Structure and Biochemistry of Cytochromes P450 Involved in the Biosynthesis of Macrolide Antibiotics

by

Matthew D. DeMars II

A dissertation submitted in partial fulfillment
of the requirements for the degree of
Doctor of Philosophy
(Chemical Biology)
in the University of Michigan
2017

Doctoral Committee:

Professor David H. Sherman, Chair
Professor David P. Ballou
Professor John Montgomery
Professor Stephen W. Ragsdale
Professor Janet L. Smith

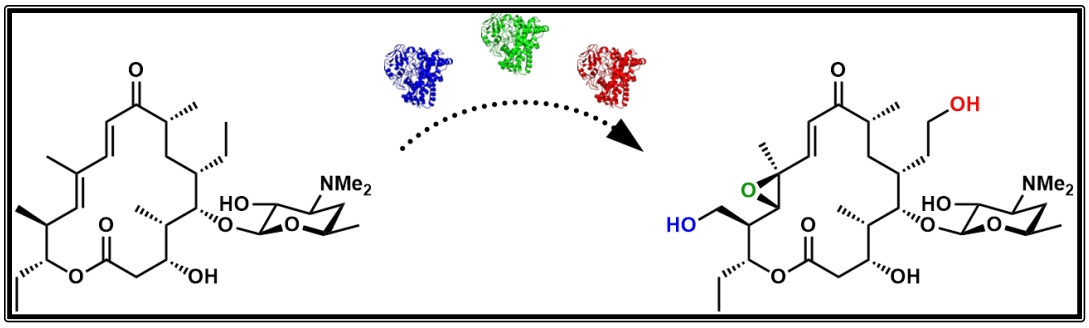
O
NMe2
HO
O
O
O
OH
O
OH
HO
O
O
O
NMe2
HO
O
O
OH

Matthew D. DeMars II
mdemars@umich.edu
ORCID iD: 0000-0002-7268-5286

Dedication

This work is dedicated to the memory of my father, Matthew David DeMars.

Acknowledgments

I have been exceedingly fortunate to have worked with some exemplary scientists during the formative years of my scientific career, and it would simply be impossible to express the full depth and breadth of my gratitude in the rather limiting context of this acknowledgments section. Quite fortuitously, I joined the laboratory of Dr. Rudi Fasan as an undergraduate student at the University of Rochester. Although I had limited experience in carrying out research at the interface of chemistry and biology, Dr. Fasan recognized my potential as well as genuine interest in the project he had assigned me and provided me with a considerable degree of autonomy shortly after I joined his lab. The work that I carried out as an undergraduate helped to solidify my fundamental affinity for interdisciplinary research, providing me with the drive to apply to and matriculate at the University of Michigan in pursuit of an advanced degree in chemical biology. As I look back five years, it is surprising that Dr. David Sherman was barely even on my radar of potential research advisors when I was considering labs in which to rotate. However, my decision to come to Michigan and ultimately to join his lab is one that I will never regret. The opportunity to perform cutting-edge and exciting research in a highly cooperative environment with some of the most skilled and intelligent people I have ever known has been a true blessing, and I could not have asked for a better lab in which to spend my tenure as a graduate student.

First and foremost, I would like to express my utmost gratitude to Dr. Sherman for giving me the freedom to pursue my own research interests and for his unabated support over the past four years. His hands-off mentoring style was appropriately complemented by his approachability and unremitting willingness to discuss and provide constructive feedback on a variety of matters whether or not they were directly related to research. Ultimately, my experience in his lab fostered my development into an independent scientist with the confidence to ask and attempt to answer my own

research questions. I also owe a debt of gratitude to my committee members: Dr. David Ballou, Dr. John Montgomery, Dr. Stephen Ragsdale, and Dr. Janet Smith. Their thoughtful questions, constructive criticisms, and valuable insights challenged me to think outside of the box and were truly instrumental in my development into a more mature researcher.

One of the most rewarding aspects of working in the Sherman lab was the opportunity to be a part of several interdisciplinary collaborations with labs across the country as well as overseas. In particular, I am extremely grateful to have gotten the chance to work with Dr. Larissa Podust, whose prolific career studying cytochromes P450 has made her a bona fide expert in the structure and biochemistry of these enzymes. Her work in solving the structures of two P450s that I extensively describe herein served as a critical foundation for many of the biochemical experiments that I later designed and carried out. More recently, we have established a collaboration with Dr. Kendall Houk, whose expertise in computational chemistry has provided an invaluable resource for better understanding dynamic processes during enzyme catalysis. I very much look forward to continuing our work with him and his lab (especially graduate student Song Yang) over the next year. Finally, I would like to thank Dr. John Montgomery and Dr. Pavel Nagorny for providing me with the opportunity to work with some of their students (Michael Gilbert, Jessica Stachowski, and Jia Hui Tay) on collaborative projects that are not described in the present body of work.

My coworkers in the Sherman lab have been and continue to be a constant source of inspiration. I have truly never met a more motivated, intelligent, and talented group of people, and it has been an honor to work alongside them for the past four years. I would especially like to thank past members Dr. Alison Narayan and Dr. Sungryeol Park as well as current members Dr. Andrew Lowell, Dr. Sean Newmister, and Dr. Ashu Tripathi for their expert advice in many areas of personal scientific ignorance. I also want to thank my bay-mates Vik Shende, Amy Fraley, and Rosa Vasquez for putting up with my antics on a daily basis. I am indebted to them along with all other members of the lab for helping to take the edge off of graduate school. Finally, I would like to extend my gratitude to Pam Schultz for being irreplaceable in her role as

lab manager as well as former and current lab secretaries Shamilya Williams and Debbie Lounds, respectively, for all of their amazing work in helping to maintain a functional and jovial work environment.

I would also like to take this opportunity to thank the Program in Chemical Biology (PCB) for admitting me as a graduate student and for being an unwavering source of support during my time here at Michigan. Program director Dr. Anna Mapp and administrators Laura Howe and Traci Swan worked hard to ensure that the entire graduate school process went as smoothly as possible for me and many others, and I sincerely thank them for all of their efforts in this respect. I feel especially fortunate to have been one of ten fantastic students that matriculated at Michigan during the 2012-2013 academic year. The camaraderie we shared is something I will forever remember and be grateful for.

During my second and third years as a graduate student at Michigan, I was fortunate enough to receive funding through the Cellular Biotechnology Training Program, which provided me with enhanced education in different areas of biotechnology. As per one of its requirements, I was able to spend Summer 2014 in South Korea working under Dr. Eung-Soo Kim in his “Microbial Molecular Biotechnology Laboratory” at Inha University. I am grateful to Dr. Sherman for presenting me with this option, to Dr. Kim for hosting me in his laboratory, and to the Center for Selective C–H Functionalization (CCHF) for funding my entire trip. As my final year in the PCB was funded by the Rackham Predoctoral Fellowship, I would also like to thank the Rackham Graduate School for its financial support.

One of the reasons I decided to come to Michigan for graduate school was the prospect of being able to simultaneously pursue my passion for early classical music. Indeed, I was afforded the opportunity to enroll in continuo and Baroque chamber ensemble courses at the School of Music starting from my very first semester as a graduate student. I want to thank Profs. Edward Parmentier and Joseph Gascho for providing me with the chance to learn about and play amazing music in a world-class university setting. Serendipitously, I also met another graduate student (Wallace Chan) whose passion for early music closely rivals mine. It has been a privilege to play music

with him and some of our mutual friends on a regular basis, and I have enjoyed going with him and his wife Mia to all of the early music concerts Ann Arbor offers every year.

Last, but certainly not least, I would like to express my deepest gratitude to my family. My parents, Matt (who just recently passed away) and Farolyn DeMars, have been there for me from the beginning and have played key roles in fostering my persistent desire to learn and create. Although they are truly unique individuals with different sets of interests and beliefs, they have always emphasized their mutual love for me and have both sacrificed so much for me to be where I am today. I'm notoriously not a very emotional person, so my gratitude and love are not always explicitly expressed, but I would like my parents to know that these feelings are always there. I also thank my stepparents, Michael Reid and Denise DeMars, for all the love and support they have given me over the years. My godparents, Larry and Jan Singer, have always taken a keen interest in my life, and I thank them for their constant love, kindness, and generosity. My grandparents, Dave and Carol DeMars, kindly hosted me in their home for several weeks every summer when I was a child/young teenager. Looking back, I cannot think of anything more they could have done to demonstrate their love for me. I would also like to thank them for providing me with the chance to take a break from writing this dissertation by joining them and the rest of the family on an Alaskan cruise this past summer. Finally, I thank my late grandfather, Jack Weinberg, who passed away just as I was starting as an undergraduate at the University of Rochester back in Fall 2008. He was someone I truly looked up to as a role model for how to treat others with kindness, warmth, and generosity, and I will forever cherish the memories I have of spending time with him.

Table of Contents

List of Figures

List of Schemes

List of Tables

List of Appendices

Abstract

Selective functionalization of chemically inert carbon-hydrogen (C–H) bonds embodies one of the grand challenges of organic chemistry and provides a key focus of research in the field. C–H functionalization can provide a valuable means to improve the efficiency of complex molecule synthesis, but significant challenges remain with respect to achieving high site selectivity in the presence of multiple unique C–H bonds in a given target. As a complement to small-molecule transition metal-based catalysts, enzymes have received increasing attention in recent years as potential biocatalysts for carrying out selective C–H bond oxidation reactions. Members of the cytochrome P450 superfamily of monooxygenases (P450s) are some of nature's most ubiquitous and versatile enzymes for performing oxidative metabolic transformations. Their unmatched ability to selectively functionalize C–H bonds has led to their growing employment in academic and industrial settings for the production of fine and commodity chemicals. Many of the most interesting and potentially biocatalytically useful P450s come from microorganisms, where they catalyze key tailoring reactions in natural product biosynthetic pathways. While most of these enzymes act on structurally complex pathway intermediates with high selectivity, they often exhibit narrow substrate scope, thus limiting their broader application. The work presented herein details studies that were carried out to biochemically and structurally characterize diverse bacterial P450s involved in the biosynthesis of 16-membered ring macrolide antibiotics with significant potential for development into robust biocatalysts for the late-stage functionalization of complex molecules. In an initial study, we investigated the reactivity of the P450 MycCI from the mycinamicin biosynthetic pathway toward a variety of macrocyclic compounds and discovered that the enzyme exhibits appreciable activity on several 16-membered ring macrolactones independent of their glycosylation state. These results were corroborated by performing equilibrium substrate binding and kinetics experiments

along with X-ray crystallographic analysis of MycCI bound to its native substrate. We also characterized TylHI, a homologous P450 from the tylosin pathway, and showed that its substrate scope is severely restricted compared with that of MycCI. Thus, the ability of the latter to hydroxylate both macrocyclic aglycones and macrolides sets it apart from related biosynthetic P450s and highlights its potential for developing novel P450 biocatalysts with broad substrate scope and high regioselectivity. Next, we performed a more in-depth analysis of TylHI in an attempt to understand the molecular basis for its substrate specificity. Turnover and equilibrium binding experiments with substrate analogs revealed that this enzyme exhibits a strict preference for 16-membered ring macrolides bearing the deoxyamino sugar mycaminose. These results were partially explained through analysis of the X-ray crystal structure of TylHI in complex with its native substrate together with biochemical characterization of several site-directed mutants. Comparative analysis of the MycCI/TylHI homolog ChmHI from the chalcomycin biosynthetic pathway provided a basis for constructing MycCI/TylHI chimeras in order to gain further insight into the features dictating the differences in the reactivity profiles of these two related P450s. These experiments unveiled the central role of the BC loop region in influencing the binding properties of 16-membered ring substrates to MycCI and TylHI. Finally, comparative analysis of several different P450s from the mycinamicin (MycCI), tylosin (TylI), and juvenimicin (JuvC and JuvD) biosynthetic pathways revealed unique substrate preferences and catalytic outcomes that facilitated their subsequent employment as biocatalysts in the chemoenzymatic synthesis of tylactone-based macrolide antibiotics.

Chapter 1: Biocatalysis and cytochrome P450

1.1 C–H functionalization, biocatalysis, and applications of cytochromes P450

1.1.1 C–H functionalization: general concepts and traditional methods

By definition, organic molecules are made up of carbon atoms, which may in turn be covalently linked to any number of other atoms, most commonly hydrogen (H), oxygen (O), nitrogen (N), or another carbon (C). The most ubiquitous of these is the C–H bond, a defining feature of organic compounds usually not explicitly depicted in standard structural formulae and typically dismissed as a viable functional group to exploit for carrying out desired chemical transformations.[1] In the broadest sense, the conversion of a C–H bond into a C–X bond, where X ≠ H, is referred to as "C–H functionalization." Unlike many other types of chemical reactions, functionalization of C–H bonds is particularly difficult to perform as a consequence of several challenges outlined below.[2-7] First, C–H bonds are quite strong (bond dissociation energies generally range from ~85 kcal/mol to ~105 kcal/mol or higher), which can lead to large kinetic barriers for C–H bond cleavage. As a result, harsh reaction conditions (e.g., high temperatures, strong oxidants, acidic or basic additives) may be required to achieve a desired outcome. Second, because most organic molecules bear multiple C–H bonds and other potentially reactive functional groups, it can be extremely difficult to target one specific site for selective modification. A commonly encountered problem associated with C–H oxidation reactions in particular is poor chemoselectivity. Because an oxidized product is typically more reactive than the unoxidized starting material, the same site may undergo further oxidation to yield undesired overoxidation products. A related issue may arise if an existing functional group in the substrate (e.g., an alcohol) is more reactive than the target site for oxidation (e.g., an unactivated alkyl C–H bond). However, the most difficult challenge by far for the practical implementation of C–H

functionalization strategies in synthetic chemistry lies in achieving the appropriate regio- and stereoselective outcome.

Despite the formidable hurdles that must be overcome in order to achieve this goal, the ability to selectively target a single C–H bond in a complex target molecule provides a powerful prospect for improving the efficiency of synthetic routes toward such compounds and could allow for the facile introduction of additional chemical functionalities at a late-stage in their construction.[8-12] In one illustrative example, the total synthesis of the potent neurotoxin (–)-tetrodotoxin was achieved in only 32 steps through judicious employment of two stereospecific C–H bond functionalization reactions[13] compared with an alternative synthesis described in the same year that required 67 steps.[14] Indeed, C–H functionalization methodology has been described as embodying a “paradigm shift” in the logic of organic synthesis.[15] The reclassification of C–H bonds from inert components of the organic molecular framework to exploitable functional groups has enabled novel retrosynthetic disconnections for complex molecule synthesis and has allowed for facile late-stage diversification of lead compounds in drug discovery efforts.[3,6,8-12,16] C–H functionalization technologies have also been successfully applied in the generation of new materials and agrochemicals.[7]

Over the past few decades, astounding progress has been made in addressing the challenges associated with performing selective C–H functionalization reactions. By and large, strategic methods involving the use of transition metals have been developed and implemented to great effect for this purpose.[2-5,17-21] While precious metals like palladium, rhodium, ruthenium, and iridium have been the most widely studied and utilized for direct functionalization of C–H bonds, more earth-abundant metals (e.g., iron, cobalt, nickel) are starting to gain prominence in the field.[22,23] In order to achieve site-selectivity in reactions using these transition metals, several strategies have been most frequently employed.[16,24] The first and most successful approach involves the use of a Lewis basic functional group on the target substrate to coordinate the metal, thereby “directing” it toward the desired site of reactivity. A second method relies on the inherent steric, electronic, and stereoelectronic properties of the different C–H bonds present in a substrate molecule to dictate the site selectivity of the reaction.[25] Although the “directing” group strategy can be used to override any inherent reactivity biases in

the substrate, it may require the installation and subsequent removal of the functional group used to chelate the metal, thereby decreasing the atom and step economy of a synthetic route. In a recent study, however, Yu and co-workers showed that transient directing groups could be used catalytically in conjunction with a palladium catalyst to selectively arylate inert C–H bonds in diverse aldehyde and ketone substrates.[26] In addition, while it has proven rather challenging to develop small-molecule catalysts that control site-selectivity independent of the substrate and without the use of directing groups,[27] this feat has successfully been achieved in recent years.[28,29] Nonetheless, a general strategy for being able to alter the selectivity of transition metal catalysts at will is not currently available. Furthermore, it remains extremely difficult to selectively functionalize sites on a molecule that are remote from any existing functionality (e.g., subterminal positions of a long alkyl chain).[1,7,20] Thus, most of the potential C–H bonds that could be targeted for functionalization remain inaccessible using these small-molecule catalyst-based methodologies.

1.1.2 Enzymatic C–H functionalization

A complementary strategy for selective C–H functionalization involves the use of biocatalysts (i.e., enzymes) to achieve desired reactivity.[30] Unlike small-molecule catalysts, enzymes typically achieve exquisite levels of site-selectivity via molecular recognition of the substrate through various noncovalent interactions (e.g., hydrophobic, hydrogen bonding, ionic) and do not require prior installation of directing or protecting groups. In addition, these biocatalysts are capable of functionalizing C–H bonds under mild reaction conditions, that is at ambient temperature/pressure under neutral conditions in aqueous solution. As Glorius and co-workers have noted, “mildness in combination with selectivity and efficiency represent the central tenets that constitute an ideal transformation.”[5] Finally, and perhaps most importantly, their catalytic properties (e.g., substrate scope, regioselectivity) can be systematically tuned via iterative rounds of mutagenesis and selection in a process called laboratory (or directed) evolution.[31]

Several different classes of enzymes have evolved in nature to catalyze reactions involving C–H bond activation.[30] Most of these enzymes possess metal- or flavin-containing cofactors that are required to mediate redox-dependent

transformations. Enzymes containing flavin mononucleotide (FMN) or flavin adenine dinucleotide (FAD) have been extensively investigated for many decades and typically carry out hydroxylation (e.g., flavin monooxygenases[32]) and halogenation (e.g., FAD-dependent halogenases[33]) reactions on electron-rich heterocyclic/aromatic compounds. Recently, a great deal of effort has focused on developing flavin-dependent halogenases into robust biocatalysts for selective C–H halogenation.[34-36] Another class of enzymes employs the 5'-deoxyadenosyl radical to abstract hydrogen atoms from a wide range of substrates, and members of this class are typically involved in catalyzing group migration, elimination, methylation, and two-electron oxidation reactions.[37] These enzymes may be classified as either adenosylcobalamin (vitamin B_{12})-dependent or *S*-adenosylmethionine (SAM)-dependent. Mononuclear non-heme iron enzymes (e.g., Fe(II)/α-ketoglutarate-dependent oxygenases) catalyze oxidation reactions via generation of high-valent iron-oxo intermediates, which can promote a variety of different oxidative transformations, including hydroxylation, halogenation, desaturation, and electrophilic aromatic substitution.[38] Other metalloenzymes, like methane monooxygenase (diiron) and tyrosinase (dicopper), are binuclear.[39] More than those from any other class, however, heme-containing enzymes (e.g., peroxidases, cytochromes P450) have served as the primary focus for the majority of work on biocatalytic C–H functionalization. These enzymes contain an iron protoporphyrin IX cofactor and generate a high-valent iron-oxo species using either hydrogen peroxide (peroxidases) or dioxygen (cytochromes P450) in order to abstract a hydrogen atom from the target substrate.[40] Finally, due to the limited capabilities of naturally occurring enzymes to perform only certain types of C–H functionalization reactions, the generation of artificial metalloenzymes has been investigated in more recent years as a potential means to expand the diversity of reactions accessible to biocatalysts.[41]

1.1.3 Applications of cytochromes P450

Owing to their impressive capacity to carry out a diverse array of oxidative transformations on many different types of substrates under mild reaction conditions and with high degrees of chemo-, regio-, and stereoselectivity, cytochromes P450 (P450s) have received increasing attention from members of the synthetic chemistry

and biotechnology communities as potential biocatalysts for selective C–H functionalization.[42-54] One of the first examples of a marketed product that was developed through the judicious application of P450 catalysis was the blue rose.[55,56] Expression of CYP75A from the blue pansy and dihydroflavonol reductase from petunia led to the production of delphinidin-derived anthocyanin pigments in roses, thereby turning them blue (**Figure 1.1A**). Successful application of P450s on an industrial scale is further exemplified by the production of the cholesterol-lowering drug pravastatin from

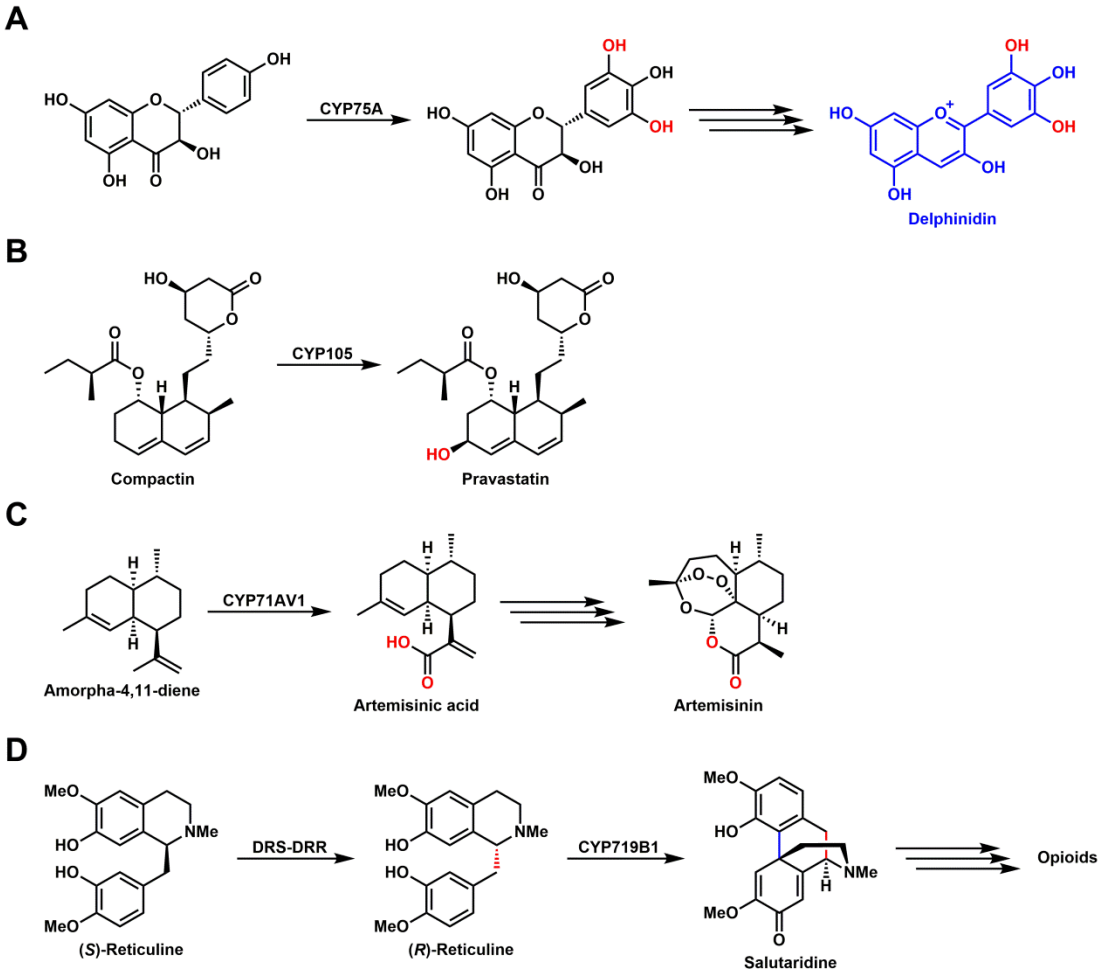

Figure 1.1. Selected biotechnological applications of cytochrome P450 enzymes. (**A**) CYP75A-catalyzed hydroxylation reactions en route to blue delphinidin-based anthocyanin pigments. (**B**) CYP105A3- and CYP105AS1-catalyzed hydroxylation of compactin for the industrial production of pravastatin. (**C**) Six-electron oxidation reaction catalyzed by CYP71AV1 in the biosynthesis of artemisinin. (**D**) DRS-DRR (1,2-dehydroreticuline synthase (CYP82Y2) + 1,2-dehydroreticuline reductase fusion enzyme) catalyzes the two-step isomerization of (*S*)-reticuline to generate (*R*)-reticuline. CYP719B1 then converts the latter to salutaridine via an oxidative C–C bond coupling reaction (new bond formed is shown in blue).

the natural product compactin via biotransformation in *Streptomyces carbophilus*, which contains a P450 (CYP105A3, or $P450_{sca-2}$) that regio- and stereoselectively hydroxylates compactin (**Figure 1.1B**).[48,57] Recently, a novel route to the industrial-scale production of pravastatin was achieved by introducing an engineered variant of CYP105AS1 from *Amycolatopsis orientalis* into the compactin producer *Penicillium chrysogenum*.[58]

Perhaps the most important P450 from a bioengineering standpoint is CYP71AV1 from *Artemisia annua*, which is responsible for converting amorpha-4,11-diene to artemisinic acid in the biosynthesis of artemisinin (**Figure 1.1C**).[59,60] This enzyme has been employed in a robust semi-synthetic process for the industrial production of this potent antimalarial compound.[61,62] More recently, the complete biosynthesis of the opioids thebaine and hydrocodone was reconstituted in yeast.[63] Two of the genes introduced were P450s from the opium poppy (a CYP82Y2-aldo-keto reductase fusion protein and CYP719B1), which acted successively to convert (*S*)-reticuline to salutaridine via (*R*)-reticuline in the biosynthetic pathway (**Figure 1.1D**). In another recent study, high-level heterologous production of oxygenated taxanes, including a precursor to paclitaxel, was achieved in *E. coli* via optimized expression of CYP725A4 (taxadiene-5α-hydroxylase) from the Pacific yew tree.[64]

P450s have seen the most widespread use in the pharmaceutical industry for the production of authentic drug metabolites.[42,46,47,49-51,53,65,66] Characterization of the pharmacological properties (e.g., toxicity, pharmacokinetics) of human drug metabolites is a critical part of the drug development pipeline, and it is necessary in order to acquire FDA approval of a new therapeutic.[67] However, given the requirement for accessing molecules incorporating the appropriate functional groups with correct regio- and stereochemistry, it can prove quite difficult to establish a feasible synthetic route to some of these metabolites.[49,50] Therefore, this process has traditionally been achieved through biotransformation methods using whole cells expressing different human hepatic P450 isoforms.[68] More recently, however, bacterial and fungal P450s have been employed to improve protein expression levels and thereby increase production yields of the final products.[46,47] For example, engineered variants of the self-sufficient $P450_{BM3}$ (CYP102A1) have frequently been used for this purpose.[49,69] A library of $P450_{BM3}$

mutants marketed by Codexis to produce drug metabolites and diversify lead compounds represents the first commercial application of engineered P450s in drug discovery and development.[70] P450s may also be used to selectively modify lead compounds in order to explore structure-activity relationships.[53] In addition to their obvious utility in the production of drugs and drug metabolites, P450s can be applied in bioremediation efforts to degrade environmental contaminants such as insecticides, pesticides, and other toxic compounds (e.g., polycyclic aromatic hydrocarbons).[44,66]

Despite these examples of how P450s have been (or can potentially be) employed in industrial processes, a number of factors have contributed to limiting their broader application in this respect.[42,44,48,51,53,65,66,71,72] First, P450s generally exhibit low levels of activity, especially on non-native substrates. Ideally, biocatalytic reactions should proceed quickly and as close to completion as possible in order to facilitate product isolation and purification. Second, P450s lack stability and display limited tolerance to organic cosolvents. Finally, and most significantly, because they are "external" monooxygenases, P450s require accessory redox partner proteins to extract electrons from NAD(P)H and deliver them to the heme iron-dioxygen intermediates in the catalytic cycle (*vide infra*). NAD(P)H itself is an expensive reagent, and in highly uncoupled redox systems, consumption of this cofactor may lead to generation of damaging reactive oxygen species (ROS) instead of productive substrate turnover. In this situation, more NAD(P)H is consumed than product is formed (i.e., less product is acquired at higher the cost).

A number of strategies have been pursued to overcome or circumvent these limitations to industrial application of P450s. In many cases, the use of whole cells expressing P450s and their redox partners can help to alleviate the drawbacks associated with using NAD(P)H-dependent enzymes, as this cofactor may be continually regenerated inside the host cell.[42,44,51,65,66,71,73] Employing whole cells as biocatalysts can also improve the overall lifetime of the catalytic system, thereby improving total substrate turnover. As a consequence, most industrial applications of P450s are restricted to whole-cell systems.[42,65,73] Alternatively, enzymatic NAD(P)H regeneration systems can be used to ensure a continual supply of this cofactor in vitro. Additional strategies to deal with the issue of electron supply may involve bypassing the

use of NAD(P)H and redox partner proteins altogether via direct reduction of the P450 using hydrogen peroxide or (electro)chemical methods. However, these techniques have not generally met with great success. By and large, issues associated with poor activity, stability, substrate scope/specificity, site selectivity, solvent tolerance, and coupling efficiency have been addressed rather effectively through a combination of rational protein design and directed evolution.[42-46,49-53,65,66] Protein engineering has been quite routinely applied to two bacterial P450s that have served as workhorses in biotechnological applications: $P450_{cam}$ (CYP101A1) and $P450_{BM3}$. In spite of the progress that has been made with respect to discovering and engineering a number of robust P450-based biocatalysts, more work is required in order to maximize their productivity levels so that they may attain more widespread application in a variety of industrial processes.[71,73]

1.2 Cytochrome P450 background

As Minor J. Coon, Professor Emeritus of Biological Chemistry at the University of Michigan, once famously said, “Cytochrome P450 [is] nature’s most versatile biological catalyst.”[74] Indeed, members of this large and growing superfamily of enzymes (thus far, >41,000 P450 sequences have been assigned systematic names[75]) are capable of performing a vast array of oxidative (and sometimes reductive) transformations, including but not limited to aliphatic/aromatic hydroxylation, epoxidation, dealkylation, heteroatom oxygenation, desaturation, decarboxylation, ring expansion/contraction, oxidative aryl/phenolic coupling, and C–C bond cleavage. Despite this vast repertoire of reactions, most of them can be rationalized mechanistically on the basis of the versatile reactivity of Compound I, the key high-valent iron-oxo species in the P450 catalytic cycle.[76-78]

P450s are heme-thiolate proteins, with an invariant cysteine residue providing a negatively charged thiolate as an axial ligand to an Fe(III) atom embedded in a protoporphyrin IX cofactor (i.e., heme). In the resting state of the enzyme, a water molecule coordinates Fe(III), serving as the sixth ligand at the distal axial position. P450s are classified as monooxygenases inasmuch as they incorporate one oxygen atom from atmospheric dioxygen (O_2) into an organic substrate while reducing the other

to water. Furthermore, because the majority of these enzymes receive the electrons required for carrying out this reaction from other proteins (redox partners), they may be more precisely called “external” monooxygenases.[79] The overall oxygenation reaction catalyzed by P450s involves the transfer of two electrons from NAD(P)H to the heme iron usually via a one- or two-component redox partner system, which facilitates heterolytic cleavage of the O–O bond to form an activated oxo-ferryl intermediate. The latter species, commonly referred to as Compound I, then acts to oxidize a bound substrate via H-atom abstraction and radical rebound.[80] Due to common secondary structural features that may nonetheless arise from unique primary sequences, all P450s share the same overall fold. Regions of structural divergence tend to reside in so-called “substrate recognition sites” (SRSs),[81] which are often experimentally found to contain residues located in proximity to bound substrate. The unique sequences and structures of these regions are frequently used to rationalize functional differences between P450 isoforms.

The P450 superfamily provides a striking example of divergent evolution from a single ancestral protein that likely existed before the emergence of eukaryotes and that probably looked and acted very much like some of the modern enzymes.[75,82,83] Indeed, despite the relatively low sequence identity (i.e., <20%) shared by P450s belonging to different families, they all retain the same overall three-dimensional fold reminiscent of an inverted triangular prism and employ a common mechanism for O_2 activation and transfer.[84,85] Indeed, the only absolutely conserved amino acid among members of the P450 superfamily is the cysteine residue that provides an axial thiolate ligand to the heme iron. While some P450 homologs lack this otherwise defining feature of the superfamily, it is not clear whether they are catalytically active.[86] In any case, it would be inappropriate to call these enzymes “P450,” as they would not exhibit the expected shift in the Soret band to ~450 nm upon reduction and carbon monoxide (CO) binding.

P450 isoforms have been identified in organisms in each of the three biological domains as well as in viruses. At present, nearly 350,000 P450 sequences have been mined and collected, a number that is expected to exceed one million within the next few years as a result of efforts to sequence the genomes of thousands of new organisms.[75] Of the P450 sequences currently identified, ~41,000 have been assigned

systematic names across >2200 different CYP families. The vast majority (>90%) of these named enzymes are found in plants, animals, and fungi while only ~7% are bacterial. P450s represent the largest family of enzymes in plant metabolism, with the corresponding genes constituting up to 1% of all protein-coding genes in these organisms.[87] For instance, in terms of raw numbers, *Arabidopsis thaliana*, *Oryza sativa* (rice), and *Vitis vinifera* (grapevine) contain 245, 332, and 315 P450 genes, respectively,[88] underscoring the breadth and diversity of plant metabolism. These enzymes are responsible for carrying out a number of important metabolic transformations involved in the biosynthesis of phytohormones and other signaling molecules (e.g., brassinosteroids, gibberellins), defense compounds (e.g., terpenoids, alkaloids, glucosinolates, phytoalexins), pigments, fatty acids, and phytosterols.[89]

In humans, 49 of the 57 identified P450 isoforms play major roles in the biosynthesis of steroid hormones, bile acids, and eicosanoids as well as in the metabolism of xenobiotics and fatty acids.[90] Human P450s are especially well known for their involvement in drug metabolism. In fact, ~75% of the enzymatic processing of small-molecule drugs that occurs in humans is mediated by P450s. The most abundant isoform in the liver and small intestine (CYP3A4) is responsible for metabolizing up to 50% of all drugs currently on the market or under development,[90] although other estimates place this number closer to 30%.[91] Notably, while expression levels of P450s involved in key basal physiological processes such as steroid hormone metabolism are generally consistent between individuals, those of the xenobiotic-metabolizing variety can exhibit substantial (i.e., more than an order of magnitude) interindividual variation.[90] Such differences may contribute to some of the pharmacokinetic variability observed among individuals taking certain drug compounds.[91] Moreover, defects in P450 genes are associated with several diseases, including rickets and congenital adrenal hyperplasia.[92] In spite of extensive research efforts over the past several decades, the physiological functions of eight human P450 isoforms have yet to be definitively established. Determining the functions of these “orphan” enzymes presents a difficult and exciting challenge for future work in this area.

P450 enzymes are also important for diverse physiological functions in fungi and bacteria. In the former, CYP51 catalyzes the 14α-demethylation of lanosterol in the rate-

limiting step of ergosterol biosynthesis.[93] Because ergosterol is a critical component of fungal cell membranes, CYP51 serves as the main target of azole-based antifungal drugs.[94] Fungal P450s also play key roles in xenobiotic detoxification as well as in the biosynthesis of mycotoxins (e.g., aflatoxin, trichothecenes) and other secondary metabolites.[95,96] While some fungal species possess many P450 genes (e.g., 155 in *Aspergillus oryzae*), others contain only a handful (e.g., 2 in *Schizosaccharomyces pombe* and 3 in *Saccharomyces cerevisiae*). Relative to eukaryotic organisms in general, however, prokaryotes tend to harbor only a small number of P450s. At one extreme, certain well-known bacterial species like *E. coli* and *Helicobacter pylori* do not have any. The genomes of various *Bacillus* species have revealed anywhere from two to eight P450s in these organisms. In contrast, mycobacteria and actinobacteria frequently contain many P450s, with 20 identified in the human pathogen *Mycobacterium tuberculosis*[97] and 18 found in the model actinomycete *Streptomyces coelicolor* A3(2).[98] It is also not uncommon for various myxobacterial species to possess around 20 or more P450 isoforms. Most notably in *Streptomyces* spp., P450s are often involved in the biosynthesis of secondary metabolites with unique and complex chemical structures.[95,99,100,101,102] Several of these enzymes will be surveyed in section 1.3.

The vast diversity of naturally occurring P450s provides great evidence that these enzymes are particularly well suited to undergoing multiple sequential rounds of mutation and selection (i.e., they are highly "evolvable"[103]). Accordingly, they have served as important starting points for directed evolution efforts aimed toward generating robust biocatalysts for performing a myriad of reactions. Work in this area goes back to the late 1990s when Arnold and co-workers used a novel fluorescence screening method to evolve $P450_{cam}$ into a peroxidase that was able to use hydrogen peroxide directly in carrying out oxygenation reactions, thus obviating the need to supply exogenous redox partners and NAD(P)H.[104] Since then, countless directed evolution campaigns have been carried out on P450s, with the catalytically self-sufficient $P450_{BM3}$ from *Bacillus megaterium* serving as the true workhorse for many of these studies.[43,46,49,52,53,103,105-109] Much of this work has focused on using a combination of different mutagenesis and screening techniques to alter the substrate scope and

regio- and stereoselectivity properties of these enzymes. It has also been possible to improve other key parameters more relevant to industrial biocatalysis such as activity, thermostability, coupling of cofactor consumption to product formation (coupling efficiency), and organic cosolvent tolerance.

Recently, P450s (and other heme-containing proteins) have been engineered to catalyze novel reactions not performed by other enzymes found in nature, including cyclopropanation, C–H amination, carbene N–H insertion, sulfimidation, and aziridination.[109-112] In order to obtain these new biocatalysts, conserved residues that were important for the natural oxygenation reaction were mutated, and synthetic reagents were fed to the enzymes to generate reactive metal carbenoid and nitrenoid intermediates. Directed evolution was then applied to improve upon suboptimal activity and selectivity. In a more extreme example of P450 engineering, Hartwig and co-workers substituted iridium-protoporphyrin IX for the natural cofactor in the thermostabile P450 CYP119 from *Sulfolobus solfataricus* to produce highly efficient biocatalysts for carbene C–H insertion[113] and C–H amination.[114] Undoubtedly, these most recent advancements testify to the intimate knowledge of P450 chemistry we have acquired over the years and point toward a future that is bright with endless possibilities for further exploiting the P450 scaffold to effect a variety of useful synthetic transformations.

1.2.1 A brief history of P450

The history of P450 can be traced back to the 1940s when techniques to obtain subcellular fractions of animal tissues were first developed. Analysis of microsomal fractions of liver cells revealed that they contained enzymes with unique metabolic and biophysical properties. A number of studies carried out in the 1950s showed that mammalian liver microsomes were capable of metabolizing various drug molecules as well as steroid hormones. Further advances in analytical techniques (e.g., mass spectrometry, spectrophotometry) that took place during this time were concomitant with the discovery in 1955 of metalloenzymes that could incorporate atmospheric dioxygen (O_2) into an organic substrate.[115,116] These enzymes would later be recognized as founding members of the oxygenase superfamily. The first experimental evidence

relating specifically to cytochrome P450 was disclosed in the same year by Axelrod and Brodie, who demonstrated that mammalian liver microsomes were capable of oxidizing xenobiotic compounds.[117,118] A few years later, Klingenberg and Garfinkel reported the detection of a carbon monoxide-binding pigment in rat and pig liver microsomes, respectively.[119,120] Notably, addition of carbon monoxide (CO) to chemically reduced microsomes led to a broad absorption band with a maximum at 450 nm. In 1962, Omura and Sato described the hemoprotein nature of this microsomal CO-binding pigment and coined the term “P450” as an abbreviation for “a pigment with a maximum absorbance at 450 nm when it is in the reduced state and bound to CO.”[121] A year later, Estabrook elucidated the physiological role of this new enzyme in steroid hydroxylation reactions.[122] Additional biochemical properties of P450 and its inactive form (P420) were subsequently detailed in further seminal reports by Omura and Sato.[123,124]

Over the next two decades, tremendous efforts put forth by many research groups established P450 as an important enzyme involved in diverse metabolic processes, ranging from steroid hormone biosynthesis in the adrenal cortex to oxidative metabolism of drugs in the liver.[125] Numerous other studies proved crucial to gaining a detailed understanding of P450 function at the molecular level. Spectroscopic characterization of the enzyme as well as model metalloporphyrin compounds confirmed that P450 was a heme-thiolate protein with a negatively charged cysteine side chain axially coordinated to the iron.[126,127] While most early experimental investigations of cytochromes P450 (P450s) focused on those obtained from mammalian tissues, the discovery of non-mammalian homologs in yeast[128] and bacteria[129,130] led to an expansion of efforts to isolate and characterize novel isoforms. Soon, the soluble P450 from *Pseudomonas putida* ($P450_{cam}$) became a robust paradigm for understanding the biochemical and biophysical properties of members of this enzyme superfamily. $P450_{cam}$ was the first P450 to be purified[130-132] and to have its full primary amino acid sequence determined.[133] In 1985, the enzyme was crystallized and analyzed by X-ray diffraction, thus producing the first three-dimensional structure of a P450.[134] Around the same time, new developments in recombinant DNA technology and heterologous protein production led to the first expression of P450s in yeast[135] and *E. coli*.[136] This work would lay an important foundation for facilitating the study of an

even broader range of prokaryotic and eukaryotic P450s in the coming decades. By 1987, at least 65 individual P450 genes had been identified, which provided an impetus for those in the field to establish a systematic nomenclature for the superfamily.[137]

With the advent of new techniques to achieve high-level heterologous expression of eukaryotic P450s for structural/functional analysis[138-140] and the elucidation of several new P450 X-ray crystal structures,[141-144] P450 research began to escalate even further throughout the 1990s. The first structure of a mammalian P450 (rabbit CYP2C5) was reported in 2000,[145] and that of a human enzyme (CYP2C9) was finally solved three years later.[146] These studies confirmed that despite considerable differences in primary sequence, the overall P450 fold is conserved between isoforms isolated from distantly related organisms. Another key insight into P450 structure in the context of its interaction with redox partners was gained when Poulos and co-workers solved the structure of $P450_{BM3}$ in complex with the FMN-binding domain of its reductase, BMR.[147] More recently, the structures of two additional P450/ferredoxin complexes have been solved: human mitochondrial CYP11A1 ($P450_{scc}$) bound to adrenodoxin (Adx)[148] and bacterial $P450_{cam}$ bound to putidaredoxin (Pdx).[149,150] Indeed, one major focus of current P450 research is to acquire a better understanding of P450-redox partner interactions and how these can dramatically impact P450 structure and catalysis. Finally, the structure of membrane-bound lanosterol 14α-demethylase (CYP51) from yeast was solved in 2014, providing the first glimpse of how the constraints of the P450 N-terminal transmembrane helix and the lipid bilayer might impact catalytic function and inhibition by azole antifungal drugs.[151] Moving into the future, functional rather than structural characterization of the countless new P450s discovered through increasingly facile genome sequencing efforts will likely become the bottleneck for understanding how these “orphan” enzymes work.[84] In addition, the isolation and characterization of the key reactive intermediate in the P450 catalytic cycle (Compound I) only recently[152] despite many attempts over the past several decades highlights the fact that even after nearly 60 years of research, we still have a great deal to learn about these amazing biocatalysts.

1.2.2 P450 catalytic mechanism

From a conceptual standpoint, the overall reaction that the standard P450 performs is rather simple: with the assistance of two electrons derived from a nicotinamide-containing cofactor (NADH or NADPH) and two protons, the enzyme takes atmospheric O_2 and inserts one of the oxygen atoms into the C–H bond of a target organic substrate with concomitant reduction of the other to water. Despite this seemingly straightforward process, the fact that C–H bonds are notoriously difficult to chemically activate, especially under mild reaction conditions (i.e., at room temperature and under atmospheric pressure), makes the observation that P450s perform this reaction quite easily and with high selectivity all the more intriguing. The key to understanding how C–H hydroxylation and many other P450-catalyzed oxidative transformations are possible lies in examining the mechanism of O_2 activation. The currently accepted P450 catalytic cycle described below (**Figure 1.2**) is the culmination of several decades' worth of work involving a plethora of different spectroscopic techniques, diagnostic substrates, synthetic metalloporphyrin model systems, and theoretical computational methods. As it has been reviewed and discussed extensively elsewhere,[80,85,153,154] only the main points will be highlighted here.

In the resting state of the enzyme, the heme iron is in the ferric state (Fe(III)) and is coordinated by a thiolate at the proximal position and a water molecule at the distal position. Upon substrate binding, the latter is displaced, changing the coordination sphere of the iron and concomitantly shifting its spin-state equilibrium from low spin to high spin. This phenomenon can be measured spectrophotometrically, as the Soret band undergoes a characteristic blue shift from ~420 nm in the resting state (low spin) to ~390 nm upon water displacement (high spin). The resulting "Type I" difference spectrum is commonly used to measure the dissociation constant associated with substrate binding to the P450. The change in the coordination state of the heme iron increases its redox potential, in turn enabling transfer of the first electron from a ferredoxin (iron-sulfur cluster-containing) or flavodoxin (flavin-containing) redox partner. In this manner, substrate binding appears to act as a regulatory mechanism to preclude unproductive NAD(P)H consumption and reduction of the heme iron in the absence of substrate, which could lead to the formation of damaging reactive oxygen species

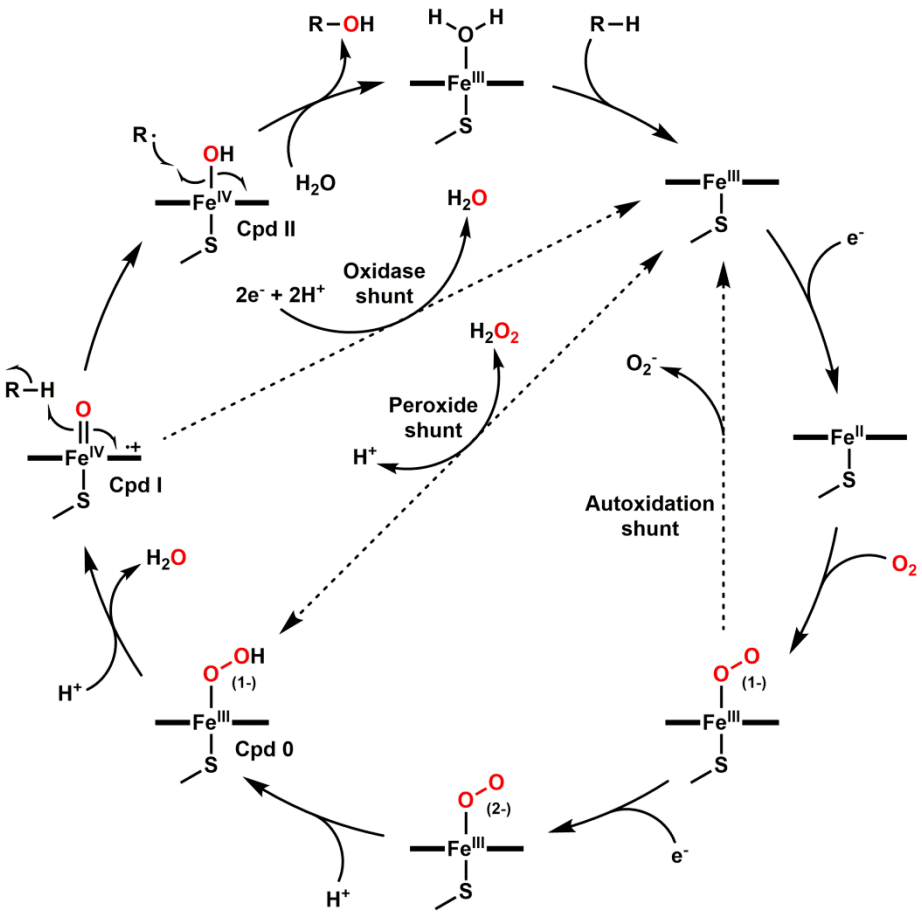

Figure 1.2. P450 catalytic cycle and shunt pathways. Compounds 0, I, and II are abbreviated Cpd 0, Cpd I, and Cpd II, respectively.

(ROS). Ferrous iron (Fe(II)) then binds O_2 at the open sixth coordination site, resulting in a ferrous dioxygen complex, although the ferric superoxide resonance form provides a more accurate representation of this species. Oxygen binding to P450s is usually fast and not a rate-limiting step for catalysis under standard reaction conditions. A second electron transfer generates a ferric peroxo intermediate, which is subsequently protonated to afford the ferric hydroperoxo complex referred to as Compound 0. While the second electron transfer step has traditionally been branded as the rate-limiting step of the catalytic cycle, the situation is likely a bit more complicated than that in practice. Indeed, given the diversity of different P450s, substrates, and redox partners currently known, it is theoretically possible that the overall rate of the reaction could be affected by any (including more than one) of the steps of the cycle.[76,155] Compound 0 is an unstable intermediate, which is rapidly protonated prior to heterolytic cleavage of the O–O bond to generate a water molecule and the oxo-ferryl (Fe(IV)) porphyrin π radical

cation species known as Compound I. This high-valent iron-oxo intermediate is the major oxidant for the vast majority of P450-catalyzed reactions. Compound I abstracts a hydrogen atom at a position on the substrate that is defined by its proximity and orientation relative to the iron-oxo group, thus producing a substrate radical and a hydroxy-ferryl species (Compound II). Finally, rapid radical rebound yields the hydroxylated substrate and the resting ferric state of the enzyme.

In a perfectly coupled system, one molecule of NAD(P)H is consumed for every molecule of oxidized product produced. This situation is rarely ever realized in practice, however, due to diversion of the catalytic cycle through one of three possible "shunt" pathways (**Figure 1.2**). The first of these is the "autoxidation shunt," wherein the ferrous dioxygen/ferric superoxide complex breaks down to release superoxide, which can rapidly disproportionate in aqueous solution to generate hydrogen peroxide and dioxygen. This shunt pathway is more likely to be followed if the second electron transfer step is slow or inefficient. The presence of substrate in the enzyme active site has been shown to increase the stability of the ferric superoxide complex in CYP3A4, thus decreasing the rate of autoxidation.[156,157] In the second shunt pathway ("peroxide shunt"), inefficient protonation of the ferric hydroperoxo complex leads to dissociation of peroxide. The proper delivery of protons to the ferric peroxo and hydroperoxo intermediates is dependent on a specific arrangement of amino acid side chains (e.g., an acid/alcohol pair) and water molecules in the active site, which together form a hydrogen-bond network in proximity to the iron-bound oxygen that facilitates protonation of these complexes en route to Compound I formation. The substrate molecule can have a significant impact on this network; minor variations in its structure can therefore be detrimental to effective proton transfer, leading to higher uncoupling. Finally, if two additional electrons and protons are supplied to Compound I, the activated oxygen atom is reduced to water, thus precluding proper insertion into the C–H bond of the target substrate. This latter pathway ("oxidase shunt") does not produce any ROS, but it consumes an additional molecule of NAD(P)H. The production of ROS (superoxide and hydrogen peroxide) that occurs in the other two shunt pathways can lead to the oxidative degradation of the enzyme and accelerate its inactivation.

Although Compound I is almost certainly the main oxidizing species in most P450-catalyzed reactions, there are a few instances in which either the ferric peroxo or the ferric hydroperoxo (Compound 0) intermediate may play the role of primary oxidant. These cases are most commonly encountered in more atypical transformations such as C–C bond cleavage and heteroatom oxidation.[158,159] Nonetheless, some previously "well-established" mechanisms may require revision as more robust biochemical/biophysical tools and techniques are developed. Among the mammalian P450s, for instance, aromatase (CYP19A1) has been one of the most intensely studied due to its central role in the formation of estrogens from androgens. It catalyzes a three-step oxidation of testosterone and androstenedione that results in the elimination of C19 as formic acid with concomitant aromatization of the A ring, generating 17β-estradiol and estrone, respectively.[90] The most cited mechanism for the final C–C bond cleavage ("lyase") step proposes that the ferric peroxo intermediate nucleophilically attacks the C19 aldehyde group to initiate a series of transformations ultimately resulting in the desired product.[160,161] However, a number of recent experimental[162-164] and theoretical[165,166] studies have further investigated this third step of the reaction sequence, concluding that Compound I rather than the ferric peroxo intermediate is the key oxidizing species.

Finally, it is worth reemphasizing that, in spite of decades of research, we continue to gain new insights into the intricacies of P450 catalysis with each passing year. Recent work by Green and co-workers has provided fundamental insight into the nature of C–H bond activation by P450s by investigating the role of thiolate ligation in controlling the reactivity properties of these enzymes. Evidence presented by these and other studies suggests that the reactivity of Compound I is largely a function of the nature of the electron-donating ligand bound at the proximal position.[167] One noteworthy observation is that thiolate-ligated heme proteins (e.g., P450s and thiolate-ligated peroxidases) are known to activate C–H bonds while related histidine-ligated peroxidases are unable to carry out these types of reactions. In a seminal study, the pK_a of the transient Fe(IV)–OH intermediate (Compound II) was determined to be ~12 in both CYP158 and CYP119.[168] This value is much higher than that of other heme enzymes and helps to explain how C–H abstraction from the target substrate

outcompetes deleterious oxidation of the protein framework. The stronger electron-donating properties of the thiolate ligand in P450s relative to those of the histidine ligand in peroxidases afford a more basic Compound II in the former, which in turn results in a significant reduction in the rate of nonproductive oxidations and increases the driving force for substrate oxidation. A follow-up study demonstrated that the Fe–S bond in P450 Compound I is significantly shorter than that in chloroperoxidase Compound I, which indicates increased electron donation from the axial thiolate ligand in the former.[169] This finding may partly explain why P450s are generally more reactive toward C–H bonds, although the underlying mechanistic details have yet to be fully elucidated. Finally, work published only a few months ago showed that selenocysteine-ligated P450 (CYP119) Compound I was more reactive than the cysteine-ligated complex.[170] This result is consistent with the hypothesis that strong electron donation from the proximal thiolate ligand is crucial for the high reactivity of P450 Compound I toward C–H bond cleavage.

1.2.3 P450 structure

In addition to the remarkable advances that have been made with respect to our understanding of the intricate details of the P450 catalytic cycle and the basis for Compound I reactivity, our knowledge of P450 structural biology has continued to expand in recent years. The first P450 structure ($P450_{cam}$ bound to camphor) was solved in 1985 by Poulos and co-workers,[134] revealing a triangular prism-like fold composed of 12 α-helical segments (A-L) and 5 small antiparallel β-sheets with the heme cofactor embedded between the proximal (L) and distal (I) helices. Several additional structures were published in the 1990s, including those for the $P450_{BM3}$ heme domain,[141] $P450_{terp}$,[142] the 6-deoxyerythronolide B hydroxylase EryF,[143,171] and fungal nitric oxide reductase ($P450_{nor}$).[144] All of these enzymes were found to share the same overall topology, with the most structural heterogeneity occurring in the six SRS regions and especially in the B', F, and G helices.[81,172] The heme cofactor was covalently bound to the cysteine residue found in the "β-bulge" region located immediately prior to the L helix, which was appropriately dubbed the "Cys-pocket." In addition, an asymmetric distribution of charge (i.e., molecular dipole) was observed in each case, which was

postulated to play a role in facilitating both cooperative redox partner interactions and the flow of protons from bulk solvent into the active site.[172] On the basis of comparing the first three P450 structures to be solved, it was predicted that all P450s would look essentially the same regardless of primary sequence or origin. Indeed, of the >120 unique P450 structures currently deposited in the Protein Data Bank (PDB), none deviates substantially from the archetypical fold.

The conserved P450 core consists of a four-helix bundle composed of three parallel helices (D, L, and I) and one antiparallel helix (E) (**Figure 1.3**).[153] As already noted, the heme group is located between the I (distal) and L (proximal) helices, and it is ligated at the proximal position by a cysteine residue located in the Cys-pocket. The sequence of this region of the protein is highly conserved across members of different P450 families and exhibits the following consensus: F-X-X-G-X_b-X-X-C-X-G, where X_b is a basic residue and C is the absolutely conserved cysteine.[173] The proximal cysteine typically hydrogen bonds with neighboring backbone amides, and an additional interaction with an amino acid side chain can be seen in some P450 isoforms. Because the electron-donating properties of the thiolate ligand can impact the reactivity of the enzyme, modulation of residues that interact with it may considerably affect catalysis. The central I helix spans the length of the protein and contains another conserved region with the following signature sequence: (A/G)-G-X-(E/D)-T. This five-residue stretch is centered at a characteristic kink in the middle of the I helix and contains a conserved acid/alcohol pair (E/D-T) that forms part of the hydrogen-bond network implicated in proton delivery to the distal oxygen atom during the catalytic cycle. In particular, the threonine residue, which is implicated in local helical distortion, participates in a hydrogen-bond network involving active site water molecules. Ordered solvent molecules near the iron-linked dioxygen are thought to act as direct proton donors to the latter, thereby promoting heterolytic cleavage of the O–O bond during the catalytic cycle. Nonetheless, the acid/alcohol pair is not present in all P450 isoforms (e.g., EryF).

Up until about 11 years ago, it was thought that all P450s contain three absolutely conserved amino acids: E-X-X-R in the K helix and the cysteine that provides the proximal thiolate ligand to the heme iron. Electrostatic interactions that occur

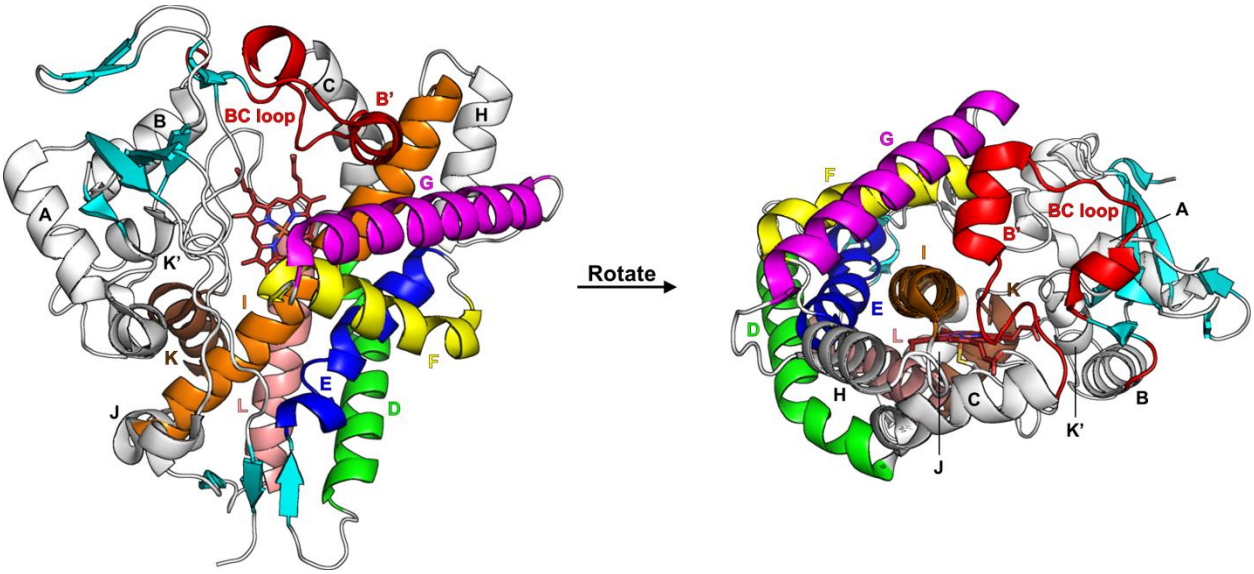

Figure 1.3. Tertiary structure of cytochrome P450. Two different viewing angles of ligand-free PikC (**PDB 2BVJ**) are shown. Select secondary structural elements are colored as follows: BC loop and B' helix (red), D helix (green), E helix (blue), F helix (yellow), G helix (magenta), I helix (orange), K helix (brown), L helix (salmon), β-strands (cyan). The heme cofactor is shown in firebrick. The axial cysteine residue can be seen coordinating the heme iron in the snapshot on the right.

between the glutamate and arginine residues of the highly conserved E-X-X-R motif are thought to be crucial for proper protein folding and stability, and they may play an important role in heme binding as well.[95,174] However, this motif is not found in a handful of P450s (CYP156B1 and CYP157 family members from *Streptomyces coelicolor*), and it was shown in 2006 that CYP157C1 from *S. coelicolor* A3(2), which has E-Q-S-L-W in place of E-X-X-R, expresses as a stable enzyme and exhibits normal P450 spectral properties.[175] Thus, only one residue (cysteine) is conserved across all naturally-occurring (and, so far as we are aware, functional) members of the P450 superfamily.

As previously mentioned, the most structurally variable regions of the protein scaffold are found in the six SRSs,[81] which play important roles in determining substrate selectivity. These portions of the sequence are found in the B' helix/BC loop (SRS1), the C-terminal portion of the F helix (SRS2), the N-terminal portion of the G helix (SRS3), the middle of the I helix (SRS4), the region immediately following the K helix that overlaps with part of the β-sheet domain (SRS5), and a portion of the loop (or β-strand) that passes above the I helix toward the C-terminus of the protein (SRS6). In large part due to disparities in the SRS regions, active site volumes vary considerably between different P450 isoforms (e.g., ~190 $Å^3$ in human CYP2E1[176]; ~2500 $Å^3$ in bacterial P450

RevI[177]). The specific shapes of P450 active sites are also quite variable and reflect the substrate selectivities of the associated enzymes.[173] Analysis of some P450 crystal structures has also revealed that they can adopt multiple different conformations as a function of substrate and/or redox partner binding. Currently, it is generally accepted that P450s undergo open/close transitions that are associated with substrate binding and that involve large movements of the BC and FG loops as well as the F and G helices.[84]

At this point, one may begin to recognize a common theme embodying P450 research and perhaps additional topics of scientific inquiry: notwithstanding the immense amount of knowledge we have acquired over the past few decades, there is an ample amount we have yet to uncover. Regarding P450 structure in particular, one of the most intriguing and mechanistically relevant questions that we have only begun to explore relates to how P450s interact with their redox partners. How do these proteins bind to P450s, and how do the structures of the latter change in response? Thus far, the structures of three P450/redox partner complexes have been solved, including $P450_{BM3}$/BMR (FMN domain only),[147] $P450_{scc}$/Adx,[148] and $P450_{cam}$/Pdx.[149,150] These snapshots have shown that ferredoxin/flavodoxin binding, which occurs on the proximal side of the heme, is largely facilitated by long- and short-range electrostatic interactions. In the case of the $P450_{cam}$/Pdx complex, Pdx plays the role of an effector by inducing structural changes in $P450_{cam}$ that are required for proper catalytic function. In spite of these initial valuable insights, more structures of P450s in complex with redox partners are needed to fully understand the breadth of possible interactions and how they can impact catalysis. Current efforts are undoubtedly focused on obtaining high-resolution X-ray crystal structures of eukaryotic P450s bound to NADPH-cytochrome P450 reductase (CPR) and other interacting partners such as cytochrome b_5 as well as those of full-length redox self-sufficient systems like $P450_{BM3}$ and $P450_{RhF}$.

1.2.4 P450 classification and diversity of redox partner systems

P450s may be classified on the basis of a number of different criteria, including type(s) of reaction(s) catalyzed, native/host organism, primary sequence/percent sequence identity to other P450s, and redox partner(s) utilized. In 1987, a classification

system for P450s based on amino acid sequence homology was developed,[137] which has since been employed to place those with ≥40% identity into the same family (e.g., CYP1, CYP2, CYP3, etc.) and those sharing ≥55% identity into a given subfamily (e.g., CYP1A, CYP1B, CYP1C, etc.). Every individual P450 is thus associated with a specific name like "CYP1A1." Later, broader groups called "clans" were introduced to highlight phylogenetic relationships between different P450 families.[178,179] Updates and additions to P450 nomenclature are routinely made by Dr. David R. Nelson, who curates the "Cytochrome P450 Homepage" (http://drnelson.uthsc.edu/cytochromeP450.html).[180] Currently, there are >300,000 P450 sequences, of which ~41,000 have been assigned systematic names.[75] These named sequences include ~13,000 from animals (>50% insectal), ~16,000 from plants, ~8000 from fungi, and ~3000 from bacteria. These and other P450s have been placed into a total of 2252 different CYP families.

As external monooxygenases, most P450s require accessory redox proteins to deliver electrons derived from NAD(P)H to the heme domain. A great diversity of redox partner systems exists, and they play crucial roles in allowing P450s to carry out their unique chemistry.[79] At least 10 different redox systems have been observed among characterized P450s (**Figure 1.4**). In bacteria, the most commonly encountered system (class I) involves a soluble FAD-containing ferredoxin reductase (FdR) and a soluble ferredoxin. The latter contains an iron-sulfur cluster ([2Fe-2S], [3Fe-4S], or [4Fe-4S]) and is responsible for shuttling electrons between FdR and the P450, which is also soluble. In *Pseudomonas putida*, for example, putidaredoxin reductase uses two electrons from NADH to reduce the [2Fe-2S]-containing putidaredoxin (Pdx), which then transfers each electron individually to $P450_{cam}$. Mitochondrial redox systems are similar to those found in bacteria with the exception that FdR is membrane-associated and P450 is bound to the inner mitochondrial membrane via an N-terminal helical anchor. In humans, CYP11A1 ($P450_{scc}$) is a mitochondrial enzyme that catalyzes the initial and rate-limiting step of steroid hormone biosynthesis from cholesterol, which involves two successive hydroxylation steps followed by oxidative C–C bond cleavage.[90] Adrenodoxin reductase oxidizes NADPH and subsequently reduces a soluble [2Fe-2S]-type ferredoxin (adrenodoxin, Adx), which then delivers the requisite electrons to $P450_{scc}$.

The most common redox system in eukaryotes comprises a membrane-bound single-component NADPH-cytochrome P450 reductase (CPR) and a membrane-bound P450 (class II). These enzymes are localized to the endoplasmic reticulum and are responsible for carrying out a wide variety of reactions in plants, animals, and fungi. CPR likely evolved as a fusion of two ancestral genes, since the N-terminal portion is homologous to bacterial FMN-containing flavodoxins while the C-terminal region exhibits homology to FAD-containing FdRs.[181,182] In addition to CPR, cytochrome b_5 reductase and cytochrome b_5 may function as electron donors to P450 in eukaryotic systems. In rare cases, these two membrane-bound proteins act independently of CPR to sequentially deliver both electrons to P450. More commonly, cytochrome b_5 is reduced by either cytochrome b_5 reductase or CPR prior to transferring only the second electron to P450. Cytochrome b_5 may also serve as an allosteric effector of P450 without acting in a standard electron-shuttling capacity.[183] Interestingly, a class II system consisting of CYP105A3 ($P450_{sca}$) and a soluble NADH-dependent CPR containing both FAD and FMN is found in the bacterium *Streptomyces carbophilus*.[184]

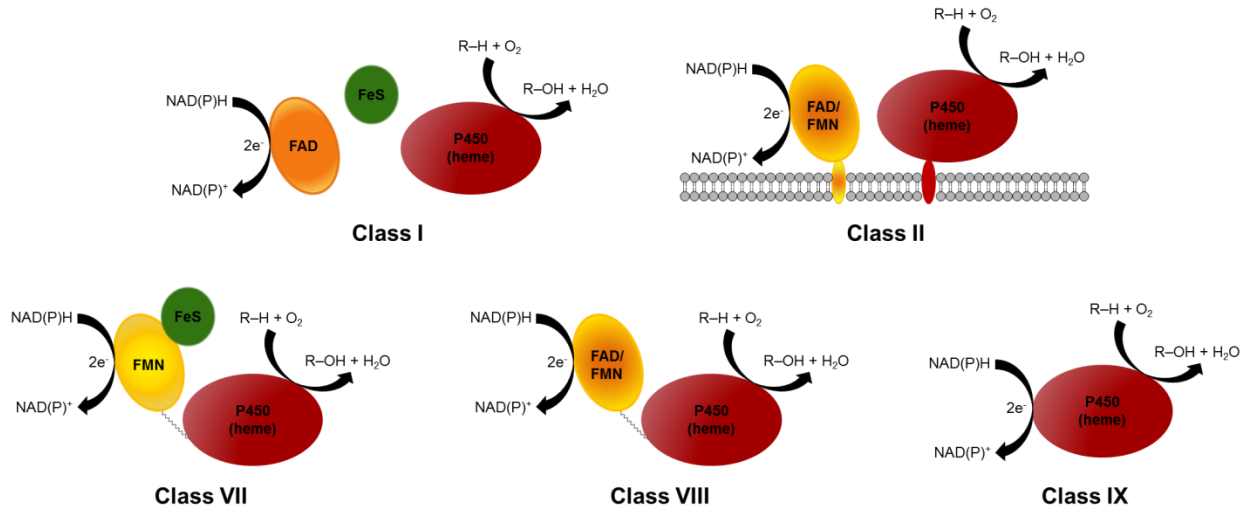

Figure 1.4. P450/redox partner systems. Selected examples described in the text are depicted. FAD = flavin adenine dinucleotide. FMN = flavin mononucleotide. FeS = iron-sulfur cluster.

Until the discovery of redox self-sufficient $P450_{BM3}$ in the 1980s (*vide infra*),[185,186] class I and class II systems were thought to be the only two that occurred in nature.[187] A variation on the class I system is presented as class III, which was initially reported in 2002.[188] CYP176A1 from *Citrobacter braakii* ($P450_{cin}$) interacts with a FMN-containing

flaxodoxin (cindoxin) instead of a ferredoxin in the host organism. However, it should be noted that the catalytic activity of many bacterial P450s can be reconstituted with flavodoxin (Fldx) in place of ferredoxin (Fdx). Class IV systems are exemplified by that involved in the reduction of CYP119 from the thermophilic archaeon *Sulfolobus solfataricus*. Instead of ultimately obtaining reducing equivalents from NAD(P)H, this enzyme depends on the action of a thiamine pyrophosphate- and [4Fe-4S]-containing 2-oxoacid:ferredoxin oxidoreductase (OFOR), which delivers electrons to Fdx following decarboxylation of pyruvate or another 2-oxoacid.[189] In class V systems, a standard FAD-containing FdR reduces a Fdx that is covalently linked to the P450 heme domain. The sterol 14α-demethylase (CYP51) from *Methylococcus capsulatus* is fused to a [3Fe-4S]-type Fdx at its C-terminus via an alanine-rich linker.[190] Class VI redox systems are the same as those of the previous class with the exception that the P450 is fused to a FMN-containing Fldx domain at its N-terminus. The explosive-degrading P450 XplA from *Rhodococcus rhodochrous* operating in conjunction with its native FdR XplB provides an example of this type of arrangement.[191] Compared with classes I and II, classes III-VI are encountered far less frequently.

The class VII redox partner arrangement was first described in 2002 with the discovery of $P450_{RhF}$ (CYP116B2) in *Rhodococcus* sp. NCIMB 9784.[192] In this system, the P450 heme domain is fused at its C-terminus to a FMN/[2Fe-2S]-containing reductase domain via a 16-amino acid linker. The reductase portion (denoted "RhFRED") shows high homology to the phthalate family of dioxygenase reductases (PFOR) and exhibits a strong preference for oxidizing NADPH over NADH.[193] RhFRED has been widely employed as a surrogate redox partner for a number of different bacterial P450s. $P450_{BM3}$ (CYP102A1) from *Bacillus megaterium* represents another completely redox self-sufficient system, but it belongs to a separate class from that of $P450_{RhF}$ (class VIII). In class VIII systems, the diflavin (FAD/FMN)-containing reductase domain is homologous to CPR from eukaryotic systems and is linked to the C-terminus of the P450 heme domain. Homologs of $P450_{BM3}$ have been found in other *Bacillus* spp., and other class VIII proteins have been identified in fungi. $P450_{foxy}$ (CYP505A1) from *Fusarium oxysporum*[194,195] and its homologs from *Phanerochaete chrysosporium*[196] possess the same domain architecture as $P450_{BM3}$, but like most

eukaryotic P450s, they are membrane bound. Another class VIII P450, Fum6p (CYP505B1), is found in *Fusarium verticillioides*, where it is involved in the biosynthesis of the fumonisin mycotoxins.[197,198]

F. oxysporum is also host to another unusual P450: $P450_{nor}$ (CYP55A1), or nitric oxide reductase.[199] Despite being of eukaryotic origin, this enzyme is completely soluble. In addition, it carries out a reduction reaction (nitric oxide to nitrous oxide) using NADH as a direct electron donor without the aid of any accessory redox proteins (class IX). Nitric oxide reductase isozymes have been identified in other fungal species as well. Some bacterial P450s are able to use hydrogen peroxide directly as a source of oxygen, generating Compound I directly via the "peroxide shunt" pathway and thereby obviating the need for delivery of electrons from a redox partner. Examples of these P450 "peroxygenases" include $P450_{SP\alpha}$ (CYP152B1) from *Sphingomonas paucimobilis* and $P450_{BS\beta}$ (CYP152A1) from *Bacillus subtilis*.[200] The peroxygenase P450 OleT (CYP152L1) from *Jeotgalicoccus* sp. ATCC 8456 is rather intriguing from a biotechnological standpoint because it catalyzes the peroxide-dependent decarboxylation of long-chain fatty acids to produce terminal alkenes.[201] Class X P450s, which are membrane-bound enzymes found in plants and animals, also do not employ redox partners. Members of the CYP74 family are present in plant chloroplast membranes and carry out rearrangement reactions that do not require O_2 or NAD(P)H. Instead, these enzymes use the acyl hydroperoxide group of the substrate as an oxygen donor to form new C–O bonds in the products. One salient example of this type of reaction is that carried out by allene oxide synthase (CYP74A), which converts lipoxygenase-derived 13-hydroperoxylinolenic acid to the corresponding allene oxide (12,13-epoxylinolenic acid) en route to jasmonic acid.[202] Examples in mammals include prostacyclin synthase (CYP8) and thromboxane synthase ($P450_{TxA}$, CYP5), which catalyze isomerization reactions of long-chain acyl peroxides in the biosynthesis of eicosanoids.[79] More recently, a bacterial class X P450 from *Streptomyces coelicolor* was discovered and characterized. This enzyme (CYP154A1) could catalyze an intramolecular cyclization reaction on a dipentaenone substrate in the absence of NAD(P)H and redox partner proteins.[203]

Other unusual P450 fusion proteins have been identified in more recent years. CYP221A1 from *Pseudomonas fluorescens* was found to be fused at its N-terminus to an acyl-CoA dehydrogenase.[78,174] The first viral P450 discovered in 2009 (CYP5253A1 from *Mimivirus*) is fused at its C-terminus to a protein of unknown function but containing several potential sites for post-translational modification.[204] The filamentous fungus *Aspergillus nidulans* encodes a P450 (PpoA) that is fused to a heme-containing dioxygenase/peroxidase domain at its N-terminus.[205] The peroxidase domain catalyzes oxidation of linoleic acid to form 8-hydroperoxyoctadecadienoic acid, which is then isomerized by the P450 domain to form 5,8-dihydroxyoctadecadienoic acid. Finally, the MpaDE fusion protein from *Penicillium brevicompactum* is involved in the biosynthesis of mycophenolic acid and consists of an N-terminal P450 domain (CYP631B5) and a C-terminal Zn-containing hydrolase domain, which act sequentially in the initial steps of the biosynthetic pathway.[206] Continued genome sequencing and functional characterization efforts will surely lead to the discovery of even more exotic P450 fusion proteins in the near future.

1.3 P450s involved in the biosynthesis of secondary metabolites

Beyond playing central roles in primary metabolic pathways ranging from steroid biosynthesis in animals and fungi to the production of phytohormones and other signaling molecules in plants, P450s represent nature's catalysts of choice for carrying out key oxidative transformations in the biosynthesis of secondary metabolites, or natural products. These small molecules are produced by many different organisms for a multitude of purposes, ultimately serving to maintain a certain level of fitness for a given organism in its environment. Thus, natural products act as robust mechanisms of self-defense, promoters of symbiosis, sexual hormones and other pheromones, metal transporting agents, and effectors of cell differentiation.[207] However, the specific endogenous function of a particular natural product is not always known. Humans have made extensive use of these compounds for centuries, often in the form of herbal remedies, elixirs, salves, and other crude concoctions, but only relatively recently have the individual molecules responsible for effecting particular biological responses been isolated and characterized. Natural products continue to serve vital roles in treating a

number of infections and diseases in humans. Indeed, from 1981 to 2014, nearly half of all new approved drugs were natural products or derivatives/mimics thereof.[208]

Microorganisms constitute an especially important source of natural products that commonly exhibit potent antibiotic, anticancer, or other therapeutically relevant properties. The biosynthetic pathways that are involved in assembling these often structurally complex and architecturally unique compounds almost invariably feature tailoring steps involving one or more P450s.[101] While these biosynthetic enzymes most commonly catalyze standard hydroxylation or epoxidation reactions, certain isoforms may carry out more exotic transformations that can lead to dramatic changes in the structure of the molecule.[209] Some of these more uncommon P450-catalyzed reactions include aryl or phenolic coupling, C–C bond formation or cleavage, ring expansion or contraction, and oxidative carbon skeleton rearrangement among others.[101,209] Thus, as new fascinating biosynthetic P450 reactions are uncovered, it becomes clearer that these versatile enzymes may be involved just as much in constructing the core scaffold of a natural product as they are in precisely decorating it with oxygen-containing functional groups. Regardless of the specific nature of the reaction performed, P450s are responsible for introducing structural and functional diversity into natural products, which can positively impact their properties with respect to how they are utilized by the producing organism. Accordingly, structural diversification of natural products can play a central role in helping the host to maintain a competitive advantage when faced with various environmental challenges.[101]

Among microorganisms, actinomycete bacteria, and especially *Streptomyces* spp., are prolific producers of natural products. In fact, over two-thirds of microbially derived antibiotics in current use along with many other important pharmaceuticals such as antifungal, anticancer, antiparasitic, and immunosuppressive agents originate from *Streptomyces*.[99,210,211] The genomes of these organisms commonly encode as many as 20-30 unique P450s, testifying to the importance of these enzymes in the production of antibiotics and other natural products.[95,99,212] To date, 184 P450s of streptomycete origin have been functionally characterized, either through in vitro methods (i.e., cloning, expression, and purification) or in vivo genetic inactivation.[212] Of these, 29 structures have been solved, but not all of them are of complexes with native substrate(s). A

number of additional genes encoding potential biosynthetic P450s in streptomycetes and other organisms that are well-known producers of natural products have been identified, but their functions have yet to be verified. For example, only ~2.4% of all P450s that have hitherto been found within the *Streptomyces* genus have been functionally characterized, and <0.4% of them have solved structures.[212] Indeed, one of the great challenges facing future work in this area is to translate existing genomic data into functional and structural information on individual P450 gene products. These studies will be sure to yield new insights into natural product biosynthesis and simultaneously lead to the discovery of even more remarkable P450 enzymology.

Among the natural products produced by *Streptomyces* and other actinomycetes, polyketides are particularly well represented. These compounds encompass an enormous number of structurally and functionally diverse secondary metabolites that quite often possess important biological activities (e.g., antibiotic, anticancer, immunosuppressive, and others). The biosynthesis of polyketides has been studied intensely at the genetic and biochemical levels for the past three or so decades and has been the subject of many extensive review articles.[213-215] Macrolactone glycosides (i.e., macrolides) constitute a large class of polyketide natural products that have been widely adopted as potent antibiotic and antifungal agents.[216] Structurally, these compounds consist of a macrocyclic lactone core to which one or more deoxysugars are attached. The most well-studied and therapeutically relevant macrolide is erythromycin, which was the first of this class of molecules to be approved for clinical use in humans back in 1952.[217] The antibiotic activity of macrolides derives from their ability to disrupt protein synthesis by binding in the nascent peptide exit tunnel of the bacterial large ribosomal subunit, although the details of the mechanism of action are still under active investigation.[218-222] Most biosynthetic pathways responsible for the construction of macrolides feature the action of one or more P450s that introduce oxidative functionality into the molecule after the macrolactone core (aglycone) has been offloaded from the terminal module of a polyketide synthase (PKS) enzyme. Although P450s are ubiquitous in macrolide biosynthetic gene clusters, the nature of the substrates as well as the positions targeted and types of reactions performed vary considerably.[99] In the following subsections, we will briefly explore the diversity of P450s involved in the

biosynthesis of various macrolides of actinomycete origin (see **Table 1.1** for a complete list of these P450s).

1.3.1 P450s involved in the biosynthesis of 12- and 14-membered ring macrolides

The erythromycin biosynthetic pathway in *Saccharopolyspora erythraea* includes two P450s that hydroxylate the 14-membered ring macrolactone scaffold at defined points in the assembly of the terminal product, erythromycin A (**Figure 1.5** and **Scheme 1.1**). EryF hydroxylates the aglycone precursor 6-deoxyerythronolide B (6-DEB) at C6[223,224] whereas EryK installs a hydroxyl group at C12 of doubly glycosylated erythromycin D.[225,226] Beyond those that carry out six-electron oxidation reactions on polyene aglycones (*vide infra*), EryF is one of the few known macrolide P450s that acts on a substrate lacking any sugar moieties. This enzyme was one of the earliest of the macrolide biosynthetic P450s to be characterized, and it was the first for which a high-resolution X-ray crystal structure was obtained.[143,171] One notable feature of EryF is that an alanine substitutes for the conserved alcohol-containing residue in the I helix. In most P450 isoforms, this threonine (or serine in some cases) is thought to play an important role in the hydrogen-bond network implicated in proton delivery to iron-linked dioxygen during the catalytic cycle. In initial EryF/6-DEB cocrystal structures, the

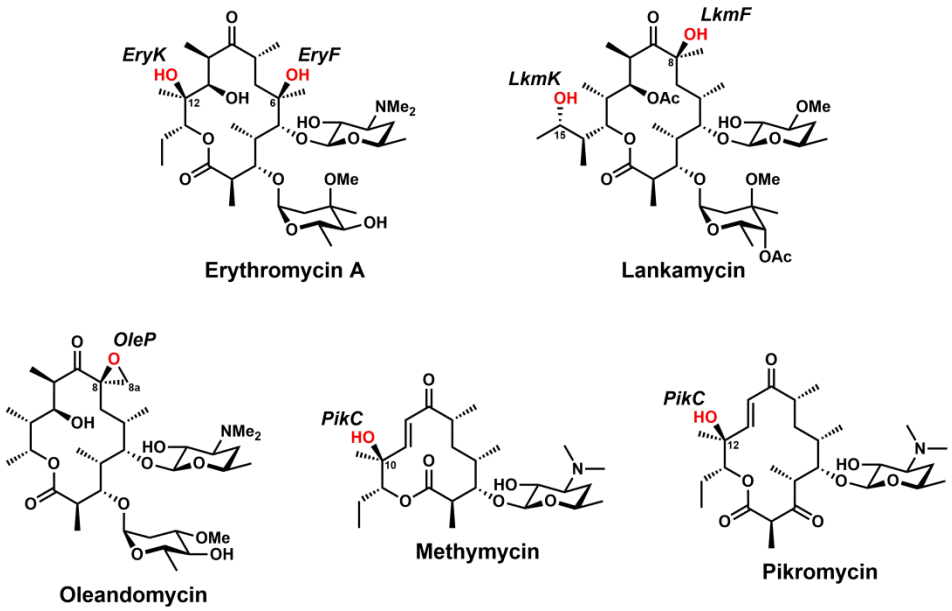

Figure 1.5. 12- and 14-membered ring macrolides. Sites of P450-catalyzed oxidation are highlighted in red.

hydroxyl group appended to C5 of the substrate was positioned to interact with a water molecule in the active site that was thought to be directly involved in donating a proton to the iron-dioxygen species en route to Compound I formation.[171,227] However, a subsequent structure of the ferrous dioxygen complex revealed that the only direct hydrogen-bond donor to dioxygen was the C5-OH group of 6-DEB.[228] This new mechanism of proton delivery invoking the substrate as a direct donor in the first protonation step to form Compound 0 has been further supported through recent molecular dynamics (MD) and quantum mechanics/molecular mechanics (QM/MM) studies.[229] The substrate-assisted catalysis hypothesis for EryF is consistent with the finding that the wild-type enzyme is unable to hydroxylate a 6-DEB analog in which the C5-OH group is oxidized to a ketone.[224] Interestingly, mutating the alanine residue in the I helix to a threonine renders EryF capable of oxidizing alternative substrates, including testosterone.[230]

Scheme 1.1. Abbreviated erythromycin biosynthetic pathway. Reactions catalyzed by P450s EryF and EryK as well as the methyltransferase EryG are shown.

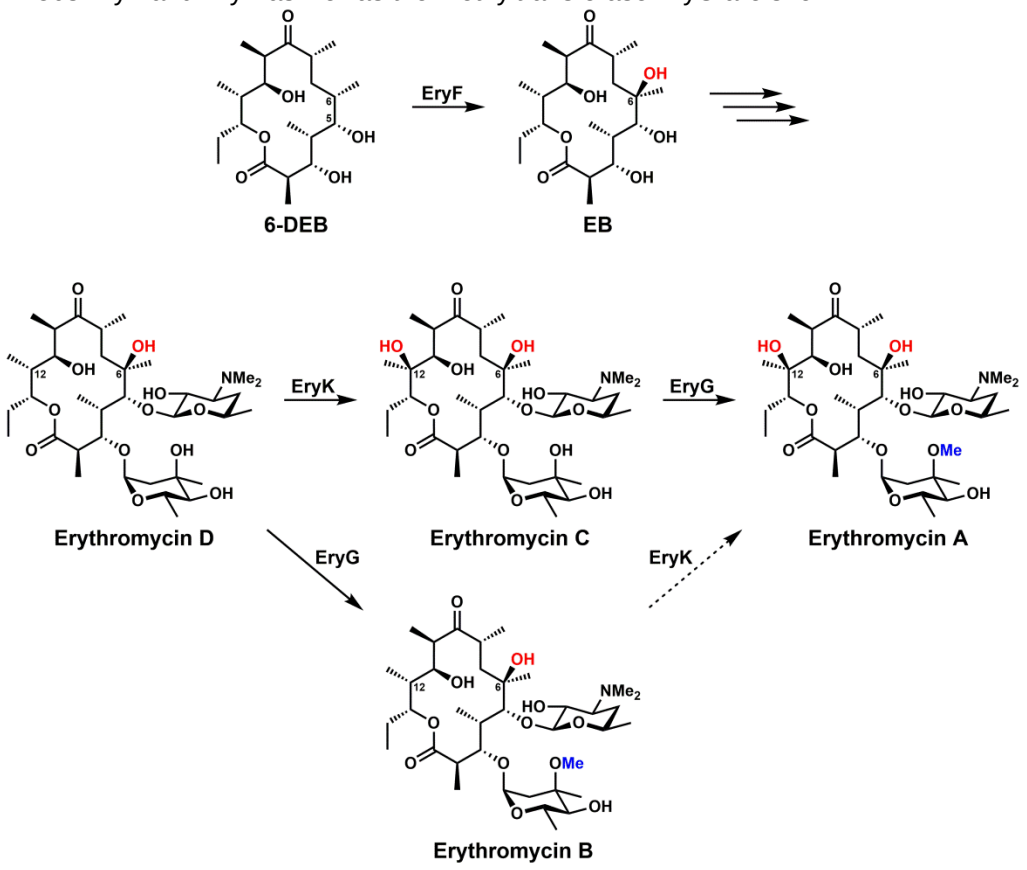

Table 1.1. List of P450s involved in the biosynthesis of macrolides in actinomycetes.[a]

P450	CYP family	Biosynthetic pathway	Macrolide type	Organism	Substrate type	Reaction type
EryF	CYP107A1	Erythromycin	14-membered	*Saccharopolyspora erythraea*	Aglycone	Hydroxylation
EryK	CYP113A1	Erythromycin	14-membered	*Saccharopolyspora erythraea*	Glycosylated	Hydroxylation
LkmF	CYP107A2	Lankamycin	14-membered	*Streptomyces rochei*	Unknown	Hydroxylation
LkmK	CYP107AP1	Lankamycin	14-membered	*Streptomyces rochei*	Unknown	Hydroxylation
OleP	CYP107D1	Oleandomycin	14-membered	*Streptomyces antibioticus*	Unknown	Desaturation/epoxidation
PikC	CYP107L1	Methymycin/pikromycin	12-/14-membered	*Streptomyces venezuelae*	Glycosylated	Hydroxylation
Cbm2	CYP113B	Carbomycin	16-membered (platenolide)	*Streptomyces thermotolerans*	Glycosylated	Four-electron oxidation
OrfA	CYP107C1	Carbomycin	16-membered (platenolide)	*Streptomyces thermotolerans*	Glycosylated	Epoxidation
Srm13	CYP113B	Spiramycin	16-membered (platenolide)	*Streptomyces ambofaciens*	Glycosylated	Four-electron oxidation
Orf6	CYP113B2	Niddamycin	16-membered (platenolide)	*Streptomyces caelestis*	Glycosylated	Four-electron oxidation
MidM	CYP113B3	Midecamycin	16-membered (platenolide)	*Streptomyces mycarofaciens*	Glycosylated	Four-electron oxidation
TylI	CYP113B1	Tylosin	16-membered (tylactone)	*Streptomyces fradiae*	Glycosylated	Four-electron oxidation
TylHI[b]	CYP105L1	Tylosin	16-membered (tylactone)	*Streptomyces fradiae*	Glycosylated	Hydroxylation
RosC	CYP113B	Rosamicin	16-membered (tylactone)	*Micromonospora rosaria*	Glycosylated	Four-electron oxidation
RosD	CYP107	Rosamicin	16-membered (tylactone)	*Micromonospora rosaria*	Glycosylated	Epoxidation
Spr5	CYP113B	Rosamicin	16-membered (tylactone)	*Salinispora pacifica*	Glycosylated	Four-electron oxidation
Spr6	CYP107	Rosamicin	16-membered (tylactone)	*Salinispora pacifica*	Glycosylated	Epoxidation
JuvC	CYP113B	Juvenimicin	16-membered (tylactone)	*Micromonospora chalcea*	Glycosylated	Four-electron oxidation
JuvD	CYP107	Juvenimicin	16-membered (tylactone)	*Micromonospora chalcea*	Glycosylated	Epoxidation
Orf1	CYP113B	Angolamycin	16-membered (tylactone)	*Streptomyces eurythermus*	Glycosylated	Four-electron oxidation
Orf10	CYP105L	Angolamycin	16-membered (tylactone)	*Streptomyces eurythermus*	Glycosylated	Hydroxylation
Orf13	CYP107	Angolamycin	16-membered (tylactone)	*Streptomyces eurythermus*	Glycosylated	Epoxidation
MycCI[c]	CYP105L2	Mycinamicin	16-membered (chalconolide)	*Micromonospora griseorubida*	Glycosylated	Hydroxylation
MycG	CYP107E1	Mycinamicin	16-membered (chalconolide)	*Micromonospora griseorubida*	Glycosylated	Hydroxylation/epoxidation
ChmHI	CYP105L	Chalcomycin	16-membered (chalconolide)	*Streptomyces bikiniensis*	Glycosylated	Hydroxylation
ChmPI	CYP107	Chalcomycin	16-membered (chalconolide)	*Streptomyces bikiniensis*	Glycosylated	Hydroxylation
ChmPII	CYP107	Chalcomycin	16-membered (chalconolide)	*Streptomyces bikiniensis*	Glycosylated	Epoxidation
AlmPI[d]	CYP105L	Aldgamycin	16-membered (chalconolide)	*Streptomyces* sp. HK-2006-1	Glycosylated	Hydroxylation
AlmPIII[d]	CYP107	Aldgamycin	16-membered (chalconolide)	*Streptomyces* sp. HK-2006-1	Glycosylated	Hydroxylation
AlmPII[d]	CYP107	Aldgamycin	16-membered (chalconolide)	*Streptomyces* sp. HK-2006-1	Glycosylated	Epoxidation
GerPIII[d]	CYP105L	Dihydrochalcomycin	16-membered (chalconolide)	*Streptomyces* sp. KCTC 0041BP	Glycosylated	Hydroxylation
GerPII[d]	CYP107	Dihydrochalcomycin	16-membered (chalconolide)	*Streptomyces* sp. KCTC 0041BP	Glycosylated	Hydroxylation
GerPI[d]	CYP107	Dihydrochalcomycin	16-membered (chalconolide)	*Streptomyces* sp. KCTC 0041BP	Glycosylated	Epoxidation
AveE	CYP171A1	Avermectin	16-membered	*Streptomyces avermitilis*	Aglycone	Furan ring formation
PimG	CYP105H3	Pimaricin	26-membered (polyene)	*Streptomyces natalensis*	Aglycone	Six-electron oxidation
PimD	CYP161A2	Pimaricin	26-membered (polyene)	*Streptomyces natalensis*	Glycosylated	Epoxidation
ScnG	CYP105H	Pimaricin	26-membered (polyene)	*Streptomyces chattanoogensis*	Aglycone	Six-electron oxidation
ScnD	CYP161A	Pimaricin	26-membered (polyene)	*Streptomyces chattanoogensis*	Glycosylated	Epoxidation
TetrG[d]	CYP105H	Tetramycin	26-membered (polyene)	*Streptomyces hygrospinosus*	Aglycone	Six-electron oxidation
TetrK[e]	CYP161A	Tetramycin	26-membered (polyene)	*Streptomyces hygrospinosus*	Glycosylated	Hydroxylation
TtmG[d]	CYP105H	Tetramycin	26-membered (polyene)	*Streptomyces ahygroscopicus*	Aglycone	Six-electron oxidation
TtmD[e]	CYP161A	Tetramycin	26-membered (polyene)	*Streptomyces ahygroscopicus*	Glycosylated	Hydroxylation
RimG	CYP105H	Rimocidin/CE-108	28-membered (polyene)	*Streptomyces diastaticus*	Aglycone	Six-electron oxidation
AmphN	CYP105H4	Amphotericin B	38-membered (polyene)	*Streptomyces nodosus*	Aglycone	Six-electron oxidation
AmphL	CYP161A3	Amphotericin B	38-membered (polyene)	*Streptomyces nodosus*	Glycosylated	Hydroxylation
NysN	CYP105H1	Nystatin	38-membered (polyene)	*Streptomyces noursei*	Aglycone	Six-electron oxidation
NysL	CYP161A1	Nystatin	38-membered (polyene)	*Streptomyces noursei*	Glycosylated	Hydroxylation
NppN	CYP105H	NPP	38-membered (polyene)	*Pseudonocardia autotrophica*	Aglycone	Six-electron oxidation

NppL	CYP161A	NPP	38-membered (polyene)	*Pseudonocardia autotrophica*	Glycosylated	Hydroxylation
CanC[e]	CYP105H5	Candicidin	38-membered (polyene)	*Streptomyces griseus*	Aglycone	Six-electron oxidation
FscP[e]	CYP105H5	FR-008 (candicidin)	38-membered (polyene)	*Streptomyces* sp. FR-008	Aglycone	Six-electron oxidation
AceN	CYP105H	67-121C	38-membered (polyene)	*Actinoplanes caeruleus*	Aglycone	Six-electron oxidation
SelL	CYP161A	Selvamicin	30-membered (polyene)	*Pseudonocardia* sp.	Glycosylated	Hydroxylation
IdnO1	CYP107	Incednine	24-membered (polyene)[f]	*Streptomyces* sp. ML694-90F3	Unknown	Hydroxylation
CmiM4	--[g]	Cremimycin	19-membered (polyene)[f]	*Streptomyces* sp. MJ635-86F5	Unknown	Unknown
TiaP1	--	Tiacumicin B	18-membered	*Dactylosporangium aurantiacum*	Unknown	Hydroxylation
TiaP2	CYP105	Tiacumicin B	18-membered	*Dactylosporangium aurantiacum*	Unknown	Hydroxylation
ApoP	CYP113	Apoptolidin	20-/21-membered	*Nocardiopsis* sp. FU40	Unknown	Hydroxylation
Ibo6	CYP105	Ibomycin	34-membered	WAC 2288	Unknown	Hydroxylation
GonCP	CYP105	PM100117/PM100118	36-membered	*Streptomyces caniferus*	Unknown	Four-electron oxidation
SamR0478	--	Stambomycin	51-membered	*Streptomyces ambofaciens*	Aglycone	Hydroxylation
SamR0479	--	Stambomycin	51-membered	*Streptomyces ambofaciens*	Aglycone	Hydroxylation

[a]P450s whose structures have been solved are highlighted in blue.
[b]The structure of TylHI has not yet been published, but it is described in Chapter 3.
[c]The structure of MycCI is described in Chapter 2.
[d]The following protein pairs are ≥99% identical: AlmPI/GerPIII, AlmPIII/GerPII, AlmPII/GerPI, TetrG/TtmG.
[e]The following protein pairs are 100% identical: TetrK/TtmD, CanC/FscP.
[f]Incednine and cremimycin are macrolactams.
[g]Blank space (--) indicates that the CYP family has not yet been identified.

Although its substrate scope is not quite as narrow as that of EryF, EryK exhibits a clear preference for its native substrate erythromycin D over erythromycin B, which arises as a shunt metabolite in *S. erythraea* culture broth through the promiscuous action of the methyltransferase EryG (**Scheme 1.1**).[226] The structure of EryK bound to erythromycin D was solved in 2009,[231] which facilitated subsequent structure-based design of a key M86A mutant that was capable of turning over both its native substrate and erythromycin B with equal catalytic efficiency.[232] EryK has also been demonstrated to hydroxylate the 12-membered ring macrolide YC-17 and the 14-membered ring macrolide narbomycin to afford methymycin/neomethymycin and pikromycin, respectively, demonstrating its ability to accept monoglycosylated (desosaminylated) substrates.[233]

Lankamycin is a structural analog of erythromycin that is produced by *Streptomyces rochei*. The biosynthetic gene cluster for this 14-membered ring macrolide also encodes two P450s, which exhibit some homology to those from the erythromycin pathway: LkmF (65% identical to EryF) and LkmK (49% identical to EryF and 37% identical to EryK). Genetic knockout studies confirmed that LkmF introduces a hydroxyl group at the C8 position whereas LkmK does so at C15 (**Figure 1.5**).[234] The results also suggested that LkmK acts prior to LkmF in the preferred native pathway, although the order of oxidation events may not be as strict as it is in the erythromycin pathway. However, as in vitro studies have not yet been carried out on these P450s, it is unknown whether either of them acts (or can act) upon the lankanolide precursor aglycone.

The biosynthetic pathway of the 14-membered ring macrolide antibiotic oleandomycin produced by the aptly named *Streptomyces antibioticus* features one P450, OleP (**Figure 1.5**). This enzyme is one of the most enigmatic of the P450s involved in the biosynthesis of macrolides, as its native function has never been definitively established. It is purported to install the epoxide moiety at the C8/C8a position of the final molecule, but the timing and mechanism of the reaction are currently unknown. The prevailing hypothesis is that OleP acts on the aglycone 8,8a-deoxyoleandolide (8,8a-DO), first performing a desaturation reaction to yield an exocyclic methylene, which is then primed for epoxidation (**Scheme 1.2A**).[235,236]

However, while the purified enzyme was capable of tightly binding 8,8a-deoxyoleandolide and the related 6-DEB, the OleP-RhFRED fusion protein did not exhibit appreciable turnover of these substrates in vitro (unpublished results from our lab). In one study, OleP was heterologously expressed in a *Streptomyces lividans* strain that had been engineered to produce 6-DEB. Analysis of culture extracts revealed the presence of at least six oxidized 6-DEB analogs, one of which (8,8a-dihydroxy-6-DEB) was verified by NMR (**Scheme 1.2B**).[237] This compound was postulated to arise from adventitious hydrolysis of an epoxide introduced by OleP. Thus, the results presented in this study suggested that epoxide formation precedes glycosylation in the oleandomycin biosynthetic pathway. A related study was subsequently conducted wherein 6-DEB, erythronolide B (EB), and C3-glycosylated derivatives thereof were biotransformed in strains of *S. erythraea* blocked in erythromycin biosynthesis and heterologously expressing OleP.[238] Isolation of the metabolites showed the presence of derivatives variably oxidized at the C8/C8a positions, including 3-*O*-mycarosyl-8,8a-epoxy-EB (**Scheme 1.2B**). Notably, the isolation of 8,8a-dehydro-6-DEB (**Scheme 1.2B**) along with the demonstration that it could undergo further oxidation by *S. erythraea* strains

Scheme 1.2. Role of OleP in the biosynthesis of oleandomycin. (**A**) Purported native reactions carried out by OleP. (**B**) Some of the metabolites obtained from heterologous expression of OleP in mutant strains of *S. lividans* and *S. erythraea*.

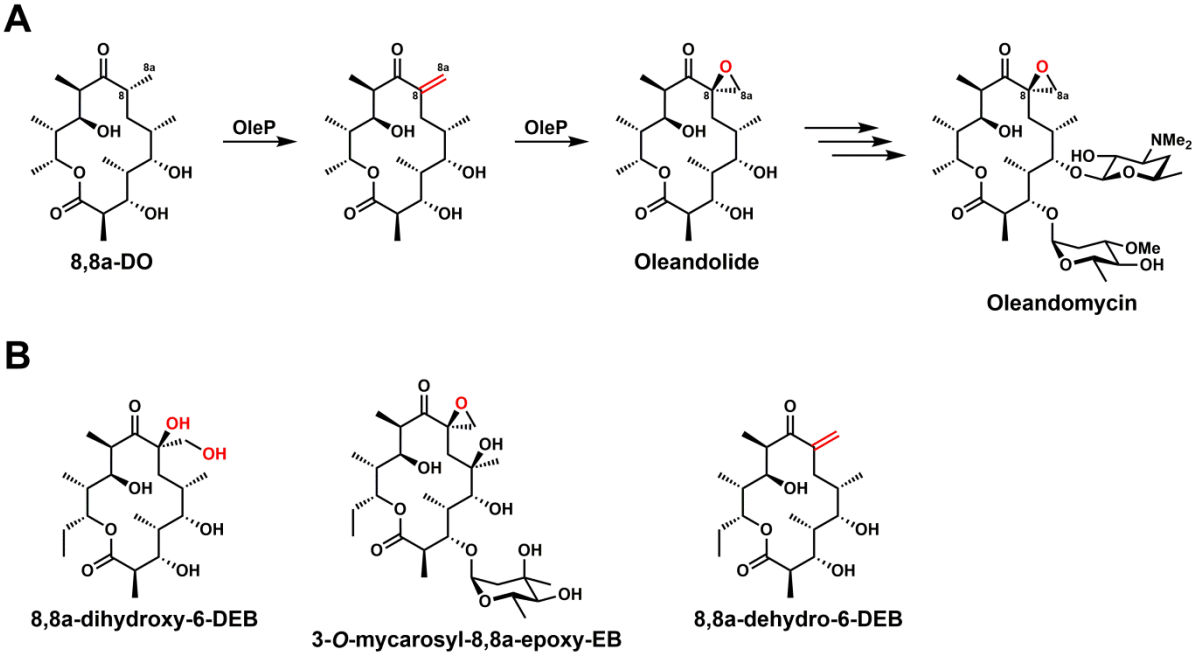

expressing OleP provided corroborating evidence that this olefin serves as an intermediate en route to the epoxide. In addition, as in the previous study, the isolation of 8,8a-dihydroxy compounds was rationalized on the basis of adventitious epoxide hydrolysis catalyzed by an endogenous enzyme in the host organism. Ultimately, the results of this work suggested that parallel pathways involving different orders of the oxidation and glycosylation steps may operate in *S. antibioticus* during the biosynthesis of oleandomycin. Recently, the X-ray crystal structure of OleP in complex with the inhibitor clotrimazole was solved.[239] Nonetheless, true in vitro functional characterization of this peculiar P450 remains to be performed (or at least published).

Finally, the P450 PikC from the methymycin/pikromycin pathway in *Streptomyces venezuelae* is one of the most well-studied macrolide hydroxylases. This enzyme is unique among other biosynthetic P450s in that it acts on both 12- and 14-membered ring macrolides as part of its native function (**Figure 1.5**).[240] Specifically, PikC hydroxylates the 12-membered ring macrolide YC-17 at either C10 or C12 to yield methymycin or neomethymycin, respectively, and it is also capable of installing a hydroxyl group at C12 of the 14-membered ring macrolide narbomycin to afford pikromycin (**Scheme 1.3**). Subsequent isolation of novamethymycin[241] as well as neopikromycin and novapikromycin[242] from *S. venezuelae* further highlighted the broad substrate scope of this enzyme. Structures of PikC bound to YC-17 and narbomycin revealed a key salt bridge interaction between the *N*,*N*-dimethylamino moiety of the desosamine sugar of these compounds and either of two proximal glutamate residues in

Scheme 1.3. Physiological reactions catalyzed by PikC.

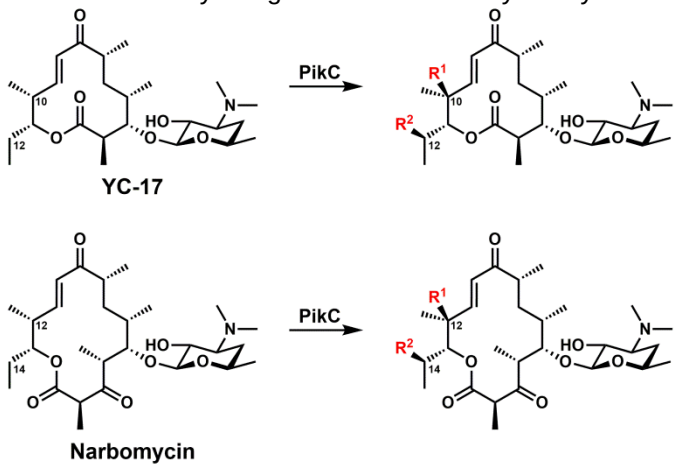

Compound	R^1	R^2
Methymycin	OH	H
Neomethymycin	H	OH
Novamethymycin	OH	OH

Compound	R^1	R^2
Pikromycin	OH	H
Neopikromycin	H	OH
Novapikromycin	OH	OH

the active site.[243,244] As a consequence of this unique substrate anchoring mechanism, PikC has been shown to accept a broad range of substrates beyond those on which it natively acts. Initial proof-of-concept studies demonstrated that appending desosamine to a variety of carbocyclic compounds was sufficient to allow for substrate binding and productive turnover by the enzyme.[245] More recent work has revealed that PikC can accept other types of substrates attached to diverse sets of nonsugar "anchors" containing the *N*,*N*-dimethylamino moiety, a functional group that is critical for proper substrate binding and orientation within the active site.[246,247] The results of MD simulations are currently being used to select specific residues in and around the PikC active site for targeted mutagenesis, thereby offering an approach that complements substrate engineering strategies to further expand the versatility of this remarkable biocatalyst.

1.3.2 P450s involved in the biosynthesis of 16-membered ring macrolides

While 14-membered ring macrolides have enjoyed more widespread clinical use than the larger 16-membered ring macrolides, the latter variety constitute a considerably broader family of compounds isolated from natural sources. Since an extensive description of 16-membered ring macrolides and their associated biosynthetic enzymes is presented in Chapter 4, the present discussion will only serve to highlight key points. These molecules can be classified into three different subgroups depending on the structure of the macrolactone core: platenolides, protylonolides (tylactones), and chalconolides (**Figure 1.6A**). Several different families of P450s are responsible for decorating these compounds with unique functional groups. Members of the CYP105L subfamily are responsible for installing a hydroxyl group at an unactivated primary carbon atom of tylactone- and chalconolide-type macrolides. The P450s MycCI and TylHI are two such enzymes (**Figure 1.6B**), and their structures and functions are explored in Chapters 2 and 3, respectively. Importantly, each CYP105L subfamily member is associated with a [3Fe-4S]-type ferredoxin present in the biosynthetic gene cluster.

CYP113B subfamily enzymes carry out four-electron oxidation reactions to generate the aldehyde moieties seen in platenolide- and tylactone-type macrolides. The

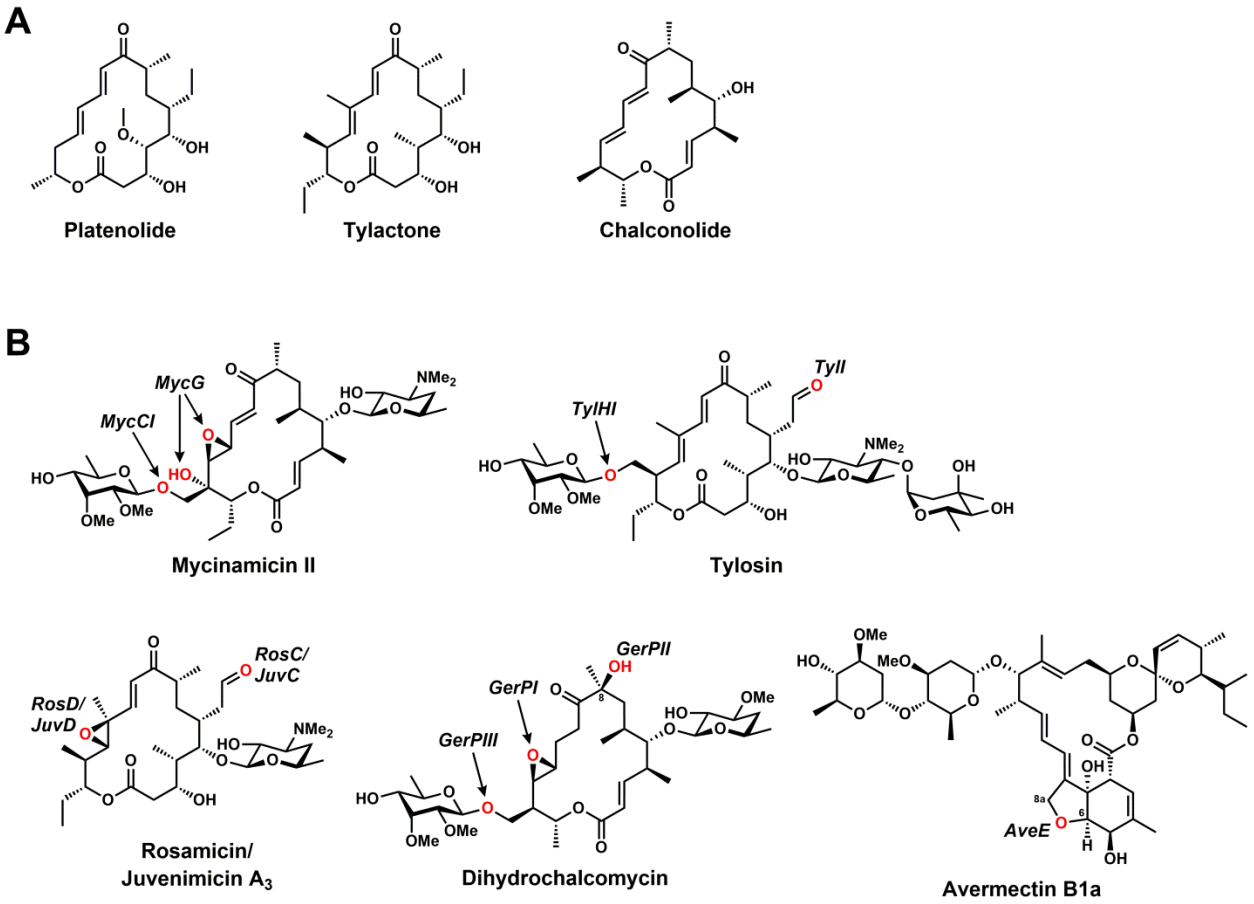

Figure 1.6. 16-membered ring macrolides. (**A**) Three main subgroups of 16-membered ring macrolides classified according to aglycone structure. (**B**) Sites of P450-catalyzed oxidation on selected 16-membered ring macrolides are highlighted in red.

activities of some members of the CYP113B subfamily (e.g., TylI, RosC, Srm13) have been verified through gene disruption and bioconversion experiments (**Figure 1.6B**), but none have been purified and tested in vitro. Chapter 4 presents work involving the expression, purification, and in vitro reconstitution of enzymatic activity of TylI and JuvC. Alignment of the primary amino acid sequences of CYP113B subfamily enzymes reveals that they cluster according to the type of macrolide they act upon. Nonetheless, these P450s likely exhibit sufficient flexibility to accept both types of macrolides. For example, it was shown that TylI could oxidize the ethyl side chains of different platenolide-type macrolides in engineered *Streptomyces fradiae* strains.[248,249] Like that of TylHI, the role of TylI in tylosin biosynthesis has hitherto been inferred from the results of various bioconversion experiments performed in the 1980s.[250-252] The predicted function of RosC was more recently confirmed via gene disruption and

complementation studies in the native rosamicin producer *Micromonospora rosaria* as well as through heterologous expression of the enzyme in *E. coli*.[253] Furthermore, the homologous P450 from the spiramycin pathway (Srm13) was shown by gene inactivation experiments to install an aldehyde moiety on a mycaminosylated intermediate to generate forocidin.[254] The putative functions of the remaining homologs are based only upon sequence alignment with those that have been functionally characterized.

A third group of P450s includes those that are part of the large CYP107 family. These enzymes carry out epoxidation and/or hydroxylation reactions on members of all three subgroups of 16-membered ring macrolides. Among them, MycG from the mycinamicin biosynthetic pathway in *Micromonospora griseorubida* has been extensively studied in vitro. This P450 is a unique multifunctional enzyme that catalyzes both hydroxylation and epoxidation reactions on its native substrate, M-IV (**Scheme 1.4**).[255] A P450 from the FD-891 pathway (GfsF) performs the same set of sequential reactions on its 16-membered ring aglycone substrate.[256,257] Whereas GfsF carries out epoxidation prior to hydroxylation, however, MycG strictly carries out these transformations in the opposite order (i.e., it cannot hydroxylate M-I, which is a shunt metabolite in the mycinamicin pathway). In addition, MycG exhibits a narrow substrate scope, as its activity on biosynthetic precursors to M-IV lacking *O*-methyl groups on the mycinose sugar is considerably diminished.[255] While several structures of this enzyme bound to some of these compounds have been solved, the substrates adopt peculiar

Scheme 1.4. Physiological reactions catalyzed by MycG.

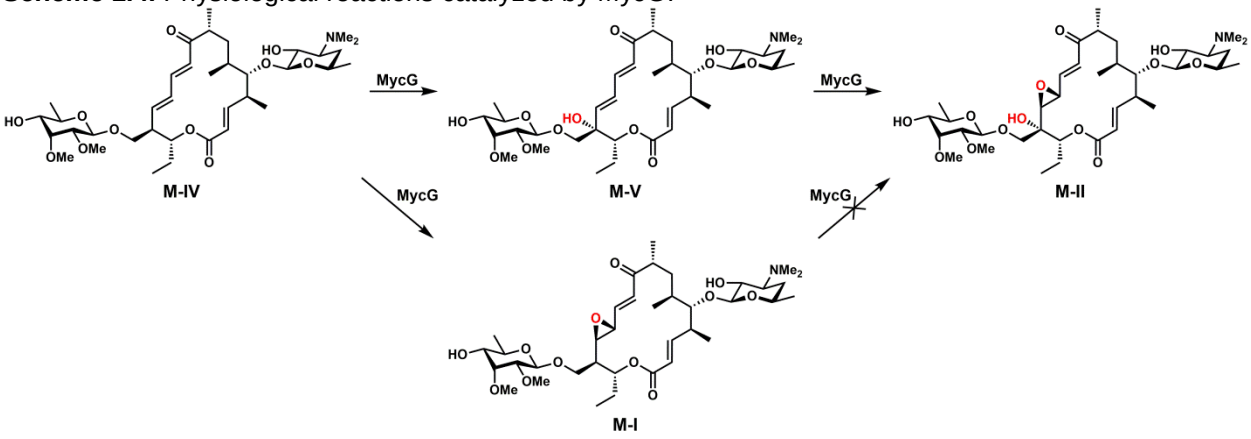

orientations in the active site that are not representative of catalytically productive binding modes.[258] Subsequent NMR[259] and MD (unpublished) studies have aided in rationalizing the observed regioselectivity properties of MycG and have provided a basis for expanding its substrate scope through protein engineering efforts.

While most members of the CYP107 family of 16-membered ring macrolide monooxygenases install epoxide groups on the macrolactone scaffold, an interesting and relatively unexplored subclass of these enzymes is responsible for hydroxylating chalconolide-type substrates at the C8 position alpha to the ketone (e.g., ChmPI, GerPII, AlmPIII). Through gene disruption and complementation experiments, GerPII was found to install a hydroxyl group at C8 prior to the epoxidation step catalyzed by GerPI in the biosynthesis of dihydrochalcomycin (**Figure 1.6B**).[260] Additional 16-membered ring macrolides exhibit structural features that are unique from those of the standard platenolide, tylactone, and chalconolide subgroups. For instance, the anthelmintic macrolide avermectin produced by *Streptomyces avermitilis* consists of four small ring systems fused to a central 16-membered ring, which in turn is linked to an oleandrose disaccharide (**Figure 1.6B**). The unique C6/C8a furan ring is forged on the aglycone precursor by the P450 AveE via a four-electron oxidation event that was verified through mutational analysis of the producing strain.[261,262] A highly homologous enzyme (MeiE) from the meilingmycin pathway in *Streptomyces nanchangensis* also catalyzes furan ring formation.[263] Notably, AveE and MeiE share 62% sequence identity, but the meilingmycins are not glycosylated compounds, further suggesting that AveE acts on avermectin aglycones.

1.3.3 P450s involved in the biosynthesis of polyene macrolides

Polyene macrolides constitute another widely studied class of natural products whose biosynthetic pathways feature important steps catalyzed by P450s. These compounds are produced by *Streptomyces* spp. as well as some rare actinomycetes, and they exhibit potent antifungal activity owing to their large macrocyclic structures and amphipathic properties. Despite extensive research over the past several decades aimed toward understanding their specific mechanisms of action, many of the details remain somewhat equivocal.[264] The primary mechanism leading to cell death is thought

to involve the formation of transmembrane channels via specific interactions with ergosterol, a critical component of fungal cell membranes, which in turn causes obstructive leakage of intracellular components.[265,266] However, other adverse effects associated with polyenes such as promotion of oxidative damage and inhibition of membrane transport proteins likely contribute to their fungicidal activity. Polyenes are also highly toxic (hemolytic) and exhibit poor water solubility properties, thus limiting their widespread use as therapeutics.

Every polyene biosynthetic gene cluster hitherto characterized contains at least one P450-encoding gene. In most cases, there are two such genes along with another encoding a [3Fe-4S]-type ferredoxin, which lies directly downstream of one of the P450 genes. The first tailoring step following PKS-catalyzed offloading and concomitant cyclization of the mature linear polyketide typically involves the sequential oxidation of an exocyclic methyl group to the corresponding carboxylic acid (**Figure 1.7A**). This reaction is carried out by a cytochrome P450 of the CYP105H subfamily with electron transfer likely mediated by the associated ferredoxin. As previously noted, genes encoding other biosynthetic P450 enzymes that belong to the CYP105L subfamily are located adjacent to those encoding [3Fe-4S]-type ferredoxins in the gene clusters of some 16-membered ring macrolides (e.g., mycinamicin (MycCI), tylosin (TylHI), chalcomycin (ChmHI)). The functions of the CYP105H enzymes in most polyene biosynthetic pathways so far investigated have been verified through targeted deletion or insertional inactivation of the gene in question. Curiously, initial attempts to inactivate these multifunctional P450s were frequently met with great difficulty, and production titers of polyene analogs lacking the exocyclic carboxyl group were often drastically reduced relative to those of the parent compounds. Ultimately, disruption of the CYP105H-encoding gene was achieved in the producers of amphotericin B,[267] nystatin,[268,269] pimaricin,[270,271] candicidin,[272] and rimocidin.[273] Not only did these experiments serve to confirm the functions of the associated enzymes, but they also led to the production of novel descarboxyl analogs that exhibited significantly reduced toxicity while retaining potent antifungal activity. To date, however, it has not been possible to overexpress and purify any of these P450s in an active form.[264] In vitro reconstitution of the relevant multistep oxidation reactions would allow for the

acquisition of more detailed mechanistic insights into the unique reactivity properties of these enzymes. In comparison with the multifunctional P450s in the macrolide pathways discussed previously, for instance, one outstanding question relates to the factors governing the extent to which a single methyl group is iteratively oxidized. Since the multifunctional polyene P450s are associated with specific ferredoxins, it is conceivable that electron transfer to these P450s is more efficient, thereby preferentially leading to full oxidation to the carboxylic acid rather than partial oxidation to the aldehyde as seen for enzymes like TylI and JuvC. Indeed, the latter enzymes are capable of producing the corresponding carboxylic acid-containing products if they are exposed directly to the aldehyde precursor (see Chapter 4), arguing against inherent differences between the P450s themselves as a tenable explanation for differential reactivity. Proper testing of this hypothesis, however, will require detailed in vitro experiments with purified P450 and ferredoxin enzymes.

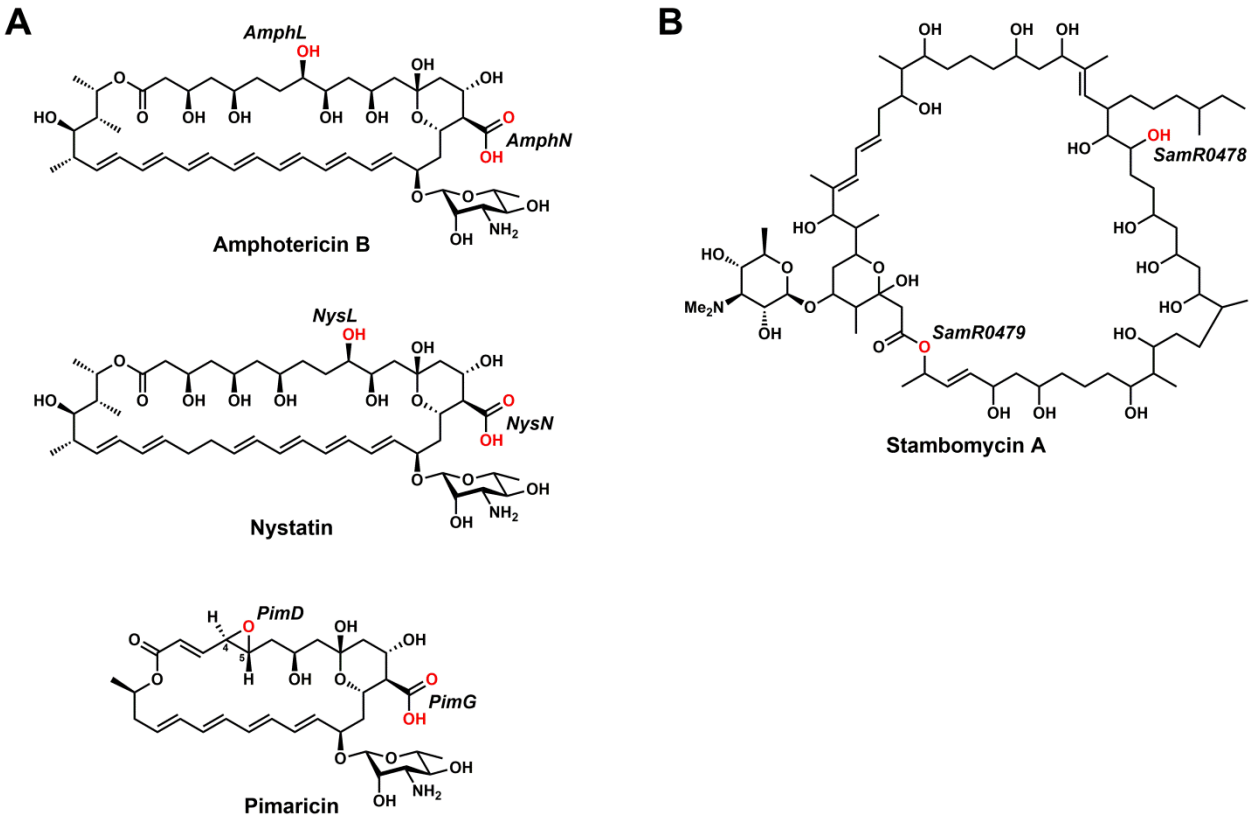

Figure 1.7. Large macrolides. (**A**) Examples of polyene antifungal compounds with sites of P450-catalyzed oxidation highlighted in red. (**B**) Structure of the 51-membered ring macrolide stambomycin A with sites of P450-catalyzed oxidation highlighted in red.

The biosynthetic pathways of 26- and 38-membered ring polyene macrolides also commonly feature a P450-catalyzed hydroxylation reaction as the final step (**Figure 1.7A**). The functions of P450s NysL and TetrK from the nystatin and tetramycin pathways, respectively, have been verified through in vitro analysis using purified enzymes.[274,275] Those of P450s AmphL and NppL from the amphotericin and NPP pathways, respectively, were confirmed through gene inactivation experiments in the native producing organisms.[276,277] A recent study explored the substrate promiscuity of these enzymes, finding that they were capable of oxidizing 4,5-desepoxypimaricin, the native substrate for a related P450 called PimD.[278] The latter enzyme is distinct from the others in that it catalyzes epoxidation rather than hydroxylation of its native substrate.[279,280] Analysis of the structure of PimD in complex with 4,5-desepoxypimaricin suggested that the ferric hydroperoxo intermediate (Compound 0) might act as the key catalytic species in carrying out the epoxidation reaction.[281] This proposal was corroborated by the results of several mechanistic biochemical experiments. Furthermore, it was hypothesized that the proton required for formation of Compound 0 could be supplied by the substrate itself in a manner analogous to the substrate-assisted catalytic mechanism observed for EryF.

1.3.4 P450s involved in the biosynthesis of other macrolides

Large non-polyene macrolides with ≥18 carbon atoms making up the core macrocycle also rely on select P450s for their biosynthesis. The functions of TiaP1 and TiaP2 in the tiacumicin B pathway were confirmed through in vivo inactivation experiments[282] while that of ApoP in the apoptolidin pathway has yet to be definitively verified.[283] Recently, a novel 34-membered ring macrolide, ibomycin, was isolated from a strain in the Wright Actinomycete Collection (WAC 2288).[284] Sequencing of the biosynthetic gene cluster revealed the presence of a single P450 gene (Ibo6), which was proposed to install a hydroxyl group on a chain elongation intermediate appended to the terminal PKS module to induce formation of a hemiketal group and subsequent macrolactonization. However, this hypothesis appears to be purely speculative. Of note, among the macrolide biosynthetic P450s, Ibo6 exhibits the highest homology to the hydroxylase TiaP2 from the tiacumicin B pathway (~50% sequence identity). In another

recent study, the installation of a ketone moiety in the novel 36-membered ring antitumor macrolides PM100117 and PM100118 by the P450 GonCP was confirmed via gene inactivation experiments.[285] Because the biosynthetic origin of a hydroxyl group adjacent to the ketone in these compounds could not be clarified, the additional involvement of GonCP in performing this reaction remains a possibility. Multiple sequence alignment with other macrolide P450s indicates that GonCP is most related to Ibo6 (~50% identity) and TiaP2 (~45% identity). In a final remarkable example, two P450s (SamR0478 and SamR0479) were shown to catalyze hydroxylation reactions in the biosynthesis of the stambomycins, 51-membered ring macrolides produced by *Streptomyces ambofaciens* (**Figure 1.7B**).[286] Gene inactivation experiments confirmed that the installation of a hydroxyl group by SamR0479 while the chain elongation intermediate is appended to the terminal PKS module is required for subsequent macrolactonization. Thus, rather than arising from the reduction of a β-keto group by a PKS ketoreductase domain, the hydroxyl group used for formation of the macrolactone is installed by a P450, representing an unprecedented mechanism for macrolactone formation in the biosynthesis of macrolide antibiotics. These studies also verified the function of SamR0478, with the data suggesting that hydroxylation by this enzyme also occurs during assembly of the polyketide chain instead of after the macrolactonization or glycosylation steps.

1.4 Dissertation outline

Despite the seemingly endless volume of literature pertaining to cytochromes P450 that has emerged over the past five and a half decades, studies aimed toward understanding their roles in the biosynthesis of natural products constitute only a small fraction of all published work on this enzyme superfamily. Because of their ability to selectively oxidize complex chemical scaffolds, biosynthetic P450s offer an as yet untapped source of novel biocatalysts for the late-stage oxidative functionalization of structurally diverse compounds. P450s involved in the biosynthesis of macrolide antibiotics are of particular interest from a bioengineering standpoint due to their inherent capacity to act on large molecules bearing a variety of different functional groups. Initial studies performed prior to the work described herein focused on

assessing the substrate scope of various P450s from the erythromycin, oleandomycin, pikromycin, tylosin, and mycinamicin pathways. A biocatalytic approach was employed to generate a panel of structurally distinct macrolactone and macrolide compounds that were subsequently used to probe the ability of these P450s to accept substrates of varying ring sizes and glycosylation states. Through these efforts, it was discovered that the P450 MycCI from the mycinamicin biosynthetic pathway displayed unprecedented promiscuity in its ability to hydroxylate both 16-membered ring aglycones as well as the corresponding macrolides. Furthermore, despite sharing relatively high sequence identity with MycCI, TylHI from the tylosin pathway exhibited significant activity only on its native substrate bearing the deoxyamino sugar mycaminose. Chapter 2 describes the results of biochemical experiments aimed toward understanding the unique catalytic properties of MycCI relative to TylHI and other P450s found in macrolide biosynthetic pathways. In collaboration with Dr. Larissa Podust (University of California, San Diego), the structure of MycCI bound to its native substrate was solved, thus providing key molecular-level insight into this interesting biocatalyst. Chapter 2 is an adaptation of an original research paper that was published in *ACS Chemical Biology* in 2016.[287] Chapter 3 provides a follow-up to several unanswered questions raised in Chapter 2 and describes further collaborative efforts with Dr. Podust to understand the molecular basis for substrate specificity in the P450 TylHI from the tylosin biosynthetic pathway. After carrying out a few additional experiments in collaboration with Dr. Kendall Houk (University of California, Los Angeles), the work presented in this chapter will be submitted for publication in the *Journal of the American Chemical Society*. In Chapter 4, several additional P450s from the tylosin and juvenimicin biosynthetic pathways are investigated, with initial biochemical characterization laying an important foundation for subsequent employment of select P450s as biocatalysts for the chemoenzymatic preparation of a panel of 16-membered ring macrolide antibiotics. Part of this work was recently published in the *Journal of the American Chemical Society*.[288] Finally, Chapter 5 provides a discussion of ongoing efforts and future directions for the research presented in Chapters 2-4.

1.5 References

(1) Yang, K. S., and Engle, K. M. (2016) Precision pruning of molecules. *Nature 533*, 183–184.
(2) Dick, A. R., and Sanford, M. S. (2006) Transition metal catalyzed oxidative functionalization of carbon–hydrogen bonds. *Tetrahedron 62*, 2439–2463.
(3) Giri, R., Shi, B.-F., Engle, K. M., Maugel, N., and Yu, J.-Q. (2009) Transition metal-catalyzed C–H activation reactions: diastereoselectivity and enantioselectivity. *Chem. Soc. Rev. 38*, 3242–3272.
(4) Lyons, T. W., and Sanford, M. S. (2010) Palladium-catalyzed ligand-directed C–H functionalization reactions. *Chem. Rev. 110*, 1147–1169.
(5) Wencel-Delord, J., Dröge, T., Liu, F., and Glorius, F. (2011) Towards mild metal-catalyzed C–H bond activation. *Chem. Soc. Rev. 40*, 4740–4761.
(6) Zheng, C., and You, S.-L. (2014) Recent development of direct asymmetric functionalization of inert C–H bonds. *RSC Adv. 4*, 6173–6214.
(7) Hartwig, J. F. (2016) Evolution of C–H bond functionalization from methane to methodology. *J. Am. Chem. Soc. 138*, 2–24.
(8) Godula, K., and Sames, D. (2006) C-H bond functionalization in complex organic synthesis. *Science 312*, 67–72.
(9) Gutekunst, W. R., and Baran, P. S. (2011) C–H functionalization logic in total synthesis. *Chem. Soc. Rev. 40*, 1976–1991.
(10) Yamaguchi, J., Yamaguchi, A. D., and Itami, K. (2012) C–H bond functionalization: emerging synthetic tools for natural products and pharmaceuticals. *Angew. Chem. Int. Ed. 51*, 8960–9009.
(11) Wencel-Delord, J., and Glorius, F. (2013) C–H bond activation enables the rapid construction and late-stage diversification of functional molecules. *Nat. Chem. 5*, 369–375.
(12) Qiu, Y., and Gao, S. (2016) Trends in applying C–H oxidation to the total synthesis of natural products. *Nat. Prod. Rep. 33*, 562–581.
(13) Hinman, A., and Du Bois, J. (2003) A stereoselective synthesis of (–)-tetrodotoxin. *J. Am. Chem. Soc. 125*, 11510–11511.
(14) Ohyabu, N., Nishikawa, T., and Isobe, M. (2003) First asymmetric total synthesis of tetrodotoxin. *J. Am. Chem. Soc. 125*, 8798–8805.
(15) Davies, H. M. L., and Morton, D. (2016) Recent advances in C–H functionalization. *J. Org. Chem. 81*, 343–350.
(16) Hartwig, J. F., and Larsen, M. A. (2016) Undirected, homogeneous C–H bond functionalization: challenges and opportunities. *ACS Cent. Sci. 2*, 281–292.
(17) Colby, D. A., Tsai, A. S., Bergman, R. G., and Ellman, J. A. (2012) Rhodium catalyzed chelation-assisted C–H bond functionalization reactions. *Acc. Chem. Res. 45*, 814–825.
(18) Neufeldt, S. R., and Sanford, M. S. (2012) Controlling site selectivity in palladium-catalyzed C–H bond functionalization. *Acc. Chem. Res. 45*, 936–946.
(19) Rouquet, G., and Chatani, N. (2013) Catalytic functionalization of C(sp^2)–H and C(sp^3)–H bonds by using bidentate directing groups. *Angew. Chem. Int. Ed. 52*, 11726–11743.
(20) Qiu, G., and Wu, J. (2015) Transition metal-catalyzed direct remote C–H functionalization of alkyl groups *via* C(sp^3)–H bond activation. *Org. Chem. Front. 2*, 169–178.
(21) Ping, L., Chung, D. S., Bouffard, J., and Lee, S.-g. (2017) Transition metal-catalyzed site- and regio-divergent C–H bond functionalization. *Chem. Soc. Rev. 46*, 4299–4328.
(22) Pototschnig, G., Maulide, N., and Schnürch, M. (2017) Direct functionalization of C–H bonds by iron, nickel, and cobalt catalysis. *Chem. Eur. J. 23*, 9206–9232.
(23) Shang, R., Ilies, L., and Nakamura, E. (2017) Iron-catalyzed C–H bond activation. *Chem. Rev. 117*, 9086–9139.
(24) Brückl, T., Baxter, R. D., Ishihara, Y., and Baran, P. S. (2012) Innate and guided C–H functionalization logic. *Acc. Chem. Res. 45*, 826–839.
(25) Newhouse, T., and Baran, P. S. (2011) If C–H bonds could talk: selective C–H bond oxidation. *Angew. Chem. Int. Ed. 50*, 3362–3374.
(26) Zhang, F.-L., Hong, K., Li, T.-J., Park, H., and Yu, J.-Q. (2016) Functionalization of C(sp^3)-H bonds using a transient directing group. *Science 351*, 252–256.
(27) White, M. C. (2012) C–H bond functionalization & synthesis in the 21st century: a brief history and prospectus. *Synlett 23*, 2746–2748.
(28) Gormisky, P. E., and White, M. C. (2013) Catalyst-controlled aliphatic C–H oxidations with a

predictive model for site-selectivity. *J. Am. Chem. Soc. 135*, 14052–14055.
(29) Liao, K., Negretti, S., Musaev, D. G., Basca, J., and Davies, H. M. L. (2016) Site-selective and stereoselective functionalization of unactivated C–H bonds. *Nature 533*, 230–234.
(30) Lewis, J. C., Coelho, P. S., and Arnold, F. H. (2011) Enzymatic functionalization of carbon-hydrogen bonds. *Chem. Soc. Rev. 40*, 2003–2021.
(31) Turner, N. J. (2009) Directed evolution drives the next generation of biocatalysts. *Nat. Chem. Biol. 5*, 567–573.
(32) van Berkel, W. J. H., Kamerbeek, N. M., and Fraaije, M. W. (2006) Flavoprotein monooxygenases, a diverse class of oxidative biocatalysts. *J. Biotechnol. 124*, 670–689.
(33) Vaillancourt, F. H., Yeh, E., Vosburg, D. A., Garneau-Tsodikova, S., and Walsh, C. T. (2006) Nature's inventory of halogenation catalysts: oxidative strategies predominate. *Chem. Rev. 106*, 3364–3378.
(34) Durak, L. J., Payne, J. T., and Lewis, J. C. (2016) Late-stage diversification of biologically active molecules via chemoenzymatic C–H functionalization. *ACS Catal. 6*, 1451–1454.
(35) Schnepel, C., and Sewald, N. (2017) Enzymatic halogenation: a timely strategy for regioselective C–H activation. *Chem. Eur. J. 23*, DOI: 10.1002/chem.201701209.
(36) Latham, J., Brandenburger, E., Shepherd, S. A., Menon, B. R. K., and Micklefield, J. (2017) Development of halogenase enzymes for use in synthesis. *Chem. Rev.* DOI: 10.1021/acs.chemrev.7b00032.
(37) Marsh, E. N. G., Patterson, D. P., and Li, L. (2010) Adenosyl radical: reagent and catalyst in enzyme reactions. *ChemBioChem 11*, 604–621.
(38) Krebs, C., Fujimori, D. G., Walsh, C. T., and Bollinger, J. M., Jr. (2007) Non-heme Fe(IV)–oxo intermediates. *Acc. Chem. Res. 40*, 484–492.
(39) Que, L., Jr., and Tolman, W. B. (2002) Bis(*μ*-oxo)dimetal "diamond" cores in copper and iron complexes relevant to biocatalysis. *Angew. Chem. Int. Ed. 41*, 1114–1137.
(40) Poulos, T. L. (2014) Heme enzyme structure and function. *Chem. Rev. 114*, 3919–3962.
(41) Upp, D. M., and Lewis, J. C. (2017) Selective C–H bond functionalization using repurposed or artificial metalloenzymes. *Curr. Opin. Chem. Biol. 37*, 48–55.
(42) Girhard, M., Bakkes, P. J., Mahmoud, O., and Urlacher, V. B. (2015) P450 biotechnology, in *Cytochrome P450: structure, mechanism, and biochemistry* (Ortiz de Montellano, P. R., Ed.) 4th ed., pp 451–520. Springer.
(43) Bernhardt, R. (2006) Cytochromes P450 as versatile biocatalysts. *J. Biotechnol. 124*, 128–145.
(44) Urlacher, V. B., and Eiben, S. (2006) Cytochrome P450 monooxygenases: perspectives for synthetic application. *Trends Biotechnol. 24*, 324–330.
(45) Grogan, G. (2011) Cytochromes P450: exploiting diversity and enabling application as biocatalysts. *Curr. Opin. Chem. Biol. 15*, 241–248.
(46) Urlacher, V. B., and Girhard, M. (2012) Cytochrome P450 monooxygenases: an update on perspectives for synthetic application. *Trends Biotechnol. 30*, 26–36.
(47) Schulz, S., Girhard, M., and Urlacher, V. B. (2012) Biocatalysis: key to selective oxidations. *ChemCatChem 4*, 1889–1895.
(48) Sakaki, T. (2012) Practical application of cytochrome P450. *Biol. Pharm. Bull. 35*, 844–849.
(49) Fasan, R. (2012) Tuning P450 enzymes as oxidation catalysts. *ACS Catal. 2*, 647–666.
(50) Caswell, J. M., O'Neill, M., Taylor, S. J. C., and Moody, T. S. (2013) Engineering and application of P450 monooxygenases in pharmaceutical and metabolite synthesis. *Curr. Opin. Chem. Biol. 17*, 271–275.
(51) Bernhardt, R., and Urlacher, V. B. (2014) Cytochromes P450 as promising catalysts for biotechnological application: chances and limitations. *Appl. Microbiol. Biotechnol. 98*, 6185–6203.
(52) Roiban, G.-D., and Reetz, M. T. (2015) Expanding the toolbox of organic chemists: directed evolution of P450 monooxygenases as catalysts in regio- and stereoselective oxidative hydroxylation. *Chem. Commun. 51*, 2208–2224.
(53) Behrendorff, J. B. Y. H., Huang, W., and Gillam, E. M. J. (2015) Directed evolution of cytochrome P450 enzymes for biocatalysis: exploiting the catalytic versatility of enzymes with relaxed substrate specificity. *Biochem. J. 467*, 1–15.
(54) Girvan, H. M., and Munro, A. W. (2016) Applications of microbial cytochrome P450 enzymes in biotechnology and synthetic biology. *Curr. Opin. Chem. Biol. 31*, 136–145.
(55) Katsumoto, Y., Fukuchi-Mizutani, M., Fukui, Y., Brugliera, F., Holton, T. A., Karan, M., Nakamura, N.,

Yonekura-Sakakibara, K., Togami, J., Pigeaire, A., Tao, G.-Q., Nehra, N. S., Lu, C.-Y., Dyson, B. K., Tsuda, S., Ashikari, T., Kusumi, T., Mason, J. G., and Tanaka, Y. (2007) Engineering of the rose flavonoid biosynthetic pathway successfully generated blue-hued flowers accumulating delphinidin. *Plant Cell Physiol. 48*, 1589–1600.

(56) Tanaka, Y., and Brugliera, F. (2013) Flower colour and cytochromes P450. *Phil. Trans. R. Soc. B 368*, 20120432.

(57) Park, J.-W., Lee, J.-K., Kwon, T.-J., Yi, D.-H., Kim, Y.-J., Moon, S.-H., Suh, H.-H., Kang, S.-M., and Park, Y.-I. (2003) Bioconversion of compactin into pravastatin by *Streptomyces* sp. *Biotechnol. Lett. 25*, 1827–1831.

(58) McLean, K. J., Hans, M., Meijrink, B., van Scheppingen, W. B., Vollebregt, A., Tee, K. L., van der Laan, J.-M., Leys, D., Munro, A. W., and van den Berg, M. A. (2015) Single-step fermentative production of the cholesterol-lowering drug pravastatin via reprogramming of *Penicillium chrysogenum*. *Proc. Natl. Acad. Sci. USA 112*, 2847–2852.

(59) Teoh, K. H., Polichuk, D. R., Reed, D. W., Nowak, G., and Covello, P. S. (2006) *Artemisia annua* L. (Asteraceae) trichome-specific cDNAs reveal CYP71AV1, a cytochrome P450 with a key role in the biosynthesis of the antimalarial sesquiterpene lactone artemisinin. *FEBS Lett. 580*, 1411–1416.

(60) Ro, D.-K., Paradise, E. M., Ouellet, M., Fisher, K. J., Newman, K. L., Ndungu, J. M., Ho, K. A., Eachus, R. A., Ham, T. S., Kirby, J., Chang, M. C. Y., Withers, S. T., Shiba, Y., Sarpong, R., and Keasling, J. D. (2006) Production of the antimalarial drug precursor artemisinic acid in engineered yeast. *Nature 440*, 940–943.

(61) Paddon, C. J., Westfall, P. J., Pitera, D. J., Benjamin, K., Fisher, K., McPhee, D., Leavell, M. D., Tai, A., Main, A., Eng, D., Polichuk, D. R., Teoh, K. H., Reed, D. W., Treynor, T., Lenihan, J., Fleck, M., Bajad, S., Dang, G., Dengrove, D., Diola, D., Dorin, G., Ellens, K. W., Fickes, S., Galazzo, J., Gaucher, S. P., Geistlinger, T., Henry, R., Hepp, M., Horning, T., Iqbal, T., Jiang, H., Kizer, L., Lieu, B., Melis, D., Moss, N., Regentin, R., Secrest, S., Tsuruta, H., Vazquez, R., Westblade, L. F., Xu, L., Yu, M., Zhang, Y., Zhao, L., Lievense, J., Covello, P. S., Keasling, J. D., Reiling, K. K., Renninger, N. S., and Newman, J. D. (2013) High-level semi-synthetic production of the potent antimalarial artemisinin. *Nature 496*, 528–532.

(62) Turconi, J., Griolet, F., Guevel, R., Oddon, G., Villa, R., Geatti, A., Hvala, M., Rossen, K., Göller, R., and Burgard, A. (2014) Semisynthetic artemisinin, the chemical path to industrial production. *Org. Process Res. Dev. 18*, 417–422.

(63) Galanie, S., Thodey, K., Trenchard, I. J., Interrante, M. F., and Smolke, C. D. (2015) Complete biosynthesis of opioids in yeast. *Science 349*, 1095–1100.

(64) Biggs, B. W., Lim, C. G., Sagliani, K., Shankar, S., Stephanopoulos, G., De Mey, M., and Ajikumar, P. K. (2016) Overcoming heterologous protein interdependency to optimize P450-mediated Taxol precursor synthesis in *Escherichia coli*. *Proc. Natl. Acad. Sci. USA 113*, 3209–3214.

(65) Chefson, A., and Auclair, K. (2006) Progress towards the easier use of P450 enzymes. *Mol. BioSyst. 2*, 462–469.

(66) O'Reilly, E., Köhler, V., Flitsch, S. L., and Turner, N. J. (2011) Cytochromes P450 as useful biocatalysts: addressing the limitations. *Chem. Commun. 47*, 2490–2501.

(67) Baillie, T. A. (2008) Metabolism and toxicity of drugs. Two decades of progress in industrial drug metabolism. *Chem. Res. Toxicol. 21*, 129–137.

(68) Schroer, K., Kittelmann, M., and Lütz, S. (2010) Recombinant human cytochrome P450 monooxygenases for drug metabolite synthesis. *Biotechnol. Bioeng. 106*, 699–706.

(69) Di Nardo, G., and Gilardi, G. (2012) Optimization of the bacterial cytochrome P450 BM3 system for the production of human drug metabolites. *Int. J. Mol. Sci. 13*, 15901–15924.

(70) Sawayama, A. M., Chen, M. M. Y., Kulanthaivel, P., Kuo, M.-S., Hemmerle, H., and Arnold, F. H. (2009) A panel of cytochrome P450 BM3 variants to produce drug metabolites and diversify lead compounds. *Chem. Eur. J. 15*, 11723–11729.

(71) Julsing, M. K., Cornelissen, S., Bühler, B., and Schmid, A. (2008) Heme-iron oxygenases: powerful industrial biocatalysts? *Curr. Opin. Chem. Biol. 12*, 177–186.

(72) Holtmann, D., and Hollmann, F. (2016) The oxygen dilemma: a severe challenge for the application of monooxygenases? *ChemBioChem 17*, 1391–1398.

(73) Lundemo, M. T., and Woodley, J. M. (2015) Guidelines for development and implementation of biocatalytic P450 processes. *Appl. Microbiol. Biotechnol. 99*, 2465–2483.

(74) Coon, M. J. (2005) Cytochrome P450: nature's most versatile biological catalyst. *Annu. Rev. Pharmacol. Toxicol. 45*, 1–25.
(75) Nelson, D. R. (2017) Cytochrome P450 diversity in the tree of life. *Biochim. Biophys. Acta, Proteins Proteomics* http://dx.doi.org/10.1016/j.bbapap.2017.05.003.
(76) Guengerich, F. P. (2001) Common and uncommon cytochrome P450 reactions related to metabolism and chemical toxicity. *Chem. Res. Toxicol. 14*, 611–650.
(77) Isin, E. M., and Guengerich, F. P. (2007) Complex reactions catalyzed by cytochrome P450 enzymes. *Biochim. Biophys. Acta 1770*, 314–329.
(78) Guengerich, F. P., and Munro, A. W. (2013) Unusual cytochrome P450 enzymes and reactions. *J. Biol. Chem. 288*, 17065–17073.
(79) Hannemann, F., Bichet, A., Ewen, K. M., and Bernhardt, R. (2007) Cytochrome P450 systems—biological variations of electron transport chains. *Biochim. Biophys. Acta 1770*, 330–344.
(80) Meunier, B., de Visser, S. P., and Shaik, S. (2004) Mechanism of oxidation reactions catalyzed by cytochrome P450 enzymes. *Chem. Rev. 104*, 3947–3980.
(81) Gotoh, O. (1992) Substrate recognition sites in cytochrome P450 family 2 (CYP2) proteins inferred from comparative analyses of amino acid and coding nucleotide sequences. *J. Biol. Chem. 267*, 83–90.
(82) Nelson, D. R., Koymans, L., Kamataki, T., Stegeman, J. J., Feyereisen, R., Waxman, D. J., Waterman, M. R., Gotoh, O., Coon, M. J., Estabrook, R. W., Gunsalus, I. C., and Nebert, D. W. (1996) P450 superfamily: update on new sequences, gene mapping, accession numbers and nomenclature. *Pharmacogenetics 6*, 1–42.
(83) Danielson, P. B. (2002) The cytochrome P450 superfamily: biochemistry, evolution and drug metabolism in humans. *Curr. Drug Metab. 3*, 561–597.
(84) Poulos, T. L., and Johnson, E. F. (2015) Structures of cytochrome P450 enzymes, in *Cytochrome P450: structure, mechanism, and biochemistry* (Ortiz de Montellano, P. R., Ed.) 4th ed., pp 3–32. Springer.
(85) Denisov, I. G., and Sligar, S. G. (2015) Activation of molecular oxygen in cytochromes P450, in *Cytochrome P450: structure, mechanism, and biochemistry* (Ortiz de Montellano, P. R., Ed.) 4th ed., pp 69–109. Springer.
(86) Sezutsu, H., Le Goff, G., and Feyereisen, R. (2013) Origins of P450 diversity. *Phil. Trans. R. Soc. B 368*, 20120428.
(87) Nelson, D., and Werck-Reichhart, D. (2011) A P450-centric view of plant evolution. *Plant J. 66*, 194–211.
(88) Nelson, D. R., Ming, R., Alam, M., and Schuler, M. A. (2008) Comparison of cytochrome P450 genes from six plant genomes. *Trop. Plant Biol. 1*, 216–235.
(89) Schuler, M. A. (2015) P450s in plants, insects, and their fungal pathogens, in *Cytochrome P450: structure, mechanism, and biochemistry* (Ortiz de Montellano, P. R., Ed.) 4th ed., pp 409–449. Springer.
(90) Guengerich, F. P. (2015) Human cytochrome P450 enzymes, in *Cytochrome P450: structure, mechanism, and biochemistry* (Ortiz de Montellano, P. R., Ed.) 4th ed., pp 523–785. Springer.
(91) Zanger, U. M., and Schwab, M. (2013) Cytochrome P450 enzymes in drug metabolism: regulation of gene expression, enzyme activities, and impact of genetic variation. *Pharmacol. Ther. 138*, 103–141.
(92) Pikuleva, I. A., and Waterman, M. R. (2013) Cytochromes P450: roles in diseases. *J. Biol. Chem. 288*, 17091–17098.
(93) Waterman, M. R., and Lepesheva, G. I. (2005) Sterol 14α-demethylase, an abundant and essential mixed-function oxidase. *Biochem. Biophys. Res. Commun. 338*, 418–422.
(94) Becher, R., and Wirsel, S. G. R. (2012) Fungal cytochrome P450 sterol 14α-demethylase (CYP51) and azole resistance in plant and human pathogens. *Appl. Microbiol. Biotechnol. 95*, 825–840.
(95) McLean, K. J., Leys, D., and Munro, A. W. (2015) Microbial cytochromes P450, in *Cytochrome P450: structure, mechanism, and biochemistry* (Ortiz de Montellano, P. R., Ed.) 4th ed., pp 261–407. Springer.
(96) Črešnar, B., and Petrič, Š. (2011) Cytochrome P450 enzymes in the fungal kingdom. *Biochim. Biophys. Acta 1814*, 29–35.
(97) Ouellet, H., Johnston, J. B., and Ortiz de Montellano, P. R. (2010) The *Mycobacterium tuberculosis* cytochrome P450 system. *Arch. Biochem. Biophys. 493*, 82–95.

(98) Lamb, D. C., Skaug, T., Song, H.-L., Jackson, C. J., Podust, L. M., Waterman, M. R., Kell, D. B., Kelly, D. E., and Kelly, S. L. (2002) The cytochrome P450 complement (CYPome) of *Streptomyces coelicolor* A3(2). *J. Biol. Chem. 277*, 24000–24005.
(99) Kelly, S. L., Lamb, D. C., Jackson, C. J., Warrilow, A. G. S., and Kelly, D. E. (2003) The biodiversity of microbial cytochromes P450. *Adv. Microb. Physiol. 47*, 131–186.
(100) Parajuli, N., Basnet, D. B., Lee, H. C., Sohng, J. K., and Liou, K. (2004) Genome analyses of *Streptomyces peucetius* ATCC 27952 for the identification and comparison of cytochrome P450 complement with other *Streptomyces*. *Arch. Biochem. Biophys. 425*, 233–241.
(101) Podust, L. M., and Sherman, D. H. (2012) Diversity of P450 enzymes in the biosynthesis of natural products. *Nat. Prod. Rep. 29*, 1251–1266.
(102) Kelly, S. L., and Kelly, D. E. (2013) Microbial cytochromes P450: biodiversity and biotechnology. Where do cytochromes P450 come from, what do they do and what can they do for us? *Phil. Trans. R. Soc. B 368*, 20120476.
(103) Jung, S. T., Lauchli, R., and Arnold, F. H. (2011) Cytochrome P450: taming a wild type enzyme. *Curr. Opin. Biotechnol. 22*, 809–817.
(104) Joo, H., Lin, Z., and Arnold, F. H. (1999) Laboratory evolution of peroxide-mediated cytochrome P450 hydroxylation. *Nature 399*, 670–673.
(105) Gillam, E. M. J. (2007) Extending the capabilities of nature's most versatile catalysts: directed evolution of mammalian xenobiotic-metabolizing P450s. *Arch. Biochem. Biophys. 464*, 176–186.
(106) Gillam, E. M. J. (2008) Engineering cytochrome P450 enzymes. *Chem. Res. Toxicol. 21*, 220–231.
(107) Lewis, J. C., and Arnold, F. H. (2009) Catalysts on demand: selective oxidations by laboratory-evolved cytochrome P450 BM3. *Chimia (Aarau). 63*, 309–312.
(108) Whitehouse, C. J. C., Bell, S. G., and Wong, L.-L. (2012) $P450_{BM3}$ (CYP102A1): connecting the dots. *Chem. Soc. Rev. 41*, 1218–1260.
(109) McIntosh, J. A., Farwell, C. C., and Arnold, F. H. (2014) Expanding P450 catalytic reaction space through evolution and engineering. *Curr. Opin. Chem. Biol. 19*, 126–134.
(110) Renata, H., Wang, Z. J., and Arnold, F. H. (2015) Expanding the enzyme universe: accessing non-natural reactions by mechanism-guided directed evolution. *Angew. Chem. Int. Ed. 54*, 3351–3367.
(111) Prier, C. K., and Arnold, F. H. (2015) Chemomimetic biocatalysis: exploiting the synthetic potential of cofactor-dependent enzymes to create new catalysts. *J. Am. Chem. Soc. 137*, 13992–14006.
(112) Hyster, T. K., and Ward, T. R. (2016) Genetic optimization of metalloenzymes: enhancing enzymes for non-natural reactions. *Angew. Chem. Int. Ed. 55*, 7344–7357.
(113) Dydio, P., Key, H. M., Nazarenko, A., Rha, J. Y.-E., Seyedkazemi, V., Clark, D. S., and Hartwig, J. F. (2016) An artificial metalloenzyme with the kinetics of native enzymes. *Science 354*, 102–106.
(114) Dydio, P., Key, H. M., Hayashi, H., Clark, D. S., and Hartwig, J. F. (2017) Chemoselective, enzymatic C–H bond amination catalyzed by a cytochrome P450 containing an Ir(Me)-PIX cofactor. *J. Am. Chem. Soc. 139*, 1750–1753.
(115) Mason, H. S., Fowlks, W. L., and Peterson, E. (1955) Oxygen transfer and electron transport by the phenolase complex. *J. Am. Chem. Soc. 77*, 2914–2915.
(116) Hayaishi, O., Katagiri, M., and Rothberg, S. (1955) Mechanism of the pyrocatechase reaction. *J. Am. Chem. Soc. 77*, 5450–5451.
(117) Axelrod, J. (1955) The enzymatic demethylation of ephedrine. *J. Pharmacol. Exp. Ther. 114*, 430–438.
(118) Brodie, B. B., Axelrod, J., Cooper, J. R., Gaudette, L., La Du, B. N., Mitoma, C., and Udenfriend, S. (1955) Detoxication of drugs and other foreign compounds by liver microsomes. *Science 121*, 603–604.
(119) Klingenberg, M. (1958) Pigments of rat liver microsomes. *Arch. Biochem. Biophys. 75*, 376–386.
(120) Garfinkel, D. (1958) Studies on pig liver microsomes. I. Enzymic and pigment composition of different microsomal fractions. *Arch. Biochem. Biophys. 77*, 493–509.
(121) Omura, T., and Sato, R. (1962) A new cytochrome in liver microsomes. *J. Biol. Chem. 237*, 1375–1376.
(122) Estabrook, R. W., Cooper, D. Y., and Rosenthal, O. (1963) The light reversible carbon monoxide inhibition of the steroid C21-hydroxylase system of the adrenal cortex. *Biochem. Z. 338*, 741–755.
(123) Omura, T., and Sato, R. (1964) The carbon monoxide-binding pigment of liver microsomes: I. Evidence for its hemoprotein nature. *J. Biol. Chem. 239*, 2370–2378.

(124) Omura, T., and Sato, R. (1964) The carbon monoxide-binding pigment of liver microsomes: II. Solubilization, purification, and properties. *J. Biol. Chem. 239*, 2379–2385.
(125) Omura, T. (2011) Recollection of the early years of the research on cytochrome P450. *Proc. Jpn. Acad., Ser. B 87*, 617–640.
(126) Stern, J. O., and Peisach, J. (1974) A model compound study of the CO-adduct of cytochrome P-450. *J. Biol. Chem. 249*, 7495–7498.
(127) Champion, P. M., Stallard, B. R., Wagner, G. C., and Gunsalus, I. C. (1982) Resonance Raman detection of an Fe-S bond in cytochrome $P450_{cam}$. *J. Am. Chem. Soc. 104*, 5469–5472.
(128) Lindenmayer, A., and Smith, L. (1964) Cytochromes and other pigments of baker's yeast grown aerobically and anaerobically. *Biochim. Biophys. Acta 93*, 445–461.
(129) Appleby, C. A. (1967) A soluble haemoprotein P 450 from nitrogen-fixing Rhizobium bacteroids. *Biochim. Biophys. Acta 147*, 399–402.
(130) Katagiri, M., Ganguli, B. N., and Gunsalus, I. C. (1968) A soluble cytochrome P-450 functional in methylene hydroxylation. *J. Biol. Chem. 243*, 3543–3546.
(131) Dus, K., Katagiri, M., Yu, C.-A., Erbes, D. L., and Gunsalus, I. C. (1970) Chemical characterization of cytochrome $P\text{-}450_{cam}$. *Biochem. Biophys. Res. Commun. 40*, 1423–1430.
(132) Yu, C.-A., and Gunsalus, I. C. (1970) Crystalline cytochrome $P\text{-}450_{cam}$. *Biochem. Biophys. Res. Commun. 40*, 1431–1436.
(133) Haniu, M., Armes, L. G., Tanaka, M., Yasunobu, K. T., Shastry, B. S., Wagner, G. C., and Gunsalus, I. C. (1982) The primary structure of the monoxygenase cytochrome $P450_{cam}$. *Biochem. Biophys. Res. Commun. 105*, 889–894.
(134) Poulos, T. L., Finzel, B. C., Gunsalus, I. C., Wagner, G. C., and Kraut, J. (1985) The 2.6-Å crystal structure of *Pseudomonas putida* cytochrome P-450. *J. Biol. Chem. 260*, 16122–16130.
(135) Oeda, K., Sakaki, T., and Ohkawa, H. (1985) Expression of rat liver cytochrome P-450MC cDNA in *Saccharomyces cerevisiae*. *DNA 4*, 203–210.
(136) Koga, H., Rauchfuss, B., and Gunsalus, I. C. (1985) $P450_{cam}$ gene cloning and expression in *Pseudomonas putida* and *Escherichia coli*. *Biochem. Biophys. Res. Commun. 130*, 412–417.
(137) Nebert, D. W., Adesnik, M., Coon, M. J., Estabrook, R. W., Gonzalez, F. J., Guengerich, F. P., Gunsalus, I. C., Johnson, E. F., Kemper, B., Levin, W., Phillips, I. R., Sato, R., and Waterman, M. R. (1987) The P450 gene superfamily: recommended nomenclature. *DNA 6*, 1–11.
(138) Larson, J. R., Coon, M. J., and Porter, T. D. (1991) Alcohol-inducible cytochrome P-450IIE1 lacking the hydrophobic NH_2-terminal segment retains catalytic activity and is membrane-bound when expressed in *Escherichia coli*. *J. Biol. Chem. 266*, 7321–7324.
(139) Porter, T. D., and Larson, J. R. (1991) Expression of mammalian P450s in *Escherichia coli*. *Methods Enzym. 206*, 108–116.
(140) Barnes, H. J., Arlotto, M. P., and Waterman, M. R. (1991) Expression and enzymatic activity of recombinant cytochrome P450 17α-hydroxylase in *Escherichia coli*. *Proc. Natl. Acad. Sci. USA 88*, 5597–5601.
(141) Ravichandran, K. G., Boddupalli, S. S., Hasemann, C. A., Peterson, J. A., and Deisenhofer, J. (1993) Crystal structure of hemoprotein domain of P450BM-3, a prototype for microsomal P450's. *Science 261*, 731–736.
(142) Hasemann, C. A., Ravichandran, K. G., Peterson, J. A., and Deisenhofer, J. (1994) Crystal structure and refinement of cytochrome $P450_{terp}$ at 2.3 Å resolution. *J. Mol. Biol. 236*, 1169–1185.
(143) Cupp-Vickery, J. R., Li, H., and Poulos, T. L. (1994) Preliminary crystallographic analysis of an enzyme involved in erythromycin biosynthesis: cytochrome P450eryF. *Proteins Struct., Funct., Genet. 20*, 197–201.
(144) Park, S.-Y., Shimizu, H., Adachi, S.-I., Nakagawa, A., Tanaka, I., Nakahara, K., Shoun, H., Obayashi, E., Nakamura, H., Iizuka, T., and Shiro, Y. (1997) Crystal structure of nitric oxide reductase from denitrifying fungus *Fusarium oxysporum*. *Nat. Struct. Biol. 4*, 827–832.
(145) Williams, P. A., Cosme, J., Sridhar, V., Johnson, E. F., and McRee, D. E. (2000) Mammalian microsomal cytochrome P450 monooxygenase: structural adaptations for membrane binding and functional diversity. *Mol. Cell 5*, 121–131.
(146) Williams, P. A., Cosme, J., Ward, A., Angove, H. C., Vinković, D. M., and Jhoti, H. (2003) Crystal structure of human cytochrome P450 2C9 with bound warfarin. *Nature 424*, 464–468.
(147) Sevrioukova, I. F., Li, H., Zhang, H., Peterson, J. A., and Poulos, T. L. (1999) Structure of a cytochrome P450–redox partner electron-transfer complex. *Proc. Natl. Acad. Sci. USA 96*, 1863–

1868.
(148) Strushkevich, N., MacKenzie, F., Cherkesova, T., Grabovec, I., Usanov, S., and Park, H.-W. (2011) Structural basis for pregnenolone biosynthesis by the mitochondrial monooxygenase system. *Proc. Natl. Acad. Sci. USA 108*, 10139–10143.
(149) Hiruma, Y., Hass, M. A. S., Kikui, Y., Liu, W.-M., Ölmez, B., Skinner, S. P., Blok, A., Kloosterman, A., Koteishi, H., Löhr, F., Schwalbe, H., Nojiri, M., and Ubbink, M. (2013) The structure of the cytochrome P450cam–putidaredoxin complex determined by paramagnetic NMR spectroscopy and crystallography. *J. Mol. Biol. 425*, 4353–4365.
(150) Tripathi, S., Li, H., and Poulos, T. L. (2013) Structural basis for effector control and redox partner recognition in cytochrome P450. *Science 340*, 1227–1230.
(151) Monk, B. C., Tomasiak, T. M., Keniya, M. V., Huschmann, F. U., Tyndall, J. D. A., O'Connell, J. D., III, Cannon, R. D., McDonald, J. G., Rodriguez, A., Finer-Moore, J. S., and Stroud, R. M. (2014) Architecture of a single membrane spanning cytochrome P450 suggests constraints that orient the catalytic domain relative to a bilayer. *Proc. Natl. Acad. Sci. USA 111*, 3865–3870.
(152) Rittle, J., and Green, M. T. (2010) Cytochrome P450 compound I: capture, characterization, and C-H bond activation kinetics. *Science 330*, 933–937.
(153) Denisov, I. G., Makris, T. M., Sligar, S. G., and Schlichting, I. (2005) Structure and chemistry of cytochrome P450. *Chem. Rev. 105*, 2253–2277.
(154) Ortiz de Montellano, P. R. (2010) Hydrocarbon hydroxylation by cytochrome P450 enzymes. *Chem. Rev. 110*, 932–948.
(155) Guengerich, F. P. (2002) Rate-limiting steps in cytochrome P450 catalysis. *Biol. Chem. 383*, 1553–1564.
(156) Denisov, I. G., Grinkova, Y. V., Baas, B. J., and Sligar, S. G. (2006) The ferrous-dioxygen intermediate in human cytochrome P450 3A4: substrate dependence of formation and decay kinetics. *J. Biol. Chem. 281*, 23313–23318.
(157) Denisov, I. G., Grinkova, Y. V., McLean, M. A., and Sligar, S. G. (2007) The one-electron autoxidation of human cytochrome P450 3A4. *J. Biol. Chem. 282*, 26865–26873.
(158) Ortiz de Montellano, P. R. (2015) Substrate oxidation by cytochrome P450 enzymes, in *Cytochrome P450: structure, mechanism, and biochemistry* (Ortiz de Montellano, P. R., Ed.) 4th ed., pp 111–176. Springer.
(159) Modi, A. R., and Dawson, J. H. (2015) Oxidizing intermediates in P450 catalysis: a case for multiple oxidants. *Adv. Exp. Med. Biol. 851*, 63–81.
(160) Akhtar, M., Wright, J. N., and Lee-Robichaud, P. (2011) A review of mechanistic studies on aromatase (CYP19) and 17α-hydroxylase-17,20-lyase (CYP17). *J. Steroid Biochem. Mol. Biol. 125*, 2–12.
(161) Di Nardo, G., and Gilardi, G. (2013) Human aromatase: perspectives in biochemistry and biotechnology. *Biotechnol. Appl. Biochem. 60*, 92–101.
(162) Khatri, Y., Luthra, A., Duggal, R., and Sligar, S. G. (2014) Kinetic solvent isotope effect in steady-state turnover by CYP19A1 suggests involvement of Compound 1 for both hydroxylation and aromatization steps. *FEBS Lett. 588*, 3117–3122.
(163) Mak, P. J., Luthra, A., Sligar, S. G., and Kincaid, J. R. (2014) Resonance Raman spectroscopy of the oxygenated intermediates of human CYP19A1 implicates a Compound I intermediate in the final lyase step. *J. Am. Chem. Soc. 136*, 4825–4828.
(164) Yoshimoto, F. K., and Guengerich, F. P. (2014) Mechanism of the third oxidative step in the conversion of androgens to estrogens by cytochrome P450 19A1 steroid aromatase. *J. Am. Chem. Soc. 136*, 15016–15025.
(165) Xu, K., Wang, Y., and Hirao, H. (2015) Estrogen formation via H-abstraction from the O–H bond of *gem*-diol by Compound I in the reaction of CYP19A1: mechanistic scenario derived from multiscale QM/MM calculations. *ACS Catal. 5*, 4175–4179.
(166) Krámos, B., and Oláh, J. (2015) The mechanism of human aromatase (CYP 19A1) revisited: DFT and QM/MM calculations support a compound I-mediated pathway for the aromatization process. *Struct. Chem. 26*, 279–300.
(167) Yosca, T. H., Ledray, A. P., Ngo, J., and Green, M. T. (2017) A new look at the role of thiolate ligation in cytochrome P450. *J. Biol. Inorg. Chem. 22*, 209–220.
(168) Yosca, T. H., Rittle, J., Krest, C. M., Onderko, E. L., Silakov, A., Calixto, J. C., Behan, R. K., and Green, M. T. (2013) Iron(IV)hydroxide pK_a and the role of thiolate ligation in C–H bond activation

by cytochrome P450. *Science 342*, 825–829.
(169) Krest, C. M., Silakov, A., Rittle, J., Yosca, T. H., Onderko, E. L., Calixto, J. C., and Green, M. T. (2015) Significantly shorter Fe–S bond in cytochrome P450-I is consistent with greater reactivity relative to chloroperoxidase. *Nat. Chem. 7*, 696–702.
(170) Onderko, E. L., Silakov, A., Yosca, T. H., and Green, M. T. (2017) Characterization of a selenocysteine-ligated P450 compound I reveals direct link between electron donation and reactivity. *Nat. Chem. 9*, 623–628.
(171) Cupp-Vickery, J. R., and Poulos, T. L. (1995) Structure of cytochrome P450eryF involved in erythromycin biosynthesis. *Nat. Struct. Biol. 2*, 144–153.
(172) Hasemann, C. A., Kurumbail, R. G., Boddupalli, S. S., Peterson, J. A., and Deisenhofer, J. (1995) Structure and function of cytochromes P450: a comparative analysis of three crystal structures. *Structure 3*, 41–62.
(173) Guengerich, F. P., Waterman, M. R., and Egli, M. (2016) Recent structural insights into cytochrome P450 function. *Trends Pharmacol. Sci. 37*, 625–640.
(174) Lamb, D. C., and Waterman, M. R. (2013) Unusual properties of the cytochrome P450 superfamily. *Phil. Trans. R. Soc. B 368*, 20120434.
(175) Rupasinghe, S., Schuler, M. A., Kagawa, N., Yuan, H., Lei, L., Zhao, B., Kelly, S. L., Waterman, M. R., and Lamb, D. C. (2006) The cytochrome P450 gene family CYP157 does not contain EXXR in the K-helix reducing the absolute conserved P450 residues to a single cysteine. *FEBS Lett. 580*, 6338–6342.
(176) Porubsky, P. R., Meneely, K. M., and Scott, E. E. (2008) Structures of human cytochrome P-450 2E1: insights into the binding of inhibitors and both small molecular weight and fatty acid substrates. *J. Biol. Chem. 283*, 33698–33707.
(177) Takahashi, S., Nagano, S., Nogawa, T., Kanoh, N., Uramoto, M., Kawatani, M., Shimizu, T., Miyazawa, T., Shiro, Y., and Osada, H. (2014) Structure-function analyses of cytochrome P450revI involved in reveromycin A biosynthesis and evaluation of the biological activity of its substrate, reveromycin T. *J. Biol. Chem. 289*, 32446–32458.
(178) Nelson, D. R. (1998) Metazoan cytochrome P450 evolution. *Comp. Biochem. Physiol. C 121*, 15–22.
(179) Nelson, D. R. (1999) Cytochrome P450 and the individuality of species. *Arch. Biochem. Biophys. 369*, 1–10.
(180) Nelson, D. R. (2009) The cytochrome P450 homepage. *Hum. Genomics 4*, 59–65.
(181) Porter, T. D., and Kasper, C. B. (1986) NADPH-cytochrome P-450 oxidoreductase: flavin mononucleotide and flavin adenine dinucleotide domains evolved from different flavoproteins. *Biochemistry 25*, 1682–1687.
(182) Smith, G. C. M., Tew, D. G., and Wolf, C. R. (1994) Dissection of NADPH-cytochrome P450 oxidoreductase into distinct functional domains. *Proc. Natl. Acad. Sci. USA 91*, 8710–8714.
(183) Porter, T. D. (2002) The roles of cytochrome b_5 in cytochrome P450 reactions. *J. Biochem. Mol. Toxicol. 16*, 311–316.
(184) Serizawa, N., and Matsuoka, T. (1991) A two component-type cytochrome *P*-450 monooxygenase system in a prokaryote that catalyzes hydroxylation of ML-236B to pravastatin, a tissue-selective inhibitor of 3-hydroxy-3-methylglutaryl coenzyme A reductase. *Biochim. Biophys. Acta 1084*, 35–40.
(185) Narhi, L. O., and Fulco, A. J. (1986) Characterization of a catalytically self-sufficient 119,000-Dalton cytochrome P-450 monooxygenase induced by barbiturates in *Bacillus megaterium*. *J. Biol. Chem. 261*, 7160–7169.
(186) Narhi, L. O., and Fulco, A. J. (1987) Identification and characterization of two functional domains in cytochrome $P\text{-}450_{BM\text{-}3}$, a catalytically self-sufficient monooxygenase induced by barbiturates in *Bacillus megaterium*. *J. Biol. Chem. 262*, 6683–6690.
(187) McLean, K. J., Sabri, M., Marshall, K. R., Lawson, R. J., Lewis, D. G., Clift, D., Balding, P. R., Dunford, A. J., Warman, A. J., McVey, J. P., Quinn, A.-M., Sutcliffe, M. J., Scrutton, N. S., and Munro, A. W. (2005) Biodiversity of cytochrome P450 redox systems. *Biochem. Soc. Trans. 33*, 796–801.
(188) Hawkes, D. B., Adams, G. W., Burlingame, A. L., Ortiz de Montellano, P. R., and De Voss, J. J. (2002) Cytochrome $P450_{cin}$ (CYP176A), isolation, expression, and characterization. *J. Biol. Chem. 277*, 27725–27732.

(189) Puchkaev, A. V., and Ortiz de Montellano, P. R. (2005) The *Sulfolobus solfataricus* electron donor partners of thermophilic CYP119: an unusual non-NAD(P)H-dependent cytochrome P450 system. *Arch. Biochem. Biophys. 434*, 169–177.
(190) Jackson, C. J., Lamb, D. C., Marczylo, T. H., Warrilow, A. G. S., Manning, N. J., Lowe, D. J., Kelly, D. E., and Kelly, S. L. (2002) A novel sterol 14*α*-demethylase/ferredoxin fusion protein (MCCYP51FX) from *Methylococcus capsulatus* represents a new class of the cytochrome P450 superfamily. *J. Biol. Chem. 277*, 46959–46965.
(191) Rylott, E. L., Jackson, R. G., Sabbadin, F., Seth-Smith, H. M. B., Edwards, J., Chong, C. S., Strand, S. E., Grogan, G., and Bruce, N. C. (2011) The explosive-degrading cytochrome P450 XplA: biochemistry, structural features and prospects for bioremediation. *Biochim. Biophys. Acta 1814*, 230–236.
(192) Roberts, G. A., Grogan, G., Greter, A., Flitsch, S. L., and Turner, N. J. (2002) Identification of a new class of cytochrome P450 from a *Rhodococcus* sp. *J. Bacteriol. 184*, 3898–3908.
(193) Roberts, G. A., Çelik, A., Hunter, D. J. B., Ost, T. W. B., White, J. H., Chapman, S. K., Turner, N. J., and Flitsch, S. L. (2003) A self-sufficient cytochrome P450 with a primary structural organization that includes a flavin domain and a [2Fe-2S] redox center. *J. Biol. Chem. 278*, 48914–48920.
(194) Nakayama, N., Takemae, A., and Shoun, H. (1996) Cytochrome P450foxy, a catalytically self-sufficient fatty acid hydroxylase of the fungus *Fusarium oxysporum*. *J. Biochem. 119*, 435–440.
(195) Kitazume, T., Takaya, N., Nakayama, N., and Shoun, H. (2000) *Fusarium oxysporum* fatty-acid subterminal hydroxylase (CYP505) is a membrane-bound eukaryotic counterpart of *Bacillus megaterium* cytochrome P450BM3. *J. Biol. Chem. 275*, 39734–39740.
(196) Syed, K., and Yadav, J. S. (2012) P450 monooxygenases (P450ome) of the model white rot fungus *Phanerochaete chrysosporium*. *Crit. Rev. Microbiol. 38*, 339–363.
(197) Seo, J.-A., Proctor, R. H., and Plattner, R. D. (2001) Characterization of four clustered and coregulated genes associated with fumonisin biosynthesis in *Fusarium verticillioides*. *Fungal Genet. Biol. 34*, 155–165.
(198) Bojja, R. S., Cerny, R. L., Proctor, R. H., and Du, L. (2004) Determining the biosynthetic sequence in the early steps of the fumonisin pathway by use of three gene-disruption mutants of *Fusarium verticillioides*. *J. Agric. Food Chem. 52*, 2855–2860.
(199) Daiber, A., Shoun, H., and Ullrich, V. (2005) Nitric oxide reductase ($P450_{nor}$) from *Fusarium oxysporum*. *J. Inorg. Biochem. 99*, 185–193.
(200) Shoji, O., and Watanabe, Y. (2014) Peroxygenase reactions catalyzed by cytochromes P450. *J. Biol. Inorg. Chem. 19*, 529–539.
(201) Rude, M. A., Baron, T. S., Brubaker, S., Alibhai, M., Del Cardayre, S. B., and Schirmer, A. (2011) Terminal olefin (1-alkene) biosynthesis by a novel P450 fatty acid decarboxylase from *Jeotgalicoccus* species. *Appl. Environ. Microbiol. 77*, 1718–1727.
(202) Song, W.-C., Funk, C. D., and Brash, A. R. (1993) Molecular cloning of an allene oxide synthase: a cytochrome P450 specialized for the metabolism of fatty acid hydroperoxides. *Proc. Natl. Acad. Sci. USA 90*, 8519–8523.
(203) Cheng, Q., Lamb, D. C., Kelly, S. L., Lei, L., and Guengerich, F. P. (2010) Cyclization of a cellular dipentaenone by *Streptomyces coelicolor* cytochrome P450 154A1 without oxidation/reduction. *J. Am. Chem. Soc. 132*, 15173–15175.
(204) Lamb, D. C., Lei, L., Warrilow, A. G. S., Lepesheva, G. I., Mullins, J. G. L., Waterman, M. R., and Kelly, S. L. (2009) The first virally encoded cytochrome P450. *J. Virol. 83*, 8266–8269.
(205) Brodhun, F., Göbel, C., Hornung, E., and Feussner, I. (2009) Identification of PpoA from *Aspergillus nidulans* as a fusion protein of a fatty acid heme dioxygenase/peroxidase and a cytochrome P450. *J. Biol. Chem. 284*, 11792–11805.
(206) Hansen, B. G., Mnich, E., Nielsen, K. F., Nielsen, J. B., Nielsen, M. T., Mortensen, U. H., Larsen, T. O., and Patil, K. R. (2012) Involvement of a natural fusion of a cytochrome P450 and a hydrolase in mycophenolic acid biosynthesis. *Appl. Environ. Microbiol. 78*, 4908–4913.
(207) Demain, A. L., and Fang, A. (2000) The natural functions of secondary metabolites, in *Advances in Biochemical Engineering/Biotechnology* (Scheper, T., and Fiechter, A., Eds.), pp 1–39. Springer, Berlin.
(208) Newman, D. J., and Cragg, G. M. (2016) Natural products as sources of new drugs from 1981 to 2014. *J. Nat. Prod. 79*, 629–661.
(209) Zhang, X., and Li, S. (2017) Expansion of chemical space for natural products by uncommon P450

reactions. *Nat. Prod. Rep.* DOI: 10.1039/c7np00028f.
(210) Bentley, S. D., Chater, K. F., Cerdeño-Tárraga, A.-M., Challis, G. L., Thomson, N. R., James, K. D., Harris, D. E., Quail, M. A., Kieser, H., Harper, D., Bateman, A., Brown, S., Chandra, G., Chen, C. W., Collins, M., Cronin, A., Fraser, A., Goble, A., Hidalgo, J., Hornsby, T., Howarth, S., Huang, C.-H., Kieser, T., Larke, L., Murphy, L., Oliver, K., O'Neil, S., Rabbinowitsch, E., Rajandream, M.-A., Rutherford, K., Rutter, S., Seeger, K., Saunders, D., Sharp, S., Squares, R., Squares, S., Taylor, K., Warren, T., Wietzorrek, A., Woodward, J., Barrell, B. G., Parkhill, J., and Hopwood, D. A. (2002) Complete genome sequence of the model actinomycete *Streptomyces coelicolor* A3(2). *Nature 417*, 141–147.
(211) Nett, M., Ikeda, H., and Moore, B. S. (2009) Genomic basis for natural product biosynthetic diversity in the actinomycetes. *Nat. Prod. Rep. 26*, 1362–1384.
(212) Rudolf, J. D., Chang, C.-Y., Ma, M., and Shen, B. (2017) Cytochromes P450 for natural product biosynthesis in *Streptomyces*: sequence, structure, and function. *Nat. Prod. Rep.* DOI: 10.1039/c7np00034k.
(213) Rawlings, B. J. (2001) Type I polyketide biosynthesis in bacteria (Part A—erythromycin biosynthesis). *Nat. Prod. Rep. 18*, 190–227.
(214) Rawlings, B. J. (2001) Type I polyketide biosynthesis in bacteria (Part B). *Nat. Prod. Rep. 18*, 231–281.
(215) Staunton, J., and Weissman, K. J. (2001) Polyketide biosynthesis: a millennium review. *Nat. Prod. Rep. 18*, 380–416.
(216) Katz, L., and Ashley, G. W. (2005) Translation and protein synthesis: macrolides. *Chem. Rev. 105*, 499–527.
(217) McGuire, J. M., Bunch, R. L., Anderson, R. C., Boaz, H. E., Flynn, E. H., Powell, H. M., and Smith, J. W. (1952) Ilotycin, a new antibiotic. *Antibiot. Chemother. 2*, 281–283.
(218) Gaynor, M., and Mankin, A. S. (2003) Macrolide antibiotics: binding site, mechanism of action, resistance. *Curr. Top. Med. Chem. 3*, 949–961.
(219) Mankin, A. S. (2008) Macrolide myths. *Curr. Opin. Microbiol. 11*, 414–421.
(220) Kannan, K., Vázquez-Laslop, N., and Mankin, A. S. (2012) Selective protein synthesis by ribosomes with a drug-obstructed exit tunnel. *Cell 151*, 508–520.
(221) Sothiselvam, S., Liu, B., Han, W., Ramu, H., Klepacki, D., Atkinson, G. C., Brauer, A., Remm, M., Tenson, T., Schulten, K., Vázquez-Laslop, N., and Mankin, A. S. (2014) Macrolide antibiotics allosterically predispose the ribosome for translation arrest. *Proc. Natl. Acad. Sci. USA 111*, 9804–9809.
(222) Kannan, K., Kanabar, P., Schryer, D., Florin, T., Oh, E., Bahroos, N., Tenson, T., Weissman, J. S., and Mankin, A. S. (2014) The general mode of translation inhibition by macrolide antibiotics. *Proc. Natl. Acad. Sci. USA 111*, 15958–15963.
(223) Andersen, J. F., and Hutchinson, C. R. (1992) Characterization of *Saccharopolyspora erythraea* cytochrome P-450 genes and enzymes, including 6-deoxyerythronolide B hydroxylase. *J. Bacteriol. 174*, 725–735.
(224) Andersen, J. F., Tatsuta, K., Gunji, H., Ishiyama, T., and Hutchinson, C. R. (1993) Substrate specificity of 6-deoxyerythronolide B hydroxylase, a bacterial cytochrome P450 of erythromycin A biosynthesis. *Biochemistry 32*, 1905–1913.
(225) Stassi, D., Donadio, S., Staver, M. J., and Katz, L. (1993) Identification of a *Saccharopolyspora erythraea* gene required for the final hydroxylation step in erythromycin biosynthesis. *J. Bacteriol. 175*, 182–189.
(226) Lambalot, R. H., Cane, D. E., Aparicio, J. J., and Katz, L. (1995) Overproduction and characterization of the erythromycin C-12 hydroxylase, EryK. *Biochemistry 34*, 1858–1866.
(227) Cupp-Vickery, J. R., Han, O., Hutchinson, C. R., and Poulos, T. L. (1996) Substrate-assisted catalysis in cytochrome P450eryF. *Nat. Struct. Biol. 3*, 632–637.
(228) Nagano, S., Cupp-Vickery, J. R., and Poulos, T. L. (2005) Crystal structures of the ferrous dioxygen complex of wild-type cytochrome P450eryF and its mutants, A245S and A245T. *J. Biol. Chem. 280*, 22102–22107.
(229) Sen, K., and Thiel, W. (2014) Role of two alternate water networks in Compound I formation in P450eryF. *J. Phys. Chem. B 118*, 2810–2820.
(230) Xiang, H., Tschirret-Guth, R. A., and Ortiz de Montellano, P. R. (2000) An A245T mutation conveys on cytochrome $P450_{eryF}$ the ability to oxidize alternative substrates. *J. Biol. Chem. 275*, 35999–

36006.
(231) Savino, C., Montemiglio, L. C., Sciara, G., Miele, A. E., Kendrew, S. G., Jemth, P., Gianni, S., and Vallone, B. (2009) Investigating the structural plasticity of a cytochrome P450: three-dimensional structures of P450 EryK and binding to its physiological substrate. *J. Biol. Chem. 284*, 29170–29179.
(232) Montemiglio, L. C., Macone, A., Ardiccioni, C., Avella, G., Vallone, B., and Savino, C. (2013) Redirecting P450 EryK specificity by rational site-directed mutagenesis. *Biochemistry 52*, 3678–3687.
(233) Lee, S. K., Basnet, D. B., Choi, C. Y., Sohng, J. K., Ahn, J. S., and Yoon, Y. J. (2004) The role of erythromycin C-12 hydroxylase, EryK, as a substitute for PikC hydroxylase in pikromycin biosynthesis. *Bioorg. Chem. 32*, 549–559.
(234) Arakawa, K., Kodama, K., Tatsuno, S., Ide, S., and Kinashi, H. (2006) Analysis of the loading and hydroxylation steps in lankamycin biosynthesis in *Streptomyces rochei*. *Antimicrob. Agents Chemother. 50*, 1946–1952.
(235) Tatsuta, K., Gunji, H., Tajima, S., Ishiyama, T., Imai, S., Okuyama, S., and Fukatsu, S. (1990) Biosynthetic studies on oleandomycin by incorporation of the chemically synthesized aglycones. *J. Antibiot. 43*, 909–911.
(236) Rodriguez, A. M., Olano, C., Méndez, C., Hutchinson, C. R., and Salas, J. A. (1995) A cytochrome P450-like gene possibly involved in oleandomycin biosynthesis by *Streptomyces antibioticus*. *FEMS Microbiol. Lett. 127*, 117–120.
(237) Shah, S., Xue, Q., Tang, L., Carney, J. R., Betlach, M., and McDaniel, R. (2000) Cloning, characterization and heterologous expression of a polyketide synthase and P-450 oxidase involved in the biosynthesis of the antibiotic oleandomycin. *J. Antibiot. 53*, 502–508.
(238) Gaisser, S., Lill, R., Staunton, J., Méndez, C., Salas, J., and Leadlay, P. F. (2002) Parallel pathways for oxidation of 14-membered polyketide macrolactones in *Saccharopolyspora erythraea*. *Mol. Microbiol. 44*, 771–781.
(239) Montemiglio, L. C., Parisi, G., Scaglione, A., Sciara, G., Savino, C., and Vallone, B. (2016) Functional analysis and crystallographic structure of clotrimazole bound OleP, a cytochrome P450 epoxidase from *Streptomyces antibioticus* involved in oleandomycin biosynthesis. *Biochim. Biophys. Acta 1860*, 465–475.
(240) Xue, Y., Wilson, D., Zhao, L., Liu, H.-w., and Sherman, D. H. (1998) Hydroxylation of macrolactones YC-17 and narbomycin is mediated by the *pikC*-encoded cytochrome P450 in *Streptomyces venezuelae*. *Chem. Biol. 5*, 661–667.
(241) Zhang, Q., and Sherman, D. H. (2001) Isolation and structure determination of novamethymycin, a new bioactive metabolite of the methymycin biosynthetic pathway in *Streptomyces venezuelae*. *J. Nat. Prod. 64*, 1447–1450.
(242) Lee, S. K., Park, J. W., Kim, J. W., Jung, W. S., Park, S. R., Choi, C. Y., Kim, E. S., Kim, B. S., Ahn, J. S., Sherman, D. H., and Yoon, Y. J. (2006) Neopikromycin and novapikromycin from the pikromycin biosynthetic pathway of *Streptomyces venezuelae*. *J. Nat. Prod. 69*, 847–849.
(243) Sherman, D. H., Li, S., Yermalitskaya, L. V., Kim, Y., Smith, J. A., Waterman, M. R., and Podust, L. M. (2006) The structural basis for substrate anchoring, active site selectivity, and product formation by P450 PikC from *Streptomyces venezuelae*. *J. Biol. Chem. 281*, 26289–26297.
(244) Li, S., Ouellet, H., Sherman, D. H., and Podust, L. M. (2009) Analysis of transient and catalytic desosamine-binding pockets in cytochrome P-450 PikC from *Streptomyces venezuelae*. *J. Biol. Chem. 284*, 5723–5730.
(245) Li, S., Chaulagain, M. R., Knauff, A. R., Podust, L. M., Montgomery, J., and Sherman, D. H. (2009) Selective oxidation of carbolide C–H bonds by an engineered macrolide P450 mono-oxygenase. *Proc. Natl. Acad. Sci. U.S.A. 106*, 18463–18468.
(246) Negretti, S., Narayan, A. R. H., Chiou, K. C., Kells, P. M., Stachowski, J. L., Hansen, D. A., Podust, L. M., Montgomery, J., and Sherman, D. H. (2014) Directing group-controlled regioselectivity in an enzymatic C–H bond oxygenation. *J. Am. Chem. Soc. 136*, 4901–4904.
(247) Narayan, A. R. H., Jiménez-Osés, G., Liu, P., Negretti, S., Zhao, W., Gilbert, M. M., Ramabhadran, R. O., Yang, Y.-F., Furan, L. R., Li, Z., Podust, L. M., Montgomery, J., Houk, K. N., and Sherman, D. H. (2015) Enzymatic hydroxylation of an unactivated methylene C–H bond guided by molecular dynamics simulations. *Nat. Chem. 7*, 653–660.
(248) Rodriguez, E., Ward, S., Fu, H., Revill, W. P., McDaniel, R., and Katz, L. (2004) Engineered

biosynthesis of 16-membered macrolides that require methoxymalonyl-ACP precursors in *Streptomyces fradiae*. *Appl. Microbiol. Biotechnol. 66*, 85–91.
(249) Reeves, C. D., Ward, S. L., Revill, W. P., Suzuki, H., Marcus, M., Petrakovsky, O. V., Marquez, S., Fu, H., Dong, S. D., and Katz, L. (2004) Production of hybrid 16-membered macrolides by expressing combinations of polyketide synthase genes in engineered *Streptomyces fradiae* hosts. *Chem. Biol. 11*, 1465–1472.
(250) Omura, S., Tanaka, H., and Tsukui, M. (1982) Biosynthesis of tylosin: oxidations of 5-*O*-mycaminosylprotylonolide at C-20 and C-23 with a cell-free extract from *Streptomyces fradiae*. *Biochem. Biophys. Res. Commun. 107*, 554–560.
(251) Baltz, R. H., Seno, E. T., Stonesifer, J., and Wild, G. M. (1983) Biosynthesis of the macrolide antibiotic tylosin: a preferred pathway from tylactone to tylosin. *J. Antibiot. 36*, 131–141.
(252) Omura, S., Tomoda, H., Yamamoto, S., Tsukui, M., and Tanaka, H. (1984) Studies on two dioxygenases involved in the synthesis of tylosin in *Streptomyces fradiae*. *Biochim. Biophys. Acta 802*, 141–147.
(253) Iizaka, Y., Higashi, N., Ishida, M., Oiwa, R., Ichikawa, Y., Takeda, M., Anzai, Y., and Kato, F. (2013) Function of cytochrome P450 enzymes RosC and RosD in the biosynthesis of rosamicin macrolide antibiotic produced by *Micromonospora rosaria*. *Antimicrob. Agents Chemother. 57*, 1529–1531.
(254) Nguyen, H.-C., Darbon, E., Thai, R., Pernodet, J.-L., and Lautru, S. (2013) Post-PKS tailoring steps of the spiramycin macrolactone ring in *Streptomyces ambofaciens*. *Antimicrob. Agents Chemother. 57*, 3836–3842.
(255) Anzai, Y., Li, S., Chaulagain, M. R., Kinoshita, K., Kato, F., Montgomery, J., and Sherman, D. H. (2008) Functional analysis of MycCI and MycG, cytochrome P450 enzymes involved in biosynthesis of mycinamicin macrolide antibiotics. *Chem. Biol. 15*, 950–959.
(256) Kudo, F., Motegi, A., Mizoue, K., and Eguchi, T. (2010) Cloning and characterization of the biosynthetic gene cluster of 16-membered macrolide antibiotic FD-891: involvement of a dual functional cytochrome P450 monooxygenase catalyzing epoxidation and hydroxylation. *ChemBioChem 11*, 1574–1582.
(257) Kudo, F., Kawamura, K., Furuya, T., Yamanishi, H., Motegi, A., Komatsubara, A., Numakura, M., Miyanaga, A., and Eguchi, T. (2016) Parallel post-polyketide synthase modification mechanism involved in FD-891 biosynthesis in *Streptomyces graminofaciens* A-8890. *ChemBioChem 17*, 233–238.
(258) Li, S., Tietz, D. R., Rutaganira, F. U., Kells, P. M., Anzai, Y., Kato, F., Pochapsky, T. C., Sherman, D. H., and Podust, L. M. (2012) Substrate recognition by the multifunctional cytochrome P450 MycG in mycinamicin hydroxylation and epoxidation reactions. *J. Biol. Chem. 287*, 37880–37890.
(259) Tietz, D. R., Podust, L. M., Sherman, D. H., and Pochapsky, T. C. (2017) Solution conformations and dynamics of substrate-bound cytochrome P450 MycG. *Biochemistry 56*, 2701–2714.
(260) Malla, S., Thuy, T. T. T., Oh, T. J., and Sohng, J. K. (2011) Identification and characterization of *gerPI* and *gerPII* involved in epoxidation and hydroxylation of dihydrochalcolactone in *Streptomyces* species KCTC 0041BP. *Arch. Microbiol. 193*, 95–103.
(261) Pang, C.-H., Matsuzaki, K., Ikeda, H., Tanaka, H., and Omura, S. (1995) Production of 6,8a-seco-6,8a-deoxy derivatives of avermectins by a mutant strain of *Streptomyces avermitilis*. *J. Antibiot. 48*, 59–66.
(262) Ikeda, H., and Omura, S. (1997) Avermectin biosynthesis. *Chem. Rev. 97*, 2591–2609.
(263) He, Y., Sun, Y., Liu, T., Zhou, X., Bai, L., and Deng, Z. (2010) Cloning of separate meilingmycin biosynthesis gene clusters by use of acyltransferase-ketoreductase didomain PCR amplification. *Appl. Environ. Microbiol. 76*, 3283–3292.
(264) Caffrey, P., De Poire, E., Sheehan, J., and Sweeney, P. (2016) Polyene macrolide biosynthesis in streptomycetes and related bacteria: recent advances from genome sequencing and experimental studies. *Appl. Microbiol. Biotechnol. 100*, 3893–3908.
(265) Ghannoum, M. A., and Rice, L. B. (1999) Antifungal agents: mode of action, mechanisms of resistance, and correlation of these mechanisms with bacterial resistance. *Clin. Microbiol. Rev. 12*, 501–517.
(266) Kong, D., Lee, M.-J., Lin, S., and Kim, E.-S. (2013) Biosynthesis and pathway engineering of antifungal polyene macrolides in actinomycetes. *J. Ind. Microbiol. Biotechnol. 40*, 529–543.
(267) Carmody, M., Murphy, B., Byrne, B., Power, P., Rai, D., Rawlings, B., and Caffrey, P. (2005)

Biosynthesis of amphotericin derivatives lacking exocyclic carboxyl groups. *J. Biol. Chem. 280*, 34420–34426.
(268) Brautaset, T., Sletta, H., Nedal, A., Borgos, S. E. F., Degnes, K. F., Bakke, I., Volokhan, O., Sekurova, O. N., Treshalin, I. D., Mirchink, E. P., Dikiy, A., Ellingsen, T. E., and Zotchev, S. B. (2008) Improved antifungal polyene macrolides via engineering of the nystatin biosynthetic genes in *Streptomyces noursei*. *Chem. Biol. 15*, 1198–1206.
(269) Brautaset, T., Sletta, H., Degnes, K. F., Sekurova, O. N., Bakke, I., Volokhan, O., Andreassen, T., Ellingsen, T. E., and Zotchev, S. B. (2011) New nystatin-related antifungal polyene macrolides with altered polyol region generated via biosynthetic engineering of *Streptomyces noursei*. *Appl. Environ. Microbiol. 77*, 6636–6643.
(270) Qi, Z., Kang, Q., Jiang, C., Han, M., and Bai, L. (2015) Engineered biosynthesis of pimaricin derivatives with improved antifungal activity and reduced cytotoxicity. *Appl. Microbiol. Biotechnol. 99*, 6745–6752.
(271) Liu, S.-P., Yuan, P.-H., Wang, Y.-Y., Liu, X.-F., Zhou, Z.-X., Bu, Q.-t., Yu, P., Jiang, H., and Li, Y.-Q. (2015) Generation of the natamycin analogs by gene engineering of natamycin biosynthetic genes in *Streptomyces chattanoogensis* L10. *Microbiol. Res. 173*, 25–33.
(272) Chen, S., Mao, X., Shen, Y., Zhou, Y., Li, J., Wang, L., Tao, X., Yang, L., Wang, Y., Zhou, X., Deng, Z., and Wei, D. (2009) Tailoring the P450 monooxygenase gene for FR-008/candicidin biosynthesis. *Appl. Environ. Microbiol. 75*, 1778–1781.
(273) Seco, E. M., Fotso, S., Laatsch, H., and Malpartida, F. (2005) A tailoring activity is responsible for generating polyene amide derivatives in *Streptomyces diastaticus* var. 108. *Chem. Biol. 12*, 1093–1101.
(274) Volokhan, O., Sletta, H., Ellingsen, T. E., and Zotchev, S. B. (2006) Characterization of the P450 monooxygenase NysL, responsible for C-10 hydroxylation during biosynthesis of the polyene macrolide antibiotic nystatin in *Streptomyces noursei*. *Appl. Environ. Microbiol. 72*, 2514–2519.
(275) Cao, B., Yao, F., Zheng, X., Cui, D., Shao, Y., Zhu, C., Deng, Z., and You, D. (2012) Genome mining of the biosynthetic gene cluster of the polyene macrolide antibiotic tetramycin and characterization of a P450 monooxygenase involved in the hydroxylation of the tetramycin B polyol segment. *ChemBioChem 13*, 2234–2242.
(276) Byrne, B., Carmody, M., Gibson, E., Rawlings, B., and Caffrey, P. (2003) Biosynthesis of deoxyamphotericins and deoxyamphoteronolides by engineered strains of *Streptomyces nodosus*. *Chem. Biol. 10*, 1215–1224.
(277) Kim, H.-J., Kim, M.-K., Lee, M.-J., Won, H.-J., Choi, S.-S., and Kim, E.-S. (2015) Post-PKS tailoring steps of a disaccharide-containing polyene NPP in *Pseudonocardia autotrophica*. *PLoS One 10*, e0123270.
(278) Santos-Aberturas, J., Engel, J., Dickerhoff, J., Dörr, M., Rudroff, F., Weisz, K., and Bornscheuer, U. T. (2015) Exploration of the substrate promiscuity of biosynthetic tailoring enzymes as a new source of structural diversity for polyene macrolide antifungals. *ChemCatChem 7*, 490–500.
(279) Mendes, M. V., Recio, E., Fouces, R., Luiten, R., Martín, J. F., and Aparicio, J. F. (2001) Engineered biosynthesis of novel polyenes: a pimaricin derivative produced by targeted gene disruption in *Streptomyces natalensis*. *Chem. Biol. 8*, 635–644.
(280) Mendes, M. V., Antón, N., Martín, J. F., and Aparicio, J. F. (2005) Characterization of the polyene macrolide P450 epoxidase from *Streptomyces natalensis* that converts de-epoxypimaricin into pimaricin. *Biochem. J. 386*, 57–62.
(281) Kells, P. M., Ouellet, H., Santos-Aberturas, J., Aparicio, J. F., and Podust, L. M. (2010) Structure of cytochrome P450 PimD suggests epoxidation of the polyene macrolide pimaricin occurs via a hydroperoxoferric intermediate. *Chem. Biol. 17*, 841–851.
(282) Xiao, Y., Li, S., Niu, S., Ma, L., Zhang, G., Zhang, H., Zhang, G., Ju, J., and Zhang, C. (2011) Characterization of tiacumicin B biosynthetic gene cluster affording diversified tiacumicin analogues and revealing a tailoring dihalogenase. *J. Am. Chem. Soc. 133*, 1092–1105.
(283) Du, Y., Derewacz, D. K., Deguire, S. M., Teske, J., Ravel, J., Sulikowski, G. A., and Bachmann, B. O. (2011) Biosynthesis of the apoptolidins in *Nocardiopsis* sp. FU 40. *Tetrahedron 67*, 6568–6575.
(284) Robbins, N., Spitzer, M., Wang, W., Waglechner, N., Patel, D. J., O'Brien, J. S., Ejim, L., Ejim, O., Tyers, M., and Wright, G. D. (2016) Discovery of ibomycin, a complex macrolactone that exerts antifungal activity by impeding endocytic trafficking and membrane function. *Cell Chem. Biol. 23*,

1383–1394.
(285) Salcedo, R. G., Olano, C., Gómez, C., Fernández, R., Braña, A. F., Méndez, C., de la Calle, F., and Salas, J. A. (2016) Characterization and engineering of the biosynthesis gene cluster for antitumor macrolides PM100117 and PM100118 from a marine actinobacteria: generation of a novel improved derivative. *Microb. Cell Fact. 15*, 44.
(286) Song, L., Laureti, L., Corre, C., Leblond, P., Aigle, B., and Challis, G. L. (2014) Cytochrome *P*450-mediated hydroxylation is required for polyketide macrolactonization in stambomycin biosynthesis. *J. Antibiot. 67*, 71–76.
(287) DeMars, M. D., II, Sheng, F., Park, S. R., Lowell, A. N., Podust, L. M., and Sherman, D. H. (2016) Biochemical and structural characterization of MycCI, a versatile P450 biocatalyst from the mycinamicin biosynthetic pathway. *ACS Chem. Biol. 11*, 2642–2654.
(288) Lowell, A. N., DeMars, M. D., II, Slocum, S. T., Yu, F., Anand, K., Chemler, J. A., Korakavi, N., Priessnitz, J. K., Park, S. R., Koch, A. A., Schultz, P. J., and Sherman, D. H. (2017) Chemoenzymatic total synthesis and structural diversification of tylactone-based macrolide antibiotics through late-stage polyketide assembly, tailoring, and C—H functionalization. *J. Am. Chem. Soc. 139*, 7913–7920.

Chapter 2: Biochemical and structural characterization of MycCI, a versatile P450 biocatalyst from the mycinamicin biosynthetic pathway*

2.1 Introduction

Cytochromes P450 (P450s) comprise one of the most widely distributed and versatile groups of enzymes found in nature, catalyzing a broad range of physiologically important oxidative transformations in organisms across all domains of life.[1-4] To date, more than 21,000 individual sequences of these ubiquitous heme-thiolate proteins have been identified.[5] Despite their vast diversity, P450s share a conserved three-dimensional fold as well as a general catalytic cycle for dioxygen activation and transfer.[6-8] Although P450s most commonly catalyze hydroxylation, epoxidation, heteroatom (e.g., N or S) oxygenation, and dealkylation reactions, their catalytic repertoire extends far beyond these well-documented transformations.[4,9,10]

With P450s, Nature has provided an impressive class of oxidation catalysts that can functionalize a diverse array of molecular scaffolds with high degrees of selectivity. Accordingly, they have garnered increasing attention in recent years as potential biocatalysts for the oxidative tailoring of molecules ranging from simple hydrocarbons to complex natural products.[11-20] In addition, since they operate under mild reaction conditions and employ earth-abundant Fe as a component of their heme cofactor, P450s have the potential to contribute to the realization of environmentally sustainable approaches toward the production of fine and commodity chemicals.[21] Microbes offer a particularly rich source of novel P450s with potential broad applicability in various biocatalytic processes.[20,22,23] In many cases, these enzymes are found in gene clusters

*This chapter has been adapted from the following publication: DeMars, M. D., II, Sheng, F., Park, S. R., Lowell, A. N., Podust, L. M., and Sherman, D. H. (2016) Biochemical and structural characterization of MycCI, a versatile P450 biocatalyst from the mycinamicin biosynthetic pathway. *ACS Chem. Biol. 11*, 2642–2654.

for the biosynthesis of secondary metabolites, where they are responsible for catalyzing a diverse array of tailoring reactions, including C–H bond hydroxylation, oxidative phenolic coupling, and C–C bond formation/cleavage among many others.[24,25]

Actinomycetes, and *Streptomyces* spp. in particular, are prolific producers of biologically active natural products, many of which have been developed into important pharmaceuticals.[25,26] Accordingly, many of the secondary metabolic (biosynthetic) P450s that have hitherto been structurally and functionally characterized originate from these organisms.[17] Whereas mammalian P450s involved in xenobiotic metabolism are known to act on a variety of different substrates, the bacterial biosynthetic enzymes typically possess limited substrate scope and catalyze oxidative transformations with high degrees of regio- and stereoselectivity. For example, EryF, which is responsible for hydroxylating the aglycone precursor to erythromycin (6-deoxyerythronolide B), exhibits an extremely narrow substrate scope and cannot tolerate even minor changes to the structure of its native substrate.[27] Conversely, a few biosynthetic P450s inherently possess some degree of substrate flexibility. PikC, a well-studied P450 from the methymycin/pikromycin pathway in *Streptomyces venezuelae*, is capable of hydroxylating both 12- and 14-membered ring macrolides at either of two positions, leading to the production of up to six unique macrolide antibiotics from a single biosynthetic pathway.[28-30] Because biosynthetic P450s often catalyze oxidation reactions on complex and densely functionalized substrates, they provide an important and underexplored starting point for the development of new biocatalysts.[20,22] Consequently, much of our lab's recent work has focused on the discovery and biochemical/structural characterization of new P450s involved in the biosynthesis of bacterial natural products.[31-35] As has been demonstrated with PikC,[36-38] these fundamental studies serve as a key starting point to guide future efforts to modulate the substrate scope and selectivity properties of P450 enzymes. Engineered biosynthetic P450s may ultimately be employed in vitro or in vivo as biocatalysts for the efficient production of novel biologically active compounds. For example, new sites of oxidation on macrolide scaffolds could enable further diversification of these molecules via chemoenzymatic synthesis, potentially leading to new and more effective antimicrobial agents.

In previous work, our lab demonstrated that the desosamine (**1**) moiety facilitates recognition and anchoring of the macrolide substrates YC-17 (**3**) and narbomycin (**5**) in the active site of PikC.[31,39] Specifically, the protonated *N*,*N*-dimethylamino group on **1** participates in a salt bridge interaction with either of two proximal glutamate residues in the enzyme active site. It was subsequently shown that the presence of **1** on a series of unfunctionalized carbocycles was sufficient for PikC to bind and hydroxylate these unnatural substrates.[36] More recently, it was demonstrated that PikC can accept a variety of other substrates attached to structurally diverse nonsugar anchors containing the *N*,*N*-dimethylamino moiety.[37,38] Although such an explicit anchoring mechanism has not been clearly established for other P450s that act on macrolide substrates, the presence of one or more sugar moieties is typically required for substrate recognition, leading in turn to effective binding and catalysis. Conversely, other P450s involved in macrolide biosynthetic pathways (e.g., EryF) strictly act on aglycone intermediates prior to glycosylation. Here, we report that the P450 MycCI from the mycinamicin (**6**) pathway in *Micromonospora griseorubida* (**Scheme 2.1A**) is able to effectively accept 16-membered ring macrolactones as substrates regardless of their glycosylation state. Our findings are further clarified on the basis of equilibrium substrate binding experiments, steady-state kinetics studies, and X-ray crystallographic analysis of the enzyme in complex with its native substrate. Comparison with TylHI, a homologous P450 from the tylosin (**7**) biosynthetic pathway (**Scheme 2.1B**), further reveals that MycCI is unique in exhibiting such unusually broad substrate tolerance.

Scheme 2.1. Abbreviated biosynthetic pathways for (**A**) mycinamicin II and (**B**) tylosin.

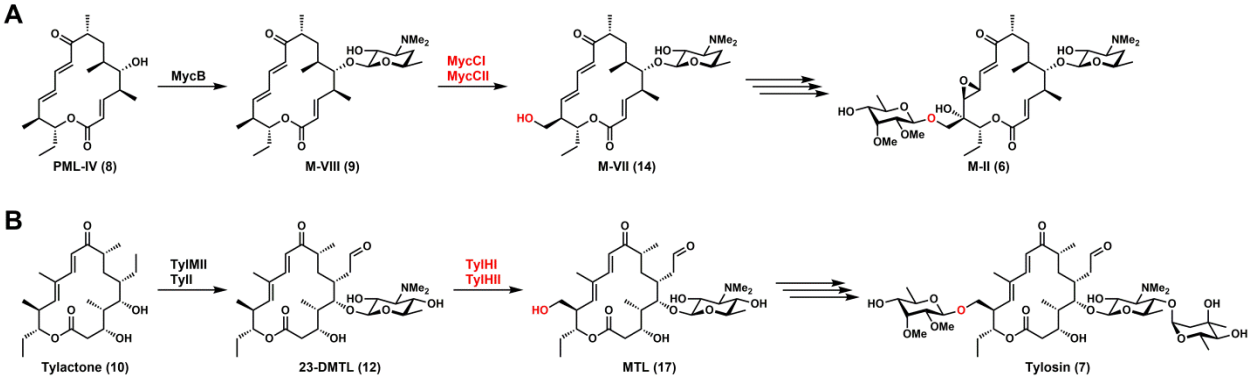

2.2 MycCI is capable of hydroxylating 16-membered ring macrolides and aglycones

To test the substrate scope of MycCI and other P450s involved in macrolide biosynthetic pathways, we envisioned generating a set of macrocyclic compounds of varying ring sizes and glycosylation states. Using a biotransformation method we previously developed for producing the macrolide antibiotics methymycin and pikromycin directly from the corresponding aglycones 10-deoxymethynolide (10-DML, **2**) and narbonolide (NBL, **4**), respectively,[40] we were able to efficiently append desosamine (**1**) to various 12-, 14-, and 16-membered ring macrolactone aglycones (**Figure 2.1**). Consistent with prior reports detailing the extremely broad substrate scope of DesVII (the native glycosyltransferase in the methymycin/pikromycin pathway in *S. venezuelae*) acting in conjunction with its effector protein DesVIII,[41,42] tylactone (**10**) was

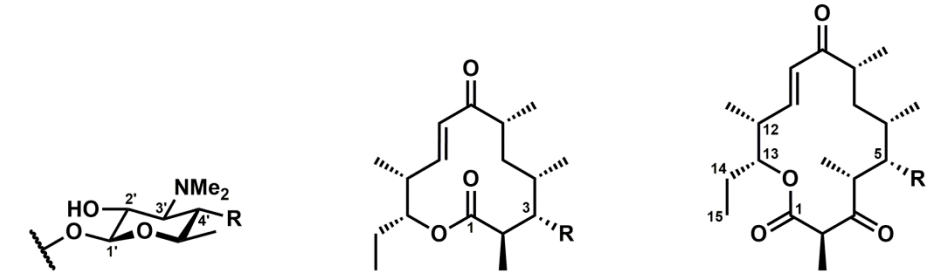

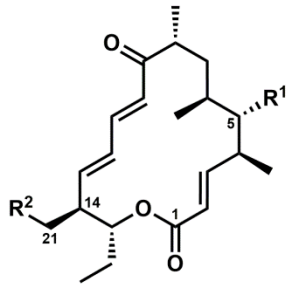

Compound	R^1	R^2
PML-IV (8)	OH	H
M-VIII (9)	1	H
ML-IV (13)	OH	OH
M-VII (14)	1	OH

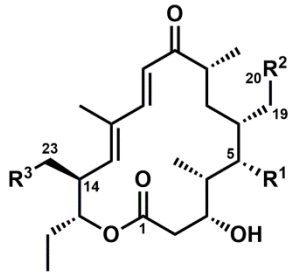

Compound	R^1	R^2	R^3
Tylactone (10)	OH	CH_3	H
DT (11)	1	CH_3	H
23-DMTL (12)	18	CHO	H
23-OH-tylactone (15)	OH	CH_3	OH
23-OH-DT (16)	1	CH_3	OH
MTL (17)	18	CHO	OH

Figure 2.1. Structures of compounds investigated in Chapter 2.

completely converted to 5-*O*-desosaminyl-tylactone (DT, **11**), and the majority (>90%) of protomycinolide IV (PML-IV, **8**) was converted to mycinamicin VIII (M-VIII, **9**) following a 24 h incubation period. An additional potential substrate, 23-deoxy-5-*O*-mycaminosyl-tylonolide (23-DMTL, **12**), was acquired through fermentation of a *Streptomyces fradiae* mutant strain that had previously been generated via chemical mutagenesis.[43] In each case, sufficient quantities of pure substrate to be used for enzymatic assays were obtained by preparative HPLC purification of crude extracts.

In the mycinamicin biosynthetic gene cluster, a gene encoding a [3Fe-4S]-type ferredoxin (*mycCII*) is located immediately downstream of *mycCI*. Previous work carried out in our lab demonstrated that MycCI converts **9** to the monohydroxylated product mycinamicin VII (M-VII, **14**) more effectively when it is paired with MycCII compared with spinach ferredoxin.[33] Therefore, we purified MycCI and MycCII expressed separately as N-terminal His-tagged constructs and used them in conjunction with purified N-terminal MBP-tagged spinach ferredoxin reductase (MBP-FdR) in small-scale in vitro reactions. MycCI exhibited equivalent activity on all three of the 16-membered ring macrolides tested (**9**, **11**, and **12**; see **Table 2.1**), demonstrating its inherent ability to accept large substrates with slight differences in overall architecture. More surprising, however, was the ability of MycCI to catalyze hydroxylation of the corresponding 16-membered ring aglycones (**8** and **10**) with only relatively minor decreases in total turnover number (TTN; **Table 2.1**). To the best of our knowledge, such tolerance with respect to the glycosylation state of the substrate has not been reported for related P450s involved in macrolide biosynthetic pathways (e.g., polyenes) or for those that play roles in the biosynthesis of other glycosylated natural products (e.g.,

Table 2.1. Total turnover numbers (TTNs) for selected enzymatic reactions.[a]

	Substrate					
Catalytic system	**5**	**8**	**9**	**10**	**11**	**12**
MycCI/MycCII[b]	6.8 ± 0.4	65 ± 1	85 ± 2	72 ± 1	87 ± 4	89 ± 2
MycCI-RhFRED	0.6 ± 0.1	18.8 ± 0.8	167 ± 13	49.3 ± 0.7	177 ± 7	114 ± 4
TylHI/TylHII[b]	0	0	0	0	1.0 ± 0.2	18.2 ± 0.8
TylHI/MycCII[b]	0	0	0	0	0.2 ± 0.1	69 ± 2
TylHI-RhFRED	0	0	0	0	0.8 ± 0.1	162 ± 6
$MycCI_{S172A}$/MycCII[b]	2.0 ± 0.1	74 ± 3	71 ± 2	77 ± 1	61 ± 4	66 ± 4

[a]TTN = mol product/mol P450. Reported errors are standard deviations calculated from experiments performed in triplicate.
[b]Includes MBP-FdR.

glycopeptides). Moreover, experiments that we performed with a suite of purified P450s from the pikromycin, erythromycin, and tylosin (*vide infra*) pathways using the substrates presented here failed to identify another P450 enzyme besides MycCI that could accept both a given glycosylated compound and the corresponding aglycone. In addition to the 16-membered ring substrates, MycCI displayed a low-level ability to catalyze oxidation of the 14-membered ring macrolide narbomycin (**5**) (**Tables 2.1** and **A.5**). In contrast to the other compounds tested, which yielded single monohydroxylated products in each case, LC-MS analysis of reaction mixtures containing **5** revealed the formation of two distinct monohydroxylated species as well as one arising from potential dihydroxylation, all in roughly equal abundance (**Figure A.4**). Interestingly, MycCI was unable to catalyze C–H oxidation of the 14-membered ring aglycone **4** or the smaller 12-membered ring compounds YC-17 (**3**) and **2**, thus highlighting a clear preference for the enzyme to act upon larger glycosylated macrolides.

Over the course of optimizing in vitro reaction conditions, it became evident that the amount of MycCII present in reaction mixtures was an important factor in determining reaction outcome as assessed by TTN. With the concentration of MycCI kept relatively low (0.5 μM), increased concentrations of MycCII (e.g., 10-100 μM) correlated with higher TTN values for all substrates tested. In contrast, increasing the amount of MBP-FdR (e.g., 1-10 μM) by itself had little to no effect on this parameter. However, when the levels of both MycCII and MBP-FdR were increased, the positive effect on TTN was synergistic (**Figure A.6**). MycCII interacts directly with MycCI to deliver the requisite electrons for P450 Compound I formation, and an apparent dissociation constant (K_d) of 7 μM has previously been reported for N-terminal His-tagged MycCII binding to MycCI.[33] In light of this information, it is not surprising that further increases in MycCII concentration beyond values close to its K_d with respect to MycCI led to enhanced substrate turnover.

2.3 Engineering a catalytically self-sufficient MycCI biocatalyst

Although MycCI exhibited reasonable activity on **8**–**12**, we wished to further improve its efficiency since optimal turnover was dependent on relatively high levels of MycCII and MBP-FdR. Therefore, we opted to create a self-sufficient biocatalytic

system to facilitate reaction scale-up, product isolation, and structural verification. Our lab has previously succeeded in generating self-sufficient P450 C–H oxidation catalysts via genetic fusion to the FMN/[2Fe-2S]-containing reductase domain of $P450_{RhF}$ (RhFRED) from *Rhodococcus* sp. NCIMB 9784.[34,44,45] Typically, these chimeric enzymes exhibit improved activity, especially when compared with three-component systems comprising the P450 and non-native redox partners (e.g., spinach ferredoxin and spinach ferredoxin reductase). However, as the native ferredoxin partner for MycCI was known and had been demonstrated to support catalytic activity of its associated P450, we were unsure whether fusion to RhFRED (containing both the ferredoxin and reductase domains) would indeed yield a more active biocatalyst. Thus, we were pleased to verify that purified MycCI-RhFRED exhibited improved activity relative to MycCI acting in conjunction with MycCII and MBP-FdR on each of the three 16-membered ring macrolides tested. Specifically, TTN values were doubled for **9** and **11** while the improvement was more modest for **12** (**Table 2.1**). Although the fusion protein could still accept the two 16-membered ring aglycones (**8** and **10**) as substrates, TTN values were lower than those reported for the standalone MycCI protein with ferredoxin and ferredoxin reductase partners acting in trans. The decrease in activity was more pronounced for **8**, with a TTN value of 19 compared with 65 for the three-component system. MycCI-RhFRED also showed an almost complete lack of activity on the 14-membered ring macrolide **5**. As observed for the MycCI/MycCII/MBP-FdR system, the MycCI-RhFRED fusion enzyme did not accept **2**–**4** as substrates. Interestingly, TTN values for MycCI-RhFRED were increased about two-fold across **8**–**12** when the enzyme was prepared using a faster, less rigorous purification procedure, yielding "semipure" P450 enzyme that copurified with a number of additional protein contaminants (**Table A.6**; see Appendix A, section A.8 for further discussion).

2.4 Product isolation and structure elucidation

Our lab's earlier studies on the mycinamicin biosynthetic pathway established that MycCI is responsible for installing a hydroxyl group at C21 of **9** to produce the intermediate **14**, which is then primed for subsequent glycosylation and further tailoring by two methyltransferases and the multifunctional P450 MycG (**Scheme 2.1A**).[33,46]

Comparing the structure of **9** to those of **11** and **12**, we surmised that MycCI would likely introduce a hydroxyl group at C23 of the latter two compounds. In order to rigorously assess the regioselectivity of MycCI when acting upon these macrolides and the corresponding aglycones, we scaled up the reactions so that adequate product could be isolated for full NMR characterization in each case. MycCI-RhFRED was employed in large-scale reactions with macrolide substrates, which showed conversions averaging around 60% based on analytical HPLC. Because the fusion enzyme exhibited lower activity on aglycone substrates relative to wild-type MycCI acting in conjunction with MycCII and MBP-FdR, we used the latter three-component biocatalytic system in scale-up reactions involving **8** and **10**; conversions for these two compounds were ~30% and ~50%, respectively.

Following isolation of products by preparative HPLC, we used 1D and 2D NMR to confirm that **8** and **9** were both hydroxylated at C21 to produce mycinolide IV (ML-IV, **13**) and **14**, respectively, while **10**, **11**, and **12** were each hydroxylated at the corresponding C23 position, yielding 23-hydroxy-tylactone (23-OH-tylactone, **15**), 23-hydroxy-5-*O*-desosaminyl-tylactone (23-OH-DT, **16**), and 5-*O*-mycaminosyl-tylonolide (MTL, **17**), respectively (**Figure 2.1**; see Appendix A for full spectroscopic characterization of all starting materials and products). Despite the low activity of MycCI on **5**, we carried out the corresponding large-scale reaction so as to determine the regioselectivity of the enzyme on this unnatural substrate. Using the same conditions as described for the aglycone substrates, **5** was converted to two monohydroxylated products, with one representing ~2% and the other slightly more polar compound comprising ~0.5% of the reaction mixture (**Figure A.3**). Unfortunately, we were unable to isolate enough material for NMR characterization, but comparison with the products of the same reaction carried out on an analytical scale using $PikC_{D50N}$-RhFRED[36,37] revealed that hydroxylation by MycCI does not occur at C12 of **5** to produce pikromycin (**Figure A.5**). In the LC-MS trace, both products elute earlier than pikromycin and neopikromycin, suggesting that the analogs are more polar. Comparing the structure of **5** to those of the 16-membered ring substrates, we hypothesize that MycCI catalyzes hydroxylation at C14 and/or at the adjacent C15 position (**Figure 2.1**).

2.5 Binding affinities of aglycone and macrolide substrates to MycCI

In order to probe the biochemical basis for the differences in reactivity observed in the activity assays described above, we conducted substrate binding experiments on both MycCI and MycCI-RhFRED. During the P450 catalytic cycle, binding of substrate displaces the heme axial water ligand, which shifts the spin-state equilibrium of the heme iron toward high spin, resulting in a blue-shifted Soret band that can be quantified spectrophotometrically.[7,47] The established substrate titration methodology associated with this principle was used to determine the dissociation constants for each of the substrates (**Table 2.2**; **Figure A.7**). Narbomycin (**5**) and PML-IV (**8**) bound to MycCI with K_d values of 17 μM and 19 μM, respectively, while tylactone (**10**) bound more tightly with a K_d value of about 3 μM. These binding affinities are readily comparable to those reported for many P450s and their natural substrates. Unexpectedly, when initial titration experiments were conducted with the 16-membered ring macrolide compounds (**9**, **11**, and **12**) under the same conditions, saturation was observed after the addition of

Table 2.2. K_d values from equilibrium substrate binding assays.[a]

	Enzyme				
Substrate	MycCI	MycCI-RhFRED	TylHI	TylHI-RhFRED	$MycCI_{S172A}$
3	40 ± 4	40 ± 2	N.B.[b]	N.B.	63 ± 5
5	17 ± 1	15.0 ± 0.8	N.B.	N.B.	23 ± 3
8	19 ± 2	15 ± 2	N.B.	1524 ± 546	9.2 ± 1.0
9	0.001 ± 0.001	0.005 ± 0.001	1291 ± 59	1230 ± 134	0.003 ± 0.004
10	3.3 ± 0.3	3.0 ± 0.3	433 ± 40	469 ± 39	1.35 ± 0.09
11	0.006 ± 0.004	0.010 ± 0.003	275 ± 22	205 ± 20	0.04 ± 0.01
12	0.045 ± 0.006	0.038 ± 0.005	0.60 ± 0.03	0.66 ± 0.05	0.12 ± 0.04

[a] K_d values are in μM. Reported errors are those obtained from fitting data averaged from experiments performed at least in triplicate.
[b] N.B. = no binding detected.

about one molar equivalent of substrate. When substoichiometric concentrations of substrate were titrated into the enzyme solution, a linear increase in signal was observed up until the equivalence point, after which no further increase in signal was detected. At sufficiently low concentrations of enzyme, dissociation constants could be estimated by fitting the data to a quadratic tight-binding equation. M-VIII (**9**) bound with an estimated K_d of 1 nM while DT (**11**) and 23-DMTL (**12**) bound with K_d values of 6 nM and 45 nM, respectively, indicating extremely tight binding of the large macrolide substrates. These dissociation constants rival those found for the binding of azole

inhibitors to various eukaryotic and bacterial P450s. For example, ketoconazole binds to OleP[48] with K_d = 5 nM, and clotrimazole binds to EryK[49] with K_d < 10 nM. Interestingly, the 12-membered ring macrolide YC-17 (**3**) bound to MycCI more weakly (K_d = 40 μM), but the affinity was still comparable to that observed for many other P450/substrate combinations. However, as previously noted, MycCI did not exhibit catalytic activity toward this smaller compound. The aglycones 10-DML (**2**) and NBL (**4**) did not induce a concentration-dependent change in the spin state of the enzyme, which may explain why MycCI failed to hydroxylate these molecules. Consistent with prior findings,[44,50] fusion to the RhFRED domain did not substantially impact the binding affinities of the various substrates tested toward MycCI (**Table 2.2**).

In most cases, the binding affinities of the compounds correlated well with their ability to be accepted as substrates for enzymatic oxidation. However, despite the fact that **5** bound to MycCI with about the same affinity as **8**, the former was a considerably poorer substrate. Moreover, while **3** bound to MycCI with modest affinity, no substrate turnover was observed. In order to rationalize these results, we examined the degree to which each substrate was able to induce a shift of the heme iron from low spin to high spin. Normalizing the maximal change in absorbance acquired from nonlinear regression analysis of the raw data to the enzyme concentration, we found that **10** induced the largest change in the spin state for both MycCI and MycCI-RhFRED (**Table A.8**). The percentage of each enzyme in the high-spin state at saturating levels of a given substrate was estimated by assuming that each was completely converted to high spin when saturated with **10** (**Figure 2.2**; **Table A.8**). Almost all substrates bound very effectively as demonstrated by their ability to elicit particularly high changes in the spin state of the enzyme (>75%; **Figures 2.2** and **A.8**). In contrast, saturation with **3** resulted in only ~30% high spin enzyme, which provides a potential explanation for the lack of observable activity with this substrate. Curiously, **5** and **8** induced the same shift in spin state (~80%), indicating that differences in substrate binding as reflected in the spectral data could not be used to rationalize the differences in reactivity observed for these two compounds. The α,β,γ,δ-unsaturated ketone moiety present in **8** and the other 16-membered ring macrolactones may play a key role in rigidifying the structures of these molecules such that the appropriate primary C–H bond in each case is presented to the

iron-oxo species prior to C–H abstraction. The more flexible scaffold of **5** may hinder its ability to adopt one particular orientation within the enzyme active site, thereby resulting in fewer turnovers and multiple oxidized products (**Table A.5**).

Increased mobility of a substrate in the P450 active site makes it more likely that an inherently weaker C–H bond will present itself to the active iron-oxo species, leading

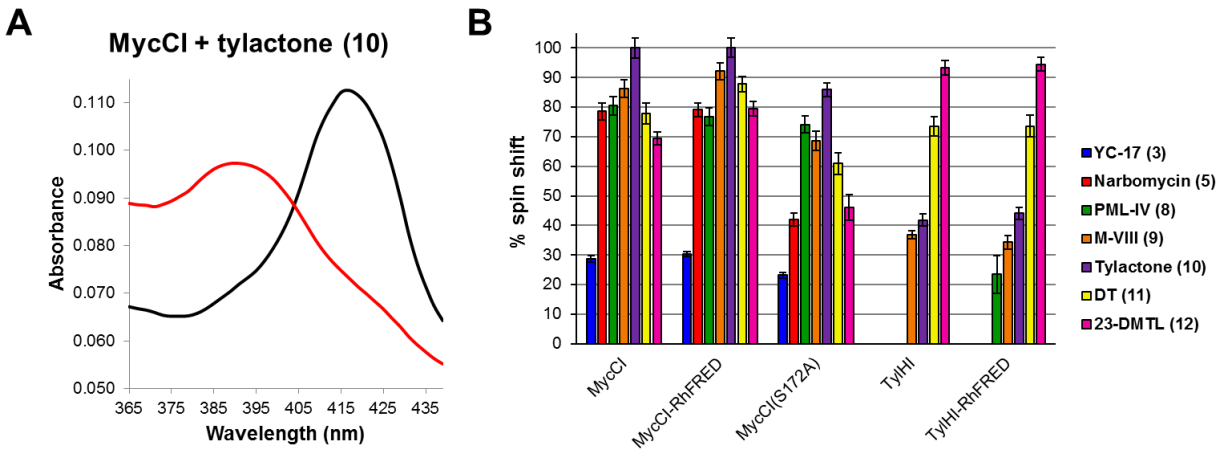

Figure 2.2. Equilibrium substrate binding analysis. (**A**) Absolute spectra of MycCI (0.5 μM) in the absence of substrate (black trace) or in the presence of 128 μM **10** (red trace). (**B**) Percent spin shift of each enzyme at saturating levels of different substrates. Values were calculated as described in Appendix A, section A.7.

to preferential oxidation of this bond over others that have stronger bond-dissociation energies. A variety of P450 ω-hydroxylases have been identified, which are highly selective for oxidizing primary unactivated C–H bonds in linear hydrocarbons (e.g., members of the CYP153 family in bacteria and the CYP52 family in fungi), linear and branched fatty acids (e.g., members of the mammalian CYP4 family), and cholesterol (e.g., CYP124A1 and CYP125A1 from *Mycobacterium tuberculosis*).[51] These remarkable enzymes are able to control their regioselectivity through specific interactions with their substrates, which typically bind tightly and whose movement in the active site is therefore severely restricted. This tight control of the bound substrate is required for ω-hydroxylation to take place over hydroxylation of more activated secondary, tertiary, or allylic carbons. In the 16-membered ring macrocyclic substrates tested here, the primary C–H bond subject to oxidation is located adjacent to a much weaker tertiary allylic C–H bond. Given the great deal of control over substrate

positioning that must be required to completely restrict access of more labile C–H bonds like this to the iron-oxo species, it is not surprising that these substrates exhibit such high affinities for MycCI.

2.6 Steady-state kinetic analysis of MycCI-catalyzed hydroxylation

Steady-state kinetics experiments were conducted for both MycCI/MycCII/MBP-FdR and MycCI-RhFRED using **8**–**12**. First, we evaluated the kinetics of product formation using the latter self-sufficient enzyme. Generally, the rates were rather slow, with k_{cat} values ranging from 1.15 ± 0.02 min^{-1} for **9** to 0.24 ± 0.02 min^{-1} for **8** (**Figure 2.3A**; **Table 2.3**). Although the latter value is lower than that observed for many other P450/substrate combinations, it is close to that reported for CYP107W1, which hydroxylates a tertiary carbon atom in the 26-membered ring macrolide oligomycin C.[52] In addition, all of the rates are higher than that determined for TamI-RhFRED acting on tirandamycin A (k_{cat} = 0.11 ± 0.01 min^{-1}),[34] which represents one of the few other examples of a biosynthetic P450 that hydroxylates an unactivated primary carbon atom.

Table 2.3. Steady-state kinetic parameters for MycCI-RhFRED.[a]

	Product formation			NADPH consumption		
Substrate	k_{cat} (min^{-1})	K_m (μM)	k_{cat}/K_m ($\mu M^{-1}min^{-1}$)	k_{cat} (min^{-1})	K_m (μM)	k_{cat}/K_m ($\mu M^{-1}min^{-1}$)
8	0.24 ± 0.02	264 ± 50	0.0009 ± 0.0002	5.4 ± 0.2	99 ± 8	0.055 ± 0.005
9	1.15 ± 0.02	2.1 ± 0.4	0.6 ± 0.1	8.0 ± 0.3	1.5 ± 0.4	5 ± 1
10	0.355 ± 0.003	28 ± 1	0.0127 ± 0.0006	6.38 ± 0.08	14.9 ± 0.9	0.43 ± 0.03
11	0.88 ± 0.04	0.9 ± 0.5	1.0 ± 0.5	9.1 ± 0.3	1.5 ± 0.3	6 ± 1
12	0.72 ± 0.03	3.9 ± 0.8	0.19 ± 0.04	8.2 ± 0.1	1.0 ± 0.1	8 ± 1

[a]Reported errors are those obtained from fitting data averaged from experiments performed at least in triplicate.

The slow rates may in part be explained by the higher activation energy required to oxidize a primary C–H bond, although examples of engineered P450s that perform similar transformations more rapidly have been reported.[53,54] Consistent with the extremely tight binding of the macrolides, the K_m values for these substrates were low and thus difficult to determine accurately. Despite much lower catalytic rates, k_{cat}/K_m values (specificity constants) were comparable to those for PikC and PikC-RhFRED acting on native substrates **3** and **5**.[44] Relative to those for the macrolides, the specificity constants for the aglycones were considerably reduced, largely due to higher

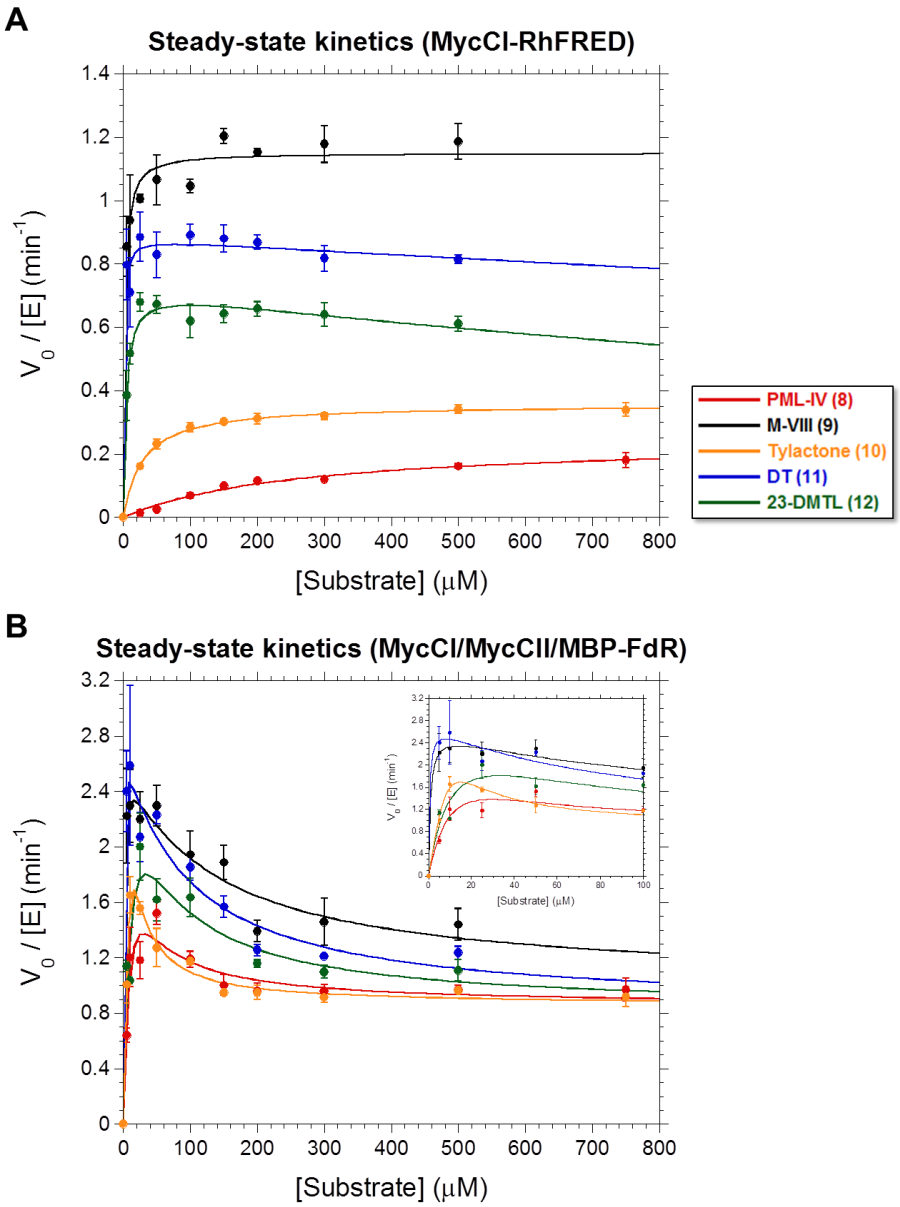

Figure 2.3. Steady-state kinetic profiles for (**A**) MycCI-RhFRED and (**B**) MycCI acting in conjunction with MycCII and MBP-FdR. Plots are of initial product formation rate (V_0) as assessed by HPLC normalized to the concentration of P450 (0.5 μM) used in the kinetics assays. Mean values and standard deviations (error bars) associated with each data point were calculated from the results of experiments performed at least in triplicate. The data were fit to the Michaelis-Menten equation (MycCI-RhFRED + **8**–**10**) or to equations describing single-site (MycCI-RhFRED + **11**, **12**) or two-site (MycCI/MycCII/MBP-FdR + **8**–**12**) substrate inhibition as described in Appendix A, section A.7. The inset in the bottom graph shows a close-up version of the data at low substrate concentrations (0-100 μM).

K_m values. k_{cat}/K_m for **10** (0.0127 ± 0.0006 $\mu M^{-1}min^{-1}$) is similar to that for CYP107W1 acting on its native substrate (0.012 $\mu M^{-1}min^{-1}$).[52] The specificity constant is ~14-fold

lower for **8** (0.0009 ± 0.0002 $\mu M^{-1}min^{-1}$), which is nevertheless slightly higher than that for the oxidation of tirandamycin A by TamI-RhFRED (0.00058 $\mu M^{-1}min^{-1}$).[34] Notably, the results of these kinetics experiments are consistent with those obtained from the TTN assays, which together indicate a clear preference for MycCI-RhFRED toward substrates bearing a deoxyamino sugar.

The same set of experiments was then conducted using MycCI in combination with MycCII and MBP-FdR. For all of the compounds tested, plots of initial rate vs substrate concentration showed a high degree of partial substrate inhibition (**Figure 2.3B**). The data revealed relatively "high" turnover rates at low substrate concentrations (e.g., 2.3 ± 0.3 min^{-1} at 10 μM **9**) that quickly diminished to ~1 min^{-1} in all cases as concentrations of substrate were increased. Partial substrate inhibition is a commonly observed phenomenon in P450-catalyzed reactions, although this situation is most well documented for human drug-metabolizing P450s (e.g., CYP3A4). Such inhibition occurs when saturating levels of substrate lead to incomplete inhibition of P450 activity,[55] and it is thought to occur as a consequence of substrate binding to a second site located either proximal or distal to the catalytically productive binding site.[56,57] The resulting ternary complex of enzyme bound simultaneously to two substrate molecules exhibits reduced competence with respect to product formation (see Appendix A, section A.8 for further discussion). Although the data obtained for MycCI/MycCII/MBP-FdR could be fit to a defined rate equation for an enzyme with two substrate binding sites,[56] the resulting values for k_{cat} and K_m were associated with large errors (**Table A.9**), rendering useful interpretation of their significance difficult. Since the physiological concentration of the intermediate **9** in wild-type *M. griseorubida* is likely very low,[58] substrate inhibition of MycCI may be irrelevant in vivo. Alternatively, it could represent a mechanism by which flux through the mycinamicin biosynthetic pathway is regulated.

The rates determined for product formation in the experiments described above were substantially lower than those previously reported for MycCI (e.g., k_{cat} = 104 ± 2 min^{-1} for **9**).[33] Since the previous data were determined by monitoring NADPH consumption, we posited that cofactor and substrate oxidation were highly uncoupled. In order to verify this hypothesis, steady-state kinetics experiments were repeated by spectrophotometrically monitoring rates of NADPH consumption at various

concentrations of substrate. For MycCI-RhFRED, the derived turnover rates were indeed significantly higher than those determined by monitoring product formation, indicating poor coupling efficiency (≤12% in all cases; **Tables 2.3**, **A.13**, and **A.14**). The ability to test lower substrate concentrations in the NADPH consumption assays also facilitated more accurate determination of K_m values, which were generally in agreement with those derived from product formation experiments (**Table 2.3**). Due to relatively fast NADPH oxidation rates, however, k_{cat}/K_m values were much higher.

Prohibitively high rates of NADPH consumption in the absence of substrate were observed when MycCI was tested in combination with MycCII and MBP-FdR (**Table A.11**), further precluding determination of relevant kinetic parameters for this tripartite biocatalytic system. Nonetheless, we were able to compare turnover frequency (TOF, determined at 500 μM substrate) values between MycCI/MycCII/MBP-FdR and MycCI-RhFRED (**Table 2.4**). The TOF was 1.4 ± 0.1 min^{-1} for the tripartite system with **9** as substrate; this value was only slightly reduced for the other substrates, with the lowest being ~1 min^{-1} for each of the aglycones. MycCI-RhFRED had a similar TOF for **9** (1.19 ± 0.06 min^{-1}), but the rates were more substantially decreased for the other substrates. In particular, the rates for formation of **15** and **13** were about 3-fold and 6-fold lower, respectively, than those determined using the tripartite MycCI system. These results

Table 2.4. Turnover frequencies (TOFs) for selected enzymatic reactions.[a]

	Substrate				
Catalytic system	**8**	**9**	**10**	**11**	**12**
MycCI/MycCII[b]	0.97 ± 0.03	1.4 ± 0.1	0.96 ± 0.01	1.23 ± 0.05	1.11 ± 0.08
MycCI-RhFRED	0.161 ± 0.008	1.19 ± 0.06	0.34 ± 0.01	0.81 ± 0.01	0.61 ± 0.02
TylHI/TylHII[b]	N.D.[c]	N.D.	N.D.	N.D.	0.14 ± 0.03
TylHI/MycCII[b]	N.D.	N.D.	N.D.	N.D.	1.63 ± 0.03
TylHI-RhFRED	N.D.	N.D.	N.D.	N.D.	0.76 ± 0.02
$MycCI_{S172A}$/MycCII[b]	1.15 ± 0.05	1.09 ± 0.05	0.96 ± 0.02	0.90 ± 0.03	0.86 ± 0.06

[a]TOF = mol product/mol P450 per min. Product formation was monitored by HPLC over the first 30 min of the reaction (initial rates). Reported errors are standard deviations calculated from experiments performed in triplicate.
[b]Includes MBP-FdR.
[c]N.D. = value not determined.

indicate that while electron transfer may not be rate-limiting for MycCI/MycCII/MBP-FdR, it likely is for MycCI-RhFRED. Interestingly, despite the higher TTN values obtained with MycCI-RhFRED acting on macrolide substrates **9**, **11**, and **12**, the

corresponding TOF values were all lower than those observed with MycCI/MycCII/MBP-FdR. The most likely explanation for this result is increased coupling efficiency of the self-sufficient system compared with the tripartite system, leading in turn to attenuated production of reactive oxygen species (ROS) that are involved in the oxidative degradation of the enzyme.[59] Thus, despite lower rates of catalysis, MycCI-RhFRED remains active in the reaction mixture for a longer amount of time and is thereby able to turn over more substrate molecules.

2.7 Comparative analysis of the MycCI homolog TylHI

MycCI (CYP105L2) is a member of the CYP105 family of P450 enzymes. Homologs of CYP105 have been identified in all species of *Streptomyces* hitherto characterized, where they are chiefly involved in xenobiotic metabolism and in the biosynthesis of secondary metabolites.[60] In turn, many of the latter variety are involved in polyketide biosynthesis, particularly polyene antifungals (e.g., amphotericin, pimaricin, nystatin, filipin, and candicidin) and macrocyclic antibiotics (e.g., tylosin, mycinamicin, and geldanamycin). MycCI has close homologs in the biosynthetic pathways for the production of the 16-membered ring macrolides tylosin (**7**) in *Streptomyces fradiae* (TylHI)[61,62] and chalcomycin in *Streptomyces bikiniensis* (ChmHI).[63] The pathways associated with the production of these molecules are highly homologous to each other and to that involved in the assembly of the mycinamicins in *M. griseorubida* (**Scheme 2.1**). Accordingly, the chemical structures of the final compounds are very similar in that they all consist of a 16-membered ring macrolactone core to which at least two different sugars are appended.

Like the mycinamicin biosynthetic gene cluster, the tylosin cluster contains two P450 enzymes (TylI and TylHI) whose functions have been provisionally assigned based on early cofermentation and biotransformation studies with mutants of *S. fradiae* blocked in tylosin biosynthesis[43,64,65] as well as phylogenetic comparison to homologous P450s from other pathways. The preferred order of oxidation events was also demonstrated via experiments that employed *S. fradiae* crude cell lysate for bioconversion of tylosin biosynthetic intermediates.[66] On the basis of these collective efforts, it was proposed that TylI installs the aldehyde at C20 of 5-*O*-mycaminosyl-

tylactone (MT) just prior to hydroxylation of C23 by TylHI to produce MTL (**17**) as a key intermediate (**Scheme 2.1B**). Until now, however, the lack of a robust in vitro system to explore these two P450 enzymes has allowed considerable ambiguity with respect to their substrate selectivity to persist. The primary sequence of TylHI (CYP105L1) is 55% identical to that of MycCI; therefore, they are classified as members of the same P450 subfamily. In addition, a small gene encoding a [3Fe-4S]-type ferredoxin, designated *tylHII*, is located adjacent to *tylHI* in the gene cluster.[61,62] As previously noted, the same juxtaposition of P450 and ferredoxin genes encoding MycCI and MycCII, respectively, occurs in the mycinamicin gene cluster,[67] suggesting that TylHI acts in conjunction with TylHII during C23 hydroxylation of its proposed native substrate, 23-DMTL (**12**).

Given its high homology to MycCI, we endeavored to probe the substrate scope of TylHI. Although the results of previous studies suggested that this enzyme could only act upon glycosylated substrates with an adjacent ethylaldehyde functionality,[66] we predicted that the purified enzyme might have a broader substrate scope on the basis of its close association with MycCI. Following the cloning, overexpression, and purification of TylHI and its ferredoxin partner TylHII, we tested their activity in conjunction with MBP-FdR toward all of the compounds previously employed to assess the substrate scope of MycCI. The results demonstrated that TylHI partnered with TylHII converted **12** to a monohydroxylated product with the same retention time as **17**, but the catalytic system only supported about 18 turnovers (**Table 2.1**). In addition, TylHI could hydroxylate DT (**11**) at the same relative position to produce 23-OH-DT (**16**), but only a single turnover was observed. The enzyme exhibited no activity on any of the other substrates tested, even when the concentration of TylHI in the reaction mixture was increased 10-fold to 5 μM (1.0 mol % relative to substrate). Although the gene encoding TylHII was codon optimized for expression in *E. coli*, the protein expressed much more poorly than MycCII, even when coexpressed with GroEL/GroES chaperones. Furthermore, spectrophotometric analysis of the purified protein indicated diminished absorbance at 410 nm compared with MycCII at a given concentration (**Figure A.1**), possibly signifying the presence of higher amounts of apo protein. Accordingly, we tested TylHI in combination with MycCII to determine if the low-level activity observed for this enzyme could be attributed to a suboptimal ferredoxin partner. While the TTN for

12 nearly quadrupled, that for **11** was essentially naught (**Table 2.1**). Moreover, the enzyme remained inactive on all of the other substrates, even when it was present at high concentrations (5 μM).

Since MycCI-RhFRED exhibited improved activity compared with MycCI/MycCII/MBP-FdR, we opted to construct the corresponding self-sufficient version of TylHI. Although activity increased to around 160 turnovers for native substrate **12**, no improvement was observed for **11**, and the enzyme remained inactive toward all other substrates (**Table 2.1**). These data unambiguously demonstrate that the substrate scope of TylHI is extremely narrow, especially compared with that of MycCI. While this finding is surprising given the high homology of the two enzymes, it is consistent with the results of previous studies.[66]

Subsequently, we performed substrate binding and steady-state kinetics assays with TylHI and TylHI-RhFRED, with the results providing some insights into those of the activity assays. TylHI bound **12** with very high affinity (K_d = 0.60 ± 0.03 μM), but its affinity toward **11** was considerably diminished (K_d = 275 ± 22 μM) (**Table 2.2**; **Figure A.7**). Curiously, these two compounds differ only in the identity of the deoxyamino sugar (**1** vs **18**) and the oxidation state of C20 (methyl vs formyl; **Figure 2.1**). Therefore, one or both of these features play key roles in substrate recognition. Although none of the other substrates tested were converted to monohydroxylated products by TylHI, some were able to induce a shift in the spin state of the enzyme, including aglycone **10** (**Table 2.2**; **Figures 2.2B** and **A.8**).

Steady-state kinetic analysis of the reaction between TylHI-RhFRED and **12** revealed little to no substrate inhibition and parameters for product formation that were about the same as those for MycCI-RhFRED acting on this substrate (**Figure A.9A**). However, TylHI-RhFRED oxidized NADPH at a slightly faster rate than MycCI-RhFRED when saturated with **12** (**Figure A.10C**). As for the tripartite MycCI system, partial substrate inhibition was observed for TylHI/TylHII/MBP-FdR acting on **12** (**Figure A.9B**), but the rate of product formation was nearly an order of magnitude lower (TOF = 0.14 ± 0.03 min^{-1}; **Table 2.4**). When MycCII was employed as surrogate ferredoxin, the TOF increased 12-fold to about 1.6 min^{-1}, which was higher than that observed for MycCI/MycCII/MBP-FdR acting on the same substrate.

The highly limited substrate scope of TylHI stands in stark contrast to the flexibility that MycCI exhibits toward different types of 16-membered ring macrolactones. Whereas the deoxyamino sugar is a dispensable feature of MycCI substrates, it is absolutely required for TylHI catalysis. Additionally, the identity of the sugar and/or the nature of the carbon side chains comprising the macrolactone core plays a significant role in substrate binding. On the basis of the results of our experiments, it remains unclear what specific aspects of **12** make it a far superior substrate for TylHI than **11**. The aldehyde and/or the additional hydroxyl group on the sugar appears to be critical for TylHI-catalyzed hydroxylation of **12**. Work is ongoing to solve the X-ray crystal structure of TylHI in complex with its native substrate, which will provide important insights into the specific interactions that are responsible for the high substrate specificity of the enzyme (see Chapter 3). Despite the current lack of a TylHI structure, alignment with MycCI reveals that while differences are fairly evenly distributed throughout each of the sequences, nearly half of the residues that are located within 4 Å of **9** in the MycCI cocrystal structure (*vide infra*) are different from the corresponding residues in TylHI. Moreover, most of these changes appear in residues that are proximal to the desosamine sugar moiety, including those found in and around the BC loop (substrate recognition site 1) and FG loop (substrate recognition sites 2 and 3) regions.[68] These findings are consistent with the differences observed between MycCI and TylHI with respect to the importance of the sugar moiety in substrate binding and catalysis.

Another interesting example of highly homologous P450s that nonetheless exhibit significant differences in their substrate scope can be found in glycopeptide antibiotic biosynthesis. Recent work carried out by Cryle and co-workers has demonstrated the importance of the nonribosomal peptide synthetase X-domain in helping to coordinate the P450-mediated oxidative cascade that leads to fully cyclized aglycones in the biosynthesis of vancomycin, teicoplanin, and other glycopeptides.[69-71] While the P450 OxyB from the vancomycin pathway ($OxyB_{van}$) has long been recognized as a versatile biocatalyst with the ability to accept a wide range of peptidyl carrier protein (PCP)-bound substrates,[72-75] the homolog from the teicoplanin pathway ($OxyB_{tei}$, 74% sequence identity) exhibits a much narrower substrate scope when acting

on PCP-bound peptides in the absence of the X-domain.[76] However, $OxyB_{tei}$ and homologs from other pathways are able to act on a broader range of substrates when the X-domain is present, although they tend to exhibit lower overall activity relative to $OxyB_{van}$.[69,70] Along with these fascinating studies, our results with MycCI underscore the importance of empirically testing and comparing P450 homologs from related biosynthetic pathways in order to identify those that might prove most useful in the development of novel biocatalysts.

2.8 Structural analysis of MycCI bound to M-VIII

Table 2.5. Crystallographic data summary for MycCI/M-VIII.

Protein	MycCI
Ligand	Mycinamicin VIII
PDB ID	**5FOI**
Data collection	
Space group	P1
Cell dimensions	
a, *b*, *c* (Å)	54.8, 59.5, 74.6
α, *β*, *γ* (°)	83.2, 72.2, 62.6
Molecules in AU	2
Wavelength	1.11587
Resolution (Å)	2.21
R_{sym} (%)	24.4
$I / \sigma I$	3.8 (1.3)[a]
Completeness (%)	91.1 (71.2)
Redundancy	2.0 (1.9)
Refinement	
No. reflections	34383
R_{work} / R_{free} (%)	18.2 / 25.2
No. atoms	
Protein	6013
Heme	86
Substrate	72
Solvent	147
Mean B value	27.2
B-factors	
Protein	27.9
Heme	17.0
Substrate	21.0
Solvent	28.6
RMSD	
Bond lengths (Å)	0.014
Bond angles (°)	1.907

[a]Values in parentheses are for the highest resolution shell.

In order to gain further insight into the unique reactivity properties exhibited by MycCI, we determined the crystal structure of the enzyme in complex with its native substrate M-VIII (**9**) to a resolution of 2.21 Å (**Table 2.5**). The asymmetric unit of the crystal lattice contains two molecules of MycCI; no conformational ambiguity is observed between chains A and B, both of which have substrate bound in the enzyme active site. MycCI has an overall tertiary structure typical of cytochrome P450 enzymes (**Figures 2.4A** and **A.11A**).[25] The 7000 $Å^3$ substrate binding pocket at the "distal" face of the heme macrocycle accommodates **9** bound in an orientation tilted relative to the plane of the macrocycle (**Figure 2.4B**). The 16-membered ring polyketide macrolactone and desosamine sugar moieties of the substrate are both clearly defined in the electron density map. The primary methyl group (C21) is exposed to the oxygen scission site within 4.06 Å of the iron center (distance averaged between the two MycCI molecules constituting an asymmetric unit). The proximity of C21 and the orientation of the C14–C21 bond relative to the heme iron are consistent with hydroxylation of **9**

exclusively at the C21 position. A few water molecules are observed in the active site, but only one overlaps between chains A and B (**Figure 2.4B**).

The most hydrophobic edge of the macrolactone portion of **9** is tightly packed against hydrophobic amino acid side chains emanating from the F, G, and I helices

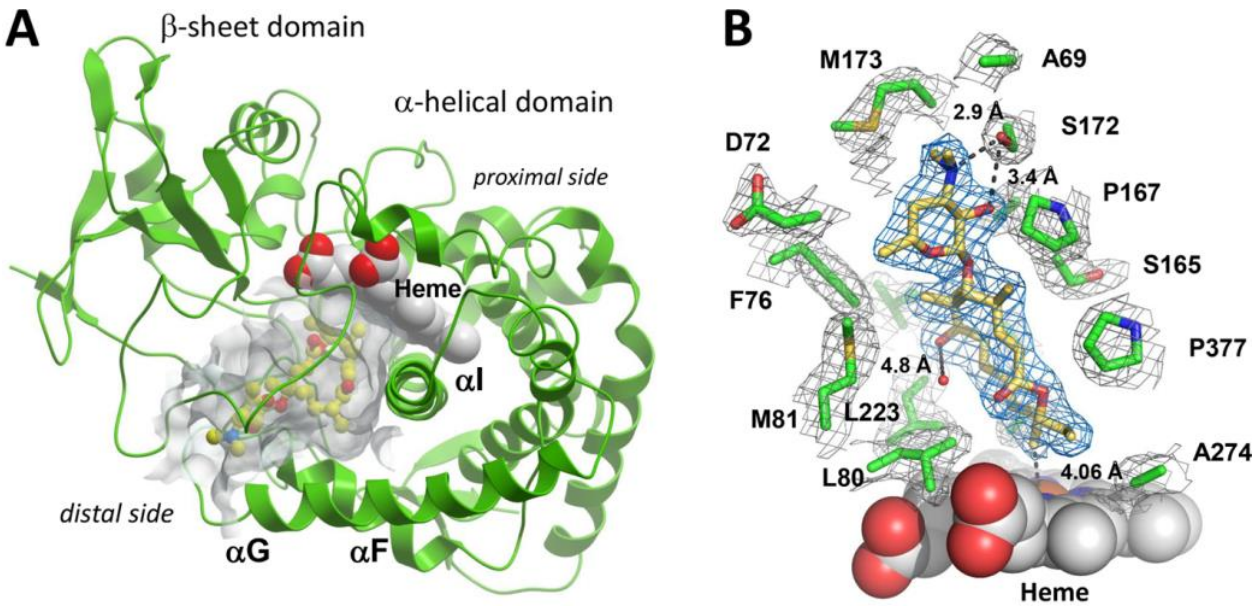

Figure 2.4. Crystal structure of MycCI with **9** bound in the active site. (**A**) The protein scaffold is represented by green ribbons. **9** (ball-and-stick mode: yellow = carbon, red = oxygen, blue = nitrogen) occupies the 7000 Å^3 pocket (semitransparent gray surface) of the α-helical domain interfacing the β-sheet domain. Image was generated using the MOLSOFT ICM-Browser.[77] (**B**) A fragment of the $2F_o$-F_c electron density map contoured at 1 σ delineates **9** (blue mesh) and a set of amino acid residues (green) within 4 Å of **9** (gray mesh). Distances reported are in Ångströms. The heme cofactor is depicted as van der Waals spheres (gray = carbon, red = oxygen, blue = nitrogen, ochre = iron). The water molecule present in both chains A and B of the asymmetric unit is shown as a small red sphere. Image was prepared using PyMOL.[78]

(shown in **Figure 2.5A** in different shades of blue). The opposite side of the binding site interfacing the β-sheet domain is more polar and loosely constructed (**Figure 2.5B**). Six hydrophobic residues (L80, L223, A227, A274, L277, and I378) form a rim adjacent to the porphyrin ring that tightly encloses the end of the macrolactone opposite desosamine (**Figure 2.5C**), serving to position it in an orientation that favors hydroxylation at C21. The binding pocket that accommodates desosamine is built by more polar residues, including S172, D70, and D72 (**Figure 2.5D**). However, the only potential specific polar contact between an amino acid side chain and the substrate occurs between the hydroxyl of S172 and the 3'-nitrogen as well as the adjacent 2'-

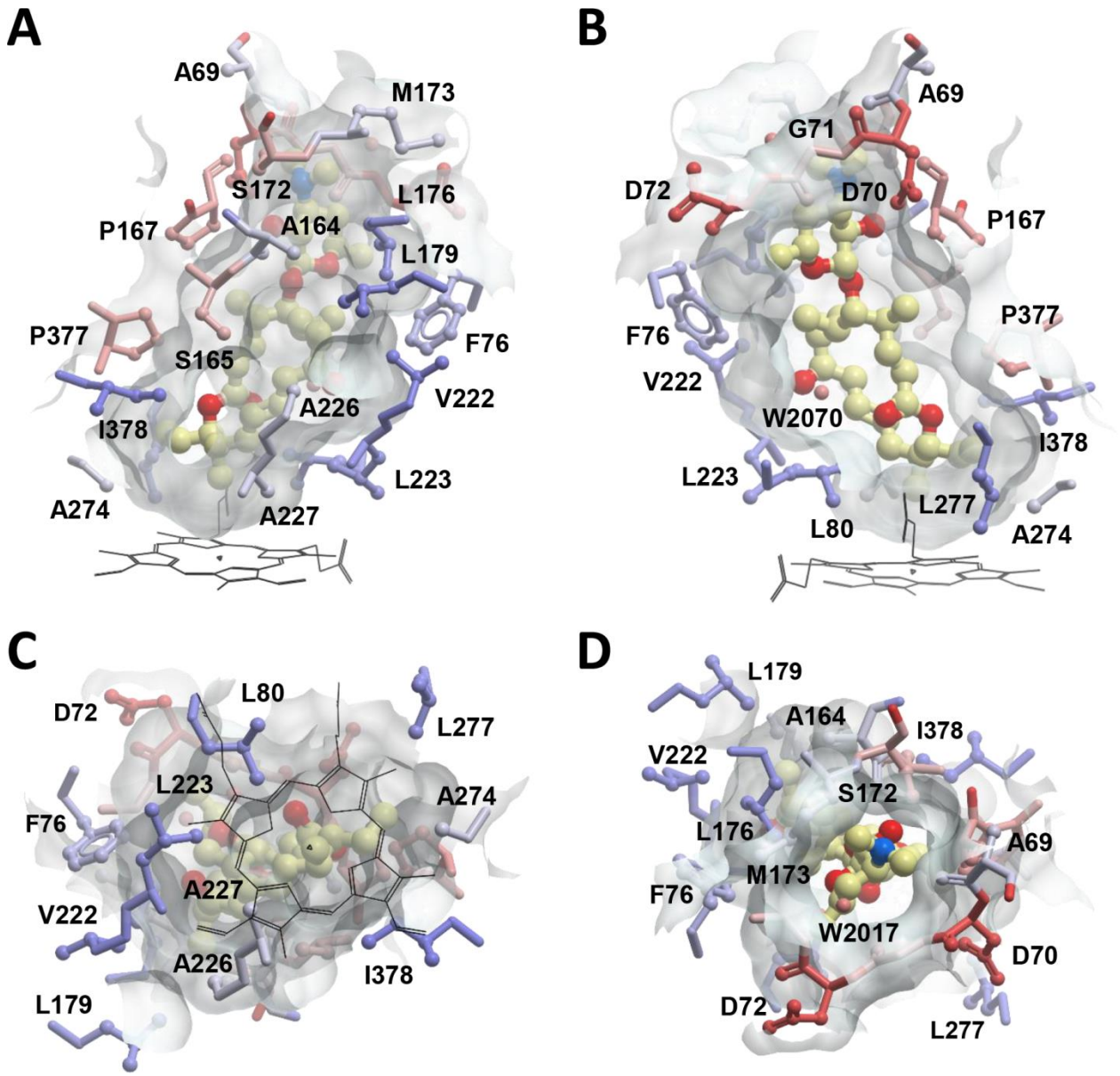

Figure 2.5. Binding site of **9** in MycCI, represented by a semitransparent surface surrounding the substrate molecule (ball-and-stick mode: yellow = carbon, red = oxygen, blue = nitrogen). Amino acid residues are in ball-and-stick mode and are colored by hydrophobicity in a color gradient ranging from ice-blue (hydrophobic) to red (hydrophilic). Water molecules are shown as small spheres. Images were generated using the MOLSOFT ICM-Browser.[77] (**A**) Side view of the binding site showing the hydrophobic wall built by lipophilic amino acids. (**B**) The opposite side of the binding pocket facing the β-sheet domain is more polar and loosely built. (**C**) Bottom view of the binding site with the heme cofactor (black lines) projected onto the semitransparent surface. Six lipophilic residues along the edge of the heme macrocycle (L80, L223, A227, A274, L277, and I378) form a pocket that surrounds the end of the M-VIII macrolactone opposite desosamine, thus positioning the C21 methyl group above the iron center. (**D**) Top view along the axis of **9** with the desosamine moiety visible through the surface opening.

hydroxyl of desosamine (**Figure 2.4B**). However, the latter is more likely to act as a hydrogen bond donor to the backbone carbonyl of A164. In order to probe the

importance of the potential interactions involving S172, the corresponding alanine mutant was generated and tested in reactions with the series of substrates previously described. Only moderate decreases in TTN were observed for the macrolide substrates (**9**, **11**, and **12**) while, surprisingly, turnover of aglycone substrates (**8** and **10**) was slightly improved for MycCI$_{S172A}$ relative to the wild-type enzyme (**Table 2.1**). Consistent with these data, the mutant bound the 16-membered ring macrolide compounds with slightly weaker affinity, but the dissociation constants were still in the nanomolar range. In contrast, **8** and **10** bound about twice as tightly to the mutant (**Table 2.2**). Despite the marginal impact that the S172A mutation had on substrate binding affinity, a lower percentage of the mutant was shifted to the high-spin state at saturating levels of each substrate compared with the wild-type enzyme (**Figure 2.2B**; **Table A.8**). This decrease in percent spin shift was largest for **5**, which shifted only ~40% of the mutant to high spin at saturating levels compared with ~80% of the wild-type. Finally, kinetic analysis revealed modest (~25%) reductions in TOF for each of the macrolide substrates while rates either improved (**8**) or remained unchanged (**10**) for the aglycones (**Table 2.4**). Taken together, these data demonstrate that S172 plays a minor role in facilitating substrate binding and catalysis for MycCI. However, this result is not surprising given that we have already shown the entire sugar moiety to be an unnecessary feature of suitable MycCI substrates. In contrast to what has been observed for PikC, the tertiary amine of desosamine, which carries a positive charge at neutral pH, does not interact with the negatively charged carboxylate-containing residues of MycCI. As previously noted, salt bridge interactions between the *N*,*N*-dimethylamino group of desosamine and the side chains of acidic residues (E85 and E94) play a critical role in positioning both native and semisynthetic substrates in the active site of PikC.[31,36,37,39] In the MycCI crystal structure, the carboxylate groups of both D70 and D72 actually point away from desosamine. Furthermore, the negative charge of the D70 side chain is neutralized by forming a salt bridge with the positively charged guanidinium side chain of R278. Thus, substrate recognition and binding operate by a completely different mechanism in MycCI, mostly mediated by hydrophobic interactions between the substrate and the plethora of nonpolar amino acid side chains that line the binding pocket.

Previous studies had initially led us to hypothesize that MycCI employs a mechanism analogous to that used by PikC for binding its natural desosaminylated substrate **9**, as conversion of the corresponding aglycone **8** to a monohydroxylated product was not observed.[33] The reason for the discrepancy between these prior results and our current findings remains unclear. In the initial report, the MycCI construct employed in analytical-scale reactions had a C-terminal His-tag and showed activity toward **9** comparable to that exhibited by the N-terminal His-tagged enzyme. However, the relative activity of the C-terminal His-tagged construct on **8** may have been diminished to the extent that no product could be detected at all. Moreover, the concentration of MycCII in the reported reactions was significantly lower (3.5 μM vs 100 μM in the present work), and a NADPH regeneration system was not employed in these prior studies. As noted before, the extent of substrate turnover was highly dependent on the amount of MycCII present in the reaction mixture. It is likely that suboptimal concentrations of this important redox partner along with the lack of continual in situ NADPH regeneration would preclude formation of detectable amounts of monohydroxylated **8**. Indeed, similar unoptimized conditions were used when we made the initial discovery that MycCI could hydroxylate **10**, with LC-MS analysis indicating only a few percent total conversion of this substrate.

2.9 Conclusions

We have demonstrated that MycCI, a P450 monooxygenase from the mycinamicin biosynthetic pathway, is capable of catalyzing the hydroxylation of unactivated primary carbons in diverse aglycone and macrolide substrates. This ability sets it apart from related P450s involved in macrolide biosynthesis and highlights its potential to serve as a basis for developing novel hydroxylation biocatalysts with broad substrate scope and high regioselectivity. The crystal structure of MycCI in complex with its native 16-membered ring macrolide substrate M-VIII (**9**) provides some insight into the mechanism of substrate binding, revealing the dominance of hydrophobic interactions in properly positioning it to undergo the energetically unfavorable oxidation of a primary C–H bond. Our work further underscores the importance of exploratory

efforts in discovering new P450s from diverse organisms that exhibit unexpected and biocatalytically useful properties.

2.10 References

(1) Ortiz de Montellano, P. R. (Ed.). (2005) Cytochrome P450: structure, mechanism, and biochemistry 3rd ed. Kluwer Academic/Plenum Publishers, New York.

(2) McLean, K. J., Girvan, H. M., Mason, A. E., Dunford, A. J., and Munro, A. W. (2011) Structure, mechanism and function of cytochrome P450 enzymes, in *Iron-containing enzymes: versatile catalysts of hydroxylation reactions in nature* (de Visser, S. P., and Kumar, D., Eds.), pp 255–280. Royal Society of Chemistry, Cambridge.

(3) Munro, A. W., Girvan, H. M., Mason, A. E., Dunford, A. J., and McLean, K. J. (2013) What makes a P450 tick? *Trends Biochem. Sci. 38*, 140–150.

(4) Guengerich, F. P. (2001) Common and uncommon cytochrome P450 reactions related to metabolism and chemical toxicity. *Chem. Res. Toxicol. 14*, 611–650.

(5) Nelson, D. R. (2009) The Cytochrome P450 Homepage. *Hum. Genomics 4*, 59–65.

(6) Meunier, B., de Visser, S. P., and Shaik, S. (2004) Mechanism of oxidation reactions catalyzed by cytochrome P450 enzymes. *Chem. Rev. 104*, 3947–3980.

(7) Denisov, I. G., Makris, T. M., Sligar, S. G., and Schlichting, I. (2005) Structure and chemistry of cytochrome P450. *Chem. Rev. 105*, 2253–2277.

(8) Ortiz de Montellano, P. R. (2010) Hydrocarbon hydroxylation by cytochrome P450 enzymes. *Chem. Rev. 110*, 932–948.

(9) Isin, E. M., and Guengerich, F. P. (2007) Complex reactions catalyzed by cytochrome P450 enzymes. *Biochim. Biophys. Acta 1770*, 314–329.

(10) Guengerich, F. P., and Munro, A. W. (2013) Unusual cytochrome P450 enzymes and reactions. *J. Biol. Chem. 288*, 17065–17073.

(11) Bernhardt, R. (2006) Cytochromes P450 as versatile biocatalysts. *J. Biotechnol. 124*, 128–145.

(12) Urlacher, V. B., and Eiben, S. (2006) Cytochrome P450 monooxygenases: perspectives for synthetic application. *Trends Biotechnol. 24*, 324–330.

(13) Munro, A. W., Girvan, H. M., and McLean, K. J. (2007) Variations on a (t)heme—novel mechanisms, redox partners and catalytic functions in the cytochrome P450 superfamily. *Nat. Prod. Rep. 24*, 585–609.

(14) O'Reilly, E., Köhler, V., Flitsch, S. L., and Turner, N. J. (2011) Cytochromes P450 as useful biocatalysts: addressing the limitations. *Chem. Commun. 47*, 2490–2501.

(15) Grogan, G. (2011) Cytochromes P450: exploiting diversity and enabling application as biocatalysts. *Curr. Opin. Chem. Biol. 15*, 241–248.

(16) Fasan, R. (2012) Tuning P450 enzymes as oxidation catalysts. *ACS Catal. 2*, 647–666.

(17) Urlacher, V. B., and Girhard, M. (2012) Cytochrome P450 monooxygenases: an update on perspectives for synthetic application. *Trends Biotechnol. 30*, 26–36.

(18) Caswell, J. M., O'Neill, M., Taylor, S. J. C., and Moody, T. S. (2013) Engineering and application of P450 monooxygenases in pharmaceutical and metabolite synthesis. *Curr. Opin. Chem. Biol. 17*, 271–275.

(19) Bernhardt, R., and Urlacher, V. B. (2014) Cytochromes P450 as promising catalysts for biotechnological application: chances and limitations. *Appl. Microbiol. Biotechnol. 98*, 6185–6203.

(20) Behrendorff, J. B. Y. H., Huang, W., and Gillam, E. M. J. (2015) Directed evolution of cytochrome P450 enzymes for biocatalysis: exploiting the catalytic versatility of enzymes with relaxed substrate specificity. *Biochem. J. 467*, 1–15.

(21) Guengerich, F. P. (2002) Cytochrome P450 enzymes in the generation of commercial products. *Nat. Rev. Drug Discov. 1*, 359–366.

(22) Kelly, S. L., Lamb, D. C., Jackson, C. J., Warrilow, A. G. S., and Kelly, D. E. (2003) The biodiversity of microbial cytochromes P450, in *Advances in Microbial Physiology, Vol. 47* (Poole, R. K., Ed.), pp 131–186. Academic Press, London.

(23) Kelly, S. L., and Kelly, D. E. (2013) Microbial cytochromes P450: biodiversity and biotechnology. Where do cytochromes P450 come from, what do they do and what can they do for us? *Phil. Trans. R. Soc. B 368*.

(24) Cryle, M. J., Stok, J. E., and De Voss, J. J. (2003) Reactions catalyzed by bacterial cytochromes P450. *Aust. J. Chem. 56*, 749–762.

(25) Podust, L. M., and Sherman, D. H. (2012) Diversity of P450 enzymes in the biosynthesis of natural products. *Nat. Prod. Rep. 29*, 1251–1266.

(26) Newman, D. J., and Cragg, G. M. (2016) Natural products as sources of new drugs from 1981 to 2014. *J. Nat. Prod. 79*, 629–661.
(27) Andersen, J. F., Tatsuta, K., Gunji, H., Ishiyama, T., and Hutchinson, C. R. (1993) Substrate specificity of 6-deoxyerythronolide B hydroxylase, a bacterial cytochrome P450 of erythromycin A biosynthesis. *Biochemistry 32*, 1905–1913.
(28) Xue, Y., Wilson, D., Zhao, L., Liu, H.-w., and Sherman, D. H. (1998) Hydroxylation of macrolactones YC-17 and narbomycin is mediated by the *pikC*-encoded cytochrome P450 in *Streptomyces venezuelae*. *Chem. Biol. 5*, 661–667.
(29) Zhang, Q., and Sherman, D. H. (2001) Isolation and structure determination of novamethymycin, a new bioactive metabolite of the methymycin biosynthetic pathway in *Streptomyces venezuelae*. *J. Nat. Prod. 64*, 1447–1450.
(30) Lee, S. K., Park, J. W., Kim, J. W., Jung, W. S., Park, S. R., Choi, C. Y., Kim, E. S., Kim, B. S., Ahn, J. S., Sherman, D. H., and Yoon, Y. J. (2006) Neopikromycin and novapikromycin from the pikromycin biosynthetic pathway of *Streptomyces venezuelae*. *J. Nat. Prod. 69*, 847–849.
(31) Sherman, D. H., Li, S., Yermalitskaya, L. V., Kim, Y., Smith, J. A., Waterman, M. R., and Podust, L. M. (2006) The structural basis for substrate anchoring, active site selectivity, and product formation by P450 PikC from *Streptomyces venezuelae*. *J. Biol. Chem. 281*, 26289–26297.
(32) Ding, Y., Seufert, W. H., Beck, Z. Q., and Sherman, D. H. (2008) Analysis of the cryptophycin P450 epoxidase reveals substrate tolerance and cooperativity. *J. Am. Chem. Soc. 130*, 5492–5498.
(33) Anzai, Y., Li, S., Chaulagain, M. R., Kinoshita, K., Kato, F., Montgomery, J., and Sherman, D. H. (2008) Functional analysis of MycCI and MycG, cytochrome P450 enzymes involved in biosynthesis of mycinamicin macrolide antibiotics. *Chem. Biol. 15*, 950–959.
(34) Carlson, J. C., Li, S., Gunatilleke, S. S., Anzai, Y., Burr, D. A., Podust, L. M., and Sherman, D. H. (2011) Tirandamycin biosynthesis is mediated by co-dependent oxidative enzymes. *Nat. Chem. 3*, 628–633.
(35) Li, S., Tietz, D. R., Rutaganira, F. U., Kells, P. M., Anzai, Y., Kato, F., Pochapsky, T. C., Sherman, D. H., and Podust, L. M. (2012) Substrate recognition by the multifunctional cytochrome P450 MycG in mycinamicin hydroxylation and epoxidation reactions. *J. Biol. Chem. 287*, 37880–37890.
(36) Li, S., Chaulagain, M. R., Knauff, A. R., Podust, L. M., Montgomery, J., and Sherman, D. H. (2009) Selective oxidation of carbolide C–H bonds by an engineered macrolide P450 mono-oxygenase. *Proc. Natl. Acad. Sci. U.S.A. 106*, 18463–18468.
(37) Negretti, S., Narayan, A. R. H., Chiou, K. C., Kells, P. M., Stachowski, J. L., Hansen, D. A., Podust, L. M., Montgomery, J., and Sherman, D. H. (2014) Directing group-controlled regioselectivity in an enzymatic C–H bond oxygenation. *J. Am. Chem. Soc. 136*, 4901–4904.
(38) Narayan, A. R. H., Jiménez-Osés, G., Liu, P., Negretti, S., Zhao, W., Gilbert, M. M., Ramabhadran, R. O., Yang, Y.-F., Furan, L. R., Li, Z., Podust, L. M., Montgomery, J., Houk, K. N., and Sherman, D. H. (2015) Enzymatic hydroxylation of an unactivated methylene C–H bond guided by molecular dynamics simulations. *Nat. Chem. 7*, 653–660.
(39) Li, S., Ouellet, H., Sherman, D. H., and Podust, L. M. (2009) Analysis of transient and catalytic desosamine-binding pockets in cytochrome P-450 PikC from *Streptomyces venezuelae*. *J. Biol. Chem. 284*, 5723–5730.
(40) Hansen, D. A., Rath, C. M., Eisman, E. B., Narayan, A. R. H., Kittendorf, J. D., Mortison, J. D., Yoon, Y. J., and Sherman, D. H. (2013) Biocatalytic synthesis of pikromycin, methymycin, neomethymycin, novamethymycin, and ketomethymycin. *J. Am. Chem. Soc. 135*, 11232–11238.
(41) Borisova, S. A., Zhang, C., Takahashi, H., Zhang, H., Wong, A. W., Thorson, J. S., and Liu, H.-w. (2006) Substrate specificity of the macrolide-glycosylating enzyme pair DesVII/DesVIII: opportunities, limitations, and mechanistic hypotheses. *Angew. Chem. Int. Ed. 45*, 2748–2753.
(42) Borisova, S. A., Kim, H. J., Pu, X., and Liu, H.-w. (2008) Glycosylation of acyclic and cyclic aglycone substrates by macrolide glycosyltransferase DesVII/DesVIII: analysis and implications. *ChemBioChem 9*, 1554–1558.
(43) Baltz, R. H., and Seno, E. T. (1981) Properties of *Streptomyces fradiae* mutants blocked in biosynthesis of the macrolide antibiotic tylosin. *Antimicrob. Agents Chemother. 20*, 214–225.
(44) Li, S., Podust, L. M., and Sherman, D. H. (2007) Engineering and analysis of a self-sufficient biosynthetic cytochrome P450 PikC fused to the RhFRED reductase domain. *J. Am. Chem. Soc. 129*, 12940–12941.
(45) Zhang, W., Liu, Y., Yan, J., Cao, S., Bai, F., Yang, Y., Huang, S., Yao, L., Anzai, Y., Kato, F., Podust,

L. M., Sherman, D. H., and Li, S. (2014) New reactions and products resulting from alternative interactions between the P450 enzyme and redox partners. *J. Am. Chem. Soc. 136*, 3640–3646.
(46) Anzai, Y., Tsukada, S., Sakai, A., Masuda, R., Harada, C., Domeki, A., Li, S., Kinoshita, K., Sherman, D. H., and Kato, F. (2012) Function of cytochrome P450 enzymes MycCI and MycG in *Micromonospora griseorubida*, a producer of the macrolide antibiotic mycinamicin. *Antimicrob. Agents Chemother. 56*, 3648–3656.
(47) Luthra, A., Denisov, I. G., and Sligar, S. G. (2011) Spectroscopic features of cytochrome P450 reaction intermediates. *Arch. Biochem. Biophys. 507*, 26–35.
(48) Montemiglio, L. C., Parisi, G., Scaglione, A., Sciara, G., Savino, C., and Vallone, B. (2016) Functional analysis and crystallographic structure of clotrimazole bound OleP, a cytochrome P450 epoxidase from *Streptomyces antibioticus* involved in oleandomycin biosynthesis. *Biochim. Biophys. Acta 1860*, 465–475.
(49) Montemiglio, L. C., Gianni, S., Vallone, B., and Savino, C. (2010) Azole drugs trap cytochrome P450 EryK in alternative conformational states. *Biochemistry 49*, 9199–9206.
(50) Robin, A., Roberts, G. A., Kisch, J., Sabbadin, F., Grogan, G., Bruce, N., Turner, N. J., and Flitsch, S. L. (2009) Engineering and improvement of the efficiency of a chimeric [P450cam-RhFRed reductase domain] enzyme. *Chem. Commun.* 2478–2480.
(51) Johnston, J. B., Ouellet, H., Podust, L. M., and Ortiz de Montellano, P. R. (2011) Structural control of cytochrome P450-catalyzed ω-hydroxylation. *Arch. Biochem. Biophys. 507*, 86–94.
(52) Han, S., Pham, T.-V., Kim, J.-H., Lim, Y.-R., Park, H.-G., Cha, G.-S., Yun, C.-H., Chun, Y.-J., Kang, L.-W., and Kim, D. (2015) Functional characterization of CYP107W1 from *Streptomyces avermitilis* and biosynthesis of macrolide oligomycin A. *Arch. Biochem. Biophys. 575*, 1–7.
(53) Meinhold, P., Peters, M. W., Hartwick, A., Hernandez, A. R., and Arnold, F. H. (2006) Engineering cytochrome P450 BM3 for terminal alkane hydroxylation. *Adv. Synth. Catal. 348*, 763–772.
(54) Zhang, K., Shafer, B. M., Demars, M. D., II, Stern, H. A., and Fasan, R. (2012) Controlled oxidation of remote sp^3 C–H bonds in artemisinin via P450 catalysts with fine-tuned regio- and stereoselectivity. *J. Am. Chem. Soc. 134*, 18695–18704.
(55) Hutzler, J. M., and Tracy, T. S. (2002) Atypical kinetic profiles in drug metabolism reactions. *Drug Metab. Dispos. 30*, 355–362.
(56) Korzekwa, K. R., Krishnamachary, N., Shou, M., Ogai, A., Parise, R. A., Rettie, A. E., Gonzalez, F. J., and Tracy, T. S. (1998) Evaluation of atypical cytochrome P450 kinetics with two-substrate models: evidence that multiple substrates can simultaneously bind to cytochrome P450 active sites. *Biochemistry 37*, 4137–4147.
(57) Lin, Y., Lu, P., Tang, C., Mei, Q., Sandig, G., Rodrigues, A. D., Rushmore, T. H., and Shou, M. (2001) Substrate inhibition kinetics for cytochrome P450-catalyzed reactions. *Drug Metab. Dispos. 29*, 368–374.
(58) Kinoshita, K., Imura, Y., Takenaka, S., and Hayashi, M. (1989) Mycinamicins, new macrolide antibiotics. XI. Isolation and structure elucidation of a key intermediate in the biosynthesis of the mycinamicins, mycinamicin VIII. *J. Antibiot. 42*, 1869–1872.
(59) Loida, P. J., and Sligar, S. G. (1993) Molecular recognition in cytochrome P-450: mechanism for the control of uncoupling reactions. *Biochemistry 32*, 11530–11538.
(60) Moody, S. C., and Loveridge, E. J. (2014) CYP105—diverse structures, functions and roles in an intriguing family of enzymes in *Streptomyces*. *J. Appl. Microbiol. 117*, 1549–1563.
(61) Fouces, R., Mellado, E., Díez, B., and Barredo, J. L. (1999) The tylosin biosynthetic cluster from *Streptomyces fradiae*: genetic organization of the left region. *Microbiology 145*, 855–868.
(62) Bate, N., and Cundliffe, E. (1999) The mycinose-biosynthetic genes of *Streptomyces fradiae*, producer of tylosin. *J. Ind. Microbiol. Biotechnol. 23*, 118–122.
(63) Ward, S. L., Hu, Z., Schirmer, A., Reid, R., Revill, W. P., Reeves, C. D., Petrakovsky, O. V., Dong, S. D., and Katz, L. (2004) Chalcomycin biosynthesis gene cluster from *Streptomyces bikiniensis*: novel features of an unusual ketolide produced through expression of the *chm* polyketide synthase in *Streptomyces fradiae*. *Antimicrob. Agents Chemother. 48*, 4703–4712.
(64) Omura, S., Sadakane, N., and Matsubara, H. (1982) Bioconversion and biosynthesis of 16-membered macrolide antibiotics. XXII. Biosynthesis of tylosin after protylonolide formation. *Chem. Pharm. Bull. 30*, 223–229.
(65) Baltz, R. H., Seno, E. T., Stonesifer, J., and Wild, G. M. (1983) Biosynthesis of the macrolide antibiotic tylosin: a preferred pathway from tylactone to tylosin. *J. Antibiot. 36*, 131–141.

(66) Omura, S., Tanaka, H., and Tsukui, M. (1982) Biosynthesis of tylosin: oxidations of 5-*O*-mycaminosylprotylonolide at C-20 and C-23 with a cell-free extract from *Streptomyces fradiae*. *Biochem. Biophys. Res. Commun. 107*, 554–560.
(67) Anzai, Y., Saito, N., Tanaka, M., Kinoshita, K., Koyama, Y., and Kato, F. (2003) Organization of the biosynthetic gene cluster for the polyketide macrolide mycinamicin in *Micromonospora griseorubida*. *FEMS Microbiol. Lett. 218*, 135–141.
(68) Gotoh, O. (1992) Substrate recognition sites in cytochrome P450 family 2 (CYP2) proteins inferred from comparative analyses of amino acid and coding nucleotide sequences. *J. Biol. Chem. 267*, 83–90.
(69) Haslinger, K., Peschke, M., Brieke, C., Maximowitsch, E., and Cryle, M. J. (2015) X-domain of peptide synthetases recruits oxygenases crucial for glycopeptide biosynthesis. *Nature 521*, 105–109.
(70) Brieke, C., Peschke, M., Haslinger, K., and Cryle, M. J. (2015) Sequential in vitro cyclization by cytochrome P450 enzymes of glycopeptide antibiotic precursors bearing the X-domain from nonribosomal peptide biosynthesis. *Angew. Chem. Int. Ed. 54*, 15715–15719.
(71) Peschke, M., Haslinger, K., Brieke, C., Reinstein, J., and Cryle, M. J. (2016) Regulation of the P450 oxygenation cascade involved in glycopeptide antibiotic biosynthesis. *J. Am. Chem. Soc. 138*, 6746–6753.
(72) Woithe, K., Geib, N., Zerbe, K., Li, D. B., Heck, M., Fournier-Rousset, S., Meyer, O., Vitali, F., Matoba, N., Abou-Hadeed, K., and Robinson, J. A. (2007) Oxidative phenol coupling reactions catalyzed by OxyB: a cytochrome P450 from the vancomycin producing organism. Implications for vancomycin biosynthesis. *J. Am. Chem. Soc. 129*, 6887–6895.
(73) Woithe, K., Geib, N., Meyer, O., Wörtz, T., Zerbe, K., and Robinson, J. A. (2008) Exploring the substrate specificity of OxyB, a phenol coupling P450 enzyme involved in vancomycin biosynthesis. *Org. Biomol. Chem. 6*, 2861–2867.
(74) Schmartz, P. C., Wölfel, K., Zerbe, K., Gad, E., El Tamany, E. S., Ibrahim, H. K., Abou-Hadeed, K., and Robinson, J. A. (2012) Substituent effects on the phenol coupling reaction catalyzed by the vancomycin biosynthetic P450 enzyme OxyB. *Angew. Chem. Int. Ed. 51*, 11468–11472.
(75) Brieke, C., Kratzig, V., Haslinger, K., Winkler, A., and Cryle, M. J. (2015) Rapid access to glycopeptide antibiotic precursor peptides coupled with cytochrome P450-mediated catalysis: towards a biomimetic synthesis of glycopeptide antibiotics. *Org. Biomol. Chem. 13*, 2012–2021.
(76) Haslinger, K., Maximowitsch, E., Brieke, C., Koch, A., and Cryle, M. J. (2014) Cytochrome P450 $OxyB_{tei}$ catalyzes the first phenolic coupling step in teicoplanin biosynthesis. *ChemBioChem 15*, 2719–2728.
(77) Abagyan, R. Internal Coordinate Mechanics (ICM) version 3.8-4a, http://www.molsoft.com/icm_pro.html.
(78) DeLano, W. L. (2002) The PyMOL Molecular Graphics System. DeLano Scientific, San Carlos, CA, USA.

Chapter 3: Molecular basis for substrate specificity in the cytochrome P450 TylHI from *Streptomyces fradiae*[*]

3.1 Introduction

Since their first discovery in the 1950s as components of mammalian liver microsomes,[1-3] thousands of unique cytochrome P450 enzymes (P450s) have been identified in organisms across all domains of life. All P450s are heme-thiolate proteins, and every member of this superfamily that has thus far been structurally characterized adopts the same triangular prism-like fold.[4,5] Most P450s also share a common mechanism of dioxygen activation and typically act via a radical pathway to insert a single atom of oxygen into a C–H bond of a target substrate.[6,7] However, the nature of their catalytic cycle renders these enzymes capable of effecting a broad array of reactions, including epoxidation, heteroatom oxidation, dealkylation, oxidative phenolic coupling, and C–C bond formation/cleavage among many others.[8-11] From a functional perspective, P450s play critical roles in cellular metabolism, ranging from xenobiotic metabolism in humans to secondary metabolite biosynthesis in plants, fungi, and bacteria.

The abundance of genes encoding P450s in microorganisms underscores the importance of this class of enzymes in carrying out key biochemical steps in primary and secondary metabolic pathways.[4] In particular, actinobacteria often contain large numbers of P450 genes, where they are frequently coupled to the production of secondary metabolites. *Streptomyces* species are particularly rich sources of natural products possessing a range of biological activities (e.g., antibacterial, antifungal, antitumor, and immunosuppressive), and P450s have been identified to play key roles in the biosynthesis of many of these compounds.[12-16] Members of the CYP105 and

[*]The work described in this chapter was a collaborative effort between Matthew D. DeMars II and Dr. Larissa M. Podust (UCSD). M.D.D. II performed all biochemical experiments, and L.M.P. determined the X-ray crystal structure of TylHI in complex with 23-DMTL.

CYP107 families are particularly well represented among actinomycetes and include those that have been characterized as having broad substrate scope (e.g., MoxA (CYP105AB3)[17,18]; PikC (CYP107L1)[19]). Homologs of CYP105 have been identified in all *Streptomyces* species that have been investigated thus far.[20] At least 17 subfamilies make up the CYP105 family in streptomycetes. These enzymes are chiefly involved in the metabolism of xenobiotics and in the biosynthesis of natural products, many of which are macrocyclic polyketides.

Scheme 3.1. Tylosin biosynthetic pathway in *Streptomyces fradiae*. The hydroxylation reaction catalyzed by TylHI acting in conjunction with its ferredoxin partner TylHII is depicted in red.

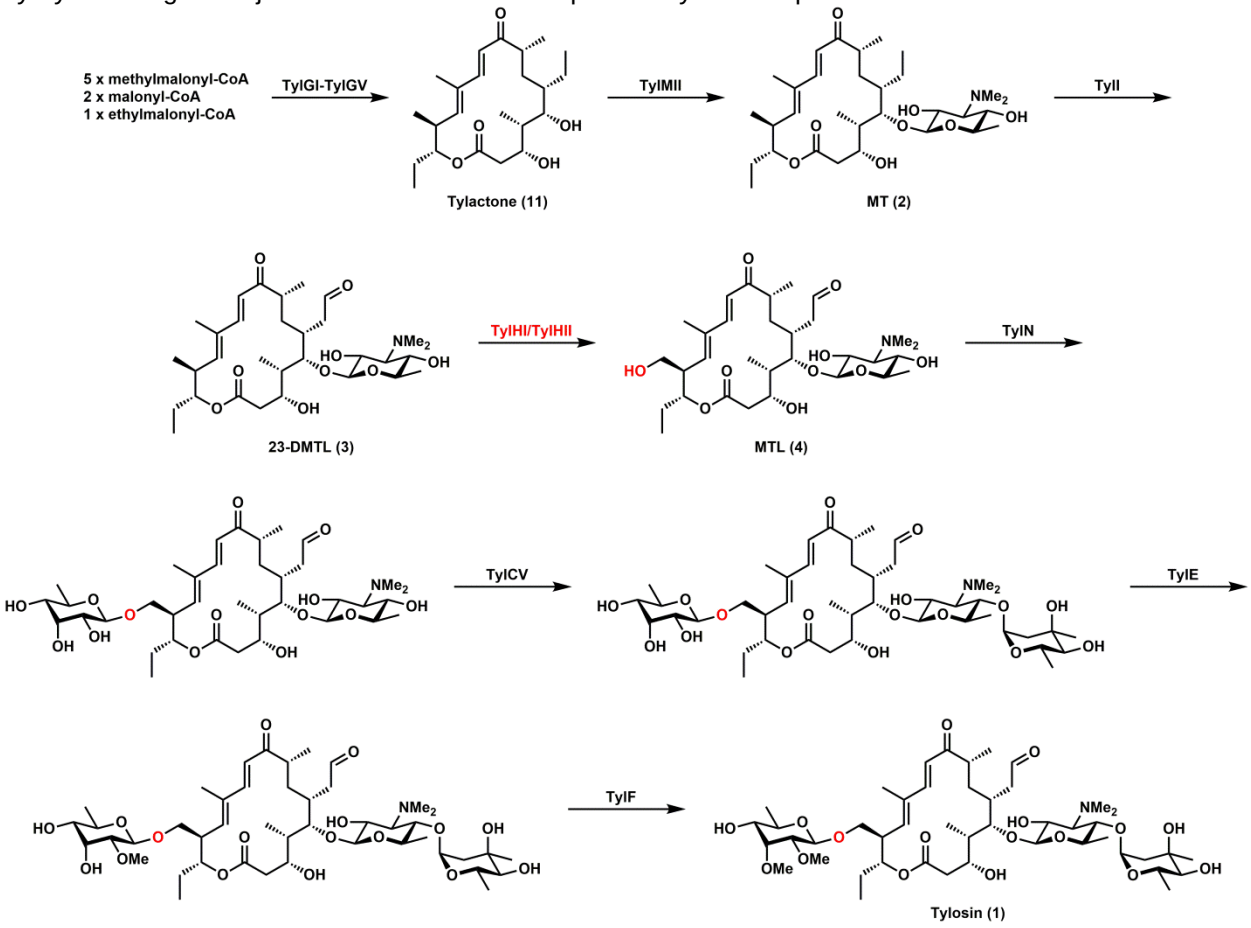

Tylosin (**1**) is a 16-membered ring macrolide antibiotic produced by several *Streptomyces* species, including *S. fradiae*, *S. rimosus*, and *S. hygroscopicus*.[21-23] Although not used clinically in humans, it has been widely adopted in veterinary medicine as an antibacterial agent as well as in the livestock industry as a growth

promoter. The biosynthesis of **1** in *S. fradiae* has been intensely studied over the past four decades (**Scheme 3.1**).[24] Many of the steps of the biosynthetic pathway were initially elucidated in the early 1980s based on analysis of metabolites produced by blocked mutants[25] as well as on the results of whole-cell and cell-free bioconversion experiments.[26-31] It was not until later that the genes associated with the biosynthetic cluster were identified and sequenced.[32,33] The tylosin gene cluster contains two P450s whose functional roles were originally assigned by investigating the ability of *S. fradiae* cell-free extracts to oxidize various tylosin biosynthetic intermediates in the presence of different cofactors.[29,31] However, only recently have the activities of the two purified enzymes been confirmed by our group through in vitro biochemical analysis (see Chapters 2[34] and 4[35]). TylI performs a four-electron oxidation at C20 of 5-*O*-mycaminosyl-tylactone (MT, **2**) to produce 23-deoxy-5-*O*-mycaminosyl-tylonolide (23-DMTL, **3**), which TylHI then hydroxylates at C23 to give 5-*O*-mycaminosyl-tylonolide (MTL, **4**) (**Scheme 3.1**). Interestingly, a third P450 gene (*orf16**) is also found in the tylosin biosynthetic gene cluster, where it may be involved in the transcriptional regulatory cascade that controls tylosin production.[36,37]

Previously, we explored the substrate scope of MycCI (CYP105L2), a P450 from the related mycinamicin (**5**) pathway (**Scheme 3.2B**), and found that it was capable of hydroxylating a relatively broad range of 16-membered ring macrolactones and macrolides (see Chapter 2).[34] However, parallel characterization of its close homolog TylHI (CYP105L1; 55% sequence identity) revealed that the latter was unable to tolerate even subtle changes to its native substrate. Differences in catalytic activity between P450 isozymes that are part of the same subfamily (≥55% identity) and that act on similar types of substrates have frequently been observed among mammalian P450s. For example, despite differing by only 11 amino acids, rabbit CYP2B4 and CYP2B5 exhibit differential regioselectivity in the hydroxylation of androstenedione as well as distinct substrate profiles.[38-40] In another noteworthy example, the insect P450 homologs CYP6B1 (*Papilio polyxenes*) and CYP6B8 (*Helicoverpa zea*) share 53% sequence identity, but the latter has a considerably broader substrate scope than the former.[41] Similar cases can be found among P450s involved in the biosynthesis of natural products in bacteria. The P450 $OxyB_{van}$, which catalyzes the first oxidative

phenolic coupling reaction in the biosynthesis of vancomycin, is well-known for its ability to tolerate a number of non-natural peptide substrates whereas its homolog from the teicoplanin pathway ($OxyB_{tei}$; 74% identity) exhibits a high degree of selectivity for its

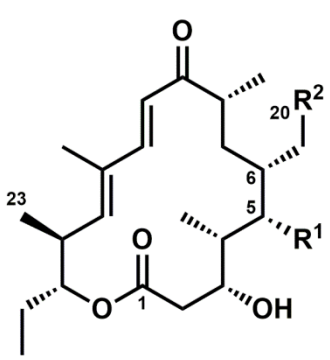

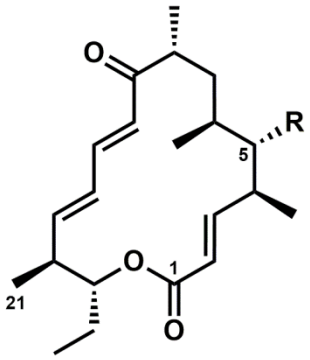

Compound	R^1	R^2
MT (**2**)	Mycaminose	CH_3
23-DMTL (**3**)	Mycaminose	CHO
20-OH-MT (**8**)	Mycaminose	CH_2OH
DT (**6**)	Desosamine	CH_3
23-DDTL (**7**)	Desosamine	CHO
20-OH-DT (**9**)	Desosamine	CH_2OH
Tylactone (**11**)	OH	CH_3

Compound	R
M-VIII (**10**)	Desosamine
PML-IV (**13**)	OH

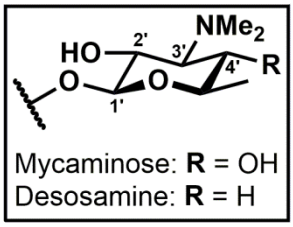

Mycaminose: **R** = OH
Desosamine: **R** = H

Figure 3.1. Structures of compounds investigated in Chapter 3.

native substrate and closely related peptides.[42] Moreover, whereas the P450s HmtT and HmtN involved in himastatin biosynthesis are 55% identical, they catalyze different types of reactions at unique sites on nearly identical substrates.[43,44] Drawing additional inspiration from these interesting examples, we sought to acquire detailed insight into the molecular basis for substrate specificity in the P450 TylHI using a combination of chemical, biochemical, and structural approaches. Ultimately, we aimed to use this information to understand the factors governing the differences in the reactivity profiles of this selective enzyme and its promiscuous homolog.

3.2 TylHI activity and binding assays with substrate analogs

In our previous studies describing the catalytic versatility of MycCI, we found that its homolog TylHI possessed a surprisingly restricted substrate scope in comparison.[34]

Whereas it readily converted its native substrate 23-DMTL (**3**) to the expected product (MTL, **4**), minor alterations to the structure of this compound rendered it essentially unacceptable as a substrate for the enzyme. Specifically, an analog lacking the C20-aldehyde and the C4'-hydroxyl (5-*O*-desosaminyl-tylactone, DT, **6**) bound with nearly 500-fold lower affinity and was turned over less than once (mol product/mol P450) over the course of an overnight in vitro reaction. Given the difference in only two functional groups between these two molecules, we questioned whether one might have a more significant impact on binding and subsequent catalysis than the other. Thus, we envisioned acquiring two additional substrate analogs via semisynthesis, one bearing the aldehyde and lacking the sugar hydroxyl group (23-deoxy-5-*O*-desosaminyl-tylonolide, 23-DDTL, **7**) and another lacking the former but maintaining the latter (5-*O*-mycaminosyl-tylactone, MT, **2**). In our recent work detailing the chemoenzymatic total synthesis of tylactone-based macrolides, we reported the efficient in vitro TylI-catalyzed hydroxylation of **6** at C20 followed by selective chemical oxidation at the same site to give **7**, a biologically active macrolide referred to in our report as M-4365 G_2 (see Chapter 4).[35] To access **2**, we followed a previously established scheme with some variations in reaction conditions (**Scheme B.1**). Reduction of the aldehyde of **3** with sodium borohydride was followed by iodination of the alcohol (20-hydroxy-5-*O*-mycaminosyl-tylactone, 20-OH-MT, **8**) and subsequent borohydride-mediated reduction to afford **2**. In addition to the target substrates, we opted to test the C20-hydroxylated synthetic intermediates **8** and 20-hydroxy-5-*O*-desosaminyl-tylactone (20-OH-DT, **9**) against TylHI in parallel activity assays.

Analytical-scale reactions with each of the substrates were performed with purified TylHI and MBP-tagged spinach ferredoxin reductase (MBP-FdR) along with native ferredoxin TylHII or its homolog MycCII. The single-component TylHI-RhFRED previously generated[34] was also tested. While reduction of the aldehyde in the native substrate (**3**) to the alcohol (**8**) had no impact on conversion, further reduction to the alkane (**2**) resulted in a modest decrease in enzymatic activity (91% conversion of **3** vs 40% conversion of **2** by TylHI/MycCII; see **Figure 3.2** and **Table B.2**). However, substitution of desosamine for mycaminose while maintaining the oxidation state of C20 had a more significant negative effect on substrate turnover (6% conversion of **7** by

TylHI/MycCII). The same trend was observed for the other catalytic systems, with the native partnering of TylHI/TylHII somewhat tempering the damaging impact of substrate

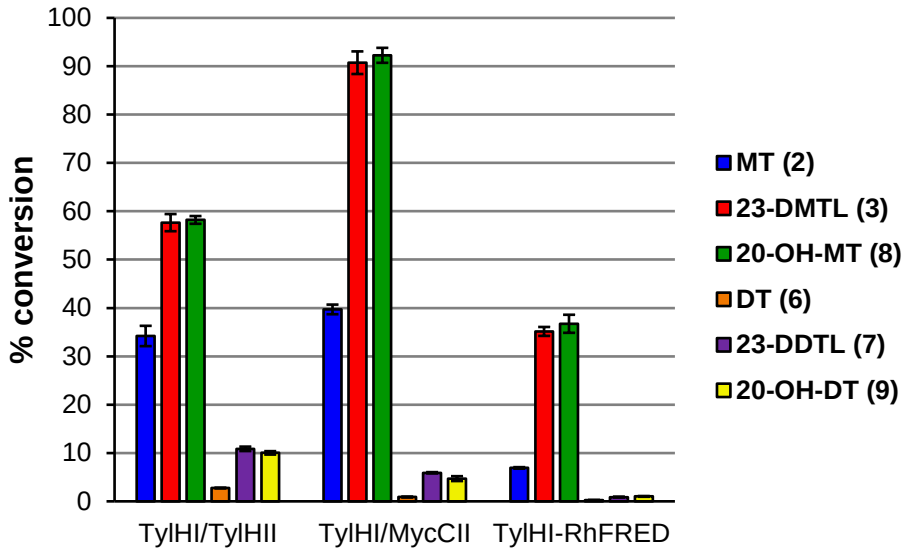

Figure 3.2. Results of activity assays with TylHI and selected substrates. See **Table B.2** for raw numerical values.

modification on activity and the artificial TylHI-RhFRED self-sufficient catalyst exacerbating it. It is difficult to rationalize why TylHI is more active on desosaminylated substrates but less so on those bearing mycaminose (including its native substrate **3**) when it is partnered with TylHII compared with when it is acting in conjunction with MycCII. One possibility relates to the kinetics of the electron transfer steps from MBP-FdR to the ferredoxin and then from the ferredoxin to the P450. NADPH consumption experiments performed previously[34] suggested that MBP-FdR exhibits a preference to reduce MycCII over TylHII (see Appendix A, **Table A.11**). The former expresses significantly better in *E. coli* and has a higher extinction coefficient at 408 nm, which may indicate that more of these protein molecules contain the appropriate [3Fe-4S] cluster. Thus, the ability of TylHII to shuttle electrons from the reductase to the P450 could be attenuated due to suboptimal folding during expression or general instability. Indeed, the turnover frequency for the tripartite TylHI/TylHII/MBP-FdR catalytic system acting on **3** was found to be about 12-fold lower than that for the same system where MycCII was substituted for TylHII. However, since TylHII may interact more favorably with TylHI, the kinetics of electron transfer could be less negatively impacted for TylHII

relative to MycCII when TylHI binds the non-native desosaminylated substrates (**6**, **7**, and **9**).

In order to corroborate the results of the activity assays, equilibrium substrate binding experiments were carried out (K_d values are shown in **Table 3.1**; see **Table B.3** for percent spin shift values). Generally, the binding affinities of the substrates tested were consistent with the degrees to which they were converted to their respective products. Reduction of the aldehyde in **3** to the alcohol (**8**) modestly increased the K_d from ~0.5 μM to 3.5 μM, and further reduction to the alkane (**2**) had a comparable impact on binding (K_d = 26 μM for **2**). Mirroring the effect of removing the C4'-hydroxyl group on substrate turnover, the K_d for binding of **7** to TylHI (271 μM) was more than 500-fold higher than that for binding of **3**. While turnover of the other desosaminylated substrates (**6** and **9**) was lower than turnover of **7**, they bound with slightly (i.e., less than two-fold) higher affinities to TylHI.

Table 3.1. Dissociation constants of selected substrates against wild-type TylHI.[a]

Substrate	K_d (μM)
2	26 ± 5
3	0.48 ± 0.03
8	3.5 ± 0.3
6	154 ± 12
7	271 ± 17
9	201 ± 19

[a]Reported errors are those obtained from fitting data averaged from experiments performed in duplicate.

Taken together, these experiments performed with key analogs of the native substrate (**3**) have revealed that, independent of the oxidation state of C20, compounds with mycaminose as the deoxyamino sugar are strongly preferred over those bearing desosamine. While TylHI preferentially accepts substrates in which the ethyl side chain is oxidized to some degree, the presence or absence of a hydroxyl group attached to C4' has a much more significant impact on substrate binding and subsequent turnover. On the basis of these conclusions, one would expect to observe important polar interactions with the sugar hydroxyl group as well as possible hydrogen bonds with the aldehyde in a crystal structure of the enzyme in complex with **3** (*vide infra*). Notably, these results are consistent with those of early in vivo and in vitro biotransformation experiments employing *Streptomyces fradiae* whole-cell cultures and cell-free

extracts.[25,29,31] In these studies, metabolites bearing a hydroxyl group at C23 independent of the oxidation state of C20 were observed, suggesting that the C23 hydroxylase could tolerate minor alterations to its native substrate. However, hydroxylation at C23 was considerably diminished in the absence of the aldehyde functionality at C20, indicating a clear substrate preference for the associated enzyme and thus helping to establish a preferred biosynthetic pathway for tylosin (**Scheme 3.1**).[30]

3.3 Structural characterization of TylHI bound to 23-DMTL

Table 3.2. Crystallographic data summary for TylHI/23-DMTL.

Protein	TylHI
Ligand	23-DMTL
PDB ID	**6B11**
Data collection	
Space group	$P2_12_12_1$
Cell dimensions	
a, *b*, *c* (Å)	63.7, 109.2, 150.1
α, *β*, *γ* (°)	90.0, 90.0, 90.0
Molecules in AU	2
Wavelength	1.11587
Resolution (Å)	1.99
R_{merge}	0.07 (1.74)[a]
I / σI	14.6 (1.39)
Completeness (%)	95.6 (69.7)
Redundancy	6.2 (3.2)
Refinement	
No. reflections	66461
R_{work} / R_{free} (%)	19.4 / 24.0
No. atoms	
Protein	5907
Heme	86
Substrate	123
Solvent	234
Mean B value	46.5
B-factors	
Protein	47.0
Heme	36.9
Substrate	38.6
Solvent	49.3
RMSD	
Bond lengths (Å)	0.019
Bond angles (°)	1.966

[a]Values in parentheses are for the highest resolution shell.

In order to acquire more detailed insights into the specific interactions involved in TylHI substrate binding, we solved the crystal structure of the enzyme in complex with its native substrate 23-DMTL (**3**) to a resolution of 1.99 Å (**Table 3.2**; **Figure 3.3**). The asymmetric unit of the crystal lattice contains two protein molecules and, in each case, electron density for the first 31 amino acids is not observed. Interestingly, alignment of the primary amino acid sequence of TylHI with that of its structural and functional homolog MycCI reveals that the first 31 residues of the former are completely absent from the latter, with the MycCI sequence starting at residue 32 of TylHI (see **Figure 3.7**). In order to probe any potential role for this N-terminal portion of the TylHI sequence, the corresponding N-terminal truncated protein was generated and tested in parallel with the wild-type enzyme. No significant differences in activity or protein stability were observed, raising the possibility that the N-terminal sequence may function in some unknown capacity in the protein's native host organism (see **Table B.2** for results of activity assays employing $TylHI_{\Delta 2\text{-}33}$).

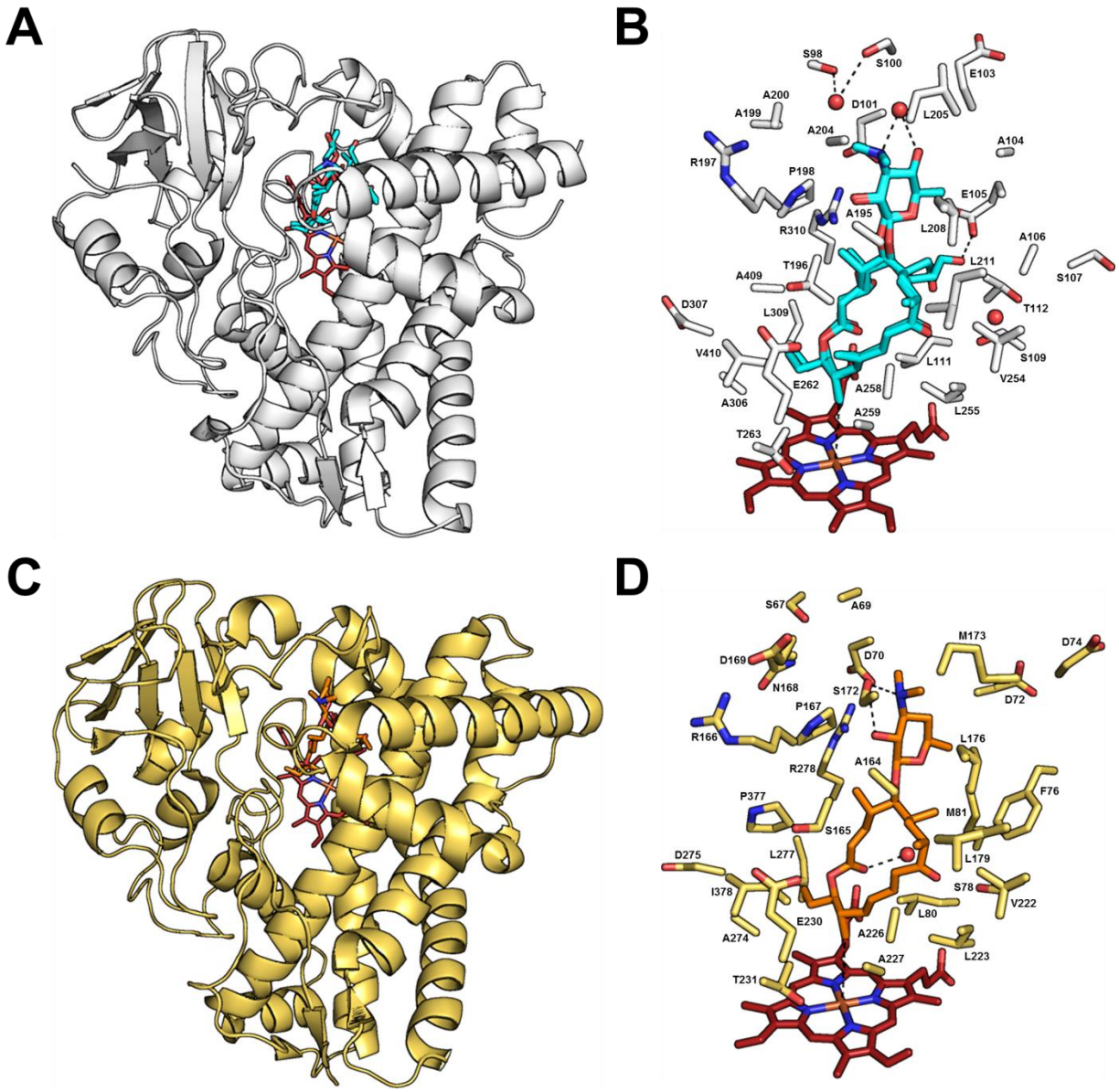

Figure 3.3. Comparison of the crystal structures of TylHI and MycCI (**PDB 5FOI**) bound to **3** and **10**, respectively. (**A**) Overall tertiary structure of TylHI. (**B**) Binding pocket of **3** in TylHI. The substrate (**3**) is depicted in cyan, the heme cofactor is shown in firebrick, and the side chains of residues within 5 Å of **3** are white and appropriately labeled. The three water molecules present in both chains of the asymmetric unit are shown as small red spheres. Potential hydrogen bonding interactions are depicted as black dashes. A black dash is also drawn between the heme iron and the carbon atom (C23) targeted for hydroxylation. (**C**) Overall tertiary structure of MycCI. (**D**) Binding pocket of **10** in MycCI shown in the same relative orientation as that of **3** in TylHI. The substrate (**10**) is depicted in orange, the heme cofactor is shown in firebrick, and the side chains of residues within 5 Å of **10** are yellow-orange and appropriately labeled. The single water molecule present in both chains of the asymmetric unit is shown as a small red sphere. Potential hydrogen bonding interactions are depicted as black dashes. A black dash is also drawn between the heme iron and the carbon atom (C21) targeted for hydroxylation.

The two chains in the asymmetric unit exhibit minimal conformational ambiguity (RMSD = 0.26 Å). However, a few minor differences between chains A and B can be discerned. Notably, while **3** is bound in both monomers, the ethylaldehyde moiety adopts two different orientations relative to the rest of the macrocycle in chain A (**Figure 3.3B**). Moreover, E103 is found in slightly altered positions between the two chains; in both cases, however, the carboxylate is pointing away from the substrate and is completely solvent exposed. Finally, the binding pocket of **3** in chain A is more hydrated than that in chain B. Three water molecules overlap between the two chains, only one of which, located above the sugar near the surface of the protein, is poised to interact directly with **3** (see **Figure 3.3B** for potential interactions between this water molecule and polar groups on the mycaminose sugar of **3** depicted as black dashes).

TylHI exhibits an overall tertiary structure very similar to that of MycCI (RMSD = 0.76 Å; **Figures 3.3A/C** and **3.8A**) and many other P450 enzymes. In addition, despite some differences in chemical structure between the bound substrates for each of these two proteins, superposition of the two structures demonstrates that the carbon framework of **3** almost perfectly overlaps with that of M-VIII (**10**) bound in the MycCI active site (**Figure 3.8**). Like that of the latter, the binding pocket of TylHI is highly hydrophobic and accommodates the macrocyclic substrate bound diagonally above the distal face of the heme cofactor (**Figure 3.3B**). The primary methyl group (C23) is located within 3.8 Å of the heme iron center, and its orientation relative to the cofactor is consistent with the experimentally observed site of hydroxylation.

Like in MycCI, the base of the substrate proximal to the heme is surrounded by six hydrophobic residues (L111, L255, A259, A306, L309, and V410) that help to position it in the proper orientation for activation of the target C–H bond. With the exception of V410 (I378 in MycCI), these residues are identical to those found in MycCI and are located in the same relative positions (**Figure 3.3B/D**). Other amino acid side chains that form part of the hydrophobic wall of the binding pocket near the I helix (e.g., A195, L208, L211, V254, and A258) are also identical to those present in MycCI. Despite these similarities between the two proteins, key differences are readily apparent, which include the identity and relative positioning of several residues in the BC and FG loop regions. For example, smaller polar amino acids in TylHI (S107 and

T112) replace larger hydrophobic residues in MycCI (F76 and M81, respectively). In addition, S107 is notably positioned further away from the substrate compared with F76, illustrating only one of several similar instances in which the position and/or orientation of a particular residue in the BC loop is altered between the two structures (**Figures 3.3**, **3.4**, and **3.8**). Although more than half of the residues that make up the BC loop are conserved between MycCI and TylHI and many of the substitutions are relatively conservative, differences in the positions of several side chains that reflect deviations in the Cα backbone are evident. One particular region in the middle of the TylHI BC loop contains residues that closely approach bound **3** (S100-A106) as well as those whose positions are displaced relative to the homologous residues in MycCI (R96, E103, E105, S107, and R108 in TylHI corresponding to R65, D72, D74, F76, and R77 in MycCI; **Figures 3.4** and **3.8**).

Additional differences in amino acid composition and positioning are observed in the FG loop and N-terminal portion of the G helix, most markedly in substitutions of small residues (A199, A200, and G201 in TylHI) for larger polar/charged residues (N168, D169, and D170 in MycCI), insertion of a carboxylate (E202 in TylHI with no counterpart in MycCI), and charge reversal (E203 in TylHI in place of R171 in MycCI). However, the side chains of these amino acids do not interact with bound substrate in either structure, and the overall fold of the region is unperturbed.

The mycaminose binding pocket is composed of residues that are mostly found in the BC and FG loops of TylHI. These residues are typically more polar than those that make up the binding pocket for the rest of the macrocycle. A salt bridge network involving R96, D101, E105, and R310 is observed surrounding one side of the substrate proximal to the sugar (**Figure 3.4A**). Despite the presence of similar residues in MycCI (R65, D70, D74, and R278), they do not all interact to form a cohesive network around the desosamine unit of **10** (**Figure 3.4B**). While the D70-R278 interaction is present in MycCI, R65 and D74 are completely displaced out of the pocket and exposed to bulk solvent.

Specific polar interactions with **3** are confined to the aldehyde substituent and portions of the deoxyamino sugar (**Figure 3.4A**). In chain A, the electron density surrounding the ethylaldehyde moiety suggests that this part of the substrate adopts two

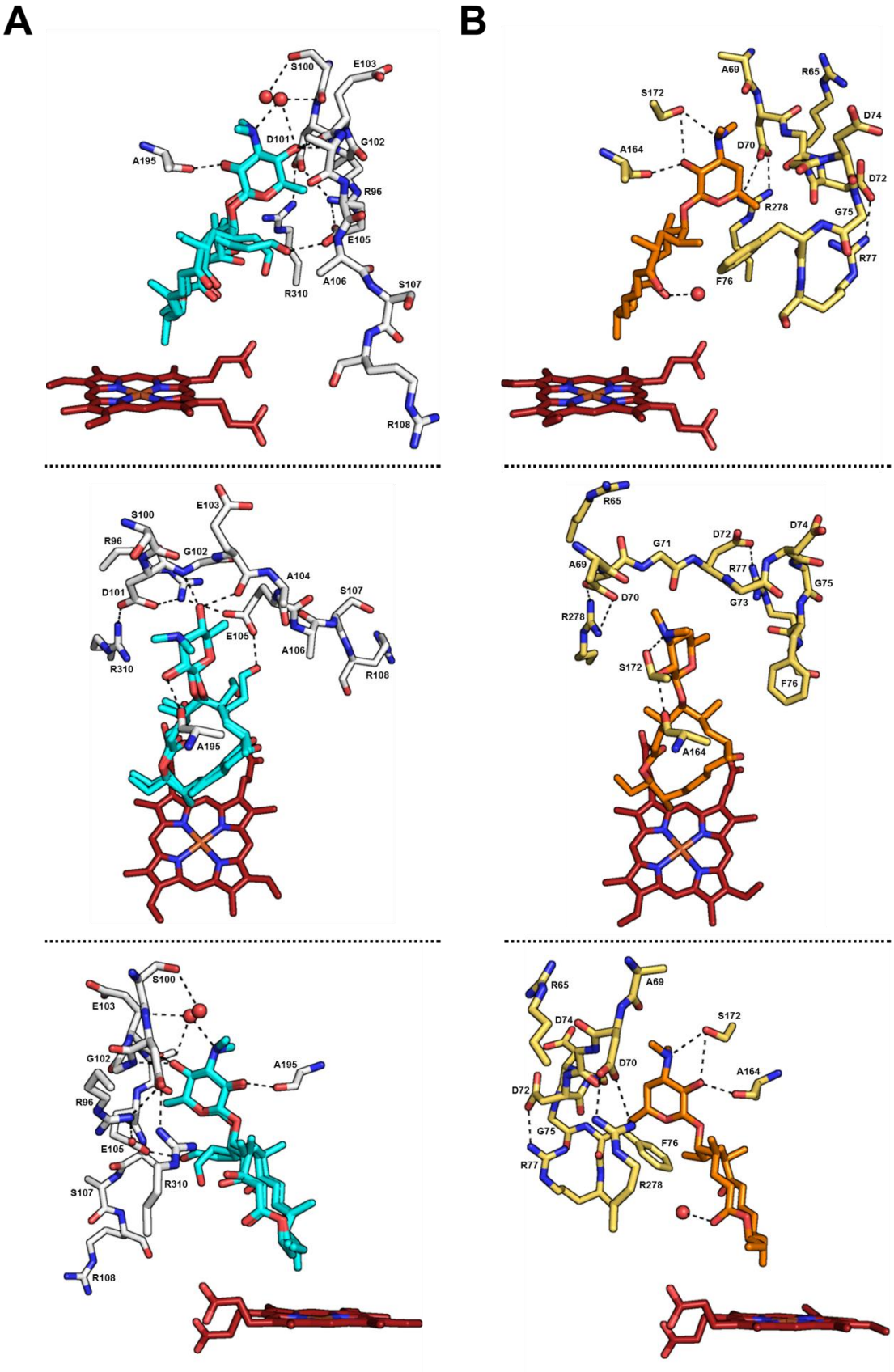
A
B
S100
E103
D101
G102
A195
R96
E105
A106
S107
R310
R108
A69
R65
S172
D74
A164
D70
D72
R278
G75
R77
F76
E103
S100
R96
G102
A104
D101
S107
E105
A106
R310
R108
A195
R65
D74
G71
D72
A69
R77
G75
D70
G73
R278
S172
F76
A164
S100
E103
A195
G102
R96
E105
R310
S107
R108
R65
A69
D74
S172
D70
A164
D72
G75
F76
R77
R278

Figure 3.4. Comparison of substrate contacts and other key interactions in the active sites of (**A**) TylHI and (**B**) MycCI. Substrates and amino acid residues are colored as in **Figure 3.3**. Main chain atoms are depicted for residues S100-R108 and A195 in TylHI and for residues A69-R77 and A164 in MycCI. Black dashes are drawn between atoms involved in potential polar contacts. For improved clarity, water molecules are omitted from the middle panels in each case.

different conformations when bound to TylHI. In the particular conformation closer to that observed in chain B, the carbonyl of the aldehyde is poised to accept a hydrogen bond from the side chain of E105 in its protonated form and/or a neighboring water molecule. However, given its proximity to R96, E105 likely exists in the deprotonated form more often, thus preventing it from acting as an effective hydrogen bond donor to the aldehyde. The possible lack of any significant polar interaction between these two functional groups is further substantiated by the presence of the other conformation of the aldehyde in chain A wherein the carbonyl oxygen is pointed away from the E105 carboxylate. Moreover, disruption of any potential interactions via modification of the substrate (*vide supra*) or site-directed mutagenesis (*vide infra*) has a relatively modest effect on enzymatic activity and substrate binding affinity, further supporting the idea that the aldehyde plays a marginal role as a substrate recognition element for TylHI. As previously demonstrated, when the aldehyde of **3** is reduced to a hydroxyl group, the resulting substrate (20-OH-MT, **8**) is readily accepted by TylHI, with no differences in turnover and only a minor decrease in binding affinity observed. While E105 can only act as a hydrogen bond donor to **3**, it can possibly accept a hydrogen bond from **8**. The complete lack of a suitable hydrogen bond donor or acceptor in the fully reduced substrate (MT, **2**) leads to partial disruption of effective binding, thereby moderately decreasing enzymatic conversion.

Two additional direct polar interactions between TylHI and bound **3** are localized to the mycaminose substituent (**Figure 3.4A**). As seen in the MycCI/**10** structure (**Figure 3.4B**), the 2'-hydroxyl group of the sugar donates a hydrogen bond to the backbone carbonyl of A195 (A164 in MycCI). Furthermore, the 4'-hydroxyl appended to mycaminose, but not to desosamine, interacts with the backbone amide nitrogen and carbonyl oxygen atoms of G102 and E103, respectively (**Figure 3.4A**). On the basis of the results of activity and binding assays with substrate analogs (*vide supra*), these polar interactions appear to be critical for substrate recognition in TylHI. Indeed, the

simple removal of the C4'-hydroxyl of mycaminose results in a drastic reduction in binding affinity and a concomitant decrease in substrate conversion.

It is also important to note that no direct interactions with the 3'-nitrogen of mycaminose are observed in either chain of the crystal structure. In MycCI, the side chain hydroxyl of S172 was shown to participate in potential hydrogen bonding interactions with the 3'-nitrogen as well as the adjacent 2'-hydroxyl of desosamine (**Figures 3.3D** and **3.4B**). However, the S172A mutant only minimally perturbed substrate binding and enzyme activity across a panel of desosaminylated substrates, suggesting that these interactions play a nominal role in substrate recognition.[34] In TylHI, the corresponding residue (A204) does not contain a polar side chain and thus cannot hydrogen bond with any functional groups on the deoxyamino sugar. Rather, a water molecule is located between the 3'-nitrogen and the 4'-hydroxyl of mycaminose, which in turn is positioned to interact with the backbone carbonyl oxygen of S100 (**Figure 3.4A**). The carboxylate of D101 in TylHI is located ~5 Å away from the 3'-nitrogen of mycaminose, which is not close enough to provide a salt bridge contact. In addition, because the negative charge of the D101 side chain is probably neutralized via interactions with R96 and R310, it likely plays a minimal role in helping to compensate for the positive charge of the protonated tertiary amine.

3.4 Analysis of TylHI site-directed mutants

Analysis of the TylHI/**3** cocrystal structure provided key insights into the molecular basis for substrate recognition, highlighting several notable differences from the homologous MycCI/**10** system. In order to validate and further probe the roles of certain amino acid residues in substrate binding, several mutants were generated and tested against the panel of six compounds previously described. The results of the activity and binding assays with **2** demonstrated that the aldehyde portion of the native substrate (**3**) does not provide a critical recognition element for TylHI. While the side chain of E105 is positioned to interact with the aldehyde in the crystal structure, the ambiguity surrounding the protonation state of the former as well as the conformation of the latter made it difficult to assign a definitive role for this residue. Therefore, several site-directed mutants were created, including E105Q and E105A. As expected, only

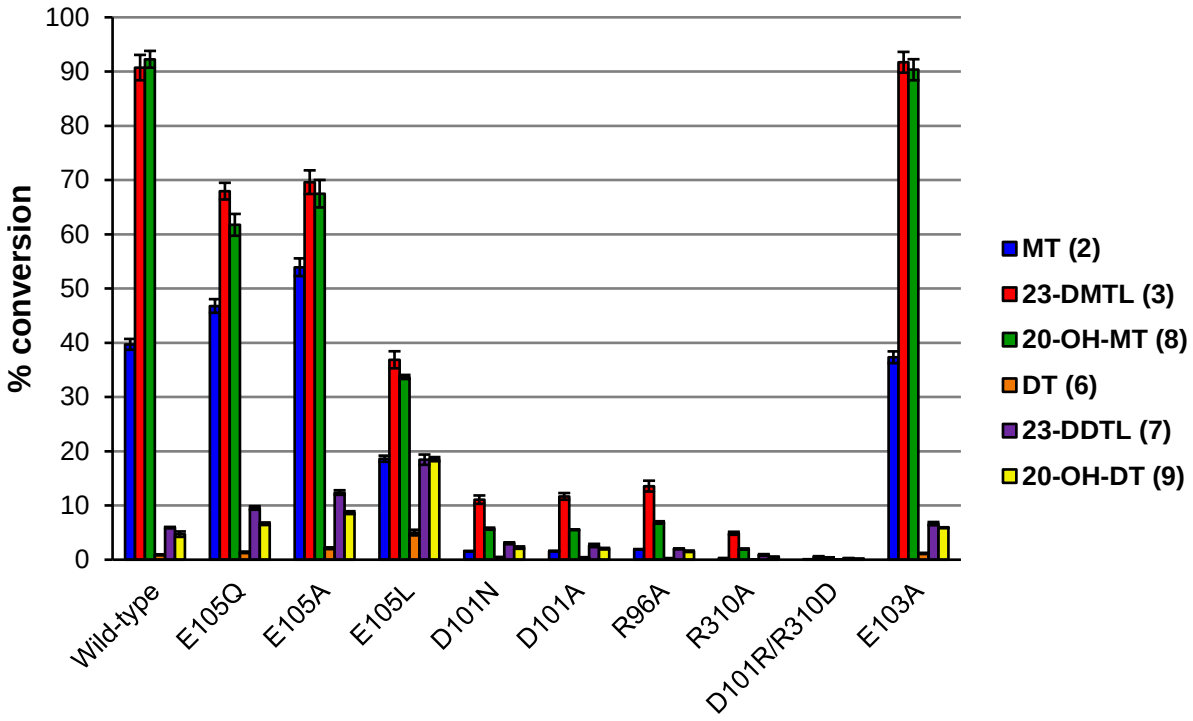

Figure 3.5. Results of activity assays with TylHI mutants and selected substrates. All reactions were carried out using MycCII and MBP-FdR as surrogate ferredoxin and ferredoxin reductase partners, respectively. See **Table B.2** for raw numerical values.

modest reductions in activity were observed for these mutants acting on **3** (~70% conversion for the mutants vs ~90% conversion for the wild-type) and its reduced analog **8** (**Figure 3.5** and **Table B.2**). However, activity marginally increased across the various other substrates tested. We initially anticipated that the E105A mutation might have a more substantial negative effect on activity due to the loss of key van der Waals interactions that could be stabilizing this region of the protein. Therefore, the E105L mutant was generated to control for any decrease in activity possibly resulting from disruption of these important intraprotein contacts. Interestingly, while activity on the mycaminosylated substrates (**2**, **3**, and **8**) decreased relative to the wild-type enzyme (e.g., 37% conversion of **3**), the E105L mutation conferred upon TylHI the ability to more effectively hydroxylate the desosaminylated substrates (**6**, **7**, and **9**; ~3-4-fold increased conversion compared with the wild-type; **Figure 3.5** and **Table B.2**). The loss of a negative charge and concomitant addition of a methyl group to the side chain of the target residue likely increased the hydrophobicity of the binding pocket, leading to better binding of suboptimal substrates bearing desosamine. Consistent with the results of the

activity assays, relatively minor decreases in affinity were associated with binding of **3** to each of the mutants (**Table 3.3**).

Table 3.3. Dissociation constants of 23-DMTL (**3**) against TylHI mutants.[a]

TylHI mutant	K_d (μM)
Wild-type	0.48 ± 0.03
E105Q	14.1 ± 0.8
E105A	4.3 ± 0.2
E105L	45 ± 3
D101N	195 ± 12
D101A	176 ± 17
R96A	139 ± 8
R310A	168 ± 9
D101R/R310D	351 ± 39
E103A	0.70 ± 0.04

[a]Reported errors are those obtained from fitting data averaged from experiments performed in duplicate.

Additional mutagenesis targets consisted of several charged residues in the BC loop forming part of the mycaminose binding pocket. One such residue (D101) was found in proximity to the *N*,*N*-dimethylamino group of the sugar, potentially helping to neutralize the positive charge associated with the protonated tertiary amine. However, any electrostatic interactions with adjacent basic residues (R96 and R310) would likely undermine its role in this capacity (**Figure 3.4A**). Both the D101N and D101A mutants exhibited substantial losses in activity across all substrates tested, with conversion of **3** diminishing to 11-12% and that of the other substrates falling at or below 6% (**Figure 3.5** and **Table B.2**). Binding of **3** was substantially weakened as well, with K_d values roughly equivalent to those observed for binding of the desosaminylated substrates to the wild-type enzyme (**Tables 3.1** and **3.3**). Nonetheless, these data alone were not enough to gain a complete understanding of the specific role of this residue in mediating substrate binding.

Since D101 is located in the middle of a potential salt bridge network involving R96 and R310 (**Figure 3.4A**), the latter residues were subsequently targeted for mutagenesis to explore whether further disruption of this network could be used to help explain attenuated substrate binding and turnover. Each of the corresponding arginine-to-alanine mutants showed a loss in catalytic activity that was comparable to that observed for the D101 mutants; R310A exhibited the most dramatic effect, with conversion of **3** under standard reaction conditions dropping to 5% (**Figure 3.5** and

Table B.2). The R96/R310 mutants also had substrate dissociation constants that were similar to those for the D101 mutants (**Table 3.3**). Incidentally, these values approached that for the corresponding aglycone (tylactone, **11**) binding to the wild-type enzyme (K_d **=** 284 μM; **Table 3.4**).

Taken together, these results are consistent with the important role of salt bridge contacts between R96, D101, and R310 in facilitating the formation of a binding pocket for the deoxyamino sugar moiety of the substrate. However, we cannot rule out the possibility that disruption of important van der Waals or hydrophobic interactions between the methylene units of the mutated arginine residues and other neighboring amino acids led to more general destabilization of the binding pocket. While this triad of charged residues is identical between TylHI and MycCI, only one salt bridge is preserved (D101-R310 in TylHI, corresponding to D70-R278 in MycCI). However, in contrast to the drastic loss in activity and substrate binding that TylHI incurred upon mutation of D101, no such impact was observed for D70 mutants of MycCI (**Table B.4**). Because MycCI is equipped to effectively bind substrates without deoxyamino sugars, any disruption of the binding pocket proximal to the sugar is likely to have a relatively insignificant effect.

While the results of the previous mutagenesis experiments suggest that the D101-R310 salt bridge interaction may play a key part in forming a functional binding pocket for mycaminose, it is unlikely to be sufficient for this purpose. The D101R/R310D double mutant of TylHI that was made to test this hypothesis expressed well and folded properly, but it was almost completely devoid of measurable activity (<1% conversion of **3** and K_d **=** 351 μM; **Figure 3.5**; **Tables B.2** and **3.3**). Although the effect of swapping these two charged residues on the overall structure of the binding pocket is uncertain, these data are consistent with the notion that interactions beyond D101-R310 play equally if not more important roles in shaping the enzyme active site.

Finally, analysis of the crystal structure demonstrated that the side chain of E103 did not form any specific contacts with substrate or other amino acids, appearing to be entirely exposed to bulk solvent. Nevertheless, given its spatial proximity to the other charged residues targeted for mutagenesis, we opted to generate and test the E103A mutant to verify that this residue was minimally involved in substrate binding and

catalysis. Consistent with our prediction, no effect on either parameter was observed (**Figure 3.5**; **Tables B.2** and **3.3**), helping to validate the reliability of the structural data we had obtained for TylHI bound to its native substrate.

3.5 Comparative analysis of the TylHI/MycCI homolog ChmHI

The results of biochemical experiments employing substrate analogs as well as the details of the crystal structure and functional effects of site-directed mutations described thus far had provided some important insights into the molecular basis for substrate recognition in TylHI and enriched our understanding of it as a highly specific enzyme compared with MycCI. However, it still proved difficult to rationalize why MycCI could bind and hydroxylate both mycinamicin-type and tylosin-type substrates whereas

Scheme 3.2. Roles of homologous P450s in the biosynthesis of 16-membered ring macrolides. (**A**) TylHI (P450) and TylHII (ferredoxin) involved in tylosin (**1**) biosynthesis. (**B**) MycCI (P450) and MycCII (ferredoxin) involved in mycinamicin II (**5**) biosynthesis. (**C**) ChmHI (P450) and ChmHII (ferredoxin) involved in chalcomycin (**12**) biosynthesis. (**D**) Possible alternative native substrate for ChmHI in the chalcomycin pathway.

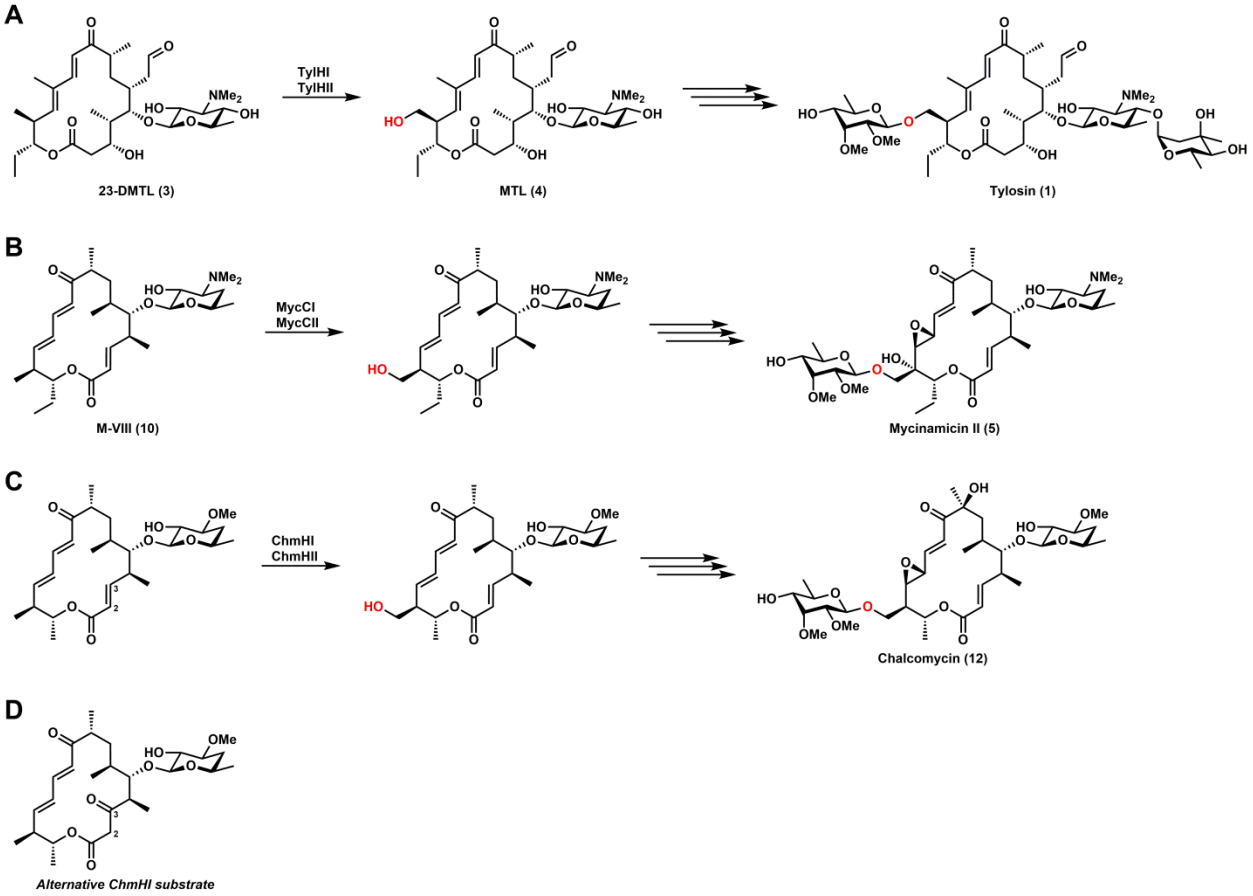

TylHI only showed appreciable activity on mycaminosylated forms of the latter. In an effort to further understand this observation, we identified ChmHI as a close homolog of both enzymes and tested its activity across a panel of macrolactone and macrolide substrates. This P450 is thought to play an analogous role in the biosynthesis of the macrolide chalcomycin (**12**) in *Streptomyces bikiniensis*, although the nature of its native substrate remains ambiguous (**Scheme 3.2C/D**).[45] Interestingly, multiple sequence alignment of the three homologous P450s reveals that ChmHI is roughly

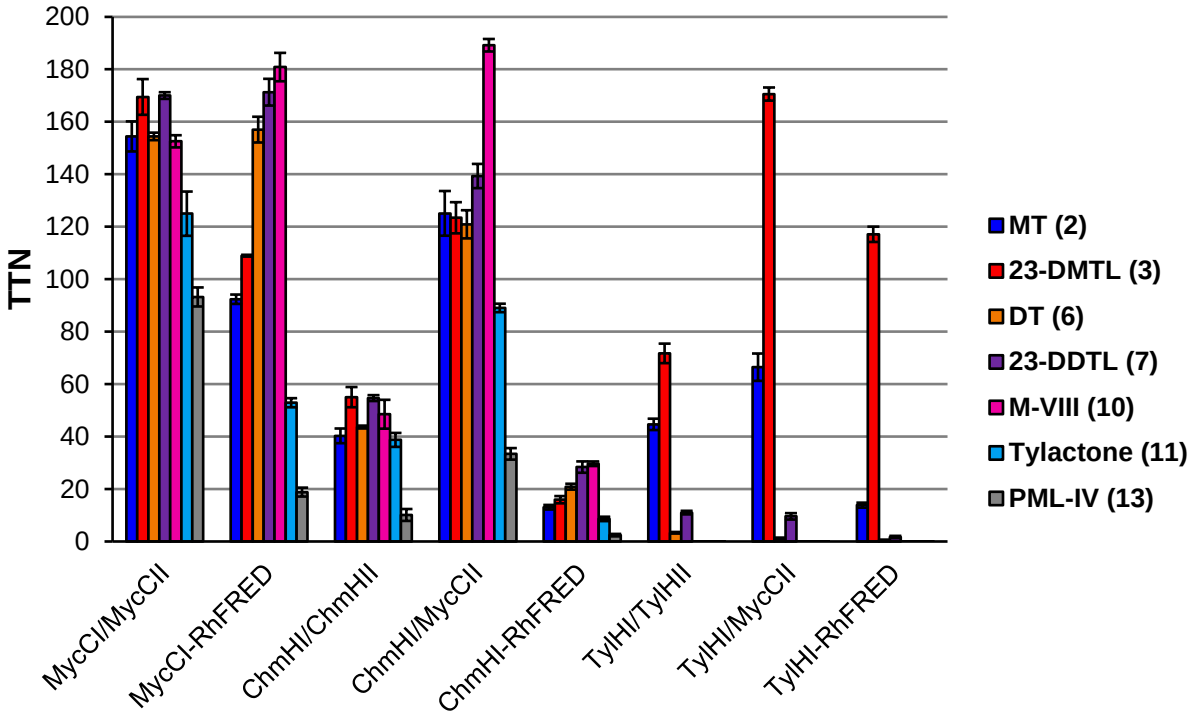

Figure 3.6. Total turnover numbers (TTNs) for enzymatic reactions involving MycCI, ChmHI, and TylHI acting in conjunction with different redox partners across a panel of selected substrates (structures shown in **Figure 3.1**). TTN = mol product/mol P450. MBP-FdR was used as surrogate ferredoxin reductase in all reactions not involving P450-RhFRED. See **Table B.5** for raw numerical values.

equally similar to both MycCI (62% identity) and TylHI (57% identity), with regions of identity and divergence scattered throughout the sequence (**Figure 3.7**). In addition, as for MycCI and TylHI, the gene encoding ChmHI is located adjacent to another that encodes a small [3Fe-4S]-type ferredoxin protein, ChmHII. Therefore, ChmHI paired with either ChmHII or the native MycCI ferredoxin (MycCII) was tested in parallel with

the catalytically self-sufficient ChmHI-RhFRED fusion protein as well as MycCI and TylHI against various macrolactone and macrolide substrates, including **3** and **10**.

Despite the absence of either of its purported native substrates from the panel, the functional activity of ChmHI was verified by its ability to convert each of the substrates tested to products with the same retention times as those of the corresponding MycCI and TylHI reactions, indicating that this P450 has a broad substrate scope similar to that of MycCI (**Figure 3.6** and **Table B.5**). As seen for TylHI, the overall activity of ChmHI was highest when it was partnered with MycCII instead of its native ChmHII, a result that was unsurprising given that the latter was found to suffer from some of the same expression and stability problems as TylHII. Curiously, ChmHI-RhFRED exhibited markedly low hydroxylation activity relative to the three-component catalytic systems across all substrates (**Figure 3.6** and **Table B.5**). Subsequent LC-MS analysis of the ChmHI-RhFRED reaction mixtures demonstrated that *N*-demethylation constituted a significant portion of the product profile for reactions involving glycosylated substrates (e.g., see **Table B.6** for LC-MS results of MycCI and ChmHI acting on the 14-membered ring macrolide narbomycin (**S2**)). Similar shifts in product distribution were observed for MycG when its activity was reconstituted with different combinations of redox partners.[46] Notably, these results suggest that ChmHI may be more inclined than MycCI and TylHI to bind its substrates in alternative conformations.

With these results in hand, we closely compared the sequences of each P450 to find any regions of similarity between MycCI and ChmHI as well as regions of divergence from TylHI (**Figure 3.7**). We envisioned that identifying these regions and mapping them onto the structures of MycCI and TylHI could yield some important clues regarding the sequence determinants for the differences in substrate scope between these enzymes. Altogether, there are 65 residues that are identical between MycCI and ChmHI but different from TylHI (an additional 2 residues are similar between MycCI/ChmHI and divergent from TylHI). These amino acid substitutions, nearly half of which represent conservative changes, are not localized to any particular region of the protein. Indeed, nonconserved patches are essentially evenly distributed throughout each of the protein sequences. Moreover, only 7 of the 65 identified residues are located near bound substrate. Among these seven, four form a near-contiguous stretch

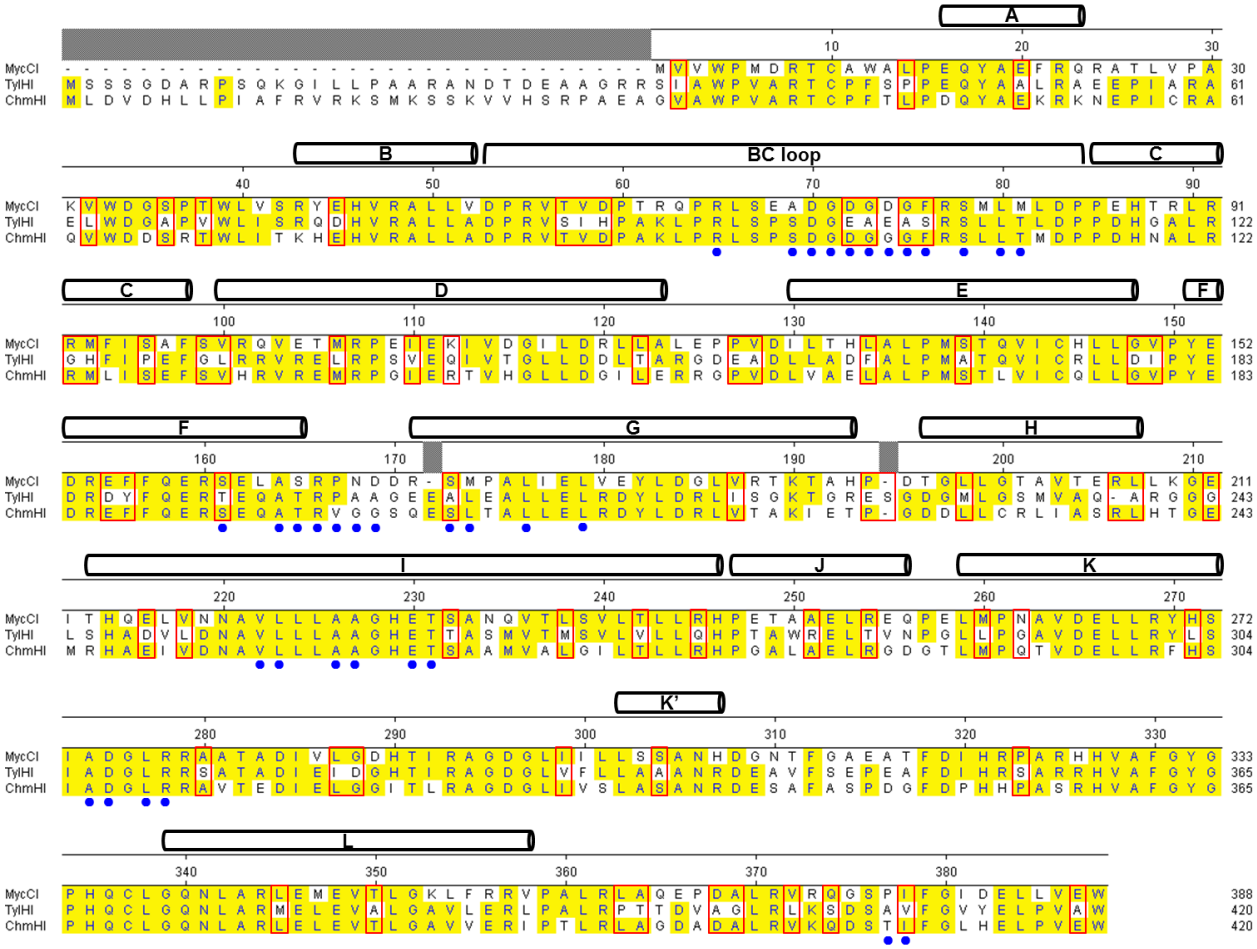

Figure 3.7. Multiple sequence alignment of MycCI, TylHI, and ChmHI. Conserved secondary structural elements (α-helices) based on the structures of MycCI and TylHI are depicted above the sequences. Residues highlighted in yellow match the consensus sequence. Red boxes enclose residues that are identical or similar between MycCI and ChmHI but divergent from TylHI. Blue circles are located below residues found within 5 Å of bound substrate in the MycCI and TylHI crystal structures.

in the middle of the BC loop while the other three stand alone in the F/G helices and the C-terminal loop region comprising substrate recognition site 6 (SRS6).[47] While the differences in the physical and chemical properties of these residues between MycCI/ChmHI and TylHI are minimal, examination of the MycCI and TylHI crystal structures reveals that the relative positions and conformations of the amino acids in the BC loop are quite different (**Figures 3.4** and **3.8**). Additionally, a serine residue (S107) in TylHI replaces phenylalanine (F76) in MycCI, although alignment of the two structures shows that the latter residue occupies a space that more closely overlaps with that occupied by A106 in TylHI.

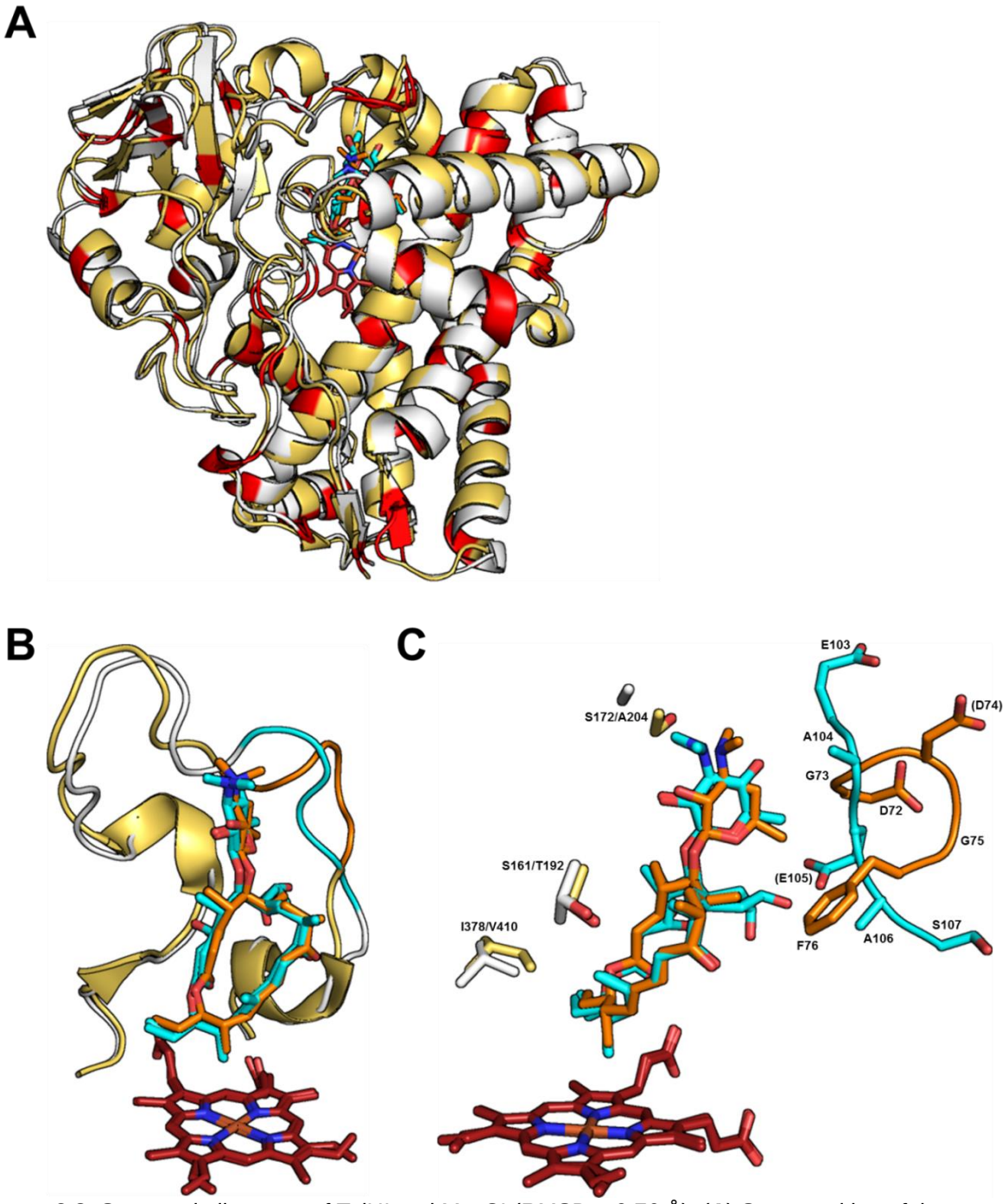

Figure 3.8. Structural alignment of TylHI and MycCI (RMSD = 0.76 Å). (**A**) Superposition of the overall tertiary structures of TylHI (white) and MycCI (yellow-orange). Regions of identity between MycCI/ChmHI and divergence from TylHI are highlighted in red (see **Figure 3.7**). (**B**) Overlay of the binding pockets of **3** (cyan) and **10** (orange) showing the BC loops of TylHI (white/cyan) and MycCI (yellow-orange/orange). The entire BC loop as well as the regions colored in cyan (TylHI) and orange (MycCI) were targeted for chimeragenesis. (**C**) Alternative view of the substrate binding pockets depicting the five-residue stretch of the BC loop targeted for chimeragenesis with side chains shown (same coloring scheme as in **B**). In addition, the side chains of the three remaining residues located in proximity to bound substrate that are identical between MycCI/ChmHI and different from TylHI are shown in white (TylHI) and yellow-orange (MycCI).

In P450s, the region between the B and C helices (referred to here as the BC loop, but it can include additional secondary structural elements like the B' helix found in many P450 isoforms) comprises an important substrate recognition site (SRS1)[47] and has been well documented as a region that plays an important role in influencing the substrate specificity of these enzymes.[48] The BC loop exhibits a high level of variability in terms of both primary sequence and three-dimensional conformation between different P450 isoforms, features that are thought to influence the selectivity of these enzymes for a broad range of substrates.[4,48,49] Significant movements involving the BC loop as well as the F/G helices and FG loop are associated with the open/close transitions of P450s that are implicated in substrate binding and catalysis.[4,49,50] The specific sequence and length of the BC loop could significantly impact the ability of certain substrates to bind productively in the active site by influencing the conformational flexibility of this region of the enzyme prior to substrate binding as well as by dictating the identities of specific residues that come into contact with the substrate once it has bound.[48,50] It has been hypothesized that the presence of a sufficiently flexible BC loop is important for the ability of some bacterial P450s to bind large, bulky molecules such as macrolides.[51,52] Furthermore, the identities of specific residues that reside in the BC loop can prove critical for proper substrate recognition (e.g., acidic residues in PikC[52]). Targeted mutations in the BC loop have been shown to impact the substrate scope as well as the regio- and stereoselectivity properties of several P450s.[53-60] On the basis of this knowledge, we set out to generate TylHI/MycCI chimeras in order to probe the role of the BC loop in affecting substrate specificity for these enzymes.

3.6 TylHI/MycCI chimeragenesis

Chimeragenesis is a method that involves replacing a set of amino acid residues in one protein with a homologous set from another protein. Traditionally, the goal of such an approach has been to acquire a clearer understanding of the roles that individual structural elements play in determining the substrate specificity and selectivity of a target enzyme. Before structures of many P450s were readily available, site-directed mutagenesis was commonly employed to determine specific amino acid

substitutions that could impart the function of one enzyme to another.[61] A number of these studies focused on trying to understand structure-function relationships among mammalian P450s with a particular emphasis on clarifying the roles of certain residues and protein subdomains in conferring distinct properties on P450s of the same subfamily (≥55% sequence identity).[62] In several exceptional cases, a single residue has been found to control the substrate specificity and even regio- and stereoselectivity of a given P450.[53,63-67] Chimeragenesis experiments are typically performed using P450s that are close homologs in order to increase the likelihood that the resulting chimeras will fold properly and exhibit catalytic activity, but useful computational algorithms have been developed to facilitate the generation of functional chimeras from proteins that have lower sequence identity.[68-71] One representative set of chimeragenesis experiments was performed using two unrelated P450s: the bacterial fatty acid hydroxylase CYP102A1 ($P450_{BM3}$) and the insect terpenoid hydroxylase CYP4C7.[72-74] It was found that replacing short contiguous strings of residues in the SRS1 and SRS5 regions of $P450_{BM3}$ with those from CYP4C7 could shift the selectivity of the former from fatty acids to farnesol, the native substrate of the latter. In addition, this approach was used to modulate the regioselectivity of oxidation of these substrates.

Following these robust precedents, we elected to generate TylHI/MycCI chimeras in order to acquire a better understanding of the role of the BC loop in influencing the notable differences in substrate specificity between these two proteins. In each of these enzymes, the BC loop consists of 32 residues, 15 of which vary between the two (**Figure 3.7**). In a first set of experiments, the entire loop region of TylHI was replaced with that of MycCI, and the resulting chimera (designated TylHI($MycCI_{T57\text{-}M81}$)) was expressed, purified, and tested against several tylosin- and mycinamicin-type 16-membered ring substrates. Remarkably, the chimera was able to convert all of the macrolide substrates to the appropriate monohydroxylated products, standing in stark contrast to the inability of wild-type TylHI to readily accept macrolides beyond those bearing mycaminose as the pendant deoxyamino sugar (**Figure 3.9** and **Table B.2**). Notably, while conversion of the native substrate **3** and its reduced analog **8** decreased, TylHI($MycCI_{T57\text{-}M81}$) turned over desosaminylated substrates (**6**, **7**, and **9**) with comparable efficiency to mycaminosylated substrates (**2**, **3**, and **8**). Moreover, whereas

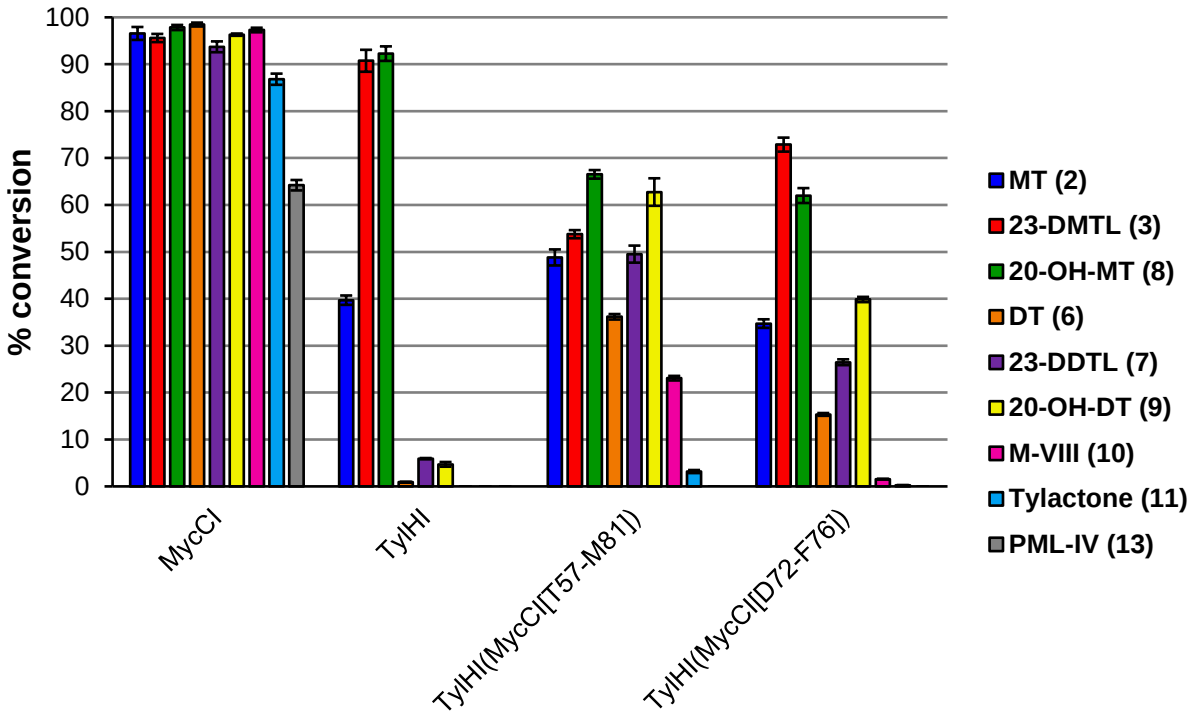

Figure 3.9. Results of activity assays with MycCI, TylHI, and MycCI/TylHI chimeras. All reactions were performed using MycCII and MBP-FdR as surrogate ferredoxin and ferredoxin reductase partners, respectively. See **Table B.2** for raw numerical values.

TylHI could scarcely bind the native substrate for MycCI (**10**), the chimera exhibited appreciable activity on this compound (23% conversion). It also displayed a low-level ability to hydroxylate the aglycone **11** (3% conversion), but it showed no activity on PML-IV (**13**). Subsequent substrate titration experiments demonstrated that all of the macrolides investigated bound with similar affinities (K_d = 19-39 μM; **Table 3.4**). While the binding affinity for **3** decreased considerably for the chimera relative to the wild-type, it stayed about the same for **2** while markedly improving for **6**, **7**, and **10**. Interestingly, **11** did not bind significantly more tightly to TylHI(MycCI$_{T57-M81}$) than to wild-type TylHI despite the ability of the former to hydroxylate this substrate, albeit to a small extent.

Encouraged by these results, we decided to further investigate a smaller portion of the BC loop previously identified as containing residues proximal to bound substrate that are shared by MycCI and ChmHI but not TylHI (**Figures 3.7** and **3.8**). Thus, the following amino acid substitutions were simultaneously introduced to TylHI, generating a chimera designated TylHI(MycCI$_{D72-F76}$): E103D, A104G, E105D, A106G, and S107F. The purified protein was roughly intermediate between wild-type TylHI and

TylHI(MycCI$_{T57\text{-}M81}$) in terms of overall activity across the substrates tested (**Figure 3.9** and **Table B.2**). Whereas relatively modest decreases in conversion were observed for mycaminosylated compounds (**2**, **3**, and **8**), TylHI(MycCI$_{D72\text{-}F76}$) was still considerably more active than wild-type TylHI on those bearing desosamine (**6**, **7**, and **9**). However, it did not turn over these substrates to the same extent as TylHI(MycCI$_{T57\text{-}M81}$), and its activity on **10** and **11** was more substantially diminished. Despite the inability to completely recapitulate the effect that replacement of the entire BC loop had on the

Table 3.4. Dissociation constants of selected substrates against TylHI and TylHI/MycCI chimeras.[a]

	Enzyme		
Substrate	TylHI (wild-type)	TylHI(MycCI$_{T57\text{-}M81}$)	TylHI(MycCI$_{D72\text{-}F76}$)
2	26 ± 5	20.0 ± 1.0	3.4 ± 0.2
3	0.48 ± 0.03	35 ± 2	2.5 ± 0.1
8	3.5 ± 0.3	--[b]	--
6	154 ± 12	24.3 ± 0.9	6.7 ± 0.4
7	271 ± 17	39 ± 2	25 ± 1
9	201 ± 19	--	--
10	686 ± 72	19 ± 1	162 ± 5
11	284 ± 16	254 ± 16	208 ± 10
13	N.B.[c]	N.B.	N.B.

[a] K_d values are in μM. Reported errors are those obtained from fitting data averaged from experiments performed in duplicate.
[b] Blank space (--) indicates that the corresponding binding experiment was not performed.
[c] N.B. = no binding detected.

catalytic activity of TylHI, the results of experiments with TylHI(MycCI$_{D72\text{-}F76}$) demonstrate that this particular region of the BC loop plays an important role in controlling the preference for the enzyme to bind mycaminosylated vs desosaminylated substrates. This finding becomes more apparent upon analysis of the binding data, which show that **6** and **7** bind with even higher affinities to TylHI(MycCI$_{D72\text{-}F76}$) than to TylHI(MycCI$_{T57\text{-}M81}$), representing more than an order of magnitude decrease in K_d values compared with those of wild-type TylHI (**Table 3.4**). However, in combination with the five-residue section targeted in these experiments, another region of the BC loop appears to play a role in conferring on TylHI(MycCI$_{T57\text{-}M81}$) the ability to more tightly bind **10**.

In MycCI, the only discernable contacts with desosamine occur between the 2'-hydroxyl and the backbone carbonyl of A164 as well as the 3'-nitrogen and the side chain hydroxyl of S172 (**Figure 3.4B**). Hydrophobic interactions with other nearby

residues (e.g., M81, M173, L176) may also contribute to the favorable energetics of binding associated with substrates bearing the desosamine moiety (K_d (**10**) = 0.001 μM vs K_d (**13**) = 19 μM). Although the mycaminose binding pocket in TylHI does not appear to differ drastically from the desosamine binding pocket in MycCI in terms of residue composition, it has been specifically tailored to bind only one of these deoxyamino sugars. On the basis of the chimeragenesis experiments, residues 103-107 in the BC loop of TylHI are of significant importance in this regard. Nonetheless, it is not immediately clear from a purely structural perspective why this is the case. Substitution of phenylalanine for serine at position 107 may provide additional hydrophobic contacts with the substrate, a possibility that is supported by the marginally tighter binding of tylactone (**11**) to TylHI(MycCI$_{D72\text{-}F76}$) (K_d = 208 μM) than to the wild-type enzyme (K_d = 284 μM). In MycCI, highly favorable binding of the core macrocycle alone renders the identity or even presence of the sugar relatively insignificant for substrate binding and subsequent turnover.[34] A more likely explanation relates to the higher degree of flexibility that the BC loop adopts in acquiring two additional glycine residues (i.e., A104G and A106G). As previously mentioned, the flexibility of this region of the enzyme can have a notable impact on substrate entry and binding, at least in part due to its effect on the nature of the active site access channel.[4,49] Thus, specific contacts with the deoxyamino sugar that are established upon substrate binding may be of secondary importance to the rate at which substrate is able to bind. Increased flexibility of the BC loop might allow for faster binding due to its ability to more easily sample different conformational states, including those that are more open and thereby more conducive to substrate entry into the active site. To validate this hypothesis, the kinetics of substrate binding to wild-type TylHI and to each of the chimeras could easily be assessed using stopped-flow spectrophotometry. Molecular dynamics simulations would also provide further insights into how differences in residue composition of the BC loop affect the conformational dynamics of this region of the protein.

On the basis of the results acquired thus far, we have seen that rational design of chimeric proteins has provided a robust experimental platform for beginning to understand the differences in substrate scope between MycCI and TylHI. However, further experiments in this vein will certainly be needed in order to start closing some of

the additional gaps that remain in our knowledge of the molecular basis for this divergence in enzymatic function. Although we have partially answered the question of why only MycCI can bind two different types of macrolide substrates and is indifferent to the identity of the appended deoxyamino sugar, the nature of its ability to effectively bind macrolactone aglycones is still unknown. Several additional sites, including those in the F (MycCI$_{S161}$/TylHI$_{T192}$) and G (MycCI$_{S172}$/TylHI$_{A204}$) helices and in SRS6 (MycCI$_{I378}$/TylHI$_{V410}$) (**Figure 3.8C**), will serve as prime targets for forthcoming mutagenesis studies. Beyond those probed in the BC loop exchange experiments already described, these residues are shared between MycCI and ChmHI and may interact directly with substrate in the binding pocket. In particular, we speculate that the additional methyl group provided by I378 in MycCI will prove to be an important feature that contributes to the ability of this enzyme to tightly bind macrolactone substrates. Nevertheless, it is likely that many questions will remain even after carrying out these targeted mutagenesis experiments. Indeed, an important lesson that can be derived from numerous directed evolution campaigns on P450s and other enzymes is that mutations at remote sites on the protein scaffold can have dramatic and otherwise unexpected effects on catalytic activity.[75-78]

It is tempting to speculate on the evolutionary relationship between homologous yet functionally distinct enzymes like MycCI and TylHI. In natural as well as in laboratory evolution, a “generalist” enzyme capable of accepting a broad range of substrates with suboptimal efficiency often serves as an early intermediate en route toward a “specialist” that exhibits high activity on one or a few substrates.[78,79] Thus, one might hypothesize that MycCI represents a generalist intermediate in an evolutionary trajectory leading from one specialist enzyme to another whereas TylHI is a specialist that has already reached its evolutionary “endpoint.” However, the question of why MycCI displays a high level of activity on a range of substrates comparable to that of TylHI on its native substrate remains to be answered. Another intriguing question relates to the evolutionary history of the CYP105L subfamily of P450s, which includes MycCI, TylHI, ChmHI, and a few others. Is the common ancestor of these enzymes a generalist like MycCI or a specialist like TylHI? One may be tempted to answer in favor of the former, but the other option is certainly plausible. As the chimeragenesis

experiments demonstrated, it is quite feasible to produce a generalist from a specialist through the manipulation of a few key residues.

3.7 Conclusions and future directions

Through a synergistic combination of biochemical and structural characterization experiments, we have begun to unravel the molecular-level details underpinning the unique catalytic divergence of two homologous biosynthetic P450s. Activity and binding assays employing substrate analogs revealed that mycaminose acts as a more important recognition element for TylHI than the aldehyde substituent of its native substrate, 23-DMTL (**3**). The crystal structure of this enzyme bound to the latter exhibited few differences from that of MycCI bound to M-VIII (**10**) with the exception of the identities and relative positions/conformations of a few residues in the BC and FG loop regions. Certain acidic and basic residues interacting to form a possible salt bridge network proximal to the deoxyamino sugar were shown by site-directed mutagenesis to play key roles in substrate binding and catalysis. However, few direct contacts with bound substrate were observed; directly apparent polar interactions with mycaminose were limited to hydrogen bonds formed between the two hydroxyl groups on the sugar and polar atoms of backbone amide bonds. Finally, comparative analysis of the homolog ChmHI aided in selecting specific regions of TylHI to replace with those of MycCI, allowing for the generation of functional chimeras that provided new insight into the importance of the BC loop in regulating the substrate flexibility of these two enzymes. Work is currently ongoing to further hone in on specific residues that contribute to the notable differences in substrate scope between MycCI and TylHI.

3.8 References

(1) Brodie, B. B., Axelrod, J., Cooper, J. R., Gaudette, L., La Du, B. N., Mitoma, C., and Udenfriend, S. (1955) Detoxication of drugs and other foreign compounds by liver microsomes. *Science 121*, 603–604.

(2) Klingenberg, M. (1958) Pigments of rat liver microsomes. *Arch. Biochem. Biophys. 75*, 376–386.

(3) Garfinkel, D. (1958) Studies on pig liver microsomes. I. Enzymic and pigment composition of different microsomal fractions. *Arch. Biochem. Biophys. 77*, 493–509.

(4) Ortiz de Montellano, P. R. (Ed.). (2015) Cytochrome P450: structure, mechanism, and biochemistry 4th ed. Springer.

(5) Munro, A. W., Girvan, H. M., Mason, A. E., Dunford, A. J., and McLean, K. J. (2013) What makes a P450 tick? *Trends Biochem. Sci. 38*, 140–150.

(6) Meunier, B., de Visser, S. P., and Shaik, S. (2004) Mechanism of oxidation reactions catalyzed by cytochrome P450 enzymes. *Chem. Rev. 104*, 3947–3980.

(7) Denisov, I. G., Makris, T. M., Sligar, S. G., and Schlichting, I. (2005) Structure and chemistry of cytochrome P450. *Chem. Rev. 105*, 2253–2277.

(8) Guengerich, F. P. (2001) Common and uncommon cytochrome P450 reactions related to metabolism and chemical toxicity. *Chem. Res. Toxicol. 14*, 611–650.

(9) Cryle, M. J., Stok, J. E., and De Voss, J. J. (2003) Reactions catalyzed by bacterial cytochromes P450. *Aust. J. Chem. 56*, 749–762.

(10) Isin, E. M., and Guengerich, F. P. (2007) Complex reactions catalyzed by cytochrome P450 enzymes. *Biochim. Biophys. Acta 1770*, 314–329.

(11) Guengerich, F. P., and Munro, A. W. (2013) Unusual cytochrome P450 enzymes and reactions. *J. Biol. Chem. 288*, 17065–17073.

(12) Kelly, S. L., Lamb, D. C., Jackson, C. J., Warrilow, A. G. S., and Kelly, D. E. (2003) The biodiversity of microbial cytochromes P450. *Adv. Microb. Physiol. 47*, 131–186.

(13) Lamb, D. C., Ikeda, H., Nelson, D. R., Ishikawa, J., Skaug, T., Jackson, C., Omura, S., Waterman, M. R., and Kelly, S. L. (2003) Cytochrome P450 complement (CYPome) of the avermectin-producer *Streptomyces avermitilis* and comparison to that of *Streptomyces coelicolor* A3(2). *Biochem. Biophys. Res. Commun. 307*, 610–619.

(14) Parajuli, N., Basnet, D. B., Lee, H. C., Sohng, J. K., and Liou, K. (2004) Genome analyses of *Streptomyces peucetius* ATCC 27952 for the identification and comparison of cytochrome P450 complement with other *Streptomyces*. *Arch. Biochem. Biophys. 425*, 233–241.

(15) Podust, L. M., and Sherman, D. H. (2012) Diversity of P450 enzymes in the biosynthesis of natural products. *Nat. Prod. Rep. 29*, 1251–1266.

(16) Rudolf, J. D., Chang, C.-Y., Ma, M., and Shen, B. (2017) Cytochromes P450 for natural product biosynthesis in *Streptomyces*: sequence, structure, and function. *Nat. Prod. Rep.* DOI: 10.1039/c7np00034k.

(17) Fujii, Y., Hirosue, S., Fujii, T., Matsumoto, N., Agematu, H., and Arisawa, A. (2006) Hydroxylation of oleanolic acid to queretaroic acid by cytochrome P450 from *Nonomuraea recticatena*. *Biosci. Biotechnol. Biochem. 70*, 2299–2302.

(18) Kabumoto, H., Miyazaki, K., and Arisawa, A. (2009) Directed evolution of the actinomycete cytochrome P450 MoxA (CYP105) for enhanced activity. *Biosci. Biotechnol. Biochem. 73*, 1922–1927.

(19) Xue, Y., Wilson, D., Zhao, L., Liu, H.-w., and Sherman, D. H. (1998) Hydroxylation of macrolactones YC-17 and narbomycin is mediated by the *pikC*-encoded cytochrome P450 in *Streptomyces venezuelae*. *Chem. Biol. 5*, 661–667.

(20) Moody, S. C., and Loveridge, E. J. (2014) CYP105—diverse structures, functions and roles in an intriguing family of enzymes in *Streptomyces*. *J. Appl. Microbiol. 117*, 1549–1563.

(21) McGuire, J. M., Boniece, W. S., Higgens, C. E., Hoehn, M. M., Stark, W. M., Westhead, J., and Wolfe, R. N. (1961) Tylosin, a new antibiotic. I. Microbiological studies. *Antibiot. Chemother. 11*, 320–327.

(22) Pape, H., and Brillinger, G. U. (1973) Metabolic products of microorganisms. 113. Biosynthesis of thymidine diphospho mycarose in a cell-free system from *Streptomyces rimosus*. *Arch. Mikrobiol. 88*, 25–35.

(23) Jensen, A. L., Darken, M. A., Schultz, J. S., and Shay, A. J. (1963) Relomycin: flask and tank

fermentation studies. *Antimicrob. Agents Chemother. 161*, 49–53.
(24) Seno, E. T., Pieper, R. L., and Huber, F. M. (1977) Terminal stages in the biosynthesis of tylosin. *Antimicrob. Agents Chemother. 11*, 455–461.
(25) Baltz, R. H., and Seno, E. T. (1981) Properties of *Streptomyces fradiae* mutants blocked in biosynthesis of the macrolide antibiotic tylosin. *Antimicrob. Agents Chemother. 20*, 214–225.
(26) Seno, E. T., and Baltz, R. H. (1981) Properties of *S*-adenosyl-L-methionine:macrocin *O*-methyltransferase in extracts of *Streptomyces fradiae* strains which produce normal or elevated levels of tylosin and in mutants blocked in specific *O*-methylations. *Antimicrob. Agents Chemother. 20*, 370–377.
(27) Seno, E. T., and Baltz, R. H. (1982) *S*-adenosyl-L-methionine: macrocin *O*-methyltransferase activities in a series of *Streptomyces fradiae* mutants that produce different levels of the macrolide antibiotic tylosin. *Antimicrob. Agents Chemother. 21*, 758–763.
(28) Omura, S., Sadakane, N., and Matsubara, H. (1982) Bioconversion and biosynthesis of 16-membered macrolide antibiotics. XXII. Biosynthesis of tylosin after protylonolide formation. *Chem. Pharm. Bull. 30*, 223–229.
(29) Omura, S., Tanaka, H., and Tsukui, M. (1982) Biosynthesis of tylosin: oxidations of 5-*O*-mycaminosylprotylonolide at C-20 and C-23 with a cell-free extract from *Streptomyces fradiae*. *Biochem. Biophys. Res. Commun. 107*, 554–560.
(30) Baltz, R. H., Seno, E. T., Stonesifer, J., and Wild, G. M. (1983) Biosynthesis of the macrolide antibiotic tylosin: a preferred pathway from tylactone to tylosin. *J. Antibiot. 36*, 131–141.
(31) Omura, S., Tomoda, H., Yamamoto, S., Tsukui, M., and Tanaka, H. (1984) Studies on two dioxygenases involved in the synthesis of tylosin in *Streptomyces fradiae*. *Biochim. Biophys. Acta 802*, 141–147.
(32) Baltz, R. H., and Seno, E. T. (1988) Genetics of *Streptomyces fradiae* and tylosin biosynthesis. *Annu. Rev. Microbiol. 42*, 547–574.
(33) Cundliffe, E., Bate, N., Butler, A., Fish, S., Gandecha, A., and Merson-Davies, L. (2001) The tylosin-biosynthetic genes of *Streptomyces fradiae*. *Antonie Van Leeuwenhoek 79*, 229–234.
(34) DeMars, M. D., II, Sheng, F., Park, S. R., Lowell, A. N., Podust, L. M., and Sherman, D. H. (2016) Biochemical and structural characterization of MycCI, a versatile P450 biocatalyst from the mycinamicin biosynthetic pathway. *ACS Chem. Biol. 11*, 2642–2654.
(35) Lowell, A. N., DeMars, M. D., II, Slocum, S. T., Yu, F., Anand, K., Chemler, J. A., Korakavi, N., Priessnitz, J. K., Park, S. R., Koch, A. A., Schultz, P. J., and Sherman, D. H. (2017) Chemoenzymatic total synthesis and structural diversification of tylactone-based macrolide antibiotics through late-stage polyketide assembly, tailoring, and C—H functionalization. *J. Am. Chem. Soc. 139*, 7913–7920.
(36) Bate, N., Butler, A. R., Gandecha, A. R., and Cundliffe, E. (1999) Multiple regulatory genes in the tylosin biosynthetic cluster of *Streptomyces fradiae*. *Chem. Biol. 6*, 617–624.
(37) Bignell, D. R. D., Bate, N., and Cundliffe, E. (2007) Regulation of tylosin production: role of a TylP-interactive ligand. *Mol. Microbiol. 63*, 838–847.
(38) Kedzie, K. M., Philpot, R. M., and Halpert, J. R. (1991) Functional expression of mammalian cytochromes P450IIB in the yeast *Saccharomyces cerevisiae*. *Arch. Biochem. Biophys. 291*, 176–186.
(39) Ryan, R., Grimm, S. W., Kedzie, K. M., Halpert, J. R., and Philpot, R. M. (1993) Cloning, sequencing, and functional studies of phenobarbital-inducible forms of cytochrome P450 2B and 4B expressed in rabbit kidney. *Arch. Biochem. Biophys. 304*, 454–463.
(40) Grimm, S. W., Dyroff, M. C., Philpot, R. M., and Halpert, J. R. (1994) Catalytic selectivity and mechanism-based inactivation of stably expressed and hepatic cytochromes P450 2B4 and 2B5: implications of the cytochrome P450 2B5 polymorphism. *Mol. Pharmacol. 46*, 1090–1099.
(41) Li, X., Baudry, J., Berenbaum, M. R., and Schuler, M. A. (2004) Structural and functional divergence of insect CYP6B proteins: from specialist to generalist cytochrome P450. *Proc. Natl. Acad. Sci. USA 101*, 2939–2944.
(42) Haslinger, K., Maximowitsch, E., Brieke, C., Koch, A., and Cryle, M. J. (2014) Cytochrome P450 $OxyB_{tei}$ catalyzes the first phenolic coupling step in teicoplanin biosynthesis. *ChemBioChem 15*, 2719–2728.
(43) Ma, J., Wang, Z., Huang, H., Luo, M., Zuo, D., Wang, B., Sun, A., Cheng, Y.-Q., Zhang, C., and Ju, J. (2011) Biosynthesis of himastatin: assembly line and characterization of three cytochrome

P450 enzymes involved in the post-tailoring oxidative steps. *Angew. Chem. Int. Ed. 50*, 7797–7802.
(44) Zhang, H., Chen, J., Wang, H., Xie, Y., Ju, J., Yan, Y., and Zhang, H. (2013) Structural analysis of HmtT and HmtN involved in the tailoring steps of himastatin biosynthesis. *FEBS Lett. 587*, 1675–1680.
(45) Ward, S. L., Hu, Z., Schirmer, A., Reid, R., Revill, W. P., Reeves, C. D., Petrakovsky, O. V., Dong, S. D., and Katz, L. (2004) Chalcomycin biosynthesis gene cluster from *Streptomyces bikiniensis*: novel features of an unusual ketolide produced through expression of the *chm* polyketide synthase in *Streptomyces fradiae*. *Antimicrob. Agents Chemother. 48*, 4703–4712.
(46) Zhang, W., Liu, Y., Yan, J., Cao, S., Bai, F., Yang, Y., Huang, S., Yao, L., Anzai, Y., Kato, F., Podust, L. M., Sherman, D. H., and Li, S. (2014) New reactions and products resulting from alternative interactions between the P450 enzyme and redox partners. *J. Am. Chem. Soc. 136*, 3640–3646.
(47) Gotoh, O. (1992) Substrate recognition sites in cytochrome P450 family 2 (CYP2) proteins inferred from comparative analyses of amino acid and coding nucleotide sequences. *J. Biol. Chem. 267*, 83–90.
(48) Hasemann, C. A., Kurumbail, R. G., Boddupalli, S. S., Peterson, J. A., and Deisenhofer, J. (1995) Structure and function of cytochromes P450: a comparative analysis of three crystal structures. *Structure 3*, 41–62.
(49) Cojocaru, V., Winn, P. J., and Wade, R. C. (2007) The ins and outs of cytochrome P450s. *Biochim. Biophys. Acta 1770*, 390–401.
(50) Pochapsky, T. C., Kazanis, S., and Dang, M. (2010) Conformational plasticity and structure/function relationships in cytochromes P450. *Antioxid. Redox Signal. 13*, 1273–1296.
(51) Xu, L.-H., Fushinobu, S., Ikeda, H., Wakagi, T., and Shoun, H. (2009) Crystal structures of cytochrome P450 105P1 from *Streptomyces avermitilis*: conformational flexibility and histidine ligation state. *J. Bacteriol. 191*, 1211–1219.
(52) Sherman, D. H., Li, S., Yermalitskaya, L. V., Kim, Y., Smith, J. A., Waterman, M. R., and Podust, L. M. (2006) The structural basis for substrate anchoring, active site selectivity, and product formation by P450 PikC from *Streptomyces venezuelae*. *J. Biol. Chem. 281*, 26289–26297.
(53) Kronbach, T., Kemper, B., and Johnson, E. F. (1991) A hypervariable region of P450IIC5 confers progesterone 21-hydroxylase activity to P450IIC1. *Biochemistry 30*, 6097–6102.
(54) Graham-Lorence, S., Truan, G., Peterson, J. A., Falck, J. R., Wei, S., Helvig, C., and Capdevila, J. H. (1997) An active site substitution, F87V, converts cytochrome P450 BM-3 into a regio- and stereoselective (14*S*,15*R*)-arachidonic acid epoxygenase. *J. Biol. Chem. 272*, 1127–1135.
(55) Oliver, C. F., Modi, S., Sutcliffe, M. J., Primrose, W. U., Lian, L.-Y., and Roberts, G. C. K. (1997) A single mutation in cytochrome P450 BM3 changes substrate orientation in a catalytic intermediate and the regiospecificity of hydroxylation. *Biochemistry 36*, 1567–1572.
(56) Roussel, F., Khan, K. K., and Halpert, J. R. (2000) The importance of SRS-1 residues in catalytic specificity of human cytochrome P450 3A4. *Arch. Biochem. Biophys. 374*, 269–278.
(57) Hayashi, K., Sugimoto, H., Shinkyo, R., Yamada, M., Ikeda, S., Ikushiro, S., Kamakura, M., Shiro, Y., and Sakaki, T. (2008) Structure-based design of a highly active vitamin D hydroxylase from *Streptomyces griseolus* CYP105A1. *Biochemistry 47*, 11964–11972.
(58) Zocher, G., Richter, M. E. A., Mueller, U., and Hertweck, C. (2011) Structural fine-tuning of a multifunctional cytochrome P450 monooxygenase. *J. Am. Chem. Soc. 133*, 2292–2302.
(59) Venkataraman, H., de Beer, S. B. A., van Bergen, L. A. H., van Essen, N., Geerke, D. P., Vermeulen, N. P. E., and Commandeur, J. N. M. (2012) A single active site mutation inverts stereoselectivity of 16-hydroxylation of testosterone catalyzed by engineered cytochrome P450BM3. *ChemBioChem 13*, 520–523.
(60) Montemiglio, L. C., Macone, A., Ardiccioni, C., Avella, G., Vallone, B., and Savino, C. (2013) Redirecting P450 EryK specificity by rational site-directed mutagenesis. *Biochemistry 52*, 3678–3687.
(61) Johnson, E. F. (1992) Mapping determinants of the substrate selectivities of P450 enzymes by site-directed mutagenesis. *Trends Pharmacol. Sci. 13*, 122–126.
(62) Domanski, T. L., and Halpert, J. R. (2001) Analysis of mammalian cytochrome P450 structure and function by site-directed mutagenesis. *Curr. Drug Metab. 2*, 117–137.
(63) Lindberg, R. L. P., and Negishi, M. (1989) Alteration of mouse cytochrome $P450_{coh}$ substrate specificity by mutation of a single amino-acid residue. *Nature 339*, 632–634.

(64) Hsu, M.-H., Griffin, K. J., Wang, Y., Kemper, B., and Johnson, E. F. (1993) A single amino acid substitution confers progesterone 6*β*-hydroxylase activity to rabbit cytochrome P450 2C3. *J. Biol. Chem. 268*, 6939–6944.
(65) Ramarao, M., and Kemper, B. (1995) Substitution at residue 473 confers progesterone 21-hydroxylase activity to cytochrome P450 2C2. *Mol. Pharmacol. 48*, 417–424.
(66) Böttner, B., Denner, K., and Bernhardt, R. (1998) Conferring aldosterone synthesis to human CYP11B1 by replacing key amino acid residues with CYP11B2-specific ones. *Eur. J. Biochem. 252*, 458–466.
(67) Schalk, M., and Croteau, R. (2000) A single amino acid substitution (F363I) converts the regiochemistry of the spearmint (–)-limonene hydroxylase from a C6- to a C3-hydroxylase. *Proc. Natl. Acad. Sci. USA 97*, 11948–11953.
(68) Voigt, C. A., Martinez, C., Wang, Z.-G., Mayo, S. L., and Arnold, F. H. (2002) Protein building blocks preserved by recombination. *Nat. Struct. Biol. 9*, 553–558.
(69) Hiraga, K., and Arnold, F. H. (2003) General method for sequence-independent site-directed chimeragenesis. *J. Mol. Biol. 330*, 287–296.
(70) Otey, C. R., Silberg, J. J., Voigt, C. A., Endelman, J. B., Bandara, G., and Arnold, F. H. (2004) Functional evolution and structural conservation in chimeric cytochromes P450: calibrating a structure-guided approach. *Chem. Biol. 11*, 309–318.
(71) Romero, P. A., Krause, A., and Arnold, F. H. (2013) Navigating the protein fitness landscape with Gaussian processes. *Proc. Natl. Acad. Sci. USA 110*, E193–E201.
(72) Munataliev, M. B., Trinh, L. N., Moser, L. V., Bates, R. B., Feyereisen, R., and Walker, F. A. (2004) Chimeragenesis of the fatty acid binding site of cytochrome P450BM3. Replacement of residues 73–84 with the homologous residues from the insect cytochrome P450 CYP4C7. *Biochemistry 43*, 1771–1780.
(73) Chen, C.-K. J., Shokhireva, T. K., Berry, R. E., Zhang, H., and Walker, F. A. (2008) The effect of mutation of F87 on the properties of CYP102A1-CYP4C7 chimeras: altered regiospecificity and substrate selectivity. *J. Biol. Inorg. Chem. 13*, 813–824.
(74) Chen, C.-K. J., Berry, R. E., Shokhireva, T. K., Munataliev, M. B., Zhang, H., and Walker, F. A. (2010) Scanning chimeragenesis: the approach used to change the substrate selectivity of fatty acid monooxygenase CYP102A1 to that of terpene ω-hydroxylase CYP4C7. *J. Biol. Inorg. Chem. 15*, 159–174.
(75) Kumar, S., Chen, C. S., Waxman, D. J., and Halpert, J. R. (2005) Directed evolution of mammalian cytochrome P450 2B1: mutations outside of the active site enhance the metabolism of several substrates, including the anticancer prodrugs cyclophosphamide and ifosfamide. *J. Biol. Chem. 280*, 19569–19575.
(76) Bloom, J. D., Meyer, M. M., Meinhold, P., Otey, C. R., MacMillan, D., and Arnold, F. H. (2005) Evolving strategies for enzyme engineering. *Curr. Opin. Struct. Biol. 15*, 447–452.
(77) Behrendorff, J. B. Y. H., Huang, W., and Gillam, E. M. J. (2015) Directed evolution of cytochrome P450 enzymes for biocatalysis: exploiting the catalytic versatility of enzymes with relaxed substrate specificity. *Biochem. J. 467*, 1–15.
(78) Tracewell, C. A., and Arnold, F. H. (2009) Directed enzyme evolution: climbing fitness peaks one amino acid at a time. *Curr. Opin. Chem. Biol. 13*, 3–9.
(79) Khersonsky, O., Roodveldt, C., and Tawfik, D. S. (2006) Enzyme promiscuity: evolutionary and mechanistic aspects. *Curr. Opin. Chem. Biol. 10*, 498–508.

Chapter 4: Comparative analysis of diverse P450 enzymes from the mycinamicin, tylosin, and juvenimicin biosynthetic pathways and their application toward the chemoenzymatic synthesis of tylactone-based macrolide antibiotics*

4.1 Introduction

Macrolides have been a mainstay of the treatment of bacterial infections in humans and other animals for well over half a century. While 14-membered ring macrolides like erythromycin and its semisynthetic derivatives have acquired the most widespread clinical use, the 16-membered ring variety constitutes the largest group isolated from natural sources. On the basis of their structural properties, these compounds can be classified into three main subgroups.[1,2] The largest of these is the "platenolide" subgroup, which includes a variety of macrolides consisting of the same aglycone scaffold (platenolide) to which the disaccharide D-mycaminosyl-L-mycarose is appended at C5 (**Figure 4.1**). The various members of this subgroup differ in the types of acyl groups attached to C3 of the macrolactone and C4'' of mycarose as well as in the oxidation states of C9 and C12/C13. The carbomycin-type compounds contain the standard C9 keto group and may (e.g., carbomycin A, deltamycins) or may not (e.g., carbomycin B, niddamycin) be epoxidized at C12/C13. In the leucomycin-type macrolides (e.g., leucomycins, kitasamycin, josamycin, midecamycin), the C9 keto group is reduced to an alcohol. The maridomycins comprise the epoxidized members of

*The work described in this chapter was a collaborative effort between Matthew D. DeMars II and Dr. Andrew N. Lowell (University of Michigan). M.D.D. II performed the P450 biochemical assays, tylactone biotransformation, and large-scale P450/chemical oxidation reactions. A.N.L. cloned P450s JuvC and JuvD, performed the chemoenzymatic synthesis of tylactone, and carried out the antimicrobial activity assay. Parts of section 4.4 were adapted from the following publication: Lowell, A. N., DeMars, M. D., II, Slocum, S. T., Yu, F., Anand, K., Chemler, J. A., Korakavi, N., Priessnitz, J. K., Park, S. R., Koch, A. A., Schultz, P. J., and Sherman, D. H. (2017) Chemoenzymatic total synthesis and structural diversification of tylactone-based macrolide antibiotics through late-stage polyketide assembly, tailoring, and C—H functionalization. *J. Am. Chem. Soc. 139*, 7913–7920.

this family. Finally, the spiramycins are unique among the platenolides in that they bear an additional deoxyamino sugar (forosamine), which is appended to the C9 alcohol. In the spiramycin biosynthetic pathway, a dedicated ketoreductase reduces the C9 keto group of platenolide I as the first post-PKS step.[3] Forosamine is likely appended as the penultimate step in the formation of spiramycin I, an unacylated congener. Among all of the 16-membered ring macrolides, only midecamycin and the spiramycins were

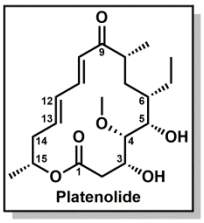

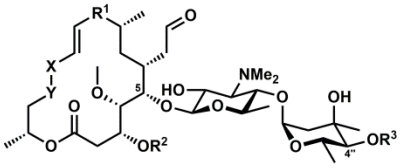

Compound	R^1	R^2	R^3	X–Y
Carbomycin A			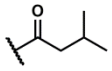	Epoxy
Deltamycins				Epoxy
Niddamycin		H		E alkene
Leucomycin A_6				E alkene
Kitasamycin		H	H	E alkene
Josamycin			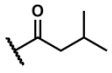	E alkene
Midecamycin A_1				E alkene
Maridomycins				Epoxy
Spiramycin I	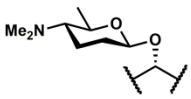	H	H	E alkene

Figure 4.1. Structure of the platenolide scaffold and representative examples of platenolide-type antibiotics.

commercialized for use in humans. Second-generation semisynthetic derivatives of the leucomycins (miocamycin and rokitamycin) were subsequently developed in order to improve their bioavailability and pharmacokinetic properties. While these antibiotics did not display enhanced in vitro potencies relative to the parent compounds, they did prove more efficacious in vivo. Nonetheless, they have not been widely adopted for clinical use.

The second subgroup of 16-membered ring macrolides consists of tylosin, rosamicin, and its relatives bearing the “tylactone” aglycone (**Figure 4.2**). Due to its widespread use in veterinary medicine and the livestock industry, tylosin is the most commercially important member of this subgroup. Like the platenolide-type macrolides, it has the mycaminosyl-mycarose disaccharide appended at the C5 position and possesses the important ethylaldehyde pharmacophore. However, unlike the platenolides, the added methyl group at C14 of tylactone provides a handle for the introduction of an additional sugar (D-mycinose). Other members of the tylactone subgroup include angolamycin as well as the cirramycins, izenamicins, juvenimicins, and M-4365 series. All of these compounds contain a deoxyamino sugar (desosamine, mycaminose, or angolosamine in the case of angolamycin) attached at C5, but additional sugars may also be present. Members of the rosamicin, izenamicin, juvenimicin, and M-4365 classes only bear desosamine, with individual species differing in the oxidation states of the ethyl side chain, the C12/C13 olefin, and the C14 methyl

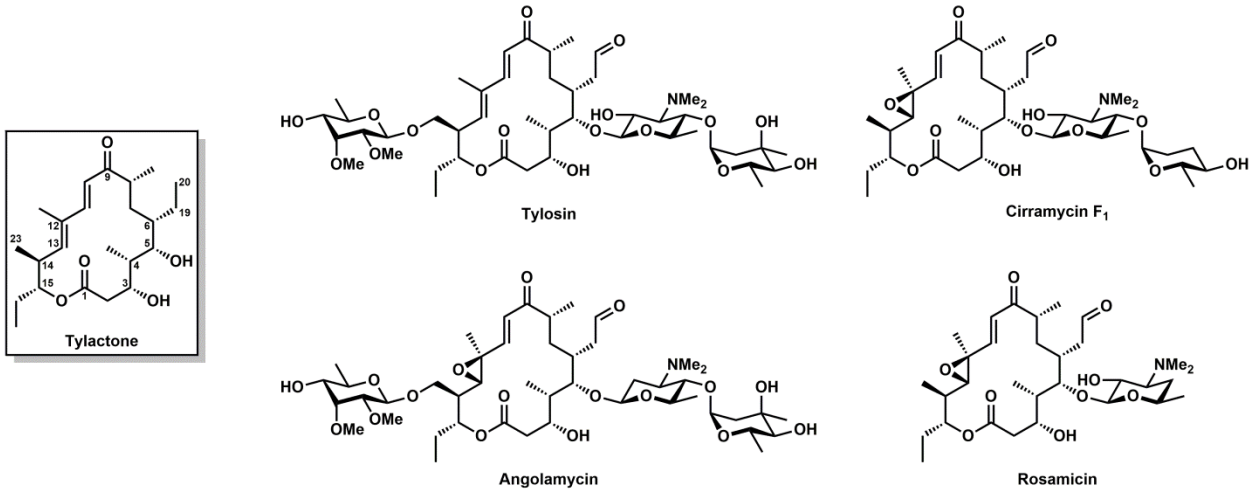

Figure 4.2. Structure of the tylactone scaffold and representative examples of tylactone-type antibiotics.

group. Fully elaborated molecules in the tylactone subgroup typically contain an ethylaldehyde moiety as well as a C12/C13 epoxide and/or a hydroxylated C14 methyl. Although it was not further developed into a drug, rosamicin was at one point tested in human clinical trials. In addition, tilmicosin and tildipirosin were developed as second-generation semisynthetic derivatives of tylosin for the prevention and treatment of bovine respiratory disease.

The third subgroup comprises macrolides constructed from the “chalconolide” scaffold and its close analogs (**Figure 4.3**). Key distinguishing features of the macrolactone include a 2,3-trans double bond and a methyl instead of an ethyl side chain at C6, thus precluding installation of an aldehyde. Notable compounds in this subgroup include the chalcomycins, neutramycins, mycinamicins, and aldgamycins. Interestingly, although chalcomycin contains a 2,3-trans double bond, the associated PKS does not contain the requisite ketoreductase and dehydratase domains in the final module to explain its formation.[4] It is still unclear how and at what point in the biosynthetic pathway the reduction and dehydration reactions occur to generate the macrolactone core seen in the final natural product. Recently, a single gene cluster was found to account for the biosynthesis of both chalcomycins and aldgamycins in a marine-derived *Streptomyces* sp., the pathways bifurcating at the point of deoxy sugar attachment to C5 of the macrolactone.[5] The mycinamicins are unique among the

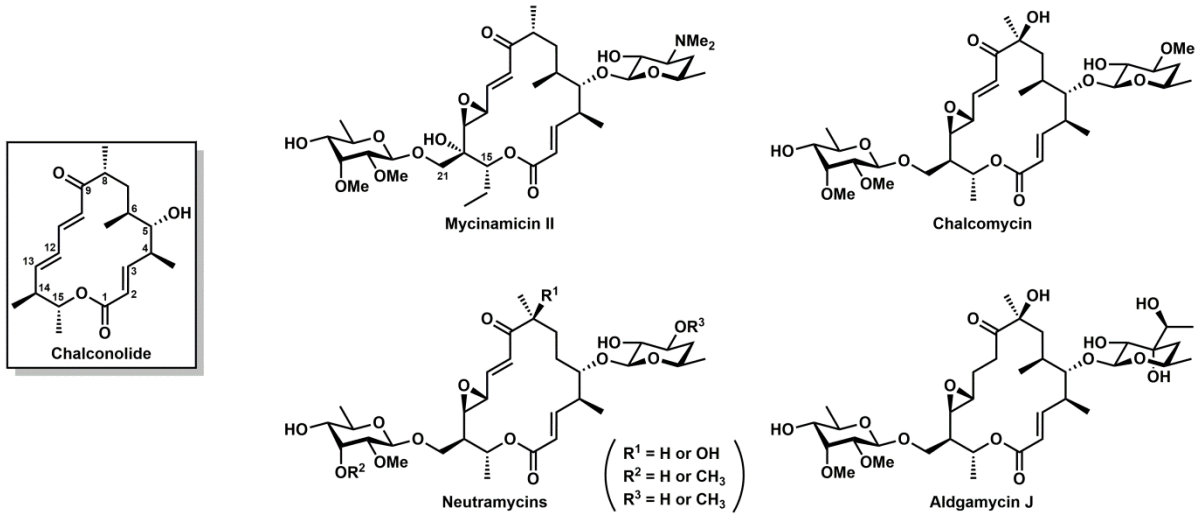

Figure 4.3. Structure of the chalconolide scaffold and representative examples of chalconolide-type antibiotics.

chalconolides in that they bear the basic deoxyamino sugar desosamine at C5 whereas the others only possess neutral sugars at this position (e.g., chalcose, aldgarose). Like many members of the tylactone subgroup, an additional sugar (javose or mycinose) is appended on the left side of the molecule. Moreover, an ethyl side chain replaces the methyl group at C15 in the mycinamicins. Novel chalconolide-type macrolides continue to be isolated from various actinomycetes as evidenced by the recent discovery of the tianchimycins[6] as well as several new aldgamycins.[7]

While 16-membered ring macrolides are generally less potent and more unstable than their 14-membered ring counterparts, they exhibit several advantages over the latter, including higher gastrointestinal tolerability and structural flexibility as well as a lack of inducible resistance.[8] Naturally occurring 16-membered ring macrolides and their semisynthetic derivatives are also often more effective against various bacterial strains that have acquired resistance to widely used 14-membered ring macrolides.[9,10] This phenomenon may be explained at least in part by the unique binding mode of 16-membered ring macrolides to the bacterial ribosome. The cocrystal structures of carbomycin, spiramycin, and tylosin bound to the 50S ribosomal subunit of the halophilic Archaeon *Haloarcula marismortui* revealed the presence of a reversible covalent bond between the ethylaldehyde substituent of the macrolides and the exocyclic amine of an adenine residue in the 23S rRNA.[11] This observation helps to explain why reduction of the aldehyde of these compounds always increases their minimum inhibitory concentrations when tested against Gram-positive bacteria. The 16-membered ring macrolides are also less susceptible to elimination from the bacterial cell by macrolide-specific efflux pumps, which constitutes an important mechanism of resistance to macrolide antibiotics.[10,12] With the increasingly significant threat that antibiotic resistance is posing to global public health, the need for new and more effective antibiotics is more acute than ever. Acquiring a detailed understanding of the biosynthetic pathways associated with the construction of these molecules will prove critical in the generation of novel analogs via pathway engineering. It will also lead to the discovery of new enzymes with unique catalytic properties that can serve as robust platforms for the development of valuable biocatalysts, which may be employed in vitro or in vivo for the more efficient production of fine and commodity chemicals.

Chapters 2 and 3 of the present thesis provided a detailed comparative analysis of P450s that perform identical reactions on 16-membered ring macrolides, namely the installation of a hydroxyl group at a particular unactivated primary carbon atom (C20 or C21 in chalconolide-type macrolides and C23 in tylactone-type macrolides). However, numerous studies on the biosynthetic pathways of these compounds have demonstrated that P450s are often responsible for several additional post-PKS modifications on the macrolide scaffold. These oxidative tailoring reactions include four-electron oxidation of the C6 ethyl side chain to yield the critical aldehyde substituent of platenolide- and tylactone-type macrolides, epoxidation of the C12/C13 olefin, and hydroxylation at the C8 position of chalconolides (**Figure 4.4** and **Table 4.1**).

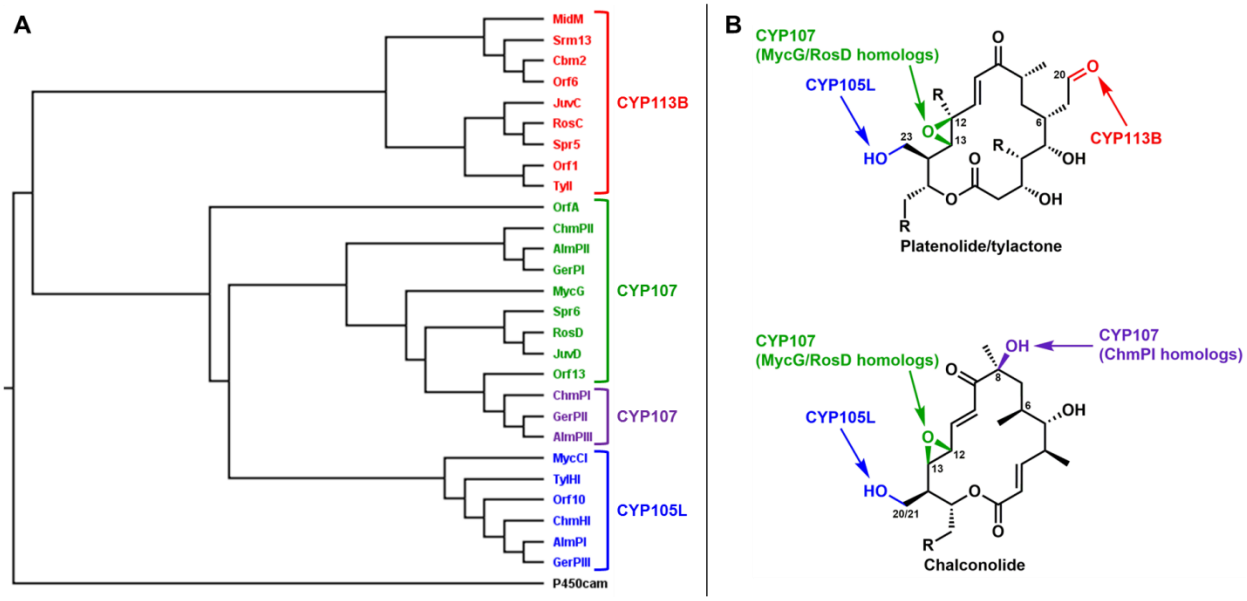

Figure 4.4. P450s involved in the biosynthesis of 16-membered ring macrolides. (**A**) Phylogenetic analysis of the 27 P450s listed in **Table 4.1**. Multiple sequence alignment was performed using Clustal Omega with $P450_{cam}$ (CYP101A1) included as an outgroup. The alignment data were rendered in tree format using FigTree. (**B**) Sites on 16-membered ring macrolides targeted by the different families of P450s listed in **Table 4.1**.

Only a handful of the associated enzymes have been directly probed, usually through gene inactivation and/or in vivo bioconversion experiments. Phylogenetic analysis of these P450s shows that they tend to cluster according to the specific reactions they have been verified or predicted to carry out (**Figure 4.4**). Homologs of MycCI and TylHI share ≥55% sequence identity and are thus all part of the CYP105L subfamily (**Table 4.1**). Notably, each of these P450s is associated with a [3Fe-4S]-type

Table 4.1. List of P450s involved in the biosynthesis of 16-membered ring macrolides.

P450	CYP family	Biosynthetic pathway	Subgroup	Organism	Reaction type	Accession number
MycCI (MycCII fdx[a])	CYP105L2	Mycinamicin	Chalconolide	*Micromonospora griseorubida*	Hydroxylation (primary C–H)	Q83WF5
ChmHI (ChmHII fdx)	CYP105L	Chalcomycin	Chalconolide	*Streptomyces bikiniensis*	Hydroxylation (primary C–H)	AAS79453
GerPIII (GerH fdx)	CYP105L	Dihydrochalcomycin	Chalconolide	*Streptomyces* sp. KCTC 0041BP	Hydroxylation (primary C–H)	ABB52539
AlmPI (AlmN fdx)	CYP105L	Aldgamycin	Chalconolide	*Streptomyces* sp. HK-2006-1	Hydroxylation (primary C–H)	ANC94973[b]
TylHI (TylHII fdx)	CYP105L1	Tylosin	Tylactone	*Streptomyces fradiae*	Hydroxylation (primary C–H)	AAD41818[c]
Orf10 (Orf9 fdx)	CYP105L	Angolamycin	Tylactone	*Streptomyces eurythermus*	Hydroxylation (primary C–H)	ABV49600
TylI	CYP113B1	Tylosin	Tylactone	*Streptomyces fradiae*	Four-electron oxidation	AAA21341
RosC	CYP113B	Rosamicin	Tylactone	*Micromonospora rosaria*	Four-electron oxidation	BAM35932
Spr5	CYP113B	Rosamicin	Tylactone	*Salinispora pacifica*	Four-electron oxidation	AKG06373
JuvC	CYP113B	Juvenimicin	Tylactone	*Micromonospora chalcea*	Four-electron oxidation	ARW71481
Orf1	CYP113B	Angolamycin	Tylactone	*Streptomyces eurythermus*	Four-electron oxidation	ABV49609
Srm13	CYP113B	Spiramycin	Platenolide	*Streptomyces ambofaciens*	Four-electron oxidation	CAM96580/AKZ58669
Cbm2	CYP113B	Carbomycin	Platenolide	*Streptomyces thermotolerans*	Four-electron oxidation	ALK28491
MidM	CYP113B3	Midecamycin	Platenolide	*Streptomyces mycarofaciens*	Four-electron oxidation	ABG67708[d]
Orf6	CYP113B2	Niddamycin	Platenolide	*Streptomyces caelestis*	Four-electron oxidation	AAC46023[e]
MycG	CYP107E1	Mycinamicin	Chalconolide	*Micromonospora griseorubida*	Epoxidation/hydroxylation	BAA03672
ChmPII	CYP107	Chalcomycin	Chalconolide	*Streptomyces bikiniensis*	Epoxidation	AAS79446
GerPI	CYP107	Dihydrochalcomycin	Chalconolide	*Streptomyces* sp. KCTC 0041BP	Epoxidation	ABB52529
AlmPII	CYP107	Aldgamycin	Chalconolide	*Streptomyces* sp. HK-2006-1	Epoxidation	ANC94979[f]
RosD	CYP107	Rosamicin	Tylactone	*Micromonospora rosaria*	Epoxidation	BAM35933
Spr6	CYP107	Rosamicin	Tylactone	*Salinispora pacifica*	Epoxidation	AKG06374
JuvD	CYP107	Juvenimicin	Tylactone	*Micromonospora chalcea*	Epoxidation	ARW71482
Orf13	CYP107	Angolamycin	Tylactone	*Streptomyces eurythermus*	Epoxidation	ABV49597
OrfA	CYP107C1	Carbomycin	Platenolide	*Streptomyces thermotolerans*	Epoxidation	BAA06420
ChmPI	CYP107	Chalcomycin	Chalconolide	*Streptomyces bikiniensis*	Hydroxylation (tertiary C–H)	AAS79447
GerPII	CYP107	Dihydrochalcomycin	Chalconolide	*Streptomyces* sp. KCTC 0041BP	Hydroxylation (tertiary C–H)	ABB52528
AlmPIII	CYP107	Aldgamycin	Chalconolide	*Streptomyces* sp. HK-2006-1	Hydroxylation (tertiary C–H)	ANC94978

[a]Each CYP105L subfamily P450 is associated with a [3Fe-4S]-type ferredoxin (fdx) as indicated in parentheses.
[b]The listed AlmPI sequence is missing the first 77 amino acids at the N-terminus.
[c]The N-terminus of the listed TylHI sequence is too long (extended by 16 amino acids).
[d]The listed MidM sequence is missing the last ~30 amino acids at the C-terminus.
[e]The listed Orf6 (NidI) sequence only contains the first 132 amino acids.
[f]The N-terminus of the listed AlmPII sequence is too long (extended by 23 amino acids).

ferredoxin, with the corresponding gene located adjacent to that encoding the P450 in the gene cluster. TylI and its homologs, which catalyze formation of the aldehyde on the C6 ethyl side chain, also form a discrete cluster and belong to the CYP113B subfamily. Although none of these enzymes have been purified and tested in vitro on their expected substrate(s), the activities of a small subset (TylI, RosC, and Srm13) have been confirmed on the basis of gene disruption and bioconversion experiments.[3,13-15] Finally, MycG, RosD, and their functional homologs are all predicted to perform epoxidation reactions on their substrates as one of the last steps in their respective biosynthetic pathways. This activity has been confirmed through in vitro reconstitution of purified MycG[16] as well as in vivo gene disruption and bioconversion studies with RosD,[15] OrfA,[17] and GerPI.[18] MycG is unique among this group of enzymes in that it is capable of performing both hydroxylation and epoxidation reactions on its native substrate (**Scheme 4.2**). Unlike the CYP105L and CYP113B subfamilies, the epoxidases do not consistently form a distinct cluster. Instead, they tend to disperse among the other groups, most notably that comprising the putative chalconolide C8 hydroxylases (ChmPI, GerPII, and AlmPIII). Interestingly, the epoxidases and C8 hydroxylases are most closely related to the P450 OleP (~50% sequence identity on average), an alleged multifunctional desaturase/epoxidase from the oleandomycin biosynthetic pathway. All of these enzymes are part of the CYP107 family, which includes a large number of bacterial secondary metabolic P450s such as the extensively characterized EryF and PikC. The function of GerPII as a C8 hydroxylase that preferentially acts prior to GerPI (P450 epoxidase) in the dihydrochalcomycin pathway has been verified through gene disruption and complementation experiments.[18]

In order to confirm the activities and explore the substrate scope of P450s beyond MycCI and TylHI, we cloned, overexpressed, and purified TylI from the tylosin pathway in *Streptomyces fradiae*[19] as well as JuvC and JuvD from the newly sequenced juvenimicin pathway in *Micromonospora chalcea* (ssp. *izumensis*). JuvD shares 84% sequence identity with RosD, the epoxidase from the rosamicin pathway in *Micromonospora rosaria*.[15] Very high sequence identity is also observed between JuvC and RosC (87%), strongly suggesting that the former performs iterative two-electron oxidations to form an aldehyde on its substrate in a similar manner to the latter, whose

function in this capacity has also been confirmed.[15] TylI is slightly more divergent from JuvC and RosC at the primary sequence level (70% and 69% identity, respectively), but it is expected to exhibit the same reactivity on the basis of previous bioconversion studies.[14,20,21] Because the native ferredoxin and ferredoxin reductase partners for these enzymes are not known, we constructed catalytically self-sufficient versions of each by fusing the FMN/[2Fe-2S]-containing reductase domain of $P450_{RhF}$ (RhFRED) to the C-terminus of the P450 as previously described.[22] The following sections of this chapter describe comparative analyses of JuvD/MycCI and JuvC/TylI and detail efforts to apply these P450s as biocatalysts in the chemoenzymatic synthesis of several tylactone-based macrolide antibiotics.

4.2 Comparative analysis of P450s JuvD and MycCI

The activities of catalytically self-sufficient JuvD-RhFRED and MycCI-RhFRED were compared across a panel of 20 macrolactone and macrolide substrates, some of which were oxidized products acquired through scale-up reactions involving these and other P450 enzymes (**Figure 4.5** and **Table 4.2**; see section 4.4). All reactions were performed on an analytical scale and analyzed by LC-MS. Overall, JuvD-RhFRED was considerably more active than MycCI-RhFRED on tylactone-type macrolides **1**–**6**, with conversions reaching ≥90% in all cases. In contrast, the highest conversions achieved by MycCI-RhFRED were around 52% for both compounds **2** and **3** (**Table 4.3**). A possible explanation for this difference in basal activity between the two enzymes relates to the higher inherent free energy barrier that must be overcome to achieve oxidation of an unactivated primary C–H bond vs epoxidation of an olefin. JuvD-RhFRED was capable of epoxidizing compounds to a similar extent regardless of the oxidation states of C20 and C4', although the enzyme seemed to exhibit a slight preference for substrates bearing mycaminose as the deoxyamino sugar (**4**–**6**). However, it is interesting to note that the juvenimicin, M-4365, and rosamicin classes of macrolides all possess desosamine, which differs from mycaminose only in its lack of a hydroxyl group at C4'. Thus, the unexpected reactivity profile of JuvD may provide interesting insight into the functions of its ancestral homologs in pathways that produced molecules with different sugar functionalities. In contrast, MycCI-RhFRED preferentially

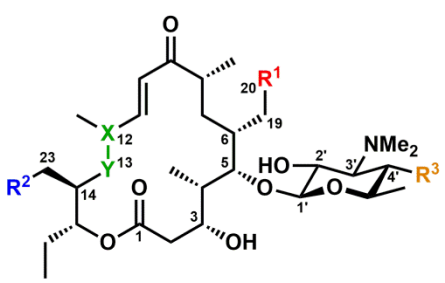

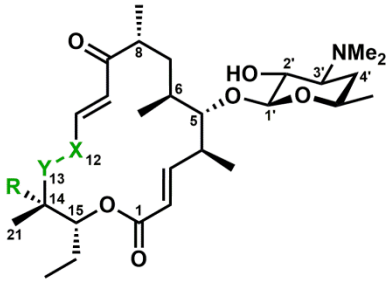

Compound	R^1	R^2	R^3	X–Y
1	CH_3	H	H	E alkene
2	CH_2OH	H	H	E alkene
3	CHO	H	H	E alkene
4	CH_3	H	OH	E alkene
5	CH_2OH	H	OH	E alkene
6	CHO	H	OH	E alkene
7	CH_3	OH	H	E alkene
8	CH_2OH	OH	H	E alkene
9	CHO	OH	H	E alkene
10	CH_3	H	H	Epoxy
11	CH_2OH	H	H	Epoxy
12	CHO	H	H	Epoxy
13	CH_3	H	H	Z alkene

Compound	R	X–Y
14	H	E alkene
15	H	Epoxy
16	OH	E alkene

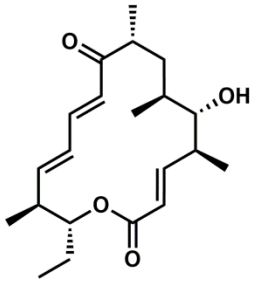

PML-IV (17)

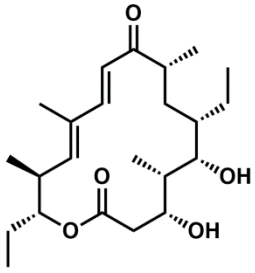

Tylactone (18)

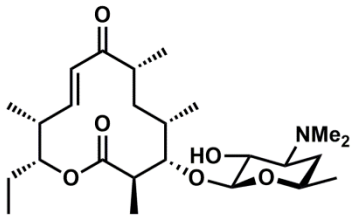

YC-17 (19)

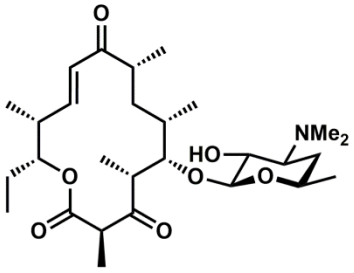

Narbomycin (20)

Figure 4.5. Structures of 20 compounds investigated in Chapter 4. Different names for compounds **1–13** are listed in **Table 4.2**. Compound **14** is mycinamicin VIII (M-VIII), and compounds **15** and **16** are previously undescribed mycinamicins.

Table 4.2. List of compounds **1–13** and associated names.

Compound	Tylactone/tylonolide	M-4365	Juvenimicin	Izenamicin	Other
1	5-*O*-desosaminyl-tylactone	G_1			
2	20-hydroxy-5-*O*-desosaminyl-tylactone	G_3	B_1	B_1	
3	23-deoxy-5-*O*-desosaminyl-tylonolide	G_2			23-DDTL
4	5-*O*-mycaminosyl-tylactone				
5	20-hydroxy-5-*O*-mycaminosyl-tylactone				
6	23-deoxy-5-*O*-mycaminosyl-tylonolide				23-DMTL
7	23-hydroxy-5-*O*-desosaminyl-tylactone				
8	20,23-dihydroxy-5-*O*-desosaminyl-tylactone		B_3	B_4	
9	5-*O*-desosaminyl-tylonolide			B_3	DTL
10	12,13-epoxy-5-*O*-desosaminyl-tylactone	A_1			
11	12,13-epoxy-20-hydroxy-5-*O*-desosaminyl-tylactone	A_3	A_4	A_2	
12	12,13-epoxy-23-deoxy-5-*O*-desosaminyl-tylonolide	A_2	A_3	A_1	Rosamicin
13	Iso-5-*O*-desosaminyl-tylactone	Iso-G_1			Mattamycin

converted desosaminylated substrates (**1**–**3**) to C23-hydroxylated products, with conversions averaging ~13% higher than those of the corresponding mycaminosylated substrates (**Table 4.3**). The enzyme also more readily accepted substrates that were oxidized at C20, leading to a cumulative effect illustrated by its ability to hydroxylate **2** and **3** (52% conversion) more than twice as effectively as **4** (23% conversion).

Table 4.3. Results of activity assays performed with MycCI-RhFRED and JuvD-RhFRED.[a]

Compound	MycCI-RhFRED	JuvD-RhFRED
1	38.3 ± 3.3	89.6 ± 2.8
2	51.9 ± 3.2	93.0 ± 0.1
3	51.7 ± 1.8	94.8 ± 0.4
4	23.4 ± 1.3	97.6 ± 0.1
5	43.1 ± 0.2	98.2 ± 0.0
6	36.6 ± 1.0	95.6 ± 0.3
7	--[b]	7.1 ± 0.8
8	--	37.3 ± 0.8
9	--	46.3 ± 0.8[c]
10	1.8 ± 0.2	--
11	8.9 ± 1.1	--
12	3.8 ± 0.6	--
13	22.5 ± 1.5[d]	2.8 ± 0.1[c]
14	52.9 ± 3.9	53.1 ± 2.2 (epoxy) 6.8 ± 0.2 (hydroxy)
15	10.0 ± 1.6	0
16	7.1 ± 0.4	12.6 ± 0.0
17	4.0 ± 0.2	0
18	6.5 ± 0.2	2.6 ± 0.3
19	0	0
20	0.1 ± 0.0	28.6 ± 1.0

[a]Average percent conversion values and standard deviations reflect the results of experiments performed and analyzed by LC-MS in duplicate.
[b]Blank space (--) indicates that the corresponding reaction was not performed.
[c]Significant *N*-demethylation (8-9%) was also observed (see **Table C.2**).
[d]At least five separate products were detected.

As expected, conversions decreased when the isolated product of one enzyme was fed to the other (**Table 4.3**). The presence of a hydroxyl group at C23 (**7**–**9**) rendered JuvD-RhFRED less capable of installing the epoxide across the adjacent C12/C13 double bond. Since modification of the oxidation state of C23 is not expected to dramatically impact the electronics of the conjugated α,β,γ,δ-unsaturated ketone moiety, the decrease in conversion likely stems from the added steric bulk of the C23-hydroxyl group. However, substrates bearing either a hydroxyl group (**8**) or an aldehyde (**9**) at C20 were epoxidized much more effectively than the corresponding non-oxidized substrate (**7**), indicating that the polar functional group installed at C20 may provide an

important recognition element for JuvD-RhFRED. This trend was not as readily observable for the other substrates because the enzyme was able to turn each of them over to a comparably high extent. Therefore, the preferred native substrate for JuvD in *Micromonospora chalcea* is most likely **3**. Interestingly, global decreases in epoxidation of the C23-hydroxylated substrates (**7**–**9**) were concomitant with increases in *N*-demethylation of these substrates relative to their C23-methyl counterparts (**1**–**3**; **Table C.2**). Products corresponding in mass to *N*-demethylated versions of the substrate are almost always observed in reactions of P450s with molecules bearing *N*,*N*-dimethylamino moieties, but these compounds are often only present in trace quantities (i.e., <1% of the total reaction mixture). However, in the reaction of JuvD-RhFRED with

Scheme 4.1. Differential regioselectivity properties of MycCI and JuvD acting on (**A**) tylactone-type and (**B**) chalconolide-type 16-membered ring macrolides.

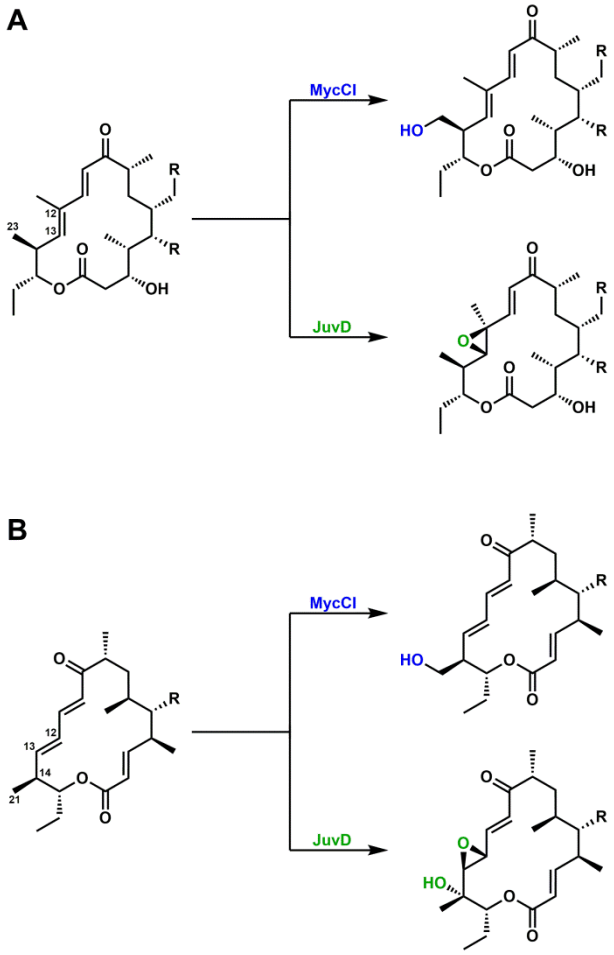

9, ~9% of the reaction mixture consisted of demethylated starting material and product (compared with ~1% in the reaction with **3**; **Table C.2**). Thus, the substrate may be more prone to adopting an alternate conformation in the JuvD active site when C23 is hydroxylated. Although this idea as it relates to the present set of results has yet to be investigated through the use of alternative redox partners, it is possible that the RhFRED reductase domain has some influence on the distribution of products in these reactions. Indeed, a recent report detailed the drastic effect that variations in redox partners can have on P450 catalytic activity, with a specific focus on the multifunctional P450 MycG acting in conjunction with RhFRED.[23] A similar finding was also previously presented in the context of the P450 ChmHI, where genetic fusion to the RhFRED domain resulted in a rather efficient biocatalyst for *N*-demethylation of 14- and 16-membered ring macrolides (see Chapter 3 and Appendix B).

The presence of an epoxide at C12/C13 of tylactone-type macrolide substrates (**10**–**12**) significantly diminished the activity of MycCI-RhFRED (2-9% conversion; **Table 4.3**), most likely due to suboptimal substrate binding or positioning within the active site. As previously observed, though, conversions were slightly better for substrates bearing an oxygen-containing functional group at C20 (**11** and **12**). Unlike JuvD-RhFRED, MycCI-RhFRED did not catalyze *N*-demethylation to an appreciable extent on these substrates (≤1%; **Table C.2**).

During the course of isolating these compounds for use in P450 activity assays, we discovered that the γ,δ-olefin was prone to photoisomerization, especially upon exposure to UV light. We then became interested in testing whether photoisomeric tylactone-type macrolides would be accepted as substrates by these enzymes. Since the photoisomer of **1** (compound **13**, which was aptly named mattamycin) was readily separable from the parent compound by preparative HPLC, we were able to isolate enough of this material to test in analytical-scale reactions with JuvD-RhFRED and MycCI-RhFRED. The former exhibited a large drop in activity on **13** compared with **1** (**Table 4.3**), which was unsurprising given that the region of the molecule immediately surrounding the normal site of oxidation had been significantly altered. Whereas ~3% of **13** was converted to a product with a mass consistent with either hydroxylation or epoxidation, ~8% of this material was *N*-demethylated (**Table C.2**; **Figure C.2**),

indicating suboptimal positioning of this substrate in the JuvD active site. More surprising, however, was the ability of MycCI-RhFRED to convert **13** to at least five different monohydroxylated and/or epoxidized products (22% total conversion). In addition, the most abundant of these products had the same retention time as that seen in the JuvD-RhFRED reaction (**Figure C.2**). Nonetheless, the reactions have not yet been scaled up to determine the identities of these compounds. The crystal structure of MycCI in complex with its native substrate M-VIII (**14**) shows that the substrate binding pocket is made up of numerous hydrophobic residues that are positioned in such a manner as to tightly bind and precisely orient the substrate so that only the C–H bond to be oxidized is favorably presented to the iron-oxo species.[24] By altering the substrate in such a dramatic fashion through photoisomerization, the binding pocket likely plays a much less effective role in substrate positioning, thereby leading to lower overall conversion and multiple oxidized products.

In addition to tylactone-type macrolides, **14** was tested as a substrate for JuvD-RhFRED in analytical-scale reactions run in parallel with MycCI-RhFRED. Whereas the latter converted 53% of this compound to a single monohydroxylated (C21) product as expected, JuvD-RhFRED gave two distinct products with longer retention times than the MycCI-RhFRED product (**Table 4.3**). After carrying out the corresponding large-scale reaction, these two products were isolated and identified as 12,13-epoxy-M-VIII (**15**, 53% analytical-scale conversion) and 14-hydroxy-M-VIII (**16**, 7% analytical-scale conversion) by NMR analysis (**Figure 4.5**). Notably, **15** and **16** are new mycinamicin compounds that have not been previously described in the literature. The C12/C13 olefin and the C14 tertiary allylic positions are the exact sites targeted by MycG later in the mycinamicin biosynthetic pathway after the second sugar (6-deoxyallose) has been appended to C21-OH and sequentially methylated.[16,25] MycG does not accept **14** as a substrate, and its ability to effectively turn over doubly glycosylated mycinamicin intermediates (M-VI, M-III, and M-IV) is highly dependent on the extent to which the second sugar has been methylated by the methyltransferases MycE and MycF (**Scheme 4.2**). Thus, unlike MycG, substrate recognition is able to effectively occur for JuvD in the absence of this additional sugar moiety.

Fortunately, the scale-up reaction provided enough of each product to further test in analytical-scale reactions with both MycCI-RhFRED and JuvD-RhFRED. As observed for the tylactone-type macrolides, epoxidation across the C12/C13 double bond

Scheme 4.2. Mycinamicin biosynthetic pathway in *Micromonospora griseorubida*. Oxidation reactions catalyzed by MycCI and MycG are highlighted in blue and green, respectively.

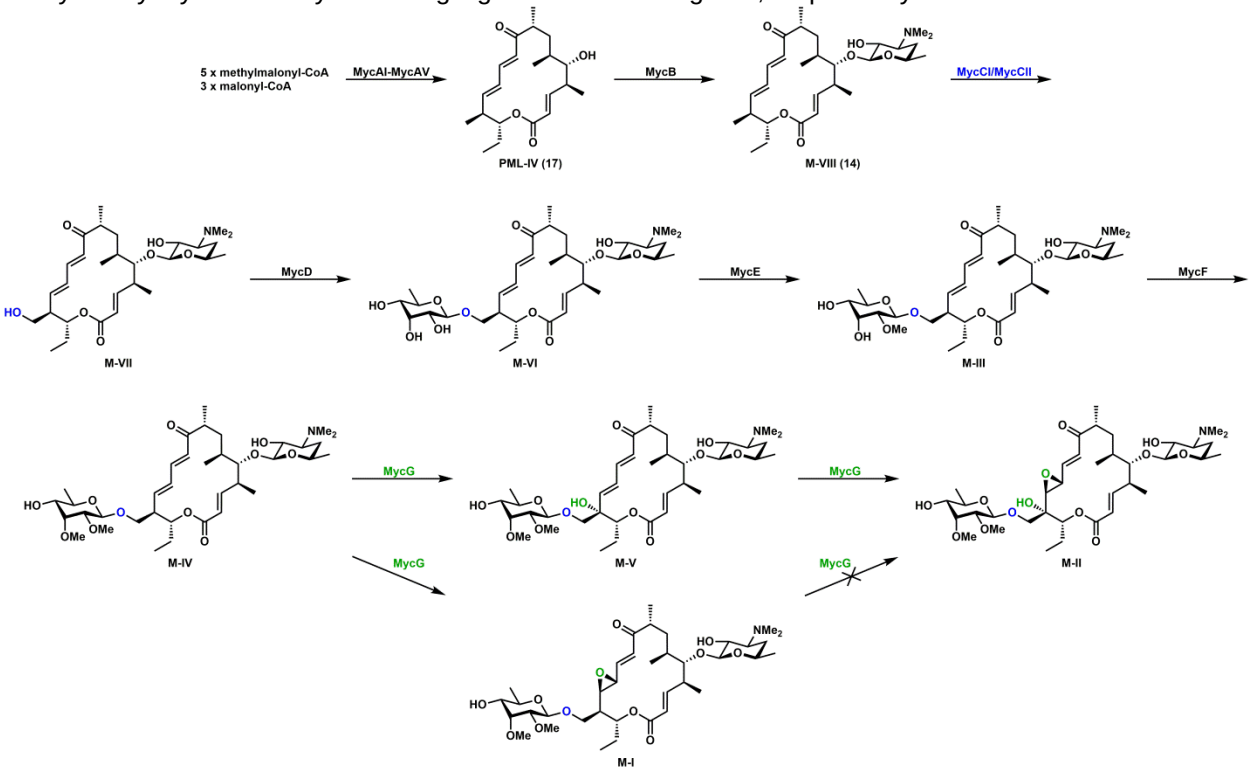

decreased the activity of MycCI-RhFRED on this analog of **14** (10% conversion of **15**; **Table 4.3**). A similar decrease in conversion (7%) occurred when the enzyme was provided with **16** as a substrate. Interestingly, while JuvD-RhFRED converted the latter to the corresponding epoxide (13%; product not yet confirmed by NMR), it was unable to hydroxylate **15**. The inability of MycG to install a hydroxyl group at C14 of the epoxidized shunt metabolite M-I (**Scheme 4.2**) most likely relates to the significant decrease in the inherent reactivity of this position when the epoxide is present, an effect that largely stems from a lack of allylic stabilization of the developing radical in the transition state for C–H abstraction (Dr. Jessica Grandner and Dr. Kendall Houk, unpublished results). Thus, while **15** may bind to JuvD-RhFRED, the prohibitively high barrier to C–H abstraction at C14 likely precludes hydroxylation at this site.

Finally, MycCI-RhFRED and JuvD-RhFRED were tested in parallel for conversion of two 16-membered ring macrolactone aglycones (**17** and **18**) as well as two smaller macrolides (**19** and **20**). Previously, we demonstrated that MycCI was able to accept both **17** and **18** as substrates, but conversion was suboptimal for the self-sufficient MycCI-RhFRED biocatalytic system.[24] In the present set of experiments, ~4% of **17** and ~6% of **18** were converted to single monohydroxylated products by MycCI-RhFRED (**Table 4.3**). Although JuvD-RhFRED did not accept **17** as a substrate, it did convert ~3% of **18** to what is likely the 12,13-epoxy analog. Although the native ferredoxin partner for JuvD is not known, employment of alternative surrogate redox partners could lead to improved conversion of **18** by this enzyme and thereby facilitate reaction scale-up to confirm the identity of the product. While neither MycCI-RhFRED nor JuvD-RhFRED accepted **19** as a substrate and the former converted **20** to a monohydroxylated product in trace quantities, JuvD-RhFRED was capable of readily oxidizing **20** (29% conversion to a single product by LC-MS). Based on its exact mass and relative HPLC retention time, the molecule appeared to represent a constitutional isomer of pikromycin, possibly neopikromycin. In order to determine its identity, a large-scale reaction was performed, and the product was isolated and analyzed by 1D and 2D

Scheme 4.3. Hypothesized hydroxylation reaction catalyzed by JuvD-RhFRED on **20** and possible degradation pathway.

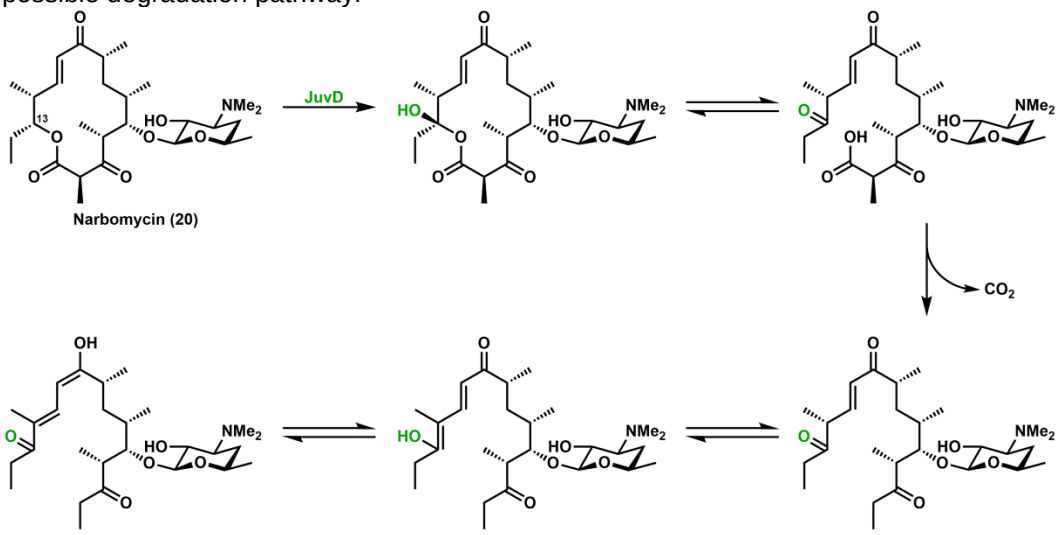

NMR. Despite straightforward HPLC purification and isolation of a single peak, the ^{1}H NMR spectrum indicated the presence of multiple molecular species. On the basis of

several lines of evidence, it appears likely that the site on **20** that JuvD-RhFRED targets for hydroxylation is the tertiary carbon (C13) adjacent to the lactone moiety. Installation of a hydroxyl group at C13 would produce a hemiketal species that could readily collapse to yield a linear acid, which could then undergo spontaneous decarboxylation and tautomerization to give a molecule with an exact mass ($[M+H]^+$) of 482 Da and a maximum absorbance (λ_{max}) around 288 nm (**Scheme 4.3**). These properties are consistent with those observed for one of the molecules isolated upon further purification of the purported hydroxy-**20** product. Moreover, the ^{1}H and ^{13}C NMR spectra of the main compound suggest the presence of additional ketone and olefin moieties relative to **20**. Work is ongoing to further purify this material and verify its exact structure.

Taken together, these results reveal JuvD as a versatile biocatalyst for the epoxidation and hydroxylation of a variety of macrolides. In comparing it with MycCI, the question of the structural basis for its unique regioselectivity properties immediately arises. Currently, we are carrying out cocrystallization trials with JuvD and its native substrate 23-DDTL (**3**). A detailed view of the specific interactions that mediate substrate binding in the JuvD active site will allow us to acquire a better understanding of the factors governing its ability to act on many of the same substrates as MycCI but preferentially install epoxides instead of hydroxyl groups. Furthermore, because JuvD exhibits appreciably higher activity on **20** compared with MycCI, it may employ an electrostatic-type substrate anchoring mechanism similar to that used by PikC, which interacts via salt bridge with the positively charged *N*,*N*-dimethylamino group of desosamine.[26,27] Accordingly, a cocrystal structure would provide a wealth of information that could be used to develop JuvD into a robust P450 biocatalyst for the selective functionalization of a range of complex molecules.

4.3 Comparative analysis of P450s TylI and JuvC

The activities of catalytically self-sufficient TylI-RhFRED and JuvC-RhFRED were compared across the same panel of 13 tylactone-type macrolides (**1**–**13**) that had been used to probe the substrate scope of JuvD-RhFRED and MycCI-RhFRED (**Figure 4.5**). TylI-RhFRED exhibited the highest activity on its native substrate **4**, with 86%

conversion to the monohydroxylated compound **5** and 9% conversion to the final aldehyde product **6** (**Table 4.4**). When the isolated intermediate **5** was subjected to the same reaction conditions, however, essentially no further conversion to **6** was observed (10%). One possible explanation for the low efficiency of the second oxidation step relative to the first relates to the use of a noncognate redox partner system for TylI in these experiments. Because the native ferredoxin and associated reductase for this P450 have not been identified in the genome of *Streptomyces fradiae*, we employed the RhFRED domain as a surrogate redox partner for TylI so that its activity could readily be reconstituted in vitro. However, as the nature of the proteins involved in electron transfer to P450 can dramatically impact the reactivity properties of the enzyme, it is likely that the ability of TylI to carry out the second oxidation reaction would greatly improve if it were acting in conjunction with its native redox partners. For example, the kinetics of MycCI-catalyzed hydroxylation of natural and non-natural substrates were notably increased when it was partnered with its native ferredoxin MycCII compared with spinach ferredoxin[16] and RhFRED.[24]

Table 4.4. Results of activity assays performed with TylI-RhFRED and JuvC-RhFRED.[a]

	TylI-RhFRED			**JuvC-RhFRED**		
Compound	CH_2OH	CHO	COOH	CH_2OH	CHO	COOH
1	78.9 ± 0.3	4.9 ± 0.2	0.1 ± 0.0	61.7 ± 0.6	4.3 ± 0.1	0.1 ± 0.0
2		7.7 ± 0.2	0.2 ± 0.0		6.4 ± 0.0	0.1 ± 0.0
3			18.0 ± 0.7			55.1 ± 1.6
4	86.4 ± 0.0	9.1 ± 0.1	0.2 ± 0.1	48.6 ± 1.4	4.5 ± 0.2	0.1 ± 0.0
5		10.4 ± 0.2	0.3 ± 0.0		7.7 ± 0.1	0.2 ± 0.0
6			22.7 ± 0.6			93.3 ± 2.4
7	51.1 ± 0.8	1.2 ± 0.0	<0.1	78.6 ± 0.9	4.0 ± 0.3	0.1 ± 0.0
8		2.5 ± 0.1	<0.1		5.1 ± 0.4	0.1 ± 0.0
9			4.8 ± 0.1			29.9 ± 2.3
10	43.8 ± 0.6	1.6 ± 0.1	0.1 ± 0.0	63.2 ± 0.6	3.8 ± 0.2	0.1 ± 0.0
11		5.0 ± 0.1	0.1 ± 0.0		6.7 ± 0.1	0.1 ± 0.0
12			12.3 ± 0.5			42.2 ± 5.5
13	17.9 ± 0.2	0.6 ± 0.0	0.1 ± 0.0	9.7 ± 0.4	0.2 ± 0.0	0.2 ± 0.0

[a]Average percent conversion values and standard deviations reflect the results of experiments performed and analyzed by LC-MS in duplicate. The percentage of the total reaction mixture consisting of hydroxyl (CH_2OH), aldehyde (CHO), and carboxylic acid (COOH) products is shown in each case.

In contrast to TylHI (see Chapter 3), the identity of the sugar (mycaminose vs desosamine) did not substantially impact the activity of TylI (**Table 4.4**). Indeed, it converted desosamine-containing **1** to both **2** (79%) and **3** (5%). Similar to the results

obtained with the native substrates **4** and **5**, feeding the hydroxylated intermediate **2** directly to TylI-RhFRED resulted in a very modest improvement in conversion to **3** (8%). Modification of the left side of **1** had a more significant effect on conversion. Installation of a hydroxyl group at C23 (**7**) reduced overall conversion to 52% (51% hydroxyl + 1% aldehyde) while epoxidation across the C12/C13 double bond (**10**) decreased conversion slightly further to 46% (44% hydroxyl + 2% aldehyde). However, TylI-RhFRED exhibited a small preference for performing the second oxidation reaction on the 12,13-epoxy substrate (5% conversion of **11** to **12**) compared with that bearing a hydroxyl group at C23 (2% conversion of **8** to **9**). Interestingly, the enzyme was also able to convert photoisomer **13** to single monohydroxylated (18%) and aldehyde (<1%) products, and an additional peak representing ~2% of the total reaction mixture was identified as a likely product of enzyme-catalyzed *N*-demethylation (this compound was seen as a major product of the JuvD-RhFRED reaction with the same substrate; **Table C.2**). Taken together, these results confirm the in vitro activity of TylI on its native substrate (**4**) for the first time and demonstrate its ability to perform sequential two-electron oxidations on a variety of different 16-membered ring macrolides. Nonetheless, unlike MycCI-RhFRED and JuvD-RhFRED, TylI-RhFRED was unable to accept the aglycone **18** as a substrate, underscoring the importance of key interactions with the deoxyamino sugar for effective substrate binding to the enzyme.

Overall, the activity of JuvC-RhFRED on these substrates mirrored that of TylI-RhFRED (**Table 4.4**). Unlike the latter, though, it displayed a moderate preference for **1** over **4** (66% and 53% overall conversion, respectively) and converted oxidized analogs of **1** with equal (**10**, 67% overall conversion) or improved (**7**, 83% overall conversion) efficiency relative to the unmodified substrate. On the basis of the reactivity profile of JuvD-RhFRED, **3** was proposed as the preferred native substrate for this enzyme in the juvenimicin pathway. However, since JuvC-RhFRED is equally capable of acting upon both **1** and **10**, and because JuvD-RhFRED shows high-level activity on **1** independent of its oxidation state at C20, identification of the “true” native substrate for each enzyme may be a senseless and impractical endeavor. Rather, as appears to be the case for the rosamicin pathway in *Micromonospora rosaria*,[15] multiple post-PKS modification routes probably operate simultaneously in the juvenimicin producer *M. chalcea*. In

contrast, given the strict substrate specificity of TylHI (Chapter 3), the preference of TylI for substrates unmodified at the C23 position, and additional corroborative results from in vivo and in vitro biotransformation studies (see Chapter 3 for references), tylosin biosynthesis in *Streptomyces fradiae* almost certainly proceeds via one predominant post-PKS tailoring pathway. Finally, like TylI-RhFRED, JuvC-RhFRED did not effectively carry out the second oxidation reaction on any of the C20-hydroxylated compounds to form the final aldehyde products (<10% conversion in all cases). In addition, its activity on **13** was diminished (10% monohydroxylation, 2% *N*-demethylation, and <1% aldehyde formation), and it was unable to hydroxylate **18**. Overall, these results clarify the role of JuvC in the juvenimicin biosynthetic pathway and demonstrate that its reactivity profile is similar to but distinct from that of TylI.

Scheme 4.4. Sequential oxidation reactions catalyzed by TylI and JuvC on tylactone-type 16-membered ring macrolides.

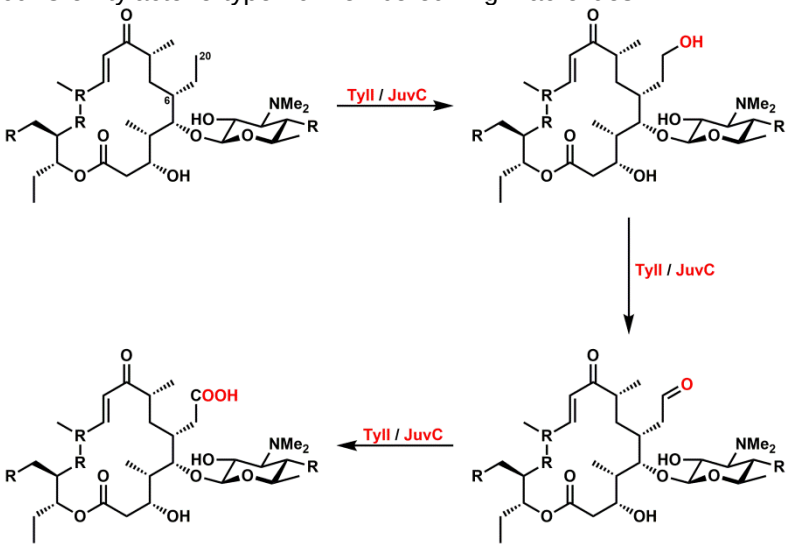

Previous reports detailed the isolation of novel 16-membered ring macrolides bearing a carboxylate moiety at C20 from *M. rosaria*[28] and an engineered strain of *S. fradiae*,[29] suggesting that endogenous enzymes were able to further oxidize the aldehyde normally present at this position. Given that a number of P450s are capable of carrying out three sequential two-electron oxidation reactions on their substrates, the most likely candidates for catalyzing these transformations were RosC (*M. rosaria*) and TylI (*S. fradiae*). In order to test this hypothesis, we examined TylI-RhFRED and JuvC-

RhFRED in parallel for catalytic activity toward four different aldehyde-containing macrolides (**3**, **6**, **9**, and **12**), all of which corresponded to the four-electron oxidation products of these two enzymes as previously described. As expected, each substrate was converted to a single product with an exact mass indicative of monohydroxylation (**Table 4.4**). Conversions were modest for TylI-RhFRED, with its native **6** serving as the best substrate (23% conversion) followed by **3** (18% conversion), **12** (12% conversion), and **9** (5% conversion). The hydroxylated version of the latter (**8**) also fared the worst among those tested for the second oxidation reaction to yield the aldehyde (*vide supra*). However, JuvC-RhFRED was able to perform the same reactions with superior catalytic efficiency as evidenced by significantly improved conversion of each aldehyde to the corresponding acid. Curiously, an inverse relationship was observed between the extent to which JuvC-RhFRED carried out the first oxidation reaction on a given substrate to afford the alcohol vs its ability to perform the third oxidation reaction on the same substrate to produce the acid (**Table 4.4**). For example, while the enzyme showed the poorest activity on **4** with respect to hydroxylation at C20, it exhibited the highest activity among the substrates tested for oxidation of the corresponding aldehyde **6** (93% conversion). Conversely, the scaffold of its best substrate for hydroxylation (**7**) served as its worst for aldehyde oxidation (**9**, 30% conversion). Despite exhibiting no preference for either **1** or **10** in the first oxidation reaction, JuvC-RhFRED converted 55% of **3** (the aldehyde of **1**) vs 42% of **12** (the aldehyde of **10**) to the corresponding acid. Incidentally, further inspection of the data revealed what could be an inherent reactivity bias for each of the aldehydes tested, as the aldehyde substrates for each enzyme followed the same order of most to least preferred (i.e., both enzymes showed the highest conversion of **6** followed in turn by **3**, **12**, and **9** to the corresponding acid products).

Although these reactions have yet to be performed on a large scale so that the purported products can be isolated and confirmed by NMR analysis, a recently published report describes the oxidation of **12** to 20-carboxy-rosamicin (**21**; **Figure 4.6**) by the P450s RosC and TylI.[30] This compound was fed to *E. coli* cells heterologously expressing these enzymes, and the product was identified as the corresponding acid by NMR. Interestingly, the antibacterial activity of **21** was considerably diminished relative

to that of the parent molecule bearing the aldehyde.[31] The latter functional group has been established as a critical pharmacophore for biological activity of these and related macrolides due to its ability to form a reversible covalent bond with a nucleobase residue of bacterial 23S rRNA.[11]

On the basis of several detailed in vitro studies that have been conducted on P450s like TylI and JuvC that carry out multistep oxidation reactions at a single site on their respective substrates, a plausible mechanism for the six-electron oxidation of the C20 methyl group of tylactone-type macrolides is shown in **Scheme 4.5**. The hydroxylated intermediate is further hydroxylated to form a *gem*-diol, which undergoes spontaneous dehydration to give the aldehyde. The latter species is then directly hydroxylated to form

Scheme 4.5. Postulated mechanism for TylI/JuvC-catalyzed six-electron oxidation of tylactone-type macrolides.

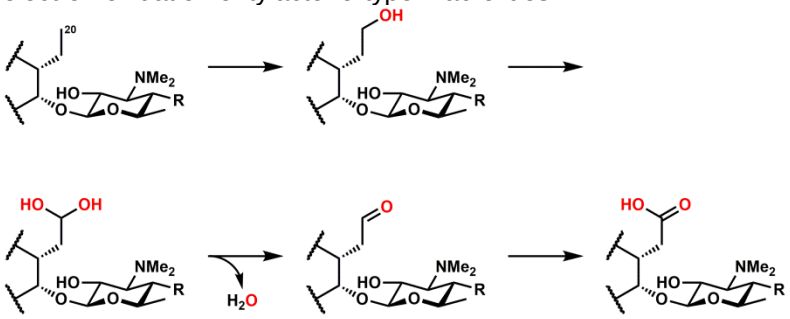

the acid. An alternative mechanism involving formation of a *gem*-triol (*ortho*-acid) from the *gem*-diol is unlikely given that the latter represents a very small fraction of the observed mass of the aldehyde substrate in the present set of experiments. Since the rates of hydration of carbonyls are relatively slow in aqueous solution, the P450 would somehow have to catalyze such a reaction in order for the *gem*-diol to be considered a viable intermediate for oxidation to the *ortho*-acid followed by dehydration to give the final carboxylic acid product.[32] Direct hydroxylation of the aldehyde could conceivably occur through either Compound I-mediated hydrogen atom abstraction or a mechanism involving addition of ferric peroxide to the carbonyl (see Chapter 5 for further discussion).

Another unanswered question relates to the processivity of the P450 in carrying out each step of the reaction sequence. While it is possible that intermediates are largely retained in the enzyme active site following each oxidation event, the results of analytical-scale reactions with TylI and JuvC presented above suggest that these P450s employ a distributive mechanism (i.e., product is released after each step). Indeed, the aldehyde product never accumulates beyond ~10% of the total reaction mixture, and approximately equal amounts of the aldehyde are observed when either unoxidized or hydroxylated compounds are used as substrates. Moreover, the carboxylic acid is only ever present in trace quantities unless the aldehyde is directly fed to the enzyme. These results are most consistent with a scenario wherein large amounts of each intermediate must build up prior to undergoing further oxidation. While several straightforward experiments (e.g., equilibrium substrate binding, steady-state kinetics) could help to resolve some of these outstanding questions, more sophisticated studies involving the measurement of kinetic isotope effects in addition to $^{18}O_2$ labeling and the employment of pulse-chase methods with radiolabeled substrate could be used to further clarify mechanism. These ideas will be further discussed as potential future directions in Chapter 5.

Through this comparative analysis of two unique P450 enzymes that catalyze six-electron oxidations on a range of macrolide substrates, we have gained important insights that can now be used to practically apply these enzymes as biocatalysts for the facile chemoenzymatic synthesis of new macrolide antibiotics (*vide infra*) as well as to design additional experiments in order to further understand the mechanistic details of the reactions they catalyze.

4.4 Chemoenzymatic synthesis of diverse 16-membered ring macrolides via P450-mediated late-stage tailoring

The incessant rise of antibiotic resistance among pathogenic microbes underscores the critical importance of developing new tools and methodologies to enable the facile synthesis of novel biologically active molecules. Building off of the strategies previously developed in our lab for the biocatalytic synthesis of 12- and 14-membered ring macrolides,[33] we set out to achieve a total chemoenzymatic synthesis of

the rosamicin, juvenimicin, and M-4365 classes of 16-membered ring macrolide antibiotics. On the basis of the robust activities and broad substrate scope of the P450s characterized in the preceding sections, we opted to employ them as biocatalysts for the late-stage diversification of chemoenzymatically generated **1** (see **Figure 4.5** for structures of compounds **1**–**20**).

To generate the tylactone aglycone scaffold (**18**), the natural tylactone hexaketide chain elongation intermediate was synthesized using traditional chemical methods. Following thiophenol activation and deprotection to afford **22**, it was loaded onto the penultimate module of the juvenimicin PKS (JuvEIV), which extended it by a single ketide unit (methylmalonyl *N*-acetylcysteamine cosubstrate) prior to passing it onto the final module (JuvEV; **Scheme 4.6A**). The latter effectively performed an additional extension using malonyl *N*-acetylcysteamine as a cosubstrate followed by offloading and concomitant macrocyclization of the completed octaketide to produce **18** (69% yield starting from **22**).

Scheme 4.6. (**A**) Chemoenzymatic synthesis of tylactone (**18**) and (**B**) biotransformation to DT (**1**) in *S. venezuelae* strain DHS316.

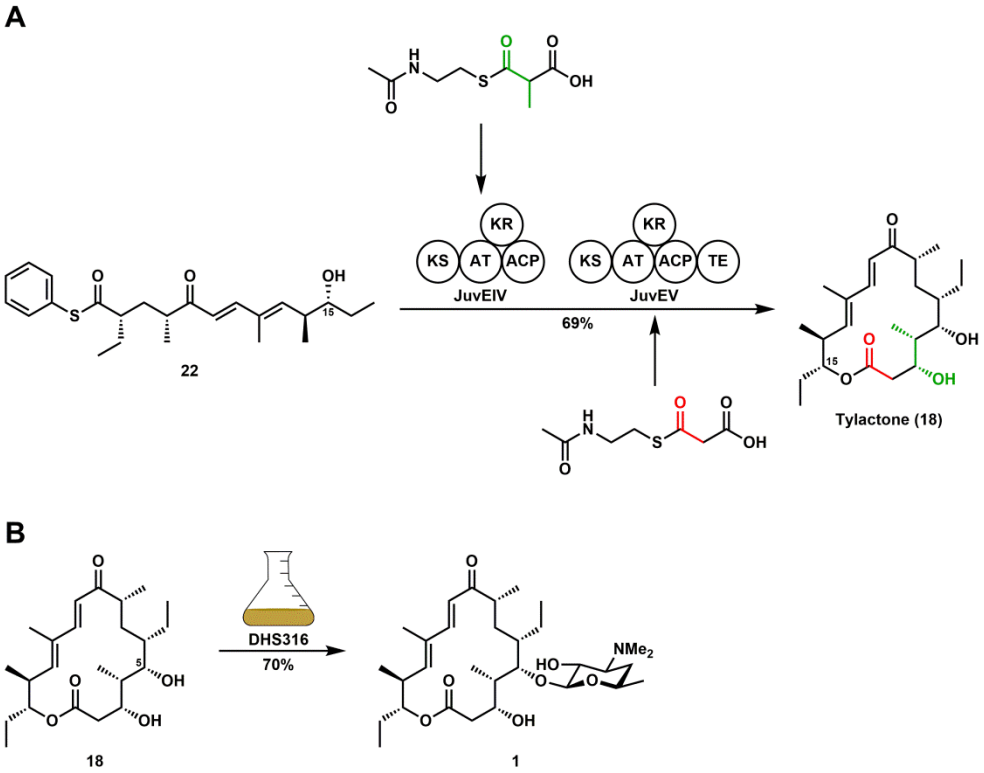

With the success of this chemoenzymatic approach to the completed macrocycle, we turned our focus to the final glycosylation and oxidative tailoring steps. We previously described an engineered strain of *Streptomyces venezuelae* (DHS316) that lacks the genes encoding the pikromycin PKS (PikAI-IV) and P450 (PikC), thereby rendering it incapable of producing its own macrolides.[24] However, as the *des* subcluster genes responsible for constructing and appending desosamine remain intact, the recombinant strain is able to biotransform exogenous macrolactones into the corresponding macrolides in a highly efficient manner. By employing DHS316 as a whole-cell biocatalyst for regioselective glycosylation, we could achieve isolated yields of **1** as high as 70% in a single step starting from **18** (**Scheme 4.6B**). The biotransformation reaction could readily be scaled up to 100 mg of starting material without compromising conversion to the desired product. This method is far superior to standard synthetic methodologies used for the desosaminylation of the pikromycin,[34] methymycin,[35] and mycinamicin[36,37] aglycones. Notably, none of these syntheses could obtain the activated sugar in greater than 50% yield despite the facile semisynthetic approach of acquiring desosamine via chemical degradation of erythromycin. This process does not even account for the additional steps required for attachment of the sugar to the macrolactone and final deprotection. For a more direct comparison of synthetic vs biocatalytic methods, the desosaminylation of PML-IV (**17**) was achieved in 24% overall yield over four chemical steps[16] whereas one-step biotransformation in DHS316 routinely afforded the desired M-VIII product (**14**) in double the yield.[24]

With significant quantities of the first macrolide (**1**) in hand, we assessed the potential for late-stage diversification to the remaining family members via P450-catalyzed oxidation. On the basis of the reactivity profiles that we had previously established for MycCI, JuvD, TylI, and JuvC, we surmised that the most efficient biocatalytic route would involve TylI-RhFRED-catalyzed hydroxylation of **1** to yield **2** followed by selective chemical oxidation to give **3**. Differential oxidative functionalization of these intermediates at the C12/C13 and C23 positions by JuvD-RhFRED and MycCI-RhFRED, respectively, would then lead to the other six target molecules. Upon scale-up, TylI-RhFRED effectively converted **1** into **2** with an isolated yield of 61% plus small amounts of the corresponding aldehyde (**3**) and recovered **1** (**Scheme 4.7**). Because

analytical-scale reactions had revealed that this enzyme poorly oxidized **2** to generate **3** (~8% conversion), we opted to utilize a copper(I)/TEMPO catalyst system[38,39] to selectively convert the C20 primary alcohol of **2** into an aldehyde. Using this strategy, **3** was obtained in a 57% isolated yield.

Next, JuvD-RhFRED was used in large-scale reactions to convert **1**, **2**, and **3** into **10**, **11**, and **12** with isolated yields of 55%, 63%, and 43%, respectively (**Scheme 4.7**). Finally, we employed MycCI-RhFRED for the selective hydroxylation of the same compounds, affording **7**, **8**, and **9** in 39%, 53%, and 47% isolated yields, respectively. Among the latter three, only **8** has been previously reported as an isolated metabolite from *M. chalcea*,[40] but **7** and **9** are potentially produced by this organism as well. The latter was isolated as izenamicin B_3 from *Micromonospora* sp. YS-02930K while a macrolide identical to **7** with the exception of a methyl in place of the ethyl group at C6

Scheme 4.7. Chemoenzymatic synthesis of diverse 16-membered ring macrolides via late-stage P450-catalyzed oxidation.

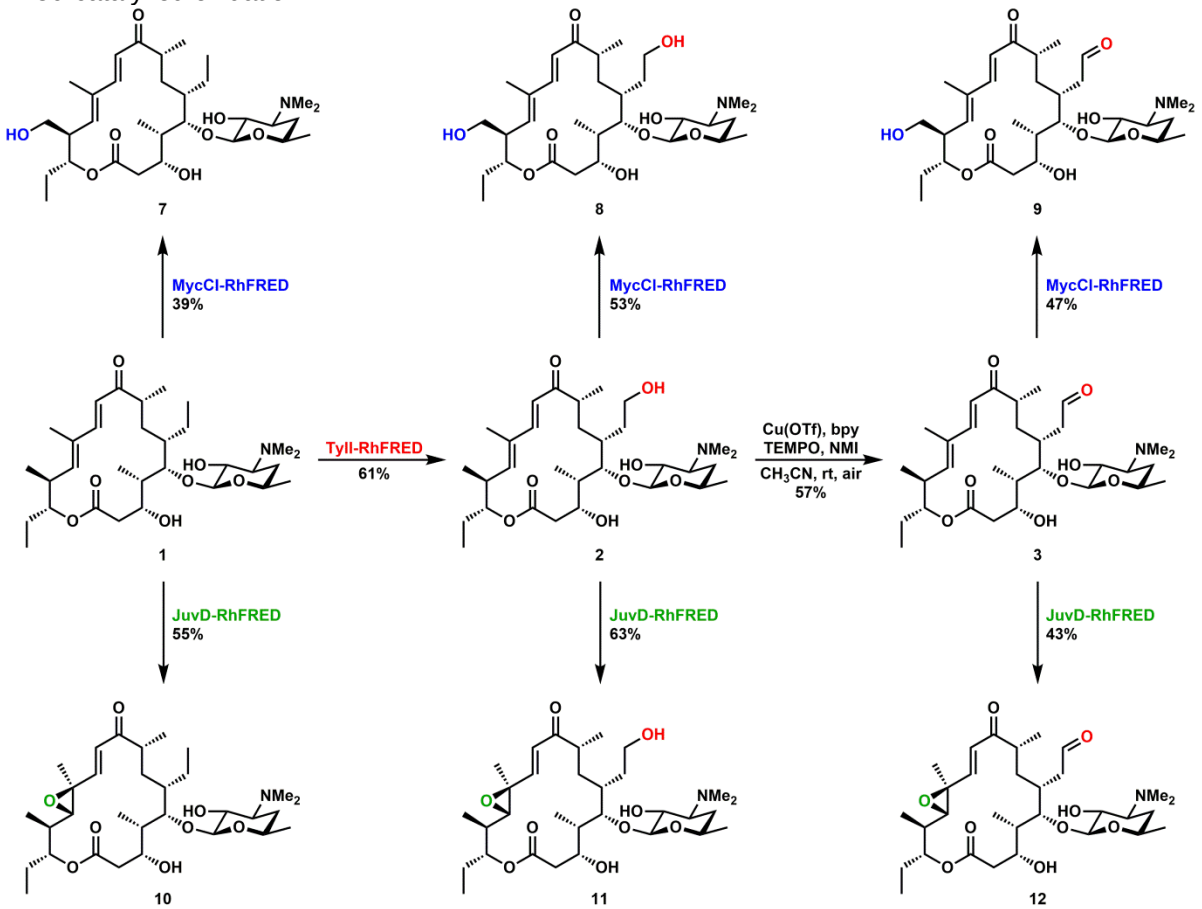

(izenamicin B_2) was isolated from the same strain, which produced additional izenamicins corresponding to rosamicin (**12**) and several juvenimicins (**2**, **8**, and **11**).[41] Compound **7** itself was first reported as a product of sequential biotransformation of **18** in two different *Streptomyces* strains,[42] but it has not been isolated as a natural product. Interestingly, izenamicin A_3 (12,13-epoxy-DTL, **23**) was also isolated from *Micromonospora* sp. YS-02930K,[41] and a reduced derivative of this compound (20-dihydro-23-hydroxy-rosamicin, **24**) was recently isolated from *Salinispora pacifica* CNS-237 (**Figure 4.6**).[43] Among the izenamicins, the B_3 variant (**9**) showed the highest antimicrobial activity against Gram-positive and Gram-negative bacteria,[41] indicating that the added epoxide in izenamicin A_3 (**23**) does not improve antibiotic potency. The analog of **23** and **24** with an unoxidized ethyl side chain (12,13-epoxy-23-OH-DT, **25**) has not been reported (**Figure 4.6**).

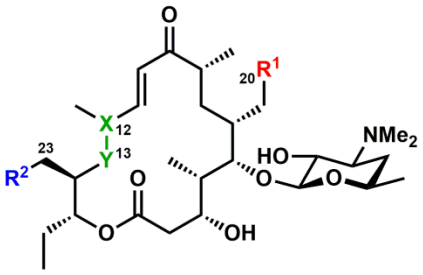

Compound	Name(s)	R^1	R^2	X–Y
21	20-carboxy-rosamicin	COOH	H	Epoxy
23	Izenamicin A_3 23-hydroxy-rosamicin	CHO	OH	Epoxy
24	20-dihydro-23-hydroxy-rosamicin	CH_2OH	OH	Epoxy
25	Unreported molecule	CH_3	OH	Epoxy
26	Unreported molecule	COOH	H	E alkene
27	Unreported molecule	COOH	OH	E alkene
28	Unreported molecule	COOH	OH	Epoxy

Figure 4.6. Structures of compounds **21** and **23**–**28**.

Scale-up and isolation of all the aforementioned compounds allowed us to test each of them as substrates for MycCI, JuvD, TylI, and JuvC (*vide supra*). A more complete understanding of the reactivity profiles of these P450s subsequently enabled us to confirm that the biocatalytic route as originally devised was the most effective

among several possible alternatives. Whereas TylI exhibited a clear preference for unoxidized substrates (i.e., **1**), MycCI preferentially hydroxylated intermediates bearing an oxidized ethyl side chain (i.e., **2** and **3**). Moreover, because JuvD could also efficiently epoxidize **8** and **9** in analytical-scale reactions, it would have likely been possible to scale these reactions up as well and isolate the previously reported compounds **24** and **23**, respectively. Unfortunately, since JuvD and MycCI did not readily accept **7** or **10** as substrates, respectively, it would not have been feasible to acquire the unreported macrolide **25** in high yield using our biocatalytic methodology. Save for **21**,[28,31,44] no carboxylated derivatives of these macrolides have been isolated or synthesized. Compared with TylI, JuvC was a superior biocatalyst for converting aldehydes into the corresponding carboxylic acids. Thus, it could be used to generate carboxylated versions of each of the molecules that we isolated in this study, yielding two (or three, if **23** were included as a viable substrate) new compounds that have not been reported previously (**26**–**28**).

Each of the ten macrolides (including **13**, the photoisomer of **1**) was tested in parallel with erythromycin and tylosin as positive controls against a panel of human bacterial pathogens in order to determine their relative minimum inhibitory concentrations (MICs; **Table C.3**). The activities of **3** and **12** were comparable to those of erythromycin and tylosin, showing strong activity against Gram-positive strains and enhanced activity against Gram-negative pathogens. These results are consistent with those previously described.[45-47] The aldehyde substituent of **3**, **9**, and **12** was critical to high activity; these compounds exhibited ~10-100-fold improvement over the corresponding C20-hydroxylated and unoxidized analogs. Testing of **13** revealed that the Z geometry at the C12/C13 olefin dramatically reduced its activity relative to that of **1**, suggesting that installation of the epoxide may serve as a protective mechanism to retain bioactivity rather than a critical pharmacophore. Indeed, the presence of this functional group did not significantly affect the activity of any of the compounds tested (**Table C.3**). Similar photoisomeric derivatives of tylosin also showed reduced activity compared with the parent molecule.[48] Hydroxylation at C23 also minimally impacted the bioactivity properties of these compounds. Further oxidation of the aldehyde to the carboxylic acid would almost certainly lead to a loss in activity due to removal of this

important pharmacophore; **21** has indeed been shown to be significantly less active than **12**.[30,31]

The work described herein represents the first efficient biocatalytic approach toward the 16-membered ring macrolactone core of tylosin along with late-stage chemoenzymatic diversification to procure nine members of the rosamicin, juvenimicin, and M-4365 family of macrolide antibiotics. The first mature natural product (**1**) was generated in 15 linear steps (21 total) with an overall yield of 4.6%. Our approach employed the native monomodular PKS enzymes responsible for completing polyketide chain elongation, processing, and macrocyclization followed by an engineered biotransformation strain to append the desosamine glycoside to the macrolactone core in the absence of protecting groups. Understanding the reactivity profiles of the P450s required for the native production of several different macrolides enabled us to implement a late-stage biocatalytic oxidation protocol to obtain a series of highly modified tylactone-type antibiotics. This strategy is uniquely divergent and allows for efficient regioselective C–H bond functionalization and/or olefin epoxidation. Thus, on the basis of the success of our efforts, judicious implementation of biocatalytic methods offers a compelling approach for modern synthetic methodology.

4.5 Summary and conclusions

Comparative analysis of P450s that act on the same substrates to effect different regiochemical outcomes provides a facile and valuable strategy by which to acquire a preliminary understanding of the factors controlling P450 selectivity. In the current study, the reactivity profiles of four P450s from three different biosynthetic pathways were assessed across a panel of up to 20 unique macrolactone and macrolide substrates. MycCI was previously shown to selectively hydroxylate a wide variety of 16-membered ring macrolactones independent of their glycosylation state. The P450 JuvD, which was identified as part of the juvenimicin biosynthetic gene cluster in *M. chalcea*, demonstrated high in vitro activity against many of the same 16-membered ring macrolide substrates as MycCI. Unlike the latter, however, it selectively installed epoxides across the C12/C13 olefins of these compounds. Because MycCI and JuvD are not highly homologous (34% sequence identity), it is improbable that the factors

governing their differential regioselectivity properties can be localized to a specific region of the enzyme. Unexpectedly, JuvD also exhibited appreciable activity on the chalconolide-type macrolide M-VIII (**14**). In this case, the major 12,13-epoxy product (**15**) was accompanied by a minor C14-hydroxylated species (**16**). These compounds represent new mycinamicins that have not been isolated or synthesized before, testifying to the biocatalytic potential of JuvD to generate novel complex molecules. It is also noteworthy to highlight the parallel role that MycG plays in the mycinamicin biosynthetic pathway, where it targets the same sites as JuvD for hydroxylation and epoxidation. In contrast to JuvD, however, MycG requires that an additional sugar residue be appended to the C21 hydroxyl group in order to facilitate binding and proper orientation of the substrate in the active site. Evidently, JuvD recognizes other parts of the macrolide to ensure effective substrate binding. One possibility is that, like in PikC, desosamine acts as an anchor by forming salt bridge contacts with acidic residues in the JuvD binding pocket. This hypothesis is supported by the observation that the 14-membered ring macrolide narbomycin (**20**) is also turned over by JuvD. Moreover, its activity on the 16-membered ring aglycone tylactone (**18**) is considerably diminished relative to that on the corresponding glycosides. Current efforts are focused on obtaining high-resolution X-ray crystal structures of JuvD in complex with several of its best substrates. The information gained from these as well as additional biochemical experiments will prove vital to understanding the unique reactivity properties of this enzyme so that it can be further engineered into a useful P450 biocatalyst.

The present chapter also presented a comparison of another newly identified P450 from the juvenimicin pathway (JuvC) and its homolog from the tylosin pathway (TylI). These two enzymes belong to a special class of P450s capable of performing consecutive oxidation reactions at a single site on a target molecule to give alcohol, aldehyde, and carboxylic acid products. In vitro reconstitution of catalytic activity achieved via fusion to the RhFRED domain revealed that these enzymes were effective hydroxylases on a range of tylactone-type macrolides. However, conversion of hydroxylated intermediates to the corresponding aldehydes was poor, possibly due to suboptimal electron transfer from the surrogate redox partner employed in these assays or ineffective binding of these compounds to the enzyme. Unexpectedly, further

oxidation of the aldehyde to the carboxylic acid was found to be much more effective, especially for JuvC. While several previous studies have clarified the roles of TylI and some of its homologs in their respective pathways through in vivo gene disruption and bioconversion experiments, no prior reports describe the expression, purification, and in vitro reconstitution of catalytic activity of these P450s. Even though TylI and JuvC share 70% sequence identity, their reactivity profiles are distinct. In addition, the broad substrate scope of both JuvC and JuvD indicates that multiple post-PKS pathways operate simultaneously in juvenimicin biosynthesis whereas the stricter substrate specificities of TylI and TylHI suggest the predominance of a single post-PKS tailoring pathway in the biosynthesis of tylosin. Future efforts will focus on designing and carrying out suitable experiments to answer several intriguing questions regarding the mechanism of these multifunctional P450s.

Finally, the inimitable catalytic properties of the P450s we characterized were leveraged to effect the late-stage diversification of a single chemoenzymatically generated 16-membered ring macrolide into eight additional members of the rosamicin, juvenimicin, and M-4365 family of antibiotics. Following in vitro PKS-catalyzed elongation of a mature synthetic hexaketide intermediate (**22**) and macrolactonization to produce **18**, a robust protocol for in vivo regioselective glycosylation allowed for production of **1** in 15 linear (21 total) steps with an overall isolated yield of 4.6%. The P450s TylI, JuvD, and MycCI along with a selective chemical oxidation protocol were then employed to afford the remaining macrolides with isolated yields averaging ~50% for each step. Subsequent antimicrobial assays confirmed the importance of the aldehyde moiety in conferring potent antibacterial activity on these compounds. Epoxidation was found to impact bioactivity only inasmuch as it precluded photoisomerization of the C12/C13 olefin, since the Z isomer of **1** (**13**) was virtually inactive as an antibiotic. The prudent implementation of biocatalytic methods for the construction of complex and diverse macrolides serves as an example of the great potential of biocatalysts to complement the vast repertoire of both new and well-established small-molecule catalysts in the synthesis of fine and commodity chemicals.

4.6 References

(1) Omura, S., and Nakagawa, A. (1981) Biosynthesis of 16-membered macrolide antibiotics, in *Biosynthesis* (Corcoran, J. W., Ed.), pp 175–192. Springer-Verlag, Berlin, Heidelberg.

(2) Katz, L., and Ashley, G. W. (2005) Translation and protein synthesis: macrolides. *Chem. Rev. 105*, 499–527.

(3) Nguyen, H.-C., Darbon, E., Thai, R., Pernodet, J.-L., and Lautru, S. (2013) Post-PKS tailoring steps of the spiramycin macrolactone ring in *Streptomyces ambofaciens*. *Antimicrob. Agents Chemother. 57*, 3836–3842.

(4) Ward, S. L., Hu, Z., Schirmer, A., Reid, R., Revill, W. P., Reeves, C. D., Petrakovsky, O. V., Dong, S. D., and Katz, L. (2004) Chalcomycin biosynthesis gene cluster from *Streptomyces bikiniensis*: novel features of an unusual ketolide produced through expression of the *chm* polyketide synthase in *Streptomyces fradiae*. *Antimicrob. Agents Chemother. 48*, 4703–4712.

(5) Tang, X.-L., Dai, P., Gao, H., Wang, C.-X., Chen, G.-D., Hong, K., Hu, D., and Yao, X.-S. (2016) A single gene cluster for chalcomycins and aldgamycins: genetic basis for bifurcation of their biosynthesis. *ChemBioChem 17*, 1241–1249.

(6) Wang, X., Tabudravu, J., Jaspars, M., and Deng, H. (2013) Tianchimycins A–B, 16-membered macrolides from the rare actinomycete *Saccharothrix xinjiangensis*. *Tetrahedron 69*, 6060–6064.

(7) Wang, C.-X., Ding, R., Jiang, S.-T., Tang, J.-S., Hu, D., Chen, G.-D., Lin, F., Hong, K., Yao, X.-S., and Gao, H. (2016) Aldgamycins J–O, 16-membered macrolides with a branched octose unit from *Streptomycetes* sp. and their antibacterial activities. *J. Nat. Prod. 79*, 2446–2454.

(8) Cui, W., and Ma, S. (2011) Recent advances in the field of 16-membered macrolide antibiotics. *Mini Rev. Med. Chem. 11*, 1009–1018.

(9) Hardy, D. J., Hensey, D. M., Beyer, J. M., Vojtko, C., McDonald, E. J., and Fernandes, P. B. (1988) Comparative in vitro activities of new 14-, 15-, and 16-membered macrolides. *Antimicrob. Agents Chemother. 32*, 1710–1719.

(10) Ajito, K., Miura, T., Furuuchi, T., and Tamura, A. (2014) Sixteen-membered macrolides: chemical modifications and future applications. *Heterocycles 89*, 281–352.

(11) Hansen, J. L., Ippolito, J. A., Ban, N., Nissen, P., Moore, P. B., and Steitz, T. A. (2002) The structures of four macrolide antibiotics bound to the large ribosomal subunit. *Mol. Cell 10*, 117–128.

(12) Leclercq, R. (2002) Mechanisms of resistance to macrolides and lincosamides: nature of the resistance elements and their clinical implications. *Clin. Infect. Dis. 34*, 482–492.

(13) Baltz, R. H., and Seno, E. T. (1981) Properties of *Streptomyces fradiae* mutants blocked in biosynthesis of the macrolide antibiotic tylosin. *Antimicrob. Agents Chemother. 20*, 214–225.

(14) Baltz, R. H., Seno, E. T., Stonesifer, J., and Wild, G. M. (1983) Biosynthesis of the macrolide antibiotic tylosin: a preferred pathway from tylactone to tylosin. *J. Antibiot. 36*, 131–141.

(15) Iizaka, Y., Higashi, N., Ishida, M., Oiwa, R., Ichikawa, Y., Takeda, M., Anzai, Y., and Kato, F. (2013) Function of cytochrome P450 enzymes RosC and RosD in the biosynthesis of rosamicin macrolide antibiotic produced by *Micromonospora rosaria*. *Antimicrob. Agents Chemother. 57*, 1529–1531.

(16) Anzai, Y., Li, S., Chaulagain, M. R., Kinoshita, K., Kato, F., Montgomery, J., and Sherman, D. H. (2008) Functional analysis of MycCI and MycG, cytochrome P450 enzymes involved in biosynthesis of mycinamicin macrolide antibiotics. *Chem. Biol. 15*, 950–959.

(17) Arisawa, A., Tsunekawa, H., Okamura, K., and Okamoto, R. (1995) Nucleotide sequence analysis of the carbomycin biosynthetic genes including the 3-*O*-acyltransferase gene from *Streptomyces thermotolerans*. *Biosci. Biotechnol. Biochem. 59*, 582–588.

(18) Malla, S., Thuy, T. T. T., Oh, T. J., and Sohng, J. K. (2011) Identification and characterization of *gerPI* and *gerPII* involved in epoxidation and hydroxylation of dihydrochalcolactone in *Streptomyces* species KCTC 0041BP. *Arch. Microbiol. 193*, 95–103.

(19) Merson-Davies, L. A., and Cundliffe, E. (1994) Analysis of five tylosin biosynthetic genes from the *tylIBA* region of the *Streptomyces fradiae* genome. *Mol. Microbiol. 13*, 349–355.

(20) Omura, S., Tanaka, H., and Tsukui, M. (1982) Biosynthesis of tylosin: oxidations of 5-*O*-mycaminosylprotylonolide at C-20 and C-23 with a cell-free extract from *Streptomyces fradiae*. *Biochem. Biophys. Res. Commun. 107*, 554–560.

(21) Omura, S., Tomoda, H., Yamamoto, S., Tsukui, M., and Tanaka, H. (1984) Studies on two

dioxygenases involved in the synthesis of tylosin in *Streptomyces fradiae*. *Biochim. Biophys. Acta 802*, 141–147.
(22) Li, S., Podust, L. M., and Sherman, D. H. (2007) Engineering and analysis of a self-sufficient biosynthetic cytochrome P450 PikC fused to the RhFRED reductase domain. *J. Am. Chem. Soc. 129*, 12940–12941.
(23) Zhang, W., Liu, Y., Yan, J., Cao, S., Bai, F., Yang, Y., Huang, S., Yao, L., Anzai, Y., Kato, F., Podust, L. M., Sherman, D. H., and Li, S. (2014) New reactions and products resulting from alternative interactions between the P450 enzyme and redox partners. *J. Am. Chem. Soc. 136*, 3640–3646.
(24) DeMars, M. D., II, Sheng, F., Park, S. R., Lowell, A. N., Podust, L. M., and Sherman, D. H. (2016) Biochemical and structural characterization of MycCI, a versatile P450 biocatalyst from the mycinamicin biosynthetic pathway. *ACS Chem. Biol. 11*, 2642–2654.
(25) Anzai, Y., Tsukada, S.-i., Sakai, A., Masuda, R., Harada, C., Domeki, A., Li, S., Kinoshita, K., Sherman, D. H., and Kato, F. (2012) Function of cytochrome P450 enzymes MycCI and MycG in *Micromonospora griseorubida*, a producer of the macrolide antibiotic mycinamicin. *Antimicrob. Agents Chemother. 56*, 3648–3656.
(26) Sherman, D. H., Li, S., Yermalitskaya, L. V., Kim, Y., Smith, J. A., Waterman, M. R., and Podust, L. M. (2006) The structural basis for substrate anchoring, active site selectivity, and product formation by P450 PikC from *Streptomyces venezuelae*. *J. Biol. Chem. 281*, 26289–26297.
(27) Li, S., Ouellet, H., Sherman, D. H., and Podust, L. M. (2009) Analysis of transient and catalytic desosamine-binding pockets in cytochrome P-450 PikC from *Streptomyces venezuelae*. *J. Biol. Chem. 284*, 5723–5730.
(28) Puar, M. S., and Schumacher, D. (1990) Novel macrolides from *Micromonospora rosaria*. *J. Antibiot. 43*, 1497–1501.
(29) Reeves, C. D., Ward, S. L., Revill, W. P., Suzuki, H., Marcus, M., Petrakovsky, O. V., Marquez, S., Fu, H., Dong, S. D., and Katz, L. (2004) Production of hybrid 16-membered macrolides by expressing combinations of polyketide synthase genes in engineered *Streptomyces fradiae* hosts. *Chem. Biol. 11*, 1465–1472.
(30) Iizaka, Y., Takeda, R., Senzaki, Y., Fukumoto, A., and Anzai, Y. (2017) Cytochrome P450 enzyme RosC catalyzes a multistep oxidation reaction to form the non-active compound 20-carboxyrosamicin. *FEMS Microbiol. Lett. 364*, doi: 10.1093/femsle/fnx110.
(31) Funaishi, K., Kawamura, K., Satoh, F., Hiramatsu, M., Hagiwara, M., and Okanish, M. (1990) New analogues of rosaramicin isolated from a *Micromonospora* strain. I. Taxonomy, fermentation, isolation and physico-chemical and biological properties. *J. Antibiot. 43*, 938–947.
(32) Guengerich, F. P., Sohl, C. D., and Chowdhury, G. (2011) Multi-step oxidations catalyzed by cytochrome P450 enzymes: processive vs. distributive kinetics and the issue of carbonyl oxidation in chemical mechanisms. *Arch. Biochem. Biophys. 507*, 126–134.
(33) Hansen, D. A., Rath, C. M., Eisman, E. B., Narayan, A. R. H., Kittendorf, J. D., Mortison, J. D., Yoon, Y. J., and Sherman, D. H. (2013) Biocatalytic synthesis of pikromycin, methymycin, neomethymycin, novamethymycin, and ketomethymycin. *J. Am. Chem. Soc. 135*, 11232–11238.
(34) Oh, H.-S., and Kang, H.-Y. (2012) Total synthesis of pikromycin. *J. Org. Chem. 77*, 1125–1130.
(35) Oh, H.-S., Xuan, R., and Kang, H.-Y. (2009) Total synthesis of methymycin. *Org. Biomol. Chem. 7*, 4458–4463.
(36) Suzuki, K., Maeta, H., Matsumoto, T., and Tsuchihashi, G.-i. (1988) New glycosidation reaction 2. Preparation of 1-fluoro-D-desosamine derivative and its efficient glycosidation by the use of Cp_2HfCl_2-$AgClO_4$ as the activator. *Tetrahedron Lett. 29*, 3571–3574.
(37) Matsumoto, T., Maeta, H., Suzuki, K., and Tsuchihashi, G.-i. (1988) First total synthesis of mycinamicin IV and VII. Successful application of new glycosidation reaction. *Tetrahedron Lett. 29*, 3575–3578.
(38) Hoover, J. M., and Stahl, S. S. (2011) Highly practical copper(I)/TEMPO catalyst system for chemoselective aerobic oxidation of primary alcohols. *J. Am. Chem. Soc. 133*, 16901–16910.
(39) Hoover, J. M., Steves, J. E., and Stahl, S. S. (2012) Copper(I)/TEMPO-catalyzed aerobic oxidation of primary alcohols to aldehydes with ambient air. *Nat. Protoc. 7*, 1161–1166.
(40) Kishi, T., Harada, S., Yamana, H., and Miyake, A. (1976) Studies on juvenimicin, a new antibiotic. II. Isolation, chemical characterization and structures. *J. Antibiot. 29*, 1171–1181.
(41) Imai, H., Suzuki, K., Morioka, M., Sasaki, T., Tanaka, K., Kadota, S., Iwanami, M., Saito, T., and Eiki, H. (1989) Izenamicins: macrolide antibiotics. *J. Antibiot. 42*, 1000–1002.

(42) Sadakane, N., Tanaka, Y., and Omura, S. (1983) Hybrid biosynthesis of a new macrolide antibiotic by a daunomycin-producing microorganism. *J. Antibiot. 36*, 921–922.
(43) Awakawa, T., Crüsemann, M., Munguia, J., Ziemert, N., Nizet, V., Fenical, W., and Moore, B. S. (2015) Salinipyrone and pacificanone are biosynthetic by-products of the rosamicin polyketide synthase. *ChemBioChem 16*, 1443–1447.
(44) Nakajima, S., Kojiri, K., Morishima, H., and Okanishi, M. (1990) New analogs of rosaramicin isolated from a *Micromonospora* strain. II. Structure determination. *J. Antibiot. 43*, 1006–1009.
(45) Wagman, G. H., Waitz, J. A., Marquez, J., Murawski, A., Oden, E. M., Testa, R. T., and Weinstein, M. J. (1972) A new *Micromonospora*-produced macrolide antibiotic, rosamicin. *J. Antibiot. 25*, 641–646.
(46) Hatano, K., Higashide, E., and Shibata, M. (1976) Studies on juvenimicin, a new antibiotic. I. Taxonomy, fermentation and antimicrobial properties. *J. Antibiot. 29*, 1163–1170.
(47) Furumai, T., Maezawa, I., Matsuzawa, N., Yano, S., Yamaguchi, T., Takeda, K., and Okuda, T. (1977) Macrolide antibiotics M-4365 produced by *Micromonospora*. I. Taxonomy, production, isolation, characterization and properties. *J. Antibiot. 30*, 443–449.
(48) Werner, J. J., Chintapalli, M., Lundeen, R. A., Wammer, K. H., Arnold, W. A., and McNeill, K. (2007) Environmental photochemistry of tylosin: efficient, reversible photoisomerization to a less-active isomer, followed by photolysis. *J. Agric. Food Chem. 55*, 7062–7068.

Chapter 5: Conclusions and future directions

5.1 Biochemical and structural characterization of P450s MycCI and TylHI

5.1.1 Conclusions

The critical discoveries that laid the foundation for the work described in this dissertation were made by judicious exploration of the substrate scope and selectivity properties of selected bacterial P450s involved in the biosynthesis of diverse macrolide antibiotics. Contrary to previously reported results,[1] the mycinamicin biosynthetic P450 MycCI exhibited robust monooxygenase activity on both its native 16-membered ring macrolide substrate (M-VIII) and the corresponding aglycone (PML-IV). Similar levels of turnover were observed on tylactone-based compounds, demonstrating the unprecedented inherent flexibility of this enzyme. Surprisingly, the homologous P450 from the tylosin biosynthetic pathway, TylHI, exhibited a strikingly narrow substrate scope, as initial experiments revealed appreciable activity of this enzyme only on its native substrate (23-DMTL). Chapters 2 and 3 described biochemical and structural studies that were carried out in order to understand the differences in the reactivity profiles of these two P450s at the molecular level. Equilibrium substrate binding assays provided a key insight, revealing the ability of MycCI to bind 16-membered ring macrolides with exceptionally high affinity (K_d < 100 nM). Thus, while removal of the desosamine glycoside from these substrates increased the dissociation constant by three to four orders of magnitude, the aglycones could still bind rather well to MycCI. A comparable decrease in binding affinity was seen with respect to TylHI binding its native macrolide substrate 23-DMTL vs the corresponding aglycone (tylactone). However, the "average" binding of 23-DMTL to TylHI (K_d = ~0.5 μM) compared with the unusually tight binding of M-VIII to MycCI (K_d = ~1 nM) rendered the binding affinity of tylactone to TylHI (K_d = 284 μM) outside of the range for acceptable substrates. Not only was the presence of a deoxyamino sugar residue essential for effective substrate binding, but its

specific identity was found to be virtually just as critical in facilitating proper recognition by TylHI. Indeed, substituting desosamine for mycaminose in the native substrate resulted in an analog that bound with the same affinity (within error) as tylactone.

The high-resolution X-ray crystal structures of both MycCI and TylHI in complex with their native substrates were solved in order to gain detailed insight into the molecular basis for substrate recognition by these two enzymes. Their overall structures were highly similar (RMSD = 0.76 Å), and the substrates bound in nearly identical positions/orientations within the active site of each enzyme. In each case, the methyl group located close to and directly above the heme iron corresponded to the experimentally observed site of hydroxylation, thus serving to validate the accuracy of the structural models. Most of the amino acids comprising the active site were identical or similar between MycCI and TylHI, with nonspecific contacts between hydrophobic residues and the substrate tending to dominate the intermolecular interaction network. Consistent with the ability of MycCI to tolerate aglycones as substrates, no important polar interactions between the desosamine moiety of M-VIII and active site residues were observed. This situation stands in stark contrast to that previously encountered with the P450 PikC, which employs an “anchoring”-like mechanism involving critical salt bridge interactions between the *N*,*N*-dimethylamino group of desosamine and carboxylate-containing residues to properly bind and position both natural and unnatural substrates in the active site. Interestingly, while it was clearly demonstrated that TylHI requires its substrates to possess a deoxyamino sugar, molecular recognition of this functionality was not mediated by electrostatics. Instead, preferential binding of substrates bearing mycaminose over desosaminylated analogs appeared to be largely facilitated by the energetically favorable burial of the 4’-hydroxyl group of mycaminose in a small hydrophilic pocket made up of the backbone amide nitrogen and carbonyl oxygen atoms of two residues in the BC loop. Substrate analog and mutagenesis studies further revealed the relative insignificance of the aldehyde substituent in assisting substrate binding.

Despite the preponderance of structural similarities between MycCI and TylHI, the identities and/or positions of several amino acid residues in the BC and FG loop regions differed between the two enzymes. For instance, while R65 in MycCI was

mostly solvent exposed, the guanidinium side chain of the corresponding R96 in TylHI was positioned in the active site to electrostatically interact with D101. In turn, the latter interacted with R310 to form a cohesive salt bridge interaction network, which was shown to be critical for proper substrate binding in TylHI. Moreover, the positions of the amino acids making up a short contiguous stretch of the BC loop deviated quite substantially between MycCI (G71-R77) and TylHI (G102-R108). Although the corresponding residues were identical or similar between the two enzymes with respect to charge and size, the two glycines in MycCI (G73/G75) that replaced alanines in TylHI (A104/A106) as well as the proline in the latter ($TylHI_{P99}$) that substituted for glutamic acid in the former ($MycCI_{E68}$) likely contributed to the differential flexibility of this region, thus leading to the observed shifts in the Cα backbone. Incidentally, the residues constituting this portion of the BC loop were also those that closely approached bound substrate in each crystal structure.

Further insight was acquired from comparative analysis of a third P450, ChmHI, which acted like a naturally occurring MycCI/TylHI chimera for the purposes of our investigations. This enzyme was more closely related to MycCI from a functional standpoint, however, in that it was capable of hydroxylating both chalconolide- and tylactone-type macrolactones and macrolides. Subsequent alignment of the primary sequences of all three homologs revealed regions of similarity between MycCI/ChmHI and divergence from TylHI. In conjunction with the comparative structural analysis of MycCI and TylHI, this information aided in the identification of the BC loop as a prime target for the construction of MycCI/TylHI chimeras in order to probe the role of this region in conferring unique reactivity profiles on these two P450s. Indeed, substituting the native BC loop in TylHI with that from MycCI resulted in a chimera that could bind and hydroxylate all of the macrolides tested. While wild-type TylHI could only appreciably turn over mycaminosylated macrolides, the chimera was capable of hydroxylating both mycaminosylated and desosaminylated substrates with comparable levels of efficiency. It could also accept the chalconolide-type macrolide M-VIII as a substrate, although conversion was not as high as that for the tylactone-type macrolides. As a first step toward further honing in on a specific portion of the BC loop that most substantially affects substrate binding, an additional chimera was generated

by targeting a stretch of five residues selected by judicious analysis of the MycCI/TylHI structures as well as the sequences of all three P450 homologs. Substrate turnover and binding assays demonstrated that this section of the BC loop played a key role in controlling the preferential binding of mycaminosylated substrates to wild-type TylHI as evidenced by a significant improvement in the ability of the quintuple TylHI mutant to bind and hydroxylate desosaminylated substrates. Work is currently ongoing to understand why the BC loop is so important in this regard.

5.1.2 Future directions

Despite the valuable questions we have thus far been able to answer with respect to the differences between MycCI and TylHI, many more remain to be explored. First and foremost among these is the molecular basis for the ability of MycCI to tightly bind macrolactone aglycones, thereby allowing them to serve as viable substrates for hydroxylation by this enzyme. The chimeragenesis experiments carried out with MycCI and TylHI showed that exchanging the BC loop of the latter with that of the former did not improve the binding of tylactone or PML-IV to TylHI. Nonetheless, the chimera was able to convert ~3% of tylactone to the monohydroxylated product. Collectively, these results are consistent with a minimal role played by the BC loop in conferring on MycCI the ability to turn over aglycone substrates. This finding is unsurprising given that the residues comprising the BC loop tend to approach the deoxyamino sugar more closely than the core macrocycle. Since ChmHI is also capable of hydroxylating aglycones, primary sequence analysis has aided in the identification of specific residues that may serve as viable candidates for further mutagenesis. One that stands out in particular is $MycCI_{I378}$/$TylHI_{V410}$ (located in SRS6), which constitutes the only difference between an otherwise completely conserved hydrophobic rim surrounding the end of the macrolactone proximal to the heme in each enzyme. The additional methyl group present in isoleucine vs valine may provide key hydrophobic contacts with the portion of the substrate close to the target site for hydroxylation. However, because MycCI binds tylactone nearly 100-fold more tightly than does TylHI, additional residues are likely to contribute in some capacity to highly effective macrolactone binding.

The MycCI/TylHI chimeragenesis studies were instrumental in unveiling the importance of the BC loop in affecting the substrate scope of these two enzymes. Whereas TylHI requires that mycaminose be appended to its substrates, MycCI is indifferent to the identity of the deoxyamino sugar. When the BC loop of MycCI was substituted for that of TylHI, the resulting chimera was capable of indiscriminately binding both mycaminosylated and desosaminylated macrolides. This effect was largely maintained when the targeted region was reduced to only five residues located in the middle of the BC loop. Because no direct contacts between the deoxyamino sugar and amino acid side chains were perturbed in generating these chimeras, the mechanism by which these mutations so profoundly affected substrate binding remains unclear. One hypothesis is that the two additional glycine residues present in the MycCI BC loop increase the flexibility of this region of the protein, which could influence substrate binding kinetics. Stopped-flow spectrophotometry would provide a robust experimental platform for determining the rates at which different substrates bind to wild-type TylHI and to each of the chimeras. One might predict that the increased flexibility of the MycCI BC loop would lead to more rapid substrate binding due to more frequent sampling of open conformational states. The relative importance of the glycine residues in this regard could be directly probed by generating and testing single and/or double mutant chimeras. Due to its bulky and hydrophobic nature, MycCI$_{F76}$ also stands out as a prime (chimera/muta)genesis target. Additional chimeras may also be created in order to explore other parts of the BC loop that do not directly contact bound substrate. Current work that we are performing in collaboration with Dr. Kendall Houk (UCLA) is focused on using molecular dynamics simulations to further understand how the differences between the MycCI and TylHI BC loops impact the local and global conformational dynamics of each enzyme. These factors may ultimately prove to be chiefly responsible for the ability of MycCI to effectively bind diverse macrolides.

Other unanswered questions relate to the fundamental mechanism of MycCI- and TylHI-catalyzed hydroxylation. Steady-state kinetic analysis revealed notable differences in the rates of product formation by MycCI as a function of the associated redox partner. The self-sufficient MycCI-RhFRED fusion enzyme displayed typical Michaelis-Menten kinetics, with k_{cat} and K_m values exhibiting significant dependence on

the substrate employed. In contrast, MycCI partnered in trans with its native ferredoxin (MycCII) and spinach ferredoxin reductase (MBP-FdR) showed partial substrate inhibition characterized by relatively “high” rates of product formation (e.g., 1-2 min^{-1}) at low concentrations of substrate that approached ~1 min^{-1} as concentrations were increased. Moreover, these rates were very similar irrespective of the identity of the substrate. One question that arises from these data relates to why MycCI-RhFRED is slower than MycCI/MycCII/MBP-FdR across all substrates tested. One obvious answer is that RhFRED provides a suboptimal redox partner compared with the native MycCII. Thus, electron transfer is a likely candidate for the rate-limiting step in reactions involving MycCI-RhFRED. Given the appreciably higher K_m values associated with steady-state turnover of the aglycones, binding of these substrates may be partially rate-limiting. However, because substrate binding is not modulated by the presence of the RhFRED domain, and since the tripartite system is able to turn over the aglycones more rapidly than the single-component catalyst, it is more plausible that one or more of the steps following substrate binding are responsible for setting the overall reaction rate. It would be prudent to repeat the kinetics experiments using different concentrations of the stand-alone RhFRED domain added in trans to reactions containing MycCI or MycCI-RhFRED. Increased reaction rates with increasing concentrations of RhFRED would provide strong evidence in favor of electron transfer as the rate-limiting step for MycCI-RhFRED.

It is less clear whether electron transfer may also be rate-limiting for the tripartite MycCI/MycCII/MBP-FdR system. In theory, the overall rate of P450-catalyzed hydroxylation could be affected by any (including more than one) of the steps of the catalytic cycle.[2] While substrate binding is usually fast, it may become rate-limiting at low concentrations.[3] As previously noted, the rate of substrate binding can be measured in the pre-steady state using stopped-flow spectrophotometry with absorbance monitored at ~390 nm, which increases upon substrate binding due to displacement of the iron-ligated water molecule. The next step in the catalytic cycle is electron transfer, which can also be measured using stopped-flow techniques. Ferrous P450 generated from the ferric resting state by one-electron reduction can be trapped as the carbon monoxide (CO) adduct under anaerobic CO-saturated conditions, thus producing the

characteristic peak at 450 nm that can be monitored over time by optical absorption spectroscopy to determine the rate of the first electron transfer step. In a complementary approach, steady-state rates of product formation could be measured with varying concentrations of MycCII in order to more thoroughly assess the impact of this ferredoxin partner on MycCI catalysis.

Dioxygen (O_2) binding to ferrous P450 occurs quite rapidly (near the diffusion limit) and is thus rarely considered as a potential rate-limiting step in P450 kinetic analyses. The subsequent electron and proton transfer steps that occur en route to Compound I formation may be probed via measurement of kinetic solvent isotope effects. The rates of transfer of the two protons to the ferric peroxo intermediate that must occur prior to O–O bond heterolysis would most likely be slower in the presence of D_2O. The difference in overall rate of product formation could be detected in the steady state if these steps were at least partially rate limiting. For some P450/substrate combinations, the C–H bond scission step itself is rate-limiting. Because the target site for oxidation in MycCI substrates is an unactivated primary C–H bond, the barrier for C–H abstraction is relatively high. While ΔG for C21–H abstraction is 19.9 kcal/mol for

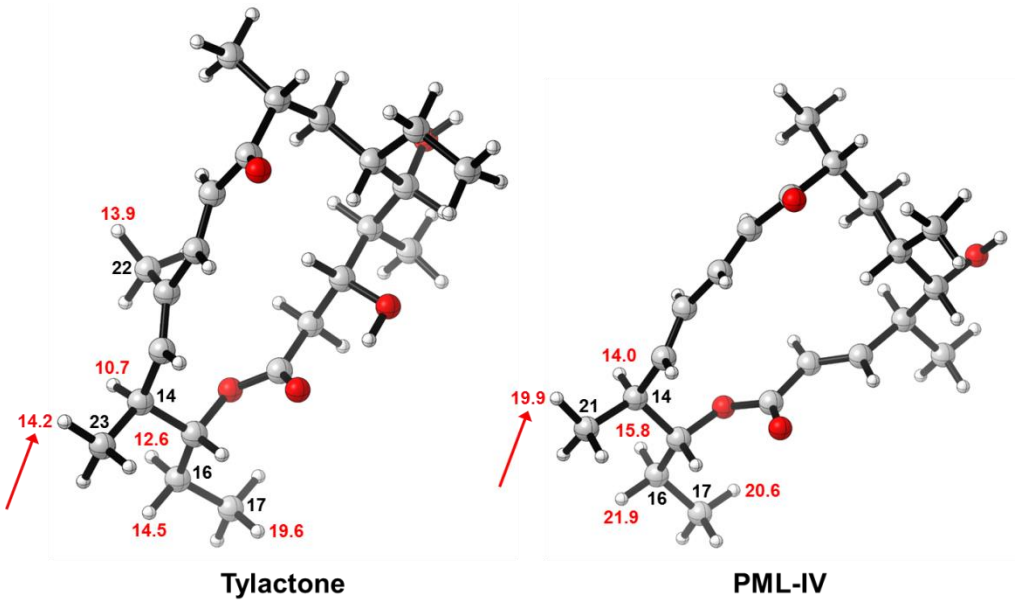

Figure 5.1. Quantum mechanical analysis of the energy associated with C–H abstraction transition states for tylactone and PML-IV. ΔG values for C–H abstraction (kcal/mol) are shown in red next to each respective hydrogen atom. Relevant carbon atoms are labeled with black numbers. Red arrows point to the sites targeted by MycCI (and TylHI) for oxidation.

PML-IV, the barrier for abstraction of the corresponding hydrogen in tylactone (C23–H) is only 14.2 kcal/mol (**Figure 5.1**; unpublished results from the Houk lab). Despite this large difference in activation energy ($\Delta\Delta G$ = 5.7 kcal/mol, $>10^4$-fold difference in uncatalyzed rate), MycCI/MycCII/MBP-FdR exhibits essentially identical kinetics for turning over these two substrates. While this step is therefore unlikely to be rate-limiting, it could be further explored by measuring primary hydrogen/deuterium kinetic isotope effects. To generate appropriate deuterated substrates, hydroxylated products could be isolated, selectively iodinated, and then reduced with a borodeuteride reagent to incorporate deuterium at the target site for hydroxylation.

Finally, if a step after product formation is rate-limiting, one would expect to observe an initial burst phase in the pre-steady state. A burst indicates that product remains in the active site after the first turnover; thus, its release or another step following product formation but preceding release (e.g., a conformational change in the enzyme) limits the steady-state rate.[2,4] It would be fairly straightforward to obtain pre-steady state kinetic parameters for MycCI using a quenched-flow apparatus. The rate of product release could also be estimated by performing spectral titration assays to determine K_d values for each of the products. Tight binding of products would provide evidence in favor of product release as at least partially rate-limiting. Steady-state kinetics assays in the presence of varying concentrations of product would also prove worthwhile in helping to answer the question of whether product inhibition plays a significant role in modulating the outcome of endpoint turnover assays (e.g., total turnover number).

Another question arising from the steady-state kinetics results relates to the mechanism of partial substrate inhibition seen for the tripartite MycCI/MycCII/MBP-FdR catalytic system across all substrates tested. The unusual kinetics profiles observed in these cases are consistent with the presence of two substrate binding sites on the enzyme. At sufficiently high concentrations of substrate, occupation of the allosteric binding site could disrupt the rate-limiting step of the reaction by any number of possible mechanisms, such as by inducing conformational changes in the P450 and/or disrupting cooperative interactions between the P450 and its ferredoxin partner (this issue is addressed more extensively in Appendix A). Performing the kinetics experiments with

RhFRED supplemented in large excess over MycCI (e.g., 200:1 molar ratio) would provide a simple means of addressing the question of whether partial substrate inhibition is specifically dependent on MycCII. However, initial rates would likely have to exceed the fastest rate observed for MycCI-RhFRED (~1.2 min^{-1}) in order for any inhibition to be detected.

Additional future efforts will aim toward further expanding the biocatalytic potential of MycCI by improving its activity on natural and unnatural substrates as well as by altering its regioselectivity. While MycCI is active on both 16-membered ring macrolides and aglycones, it exhibits a clear preference for the former. Interestingly, marginal improvements in binding and turnover of PML-IV and tylactone were evident upon introduction of the S172A mutation. These results suggest that it may be possible to shift the substrate preference for MycCI toward macrolactones by structure-based enzyme engineering and/or directed evolution. A suitable colorimetric assay could be developed for judicious implementation of the latter approach. Permethylation of 21-hydroxy-PML-IV (ML-IV) would generate a viable probe for the assay. Selective hydroxylation of the methyl group appended to the C21 hydroxyl group would produce a hemiacetal intermediate. This species would collapse to afford formaldehyde as a byproduct, which reacts with purpald reagent (4-amino-3-hydrazino-5-mercapto-1,2,4-triazole) to form a purple adduct with a maximum absorbance at 550 nm (**Scheme 5.1**). Thus, a large library of MycCI variants generated by site-saturation mutagenesis of key

Scheme 5.1. Possible high-throughput colorimetric screening assay for the directed evolution of MycCI variants with improved activity on macrolactone aglycones.

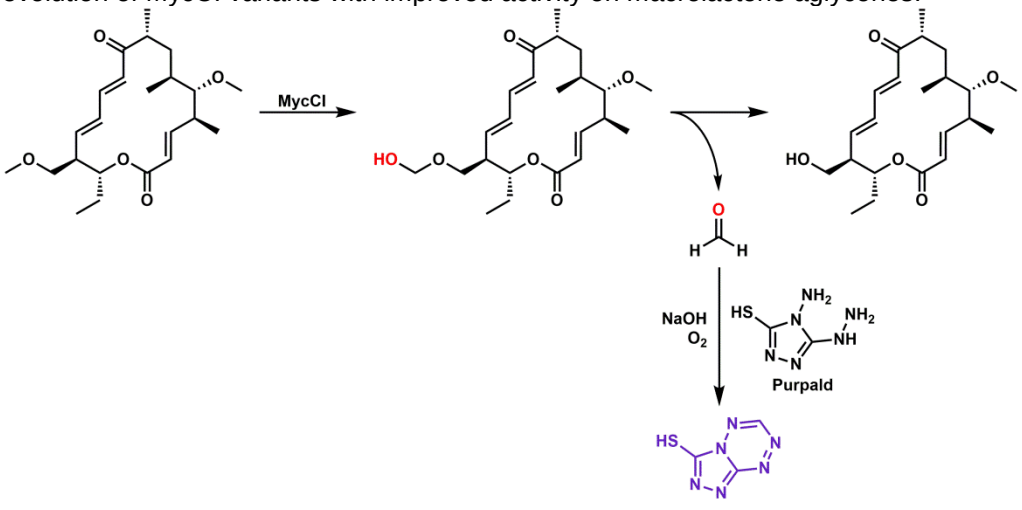

residues in and around the active site could be rapidly screened using a high-throughput spectrophotometric assay.

The reliance of P450s on other redox proteins for proper delivery of electrons has limited their broader application in biotechnology.[5-7] One commonly employed strategy to overcome this problem has been to construct artificial fusions in which these auxiliary flavin- and/or FeS-containing proteins are covalently linked to the P450 heme domain, thereby generating catalytically self-sufficient biocatalysts. The reductase domains of CYP102A1 ($P450_{BM3}$, BMR) and CYP116B2 ($P450_{RhF}$, RhFRED) have served as the most popular surrogate redox partners for various bacterial and even mammalian P450s.[8] Our lab has traditionally met with great success in generating artificial P450-RhFRED fusion constructs using bacterial P450s from different secondary metabolic pathways. Despite exhibiting slower kinetics than the tripartite system, MycCI-RhFRED showed higher total turnover numbers (TTNs) on 16-membered ring macrolide substrates. Surprisingly, TTNs for the single-component biocatalyst doubled across all substrates tested upon retention of protein impurities (e.g., molecular chaperones) despite turnover frequency (TOF) decreasing by ~30% on average compared with the pure enzyme, indicating that “semipure” MycCI-RhFRED remained active for a longer period of time in the reaction mixture.

The low coupling efficiency of the fusion enzyme (≤12%) likely contributed to its somewhat rapid oxidative degradation in vitro, leading in turn to lower substrate turnovers (see Appendix A for further discussion). Thus, the activity of MycCI-RhFRED could likely be increased even further simply by improving its coupling efficiency. Several possible strategies may be pursued in order to achieve this objective (**Figure 5.2**). One relatively straightforward approach would be to test additional reductase domains beyond RhFRED (e.g., BMR from $P450_{BM3}$; **Figure 5.2A**). Recently, artificial self-sufficient P450 nitration biocatalysts were generated by fusing TxtE from the thaxtomin biosynthetic pathway to either the RhFRED or the BMR domain.[9] The latter construct exhibited much higher activity as well as coupling efficiency relative to the former, indicating that BMR and potentially other reductase domains from $P450_{BM3}$ and $P450_{RhF}$ homologs would be worth pursuing in the context of MycCI and the other biosynthetic P450s described herein.

A second strategy to improve the coupling efficiency of MycCI-RhFRED would entail modulating the length of the linker region connecting the heme and reductase domains (**Figure 5.2B**). A number of studies have investigated the impact of this variable on P450 activity, stability, and coupling efficiency. Early studies with $P450_{BM3}$

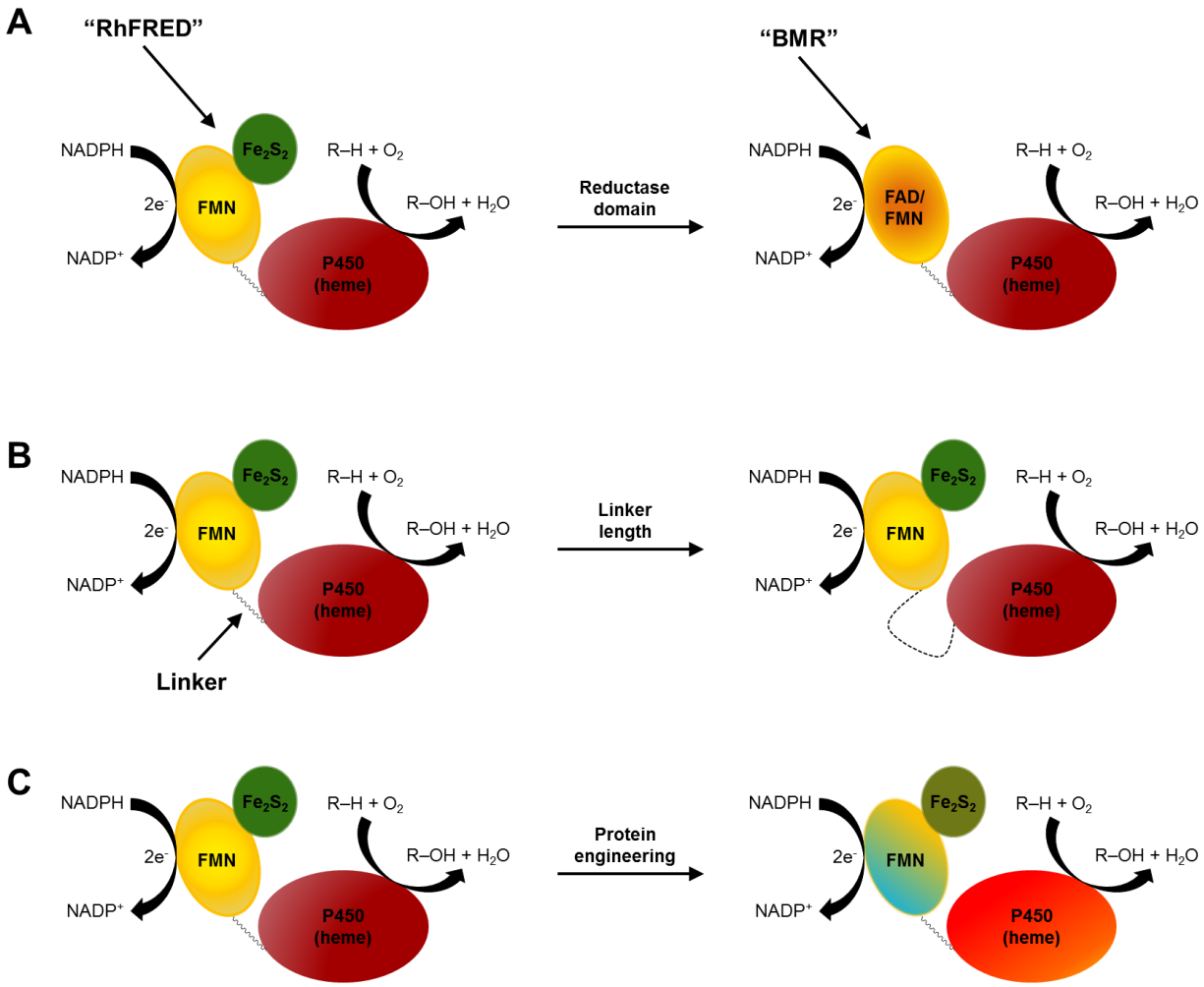

Figure 5.2. Possible strategies to enhance the coupling efficiency of an artificial catalytically self-sufficient P450 fusion protein include (**A**) changing the identity of the reductase domain (e.g., from the FMN/[2Fe-2S]-containing RhFRED domain of $P450_{RhF}$ to the FAD/FMN-containing BMR domain of $P450_{BM3}$), (**B**) altering the length of the polypeptide linking the P450 heme domain to the reductase domain, and (**C**) applying protein engineering techniques separately or in combination to each of the domains.

revealed that variation of the linker length had a more significant effect on these properties than alteration of the peptide sequence itself.[10,11] More recent work has shown that relatively small changes to the length of the polypeptide linking the heme and RhFRED (or homologs thereof from other CYP116B subfamily P450s) domains in

artificial fusion constructs can impact activity and coupling efficiency quite considerably. For instance, insertion of an additional 9-16 amino acids at the N-terminus of the natural RhFRED linker in $P450_{cam}$-RhFRED resulted in a drastic improvement in the ability of this enzyme to hydroxylate camphor in whole-cell conversion experiments.[12] In a more dramatic example, addition of only two amino acids to the linker connecting the reductase domain of CYP116B3 (PFOR) to the C-terminus of CYP153A from *Marinobacter aquaeolei* led to a 55% increase in coupling efficiency as well as similar improvements in activity and stability.[13] Thus, this strategy may prove rather effective in enhancing these parameters for MycCI-RhFRED and other P450-RhFRED constructs in our inventory.

Finally, once an optimal reductase domain and linker region have been established, domain-based protein engineering can be used to further enhance the catalytic properties of the self-sufficient biocatalyst (**Figure 5.2C**). In a landmark study, a $P450_{BM3}$ variant with relatively modest propane hydroxylase activity and poor coupling efficiency (17%) was engineered into a highly efficient P450 propane monooxygenase that could support more than 45,000 turnovers with extremely high (98%) coupling of NADPH consumption to product formation.[14,15] The engineering strategy involved initial construction of holoenzyme libraries using a combination of different mutagenesis techniques (e.g., random, site-saturation, site-directed) to independently target both the heme-containing P450 domain and the FAD/FMN-containing reductase domain. Beneficial mutations in each domain were then combined to yield an optimized enzyme with a catalytic efficiency comparable to that of wild-type $P450_{BM3}$ acting on its preferred fatty acid substrates. Following a similar approach with MycCI-RhFRED could lead to a more robust and biocatalytically useful macrolactone/macrolide hydroxylase.

In an initial effort to explore alternative MycCI redox partner fusions, a three-component chimera in which MycCII (a [3Fe-4S]-containing ferredoxin) replaced the [2Fe-2S] domain of MycCI-RhFRED was constructed. However, the enzyme displayed only ~7% of the activity of MycCI/MycCII/MBP-FdR and MycCI-RhFRED on M-VIII, which was likely due to poor reduction of MycCII by the RhFRED FMN domain and/or suboptimal binding of the former to MycCI. Since MBP-FdR (spinach ferredoxin reductase, FdR) is capable of effectively reducing MycCII, it may be possible to

engineer a functional MycCI-FdR-MycCII chimera. As previously observed, however, high concentrations of MycCII relative to MycCI are required for optimal substrate

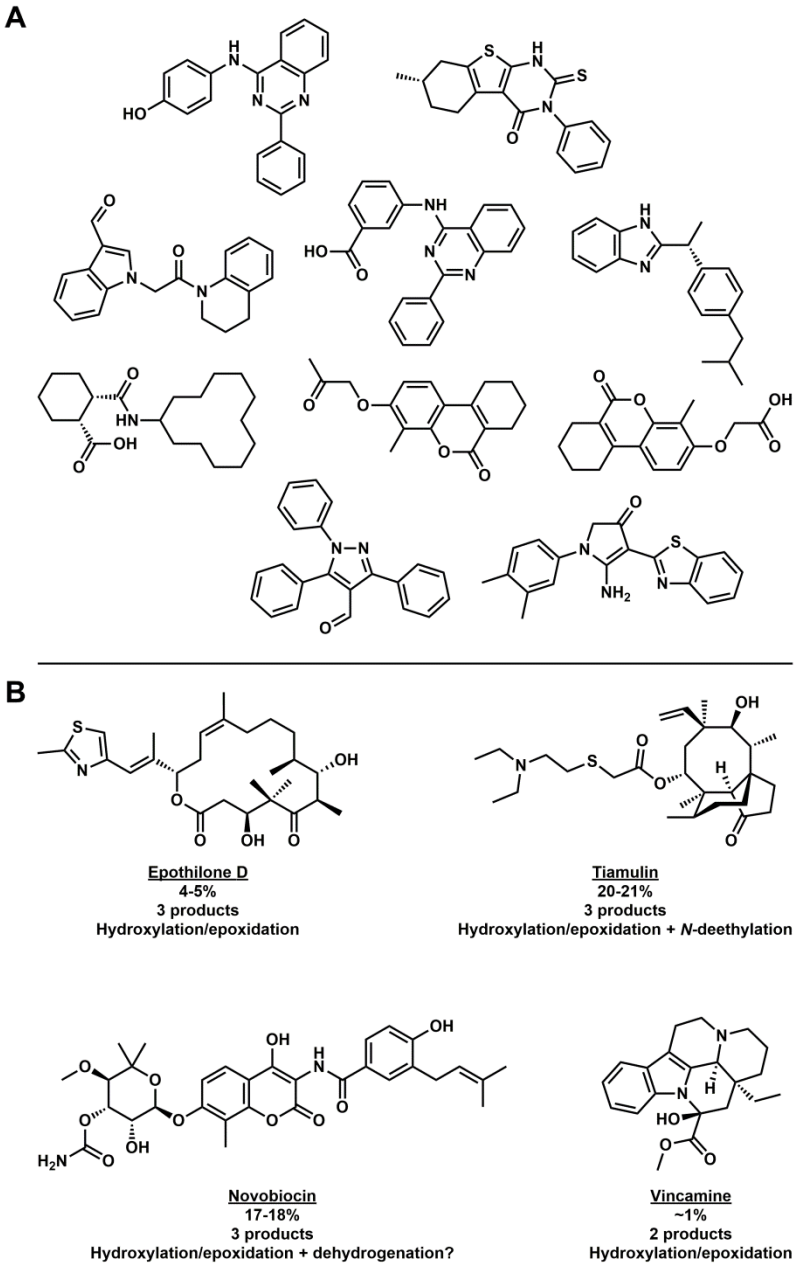

Figure 5.3. Alternative substrates for MycCI. (**A**) 10 potential MycCI substrates identified from screening ~3000 compounds from the ZINC library using AutoDock Vina. These compounds have not yet been experimentally tested. (**B**) Some non-macrolide substrates that have been experimentally tested with MycCI. Percent conversion values were estimated based on LC-MS analysis of reactions performed with MycCI in combination with MycCII ferredoxin and spinach ferredoxin reductase (MBP-FdR).

turnover. It would therefore be of interest to identify the native MycCII reductase in *Micromonospora griseorubida*, the mycinamicin producing organism.

In collaboration with the Houk lab (Song Yang), we have initiated computational studies aimed toward expanding the substrate scope of MycCI as well as altering its regioselectivity properties on native substrates. At least 10 potential non-macrolide substrates were identified based on virtual screening of the ZINC library (UCSF), which features a variety of commercially-available small molecules (**Figure 5.3A**). Experimental assessment of these substrates will provide important new insight into the inherent catalytic flexibility of MycCI. Beyond the substrates described in Chapter 2, a few additional compounds have been tested with MycCI in analytical-scale reactions (**Figure 5.3B**). Minimal conversion of these molecules to hydroxylated or dealkylated products suggests that this enzyme is fairly specific for substrates possessing the chalconolide/tylactone-type scaffold.

Thus far, molecular dynamics (MD) simulations have been used to predict specific mutations that might shift the regioselectivity of MycCI on its native substrate, M-VIII (or PML-IV, which was used in the simulations). Residues L80, M81, and S165 were proposed to play important roles in positioning the substrate in an orientation leading to preferential hydroxylation at C21 (**Figure 5.4A**). MD simulations performed with the L80G/M81G/S165W triple mutant showed that one of the hydrogens appended to C16 closely approached the iron-oxo species during the 100 ns time frame, suggesting that this site could be a viable target for hydroxylation by the mutant (**Figure 5.4B/C**). Despite successful expression and purification, MycCI$_{L80G/M81G/S165W}$ exhibited extremely poor activity on all substrates tested (<1% conversion of 16-membered ring macrolides; no conversion of macrolactones), and no changes in regioselectivity were detected on the basis of LC-MS retention times. These results were somewhat unsurprising given that, in contrast to the results of the MD simulations with the triple mutant, those with wild-type MycCI demonstrated that C21 was consistently located in proximity (≤3 Å) to the iron-oxo species over the course of the entire 100 ns time frame (**Figure 5.4C**). This observation is consistent with the extremely tight binding of M-VIII to MycCI previously seen in the spectrophotometric substrate titration assays. Additional simulations may yield novel predictions, but it will likely prove quite challenging to alter

the regioselectivity of MycCI by mutating only a few key residues. One promising strategy for selecting potential sites for mutagenesis may be to compare the MycCI

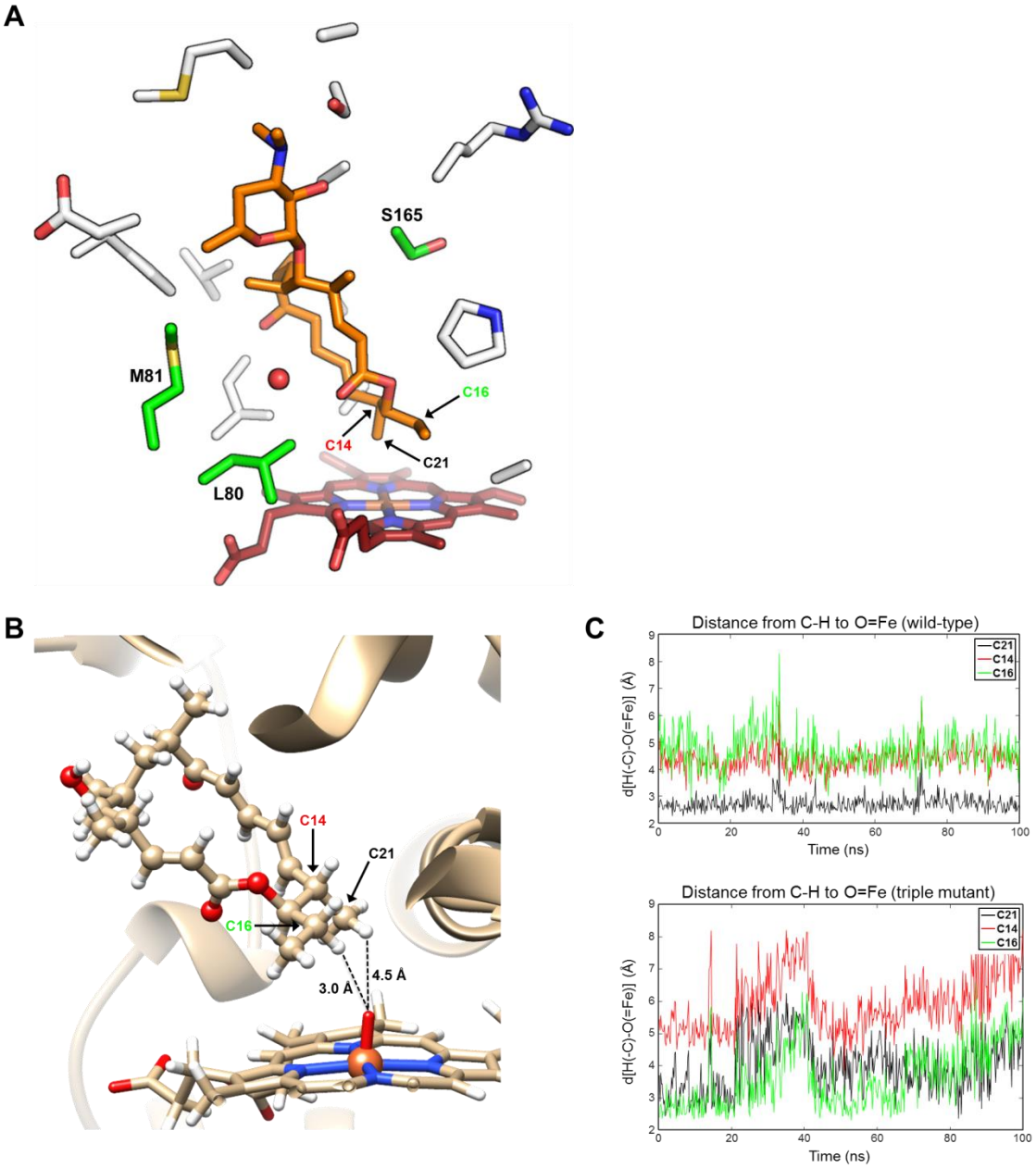

Figure 5.4. Molecular dynamics (MD) simulations of substrate-bound MycCI. (**A**) Residues highlighted in green may be important for properly positioning the substrate in the active site. Targeted mutagenesis of these residues could potentially affect the regioselectivity properties of MycCI. (**B**) Snapshot of a binding mode during the 100 ns MD simulation of a MycCI triple mutant (L80G/M81G/S165W) showing C16–H of PML-IV approaching the iron-oxo species within 3.0 Å. The target C21–H bond of the wild-type enzyme is further away from the iron-oxo species in this particular orientation (4.5 Å). (**C**) Plots of the distance (Å) between a given C–H bond and the iron-oxo species (O=Fe) as a function of time for wild-type MycCI (top) and the triple mutant (bottom).

structure with that of another P450 that targets a different position on the same set of substrates (e.g., JuvD; *vide infra*). While chimeragenesis may provide a possible means by which to identify regions of the protein that are involved in influencing regioselectivity, this method would probably only work if the other P450 in question shared significant (e.g., ≥55%) sequence identity with MycCI.

5.2 Comparative analysis of P450s JuvD, MycCI, TylI, and JuvC

5.2.1 Conclusions

The biosynthetic pathways of 16-membered ring macrolide antibiotics have been well-studied over the past several decades and have served as paradigms for understanding the construction of complex polyketides in bacteria at the genetic and biochemical levels. Most of these pathways feature multiple post-PKS tailoring steps catalyzed by P450 enzymes. The primary goal of the work described in Chapter 4 of the present dissertation was to explore the unique reactivity properties of additional P450s from the tylosin and juvenimicin pathways, ultimately culminating in their employment as biocatalysts to effect the late-stage tailoring of a chemoenzymatically generated macrolide. Isolation and sequencing of the juvenimicin biosynthetic gene cluster from *Micromonospora chalcea* (ssp. *izumensis*) revealed the presence of two genes encoding P450s (*juvC* and *juvD*) that were highly homologous to those previously characterized from the rosamicin pathway in *Micromonospora rosaria*. Along with TylI from the tylosin pathway, these P450s were cloned and expressed as fusions to the RhFRED domain in order to facilitate in vitro characterization.

In a first set of experiments, the activity of JuvD-RhFRED was compared in parallel with that of MycCI-RhFRED across a panel of different macrolactone and macrolide substrates. These studies verified that JuvD was a highly efficient epoxidase, acting on many of the same substrates as MycCI but with notably improved activity. This increase in turnover was attributed to the lower free energy barrier for olefin epoxidation relative to activation of a primary C–H bond. The preferred substrate for JuvD-RhFRED was 23-DDTL, but it exhibited essentially the same activity on the reduced analogs 20-OH-DT and DT. Unexpectedly, the enzyme also effectively converted M-VIII to two different oxidation products, 12,13-epoxy-M-VIII (major) and 14-

hydroxy-M-VIII (minor), which represented new mycinamicins that had not previously been reported. While these sites are also targeted by the multifunctional P450 MycG in the mycinamicin biosynthetic pathway, this enzyme requires that an additional sugar moiety be appended to C21-OH prior to hydroxylation and/or epoxidation. JuvD-RhFRED also readily turned over the 14-membered ring macrolide narbomycin, producing what appeared to be a single monohydroxylated product. However, the regioselectivity of the reaction could not be definitively established due to the apparent instability of the compound. Finally, JuvD-RhFRED displayed a low-level ability to oxidize the aglycone tylactone, but overall conversion was reduced compared with that observed for MycCI-RhFRED in a parallel assay. Taken together, these results highlighted JuvD as a remarkable biocatalyst for macrolide epoxidation and/or hydroxylation, thus setting the stage for a number of future directions aimed toward understanding the molecular basis for its catalytic prowess.

Subsequent studies focused on investigating the activity of the other P450 found in the juvenimicin cluster (JuvC) along with that of its homolog involved in tylosin biosynthesis (TylI). These enzymes and others found in biosynthetic pathways associated with the production of platenolide- and tylactone-type 16-membered ring macrolides are part of the CYP113B subfamily and are responsible for carrying out sequential two-electron oxidation reactions on the C6 ethyl side chain to generate the critical aldehyde pharmacophore present in the final natural products. Prior to the work described in Chapter 4, the in vitro activities of these P450s on their native substrates had not been verified. Instead, functional assignment of a select few had been based on the results of gene disruption and bioconversion experiments. A previous graduate student in our lab (Karoline Chiou) had demonstrated that purified TylI acting in conjunction with heterologous redox partners (spinach ferredoxin/ferredoxin reductase and RhFRED) was capable of hydroxylating the C20 position of a possible tylosin biosynthetic intermediate (23-hydroxy-5-*O*-mycaminosyl-tylactone). However, the preferred oxidation pathway en route to tylosin after mycaminosylation of tylactone dictates that the true native substrate for TylI should be 5-*O*-mycaminosyl-tylactone (MT). Thus, the activity of self-sufficient TylI-RhFRED on the latter as well as 12 additional tylactone-type macrolides was tested in analytical-scale in vitro reactions. As

expected, the enzyme exhibited the highest activity on MT (>95% conversion), producing a ~10:1 mixture of 20-OH-MT:23-DMTL. The second oxidation reaction proved to be rather inefficient, as TylI-RhFRED was only capable of converting ~10% of the alcohol intermediate (20-OH-MT) to the corresponding aldehyde (23-DMTL) when it was directly fed the former. Unlike TylHI, high substrate turnover was independent of the identity of the deoxyamino sugar. However, along with the observed preference for TylHI to accept C20-oxidized substrates, decreased TylI-catalyzed oxidation of 23-OH-DT relative to DT was consistent with the hypothesis that tylosin biosynthesis proceeds via one primary post-PKS tailoring pathway.

Given the high level of sequence identity shared between TylI and JuvC (70%), it was unsurprising to find that the activity of JuvC-RhFRED was similar to that of TylI-RhFRED across the various macrolide substrates tested. While its most probable native substrate was identified as DT, JuvC-RhFRED was able to turn over the corresponding epoxidized compound (12,13-epoxy-DT) equally efficiently. Together with the data demonstrating that JuvD-RhFRED activity was independent of the oxidation state of C20, these results indicated that, as observed for the rosamicin pathway in *M. rosaria*, multiple post-PKS modification routes likely operate in the biosynthesis of the juvenimicins in *M. chalcea*. Unexpectedly, while neither TylI-RhFRED nor JuvC-RhFRED was able to effectively carry out further oxidation of the C20-hydroxylated substrates to afford the corresponding aldehydes, these enzymes were able to effect subsequent oxidation of the aldehyde substrates quite readily. JuvC-RhFRED proved to be the superior biocatalyst in this respect, converting 93% of 23-DMTL and >30% of the other aldehyde substrates to the corresponding carboxylic acids.

Ultimately, the unique reactivity properties of these P450 enzymes were leveraged in order to achieve the first total biocatalytic synthesis of the rosamicin, juvenimicin, and M-4365 family of 16-membered ring macrolide antibiotics. Chemoenzymatic generation of the core aglycone (tylactone) was followed by regioselective glycosylation using an engineered *Streptomyces venezuelae* strain to afford the first macrolide (5-*O*-desosaminyl-tylactone (DT), or M-4365 G_1) in 15 linear steps (21 total) with an overall isolated yield of 4.6%. TylI-RhFRED, MycCI-RhFRED, and JuvD-RhFRED were then used for the late-stage diversification of this macrolide,

resulting in the efficient production of eight additional compounds with unique oxidative functionality. Biological testing of each macrolide confirmed the importance of the aldehyde moiety in conferring potent antibacterial activity on these molecules. Interestingly, the Z-isomer of DT (iso-DT) exhibited decreased activity relative to the E-isomer, indicating that installation of the epoxide across the C12/C13 olefin by JuvD may serve as a mechanism for this family of macrolides to retain bioactivity by precluding rapid photoisomerization at this position. This hypothesis was further evidenced by the lack of an improvement in bioactivity upon installation of the epoxide. Overall, the success of the synthetic strategy employed in this study highlights biocatalysis as a powerful approach that serves as a valuable complement to standard methodologies for the synthesis of complex molecules.

5.2.2 Future directions

Many important questions regarding the nature of the biocatalytic properties of these fascinating P450s remain to be answered. The epoxidase JuvD has emerged from our studies as a highly versatile enzyme that has great potential for further practical exploitation. Substrate binding and kinetics studies will provide additional insights that will be useful in acquiring a deeper understanding of its function, especially in relation to those of MycCI and MycG. Currently, another graduate student in our lab (Amy Fraley) has initiated cocrystallization trials with JuvD/23-DDTL. The X-ray structure of this enzyme in complex with its native substrate will undoubtedly prove vital in being able to rationalize its unique activity profile. One key issue that we hope to address through structural studies relates to the differential regioselectivity of JuvD and MycCI. These enzymes act upon the same set of substrates while effecting distinct regiochemical outcomes, providing a rare opportunity to explore the factors that govern such properties in P450 catalysis. Because JuvD-RhFRED exhibits high activity only on glycosylated macrolides (including those with 14- and 16-membered rings), it may employ a salt bridge-type anchoring mechanism similar to that used by PikC for substrate binding. If this hypothesis is supported by structural data, JuvD may likewise be able to accept a variety of unnatural substrates provided they bear the requisite *N*,*N*-dimethylamino functional group. Thus, JuvD may nicely complement PikC as a robust

biocatalyst for site-selective hydroxylation and/or epoxidation of many different types of compounds, with each enzyme potentially generating unique products.

Since JuvD targets the same sites as MycG for oxidation of the mycinamicin scaffold, it will be of further interest to compare these two enzymes from structural and functional standpoints. It has already been demonstrated that, unlike JuvD, MycG utilizes mycinose as a recognition element for properly binding its native substrate, M-IV. While this enzyme is still somewhat active on the desmethyl biosynthetic precursors M-III and M-VI, it is unable turn over M-VIII or M-VII, both of which lack a sugar appended at the C21 position. Therefore, substrate recognition by JuvD and MycG must occur via distinct mechanisms. While the former is unlikely to accept doubly glycosylated tylosin and mycinamicin intermediates as substrates, it might be worthwhile to test its activity on these compounds in order to confirm that its substrate profile does not overlap with that of MycG. In ongoing collaborative efforts with the Houk lab, we are expanding our understanding of the molecular basis for MycG function through molecular dynamics (MD) simulations. Thus far, these studies have helped to explain the observed substrate scope and regioselectivity properties of this enzyme. They have also provided a rational basis for targeted mutagenesis to relax its substrate specificity, with preliminary experimental data upholding some of these predictions. Further investigation of JuvD in this context once a structure of the enzyme becomes available may offer a nice addition to this developing story. In the meantime, additional studies with JuvD will involve further testing its substrate scope, determining the site it targets for hydroxylation on narbomycin and related 14-membered ring macrolides, and evaluating how its reactivity changes when coupled to different redox partners in trans. It might also be interesting to test its close homolog RosD (84% sequence identity) in parallel activity assays. Any differences observed between the two enzymes could prove rather straightforward to rationalize on the basis of a relatively small number of amino acid substitutions.

As for JuvD, immediate next steps for P450s TylI and JuvC will include performing substrate binding and steady-state kinetics experiments, which may help to answer several outstanding questions related to the curious reactivity profiles of these two enzymes. The endpoint turnover assays already performed appear to be consistent

with a distributive mechanism for sequential oxidation. That is, intermediates are likely released from the active site after each oxidation reaction has occurred. When fed unoxidized starting materials, these P450s primarily produce the C20 alcohols along with relatively small amounts of the corresponding aldehydes (<10% of the total reaction mixture). When the alcohol intermediates are used directly as substrates, conversion to the aldehydes is only slightly improved. These results can be rationalized by invoking any of the following three possibilities. The first (and most likely) explanation is that RhFRED serves as a suboptimal redox partner for TylI and JuvC. While other heterologous electron transfer systems may be tested (we have already cloned those from spinach, *E. coli*, and *Bacillus subtilis* into suitable expression vectors), the appropriate autologous proteins from *Streptomyces fradiae* have yet to be identified. Second, conversion of the alcohol to the aldehyde may be preferentially catalyzed by another enzyme (e.g., an alcohol dehydrogenase or another P450) located outside of the tylosin biosynthetic gene cluster. In the biosynthesis of the tirandamycins, an alcohol intermediate (tirandamycin E) is converted to the corresponding ketone (tirandamycin D) either through the formation of a *gem*-diol catalyzed by the P450 TamI or via direct dehydrogenation catalyzed by the flavin-dependent oxidase TamL. In vitro reconstitution of these reactions identified the latter as the major route,[16] so it is conceivable that a similar process operates in the tylosin pathway. Finally, the second oxidation reaction to convert the alcohol to the aldehyde may simply be inherently inefficient for TylI and JuvC. While this possibility is partially supported by the fact that nontrivial amounts of relomycin (tylosin D) and other 20-dihydro-tylosin analogs are often isolated from *S. fradiae* fermentation cultures, it has been shown that conversion of tylosin to tylosin D is catalyzed by an adventitious NADPH-dependent reductase not associated with the tylosin gene cluster.[17]

Along with the results of a recently published study,[18] those presented in Chapter 4 demonstrate that TylI and JuvC are capable of performing a third two-electron oxidation reaction at C20 of tylactone-type macrolides to generate carboxylic acid products from the corresponding aldehydes. Notably, the acid compounds were only observed in reactions in which isolated aldehyde products were directly incubated with these enzymes, further supporting a distributive mechanism for the three-step oxidation

sequence. One intriguing question arises from these findings: how are multistep oxidation reactions controlled in these and related P450/redox partner systems? While carboxylic acid-containing analogs of rosamicin and tylosin have been isolated from *M. rosaria* and *S. fradiae*,[18] these compounds do not constitute the major components of the fermentation broths. In contrast, derivatives of polyene antibiotics (e.g., amphotericin, nystatin, pimaricin) bearing hydroxyl or formyl groups in place of the carboxyl group have not been identified in producing stains. These findings suggest that the multifunctional P450s associated with the production of platenolide/tylactone-type 16-membered ring macrolides (CYP113B) and those that play similar roles in the biosynthesis of 26- and 38-membered ring polyene macrolides (CYP105H) carry out their respective multistep reactions via distinct mechanisms. Like some other biosynthetic P450s belonging to the CYP105 family (e.g., MycCI and TylHI), those from the polyene pathways are associated with dedicated [3Fe-4S]-type ferredoxins. These specific P450/ferredoxin systems may have co-evolved to maximize electron transfer efficiency, which is likely required for full conversion of a primary methyl group to a carboxylic acid. Thus, while RhFRED may serve as a viable redox partner for TylI and JuvC with respect to the initial hydroxylation step, the native ferredoxins for these P450s could play a critical role in facilitating the subsequent oxidation, especially if the C20-hydroxylated intermediate does not bind as well to the enzyme. Conversely, RhFRED might be superior to the autologous system for enabling further oxidation of the aldehyde to the carboxylic acid.

As previously alluded to, one key question that often comes up in these types of multistep P450-catalyzed reactions relates to the processivity of the enzyme (i.e., the extent to which the product of the initial step is retained in the active site prior to undergoing the next reaction in a given multistep oxidative transformation).[19] For P450s and other types of enzymes, this question has traditionally been addressed using pulse-chase-type methodologies. In these experiments, the reaction is initiated with isotope- or radiolabeled substrate (pulse) prior to addition of excess unlabeled intermediate after a given amount of time (chase). At the completion of the reaction, the amount of label retained in the final product is quantified and used to calculate the degree to which the intermediate dissociated from the enzyme during the reaction sequence. The amount of

the label carried through to the product directly reflects the extent to which the intermediate remained in the active site following the first step of the reaction. If TylI and JuvC primarily operate via a distributive mechanism, one would expect to see little if any label retained in the aldehyde or acid products. In addition to pulse-chase experiments, standard equilibrium binding and steady-state kinetics studies with unoxidized substrates as well as alcohol and aldehyde intermediates could provide useful insights into this question of processivity.

Other important questions surround the actual chemical mechanism of the multistep oxidation reaction sequence. Several plausible routes for the P450-catalyzed transformation of a primary methyl group to a carboxylic acid can be envisioned (**Scheme 5.2**). Following the first hydroxylation step, the substrate is hydroxylated again at the same site to generate a *gem*-diol, which can undergo either spontaneous dehydration to form the aldehyde or further oxidation to afford a *gem*-triol (*ortho*-acid). Subsequent direct oxidation of the former or dehydration of the latter will yield the final acid product (**Scheme 5.2A**). Furthermore, aldehyde oxidation may be rationalized via a radical pathway mediated by Compound I (**Scheme 5.2B**) or through nucleophilic addition of the ferric peroxo intermediate to the carbonyl (**Scheme 5.2C**).[3,19] Kinetic and $^{18}O_2$ incorporation studies were carried out in order to establish the mechanism of the multistep reaction catalyzed by the P450 *ent*-kaurene oxidase (KO) from *Arabidopsis thaliana*.[20] The results supported a pathway wherein dehydration of a *gem*-diol intermediate was followed by direct hydroxylation to yield *ent*-kaurenoic acid. Notably, an alternative route involving formation of the corresponding *ortho*-acid could be discounted on the basis of ^{18}O labeling results. Similar experiments may be performed with TylI and JuvC to provide support for certain mechanistic proposals while rejecting others. For example, generation of a 1:1 mixture of unlabeled and labeled aldehyde in the presence of $^{18}O_2$ with unlabeled alcohol as substrate would indicate formation of a *gem*-diol intermediate. Spontaneous dehydration would release labeled or unlabeled water, thus resulting in the observed equimolar mixture of products. Moreover, substantial incorporation of ^{18}O into the carboxylic acid product when using unlabeled aldehyde as substrate would be most consistent with a mechanism involving direct hydroxylation of the latter without formation of an *ortho*-acid intermediate. One important

issue that can complicate these types of experiments is the extent to which the aldehyde undergoes spontaneous hydration/dehydration. Aldehydes commonly exist in equilibrium with their hydrates, although the rates of hydration/dehydration in aqueous solution are relatively slow (i.e., on the order of a few minutes).[19] Therefore, it would be imperative to probe the aldehyde/solvent exchange rates using NMR and/or MS techniques before carrying out any enzymatic reactions.

Scheme 5.2. Possible mechanisms for sequential oxidation reactions catalyzed by cytochrome P450. (**A**) A carboxylic acid could arise from either direct hydroxylation of an aldehyde intermediate or spontaneous dehydration of a triol (*ortho*-acid). (**B**) Compound I-mediated oxidation of an aldehyde. Compound I is depicted as Fe^{IV}=O. (**C**) Oxidation of an aldehyde catalyzed by a ferric peroxo (Fe^{III}–O–O) species.

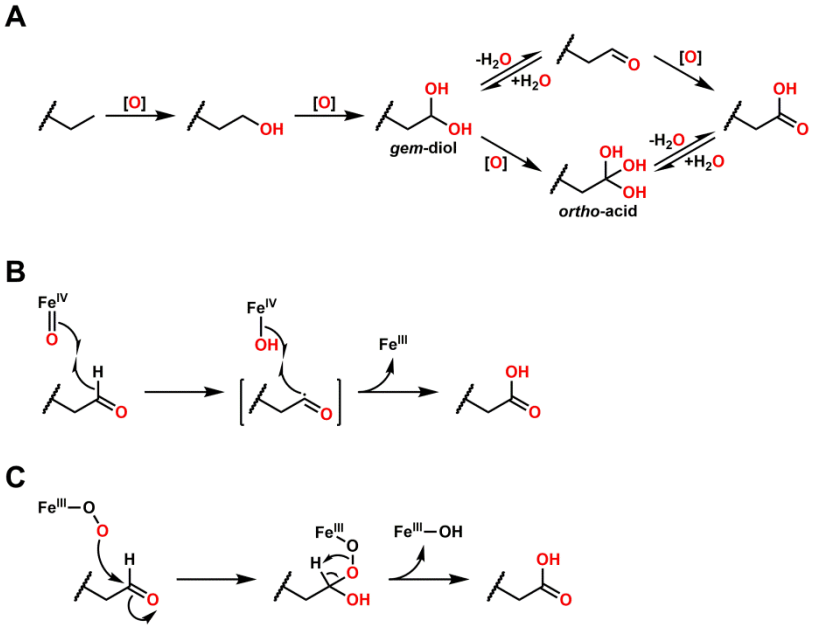

In principle, direct oxidation of an aldehyde to produce the corresponding acid could proceed through Compound I-catalyzed abstraction of the carbonyl hydrogen or via addition of the ferric peroxo species to the carbonyl (**Scheme 5.2B/C**). It might be possible to differentiate between these two mechanisms by measuring kinetic solvent isotope effects.[21,22] If the proton transfer steps are at least partially rate limiting in the catalytic cycle, one would expect to observe an isotope effect under steady-state conditions only if Compound I is the reactive intermediate. The lack of an isotope effect or the presence of an inverse isotope effect would point toward ferric peroxo as the key

catalytic species. This experiment would be relatively straightforward to perform with TylI and JuvC, and it would not require any special reagents beyond D_2O or analytical instruments other than a standard HPLC.

5.3 References

(1) Anzai, Y., Li, S., Chaulagain, M. R., Kinoshita, K., Kato, F., Montgomery, J., and Sherman, D. H. (2008) Functional analysis of MycCI and MycG, cytochrome P450 enzymes involved in biosynthesis of mycinamicin macrolide antibiotics. *Chem. Biol. 15*, 950–959.

(2) Guengerich, F. P. (2002) Rate-limiting steps in cytochrome P450 catalysis. *Biol. Chem. 383*, 1553–1564.

(3) Guengerich, F. P. (2001) Common and uncommon cytochrome P450 reactions related to metabolism and chemical toxicity. *Chem. Res. Toxicol. 14*, 611–650.

(4) Guengerich, F. P., Miller, G. P., Hanna, I. H., Sato, H., and Martin, M. V. (2002) Oxidation of methoxyphenethylamines by cytochrome P450 2D6. *J. Biol. Chem. 277*, 33711–33719.

(5) O'Reilly, E., Köhler, V., Flitsch, S. L., and Turner, N. J. (2011) Cytochromes P450 as useful biocatalysts: addressing the limitations. *Chem. Commun. 47*, 2490–2501.

(6) Sadeghi, S. J., and Gilardi, G. (2013) Chimeric P450 enzymes: activity of artificial redox fusions driven by different reductases for biotechnological applications. *Biotechnol. Appl. Biochem. 60*, 102–110.

(7) Bernhardt, R., and Urlacher, V. B. (2014) Cytochromes P450 as promising catalysts for biotechnological application: chances and limitations. *Appl. Microbiol. Biotechnol. 98*, 6185–6203.

(8) Fasan, R. (2012) Tuning P450 enzymes as oxidation catalysts. *ACS Catal. 2*, 647–666.

(9) Zuo, R., Zhang, Y., Huguet-Tapia, J. C., Mehta, M., Dedic, E., Bruner, S. D., Loria, R., and Ding, Y. (2016) An artificial self-sufficient cytochrome P450 directly nitrates fluorinated tryptophan analogs with a different regio-selectivity. *Biotechnol. J. 11*, 624–632.

(10) Govindaraj, S., and Poulos, T. L. (1995) Role of the linker region connecting the reductase and heme domains in cytochrome $P450_{BM-3}$. *Biochemistry 34*, 11221–11226.

(11) Govindaraj, S., and Poulos, T. L. (1996) Probing the structure of the linker connecting the reductase and heme domains of cytochrome P450BM-3 using site-directed mutagenesis. *Protein Sci. 5*, 1389–1393.

(12) Robin, A., Roberts, G. A., Kisch, J., Sabbadin, F., Grogan, G., Bruce, N., Turner, N. J., and Flitsch, S. L. (2009) Engineering and improvement of the efficiency of a chimeric [P450cam-RhFRed reductase domain] enzyme. *Chem. Commun.* 2478–2480.

(13) Hoffmann, S. M., Weissenborn, M. J., Gricman, L., Notonier, S., Pleiss, J., and Hauer, B. (2016) The impact of linker length on P450 fusion constructs: activity, stability and coupling. *ChemCatChem 8*, 1591–1597.

(14) Fasan, R., Chen, M. M., Crook, N. C., and Arnold, F. H. (2007) Engineered alkane-hydroxylating cytochrome $P450_{BM3}$ exhibiting nativelike catalytic properties. *Angew. Chem. Int. Ed. 46*, 8414–8418.

(15) Fasan, R., Meharenna, Y. T., Snow, C. D., Poulos, T. L., and Arnold, F. H. (2008) Evolutionary history of a specialized P450 propane monooxygenase. *J. Mol. Biol. 383*, 1069–1080.

(16) Carlson, J. C., Li, S., Gunatilleke, S. S., Anzai, Y., Burr, D. A., Podust, L. M., and Sherman, D. H. (2011) Tirandamycin biosynthesis is mediated by co-dependent oxidative enzymes. *Nat. Chem. 3*, 628–633.

(17) Huang, S.-L., Hassell, T. C., and Yeh, W.-K. (1993) Purification and properties of NADPH-dependent tylosin reductase from *Streptomyces fradiae*. *J. Biol. Chem. 268*, 18987–18993.

(18) Iizaka, Y., Takeda, R., Senzaki, Y., Fukumoto, A., and Anzai, Y. (2017) Cytochrome P450 enzyme RosC catalyzes a multistep oxidation reaction to form the non-active compound 20-carboxyrosamicin. *FEMS Microbiol. Lett. 364*, doi: 10.1093/femsle/fnx110.

(19) Guengerich, F. P., Sohl, C. D., and Chowdhury, G. (2011) Multi-step oxidations catalyzed by cytochrome P450 enzymes: processive vs. distributive kinetics and the issue of carbonyl oxidation in chemical mechanisms. *Arch. Biochem. Biophys. 507*, 126–134.

(20) Morrone, D., Chen, X., Coates, R. M., and Peters, R. J. (2010) Characterization of the kaurene oxidase CYP701A3, a multifunctional cytochrome P450 from gibberellin biosynthesis. *Biochem. J. 431*, 337–344.

(21) Gregory, M. C., Denisov, I. G., Grinkova, Y. V., Khatri, Y., and Sligar, S. G. (2013) Kinetic solvent isotope effect in human P450 CYP17A1-mediated androgen formation: evidence for a reactive peroxoanion intermediate. *J. Am. Chem. Soc. 135*, 16245–16247.

(22) Khatri, Y., Luthra, A., Duggal, R., and Sligar, S. G. (2014) Kinetic solvent isotope effect in steady-state turnover by CYP19A1 suggests involvement of Compound 1 for both hydroxylation and

aromatization steps. *FEBS Lett. 588*, 3117–3122.

Appendix A:
Experimental procedures and supplemental information for Chapter 2

A.1 Materials and general methods

Unless otherwise noted, chemical reagents and solvents were purchased from EMD Millipore, Sigma-Aldrich, and Thermo Fisher Scientific. Agarose for gel electrophoresis was purchased from BioExpress (VWR). Kanamycin sulfate, isopropyl-β-D-thiogalactopyranoside (IPTG), and dithiothreitol (DTT) were obtained from Gold Biotechnology. Tris-HCl, ampicillin disodium salt, and $NADP^+$ were purchased from Amresco. Chloramphenicol was obtained from Roche. Thiamine and NADPH were purchased from Chem-Impex. δ-aminolevulinic acid was purchased from Oakwood Chemical. Lysozyme was purchased from RPI. Imidazole was purchased from AK Scientific. Amicon Ultra centrifugal filters used for protein concentration were from EMD Millipore. PD-10 columns were purchased from GE Healthcare. Glucose-6-phosphate was from Biosynth and glucose-6-phosphate dehydrogenase (yeast) was from Alfa Aesar.

Deionized water was obtained from a Milli-Q system (EMD Millipore) using Q-Gard 2/Quantum Ex Ultrapure organex cartridges. Media components for *E. coli* growth were purchased from EMD Millipore, Sigma-Aldrich, and Thermo Fisher Scientific unless otherwise specified. Glycerol was purchased from BDH (VWR). LB broth (Miller) and LB agar (Miller) were obtained in pre-made granulated form from EMD Millipore. TB broth was made from individually purchased components and consisted of 4% (v/v) glycerol. Media and solutions were autoclaved or sterile filtered prior to use. For fermentations and biotransformation experiments, all media solutions were autoclaved and manipulations were carried out in a UV-sterilized laminar flow hood. For media, buffers, and other solutions, pH was monitored using a VWR sympHony SB70P pH

meter calibrated according to the manufacturer's specifications. When specified, room temperature (rt) was ~22-23 °C.

DNA oligonucleotides for cloning and mutagenesis were purchased from Integrated DNA Technologies. PCR was performed using a Bio-Rad iCycler thermal cycler system. Restriction endonucleases and other associated molecular biology reagents were purchased from New England Biolabs. Invitrogen PCR cleanup/gel extraction and plasmid miniprep kits were purchased from Thermo Fisher Scientific. All DNA manipulations were accomplished following the manufacturer's protocols. DNA concentrations and protein purity indexes were measured using a NanoDrop ND-1000 spectrophotometer. DNA sequencing was performed at the University of Michigan DNA Sequencing Core. *E. coli* DH5α was used for plasmid preparation and maintenance while *E. coli* BL21(DE3) was used for protein overexpression. Chemically competent *E. coli* cells were prepared using the method of Inoue.[1] Optical density (OD_{600}) was measured using an Eppendorf BioPhotometer.

Flash column chromatography was performed using Geduran Si 60 (40-63 μm) silica gel from EMD Millipore. NMR experiments were carried out on a Varian 600 MHz spectrometer. ^{1}H NMR spectra were recorded relative to the residual solvent peak (CD_3OD δ_H 3.31 ppm, $CDCl_3$ δ_H 7.26 ppm). Multiplicity abbreviations are as follows: s = singlet, d = doublet, t = triplet, q = quartet, m = multiplet. ^{13}C NMR spectra were recorded relative to the residual solvent peak (CD_3OD δ_C 49.00 ppm, $CDCl_3$ δ_C 77.16 ppm). High-resolution mass spectrometry was performed on an Agilent quadrupole time-of-flight spectrometer (Q-TOF 6500 series) via electrospray ionization (ESI).

A.2 Cloning

Cloning of MycCI and MycCII

The pET28b_MycCI and pET28b_MycCII constructs were previously generated.[2] Both proteins were expressed with N-terminal 6xHis-tags.

Construction of MycCI-RhFRED

The wild-type *mycCI* gene has two internal *EcoRI* restriction sites, which initially precluded expeditious cloning into the appropriate vector containing the $P450_{RhF}$

reductase domain (RhFRED). Thus, mutagenic primers P1 and P2 (**Table A.1**) were used to simultaneously eliminate each of these sites. The whole-plasmid PCR reaction was carried out using KOD Xtreme Hot Start DNA polymerase (EMD Millipore) and associated reagents according to the manufacturer's instructions. Positive clones were sequenced to verify the correct incorporation of both mutations. The resulting *mycCI* gene lacking internal *EcoRI* restriction sites was further amplified by PCR using primers P3_forward and P3_reverse in order to introduce flanking restriction sites and to remove the stop codon. The amplified DNA fragment was isolated and purified prior to simultaneous restriction digestion with *NdeI* and *EcoRI*. The cut *mycCI* fragment was ligated into the pET28b_PikC-RhFRED vector[3] that had previously been digested with the same restriction enzymes (to remove the *pikC* gene), yielding pET28b_MycCI-RhFRED. Sequencing results verified that the entire open reading frame was free of unwanted mutations. The following is the primary amino acid sequence of the entire translated MycCI-RhFRED protein (yellow = N-terminal His-tag; red = MycCI; green = RhFRED):

MGSSHHHHHHSSGLVPRGSHMVVWPMDRTCAWALPEQYAEFRQRATLVPAKVWDG
SPTWLVSRYEHVRALLVDPRVTVDPTRQPRLSEADGDGDGFRSMLMLDPPEHTRLRR
MFISAFSVRQVETMRPEIEKIVDGILDRLLALEPPVDILTHLALPMSTQVICHLLGVPYED
REFFQERSELASRPNDDRSMPALIELVEYLDGLVRTKTAHPDTGLLGTAVTERLLKGEI
THQELVNNAVLLLAAGHETSANQVTLSVLTLLRHPETAAELREQPELMPNAVDELLRY
HSIADGLRRAATADIVLGDHTIRAGDGLIILLSSANHDGNTFGAEATFDIHRPARHHVAF
GYGPHQCLGQNLARLEMEVTLGKLFRRVPALRLAQEPDALRVRQGSPIFGIDELLVEW
EFVLHRHQPVTIGEPAARAVSRTVTVERLDRIADDVLRLVLRDAGGKTLPTWTPGAHID
LDLGALSRQYSLCGAPDAPSYEIAVHLDPESRGGSRYIHEQLEVGSPLRMRGPRNHFA
LDPGAEHYVFVAGGIGITPVLAMADHARARGWSYELHYCGRNRSGMAYLERVAGHG
DRAALHVSEEGTRIDLAALLAEPAPGVQIYACGPGRLLAGLEDASRNWPDGALHVEHF
TSSLAALDPDVEHAFDLELRDSGLTVRVEPTQTVLDALRANNIDVPSDCEEGLCGSCE
VAVLDGEVDHRDTVLTKAERAANRQMMTCCSRACGDRLALRL

Cloning of TylHI and construction of TylHI-RhFRED

Two separate reports of the partial tylosin biosynthetic gene cluster in *Streptomyces fradiae* were published around the same time.[4,5] However, some of the gene sequences that were deduced are not identical (accession numbers AF055922[4] and AF147703[5]). In particular, the location of the translation start site for *tylHI* remained ambiguous prior to cloning the gene. Thus, the two possible genes deriving from the two

different start sites that were reported were amplified from *S. fradiae* genomic DNA using primers P4_forward/P4_reverse (start site 1) and P5_forward/P5_reverse (start site 2). Following isolation and purification of the DNA amplicons, restriction digestion was carried out with *NdeI* and *HindIII*. The cut *tylHI* fragments were then ligated into pET28b that had previously been digested with the same restriction enzymes to generate pET28b_TylHI-1 (start site 1) and pET28b_TylHI-2 (start site 2). Both plasmids were sequenced to ensure that no mutations were present in the open reading frames.

To construct the corresponding TylHI-RhFRED fusion proteins, the *tylHI* genes were further amplified by PCR using primers P4_forward/P6_reverse (start site 1) and P5_forward/P7_reverse (start site 2) in order to introduce flanking restriction sites and to remove the stop codon in each case. The amplified DNA fragments were isolated and purified prior to restriction digestion with *NdeI* and *EcoRI*. The cut *tylHI* fragments were ligated into the pET28b_PikC-RhFRED vector that had previously been digested with the same restriction enzymes, yielding pET28b_TylHI-1-RhFRED and pET28b_TylHI-2-RhFRED. Sequencing results verified that the entire open reading frame in each case was free of unwanted mutations. The following is the primary amino acid sequence of the entire translated TylHI-RhFRED protein (yellow = N-terminal His-tag; red = TylHI; green = RhFRED):

MGSSHHHHHHSSGLVPRGSHMAWAPDTVFSLRPQRVVSSSGDARPSQKGILLPAAR
ANDTDEAAGRRSIAWPVARTCPFSPPEQYAALRAEEPIARAELWDGAPVWLISRQDH
VRALLADPRVSIHPAKLPRLSPSDGEAEASRSLLTLDPPDHGALRGHFIPEFGLRRVRE
LRPSVEQIVTGLLDDLTARGDEADLLADFALPMATQVICRLLDIPYEDRDYFQERTEQA
TRPAAGEEALEALLELRDYLDRLISGKTGRESGDGMLGSMVAQARGGGLSHADVLDN
AVLLLAAGHETTASMVTMSVLVLLQHPTAWRELTVNPGLLPGAVDELLRYLSIADGLRR
SATADIEIDGHTIRAGDGLVFLLAAANRDEAVFSEPEAFDIHRSARRHVAFGYGPHQCL
GQNLARMELEVALGAVLERLPALRPTTDVAGLRLKSDSAVFGVYELPVAWEFVLHRH
QPVTIGEPAARAVSRTVTVERLDRIADDVLRLVLRDAGGKTLPTWTPGAHIDLDLGALS
RQYSLCGAPDAPSYEIAVHLDPESRGGSRYIHEQLEVGSPLRMRGPRNHFALDPGAE
HYVFVAGGIGITPVLAMADHARARGWSYELHYCGRNRSGMAYLERVAGHGDRAALH
VSEEGTRIDLAALLAEPAPGVQIYACGPGRLLAGLEDASRNWPDGALHVEHFTSSLAA
LDPDVEHAFDLELRDSGLTVRVEPTQTVLDALRANNIDVPSDCEEGLCGSCEVAVLDG
EVDHRDTVLTKAERAANRQMMTCCSRACGDRLALRL

The underlined amino acids at the N-terminus of TylHI were present in TylHI-1 and absent in TylHI-2.

Cloning of TylHII

tylHII was obtained as a synthetic codon-optimized gene from Invitrogen (GeneArt Strings DNA Fragments). The sequence (5'–3') is displayed below:

ATGCGTGTTCGTATTGATACCGGTCGTTGTGTTGGTGCAGGTCAGTGTGAACGTGCAGCACCGACCGTTTTTCG
TCAGGATGAAGATGGTGTTGGTGGTGTTCTGGATCGTACACCGCCTCCGGCAGTTTGGGAAGAAGTTCGCGAA
GCCGAAGATCTGTGTCCGGCACGTGCAGTTCTGCTGAGCGGTGATGGTACAGGTGCCGGTGCGGGTGCAGCA
GCACCGCCAACAGGTCGTGATGCATAA

The gene was amplified by PCR using primers P8_forward and P8_reverse. The amplified fragment was subsequently purified, digested with *NdeI* and *HindIII*, and ligated into pET28b that had previously been digested with the same restriction enzymes to yield pET28b_TylHII. The plasmid was sequenced to ensure that no mutations were present in the open reading frame.

Generation of MycCI$_{S172A}$

The MycCI$_{S172A}$ mutant was generated by site-directed mutagenesis using mutagenic primer P9.

A.3 Protein expression and purification

Expression and purification of MycCI for biochemical experiments

The pET28b_MycCI plasmid previously generated[2] was used to express N-terminally His-tagged MycCI. The plasmid was transformed into *E. coli* BL21(DE3) cells, and individual colonies were selected for overnight growth (37 °C) in 10 mL of LB containing kanamycin (50 µg/mL). 6 x 1 L of TB (2 L Erlenmeyer flasks) supplemented with kanamycin (50 µg/mL), thiamine (1 mM), and glycerol (4% v/v) were inoculated with the 10 mL overnight seed cultures and incubated at 37 °C (200 rpm). When the OD_{600} reached 0.6-1.0, the 1 L cultures were allowed to cool in an ice-water bath (10-20 min) before IPTG (0.1 mM) and δ-aminolevulinic acid (1 mM) were added to induce protein expression and to allow for facile production of the heme cofactor in *E. coli*, respectively. The cultures were allowed to grow at 18 °C for 18-20 h before the cells were harvested and stored at -80 °C until used for protein purification.

All subsequent steps were performed at 4 °C. The cells were thawed and resuspended in 30 mL of lysis buffer (50 mM Tris-HCl (pH = 7.4 at room temperature

(rt)), 50 mM NaCl, 10% (v/v) glycerol, 1 mM PMSF, 0.5 mg/mL lysozyme, 2 mM $MgCl_2$, 5-10 U/mL Benzonase nuclease) per 1 L of original overexpression culture (i.e., 2-3 mL per 1 g of cells). The cell suspension was incubated on a nutating shaker for 1 h prior to sonication using a Model 705 Sonic Dismembrator (Thermo Fisher Scientific) and centrifugation at 50,000 x g for 30 min to remove cellular debris. To the resulting clarified lysate were added 4 M solutions of NaCl and imidazole such that the final concentrations of each were 300 mM and 10 mM, respectively. The lysate was filtered through a syringe-operated 0.45 µm filter (Corning) prior to loading onto a 5 mL HiTrap Chelating HP column (GE Healthcare) pre-charged with Ni^{2+} via an ÄKTA FPLC system (GE Healthcare). The loaded material was washed with 5 CV of wash buffer (50 mM Tris-HCl (pH = 7.4 at rt), 300 mM NaCl, 10 mM imidazole, 10% (v/v) glycerol) followed by 10 CV of 5% elution buffer (50 mM Tris-HCl (pH = 7.4 at rt), 300 mM NaCl, 300 mM imidazole, 10% (v/v) glycerol) to remove additional protein contaminants. MycCI was eluted with a linear gradient of 10-50% elution buffer over 30 CV. Fractions containing pure material as assessed by SDS-PAGE and by monitoring absorbance (A_{420}/A_{280}) were pooled and concentrated using 30 kD MWCO centrifugal filters. Concentrated protein was desalted by loading onto PD-10 columns and eluting with storage buffer (50 mM NaH_2PO_4 (pH = 7.3), 1 mM EDTA, 0.2 mM DTT, 10% (v/v) glycerol). Aliquots of purified protein were flash frozen in liquid N_2 and stored at -80 °C until needed for biochemical experiments. Following this protocol, the yield of functional P450 (as assessed by obtaining CO difference spectra according to the established protocol[6]) was 6-7 mg per 1 L of overexpression culture, and the protein's purity index (A_{420}/A_{280}) was ~1.6. The single-site mutant $MycCI_{S172A}$ was expressed and purified in an identical manner, and no differences in yield or purity were observed.

"Semipure" MycCI was prepared by first expressing the protein in 2 x 1 L of TB as described above. Following the cell lysis and centrifugation steps, the clarified lysate was filtered through a syringe-operated 0.45 µm filter and incubated with 2 mL of pre-equilibrated Ni-NTA resin (Qiagen) on a nutating shaker for 1 h. The slurry was loaded onto an empty column and washed briefly with 6 CV of wash buffer (50 mM Tris-HCl (pH = 7.4 at rt), 300 mM NaCl, 10 mM imidazole, 10% (v/v) glycerol) prior to eluting the protein with 6 CV of elution buffer (wash buffer containing 300 mM imidazole). The

protein was subsequently concentrated, desalted, aliquoted, flash frozen, and stored at -80 °C as previously described. The yield of functional P450 was 10.2 mg per 1 L of overexpression culture, and the protein's purity index was 0.87.

MycCI crude lysate was prepared by first expressing the protein in 2 x 1 L of TB as described above. The cells were resuspended in 30 mL of storage buffer per 1 L of original overexpression culture (~2 mL per 1 g of cells). The cell suspension was sonicated and centrifuged at 50,000 x g for 20 min to remove cellular debris. Aliquots of the resulting clarified lysate were stored at -80 °C until needed. The concentration of functional P450 in the crude lysate was 6.55 ± 0.09 μM (yield per 1 L of overexpression culture = 11.4 mg), and the purity index was <0.02.

Expression and purification of MycCI-RhFRED

N-terminally His-tagged MycCI-RhFRED was expressed as described for MycCI with the following modifications. Expression of protein was contingent on coexpression of GroES/GroEL chaperones. Therefore, BL21(DE3) cells were cotransformed with pET28b_MycCI-RhFRED and pGro7 (Takara), and overexpression cultures were additionally supplemented with chloramphenicol (25 μg/mL) for pGro7 maintenance. Once the OD_{600} reached 0.6-1.0, the cultures were cooled and induced with IPTG and δ-aminolevulinic acid as described previously for MycCI as well as L-arabinose (0.5 g/L) to induce expression of the chaperones.

After harvesting cells, the protein was purified by immobilized-metal affinity chromatography (IMAC) as described for MycCI. However, a further purification step was required to remove chaperones and other contaminating *E. coli* proteins. After IMAC purification, the protein was concentrated and exchanged into anion exchange loading buffer (50 mM Tris-HCl (pH = 7.4 at rt), 50 mM NaCl, 10% (v/v) glycerol) using PD-10 columns. Using the ÄKTA FPLC system, the buffer-exchanged protein was loaded onto a 20 mL Mono Q HR 16/10 anion exchange column (GE Healthcare) and washed with 2 CV of the loading buffer followed in turn by 3 CV of 5% and 10% anion exchange elution buffer (50 mM Tris-HCl (pH = 7.4 at rt), 1 M NaCl, 10% (v/v) glycerol). MycCI-RhFRED was eluted with a linear gradient of 10-50% elution buffer over 20 CV, eluting at approximately 200 mM NaCl. Fractions containing pure material as assessed

by monitoring absorbance (A_{420}/A_{280}) were pooled, concentrated, and desalted on PD-10 columns. Protein was eluted with storage buffer, and aliquots were flash frozen in liquid N_2 and stored at -80 °C until needed. Following this protocol, the yield of functional P450 was about 1.5 mg per 1 L of overexpression culture, and the protein's purity index (A_{420}/A_{280}) was ~1.1.

"Semipure" MycCI-RhFRED was prepared in the same manner as described for MycCI. The yield of functional P450 was 2.6 mg per 1 L of overexpression culture, and the protein's purity index was 0.30.

Expression and purification of MycCII

The pET28b_MycCII plasmid previously generated[2] was used to express N-terminally His-tagged MycCII as described for MycCI with the exception that δ-aminolevulinic acid was omitted from the culture broth.

Purification of MycCII was accomplished as described for MycCI with the following modifications. 50 mM NaH_2PO_4 (pH = 8.0) replaced 50 mM Tris-HCl (pH = 7.4 at rt) in all purification buffers; the other components of each buffer remained unchanged. Following the IMAC elution step, fractions containing pure material as assessed by SDS-PAGE and by monitoring absorbance (A_{410}/A_{280}) were pooled and concentrated using 3 kD MWCO centrifugal filters. The concentration of purified MycCII was determined by the Bradford protein assay using spinach ferredoxin (Sigma-Aldrich) as standard. Based on these results, ε_{410} for MycCII was estimated to be ~4500 $M^{-1}cm^{-1}$. The overall yield was typically ~30 mg per 1 L of overexpression culture, and the protein's purity index (A_{410}/A_{280}) was ~0.56.

Expression and purification of MBP-FdR

The plasmid (pMAL-c, New England Biolabs) encoding spinach ferredoxin reductase linked to the C-terminus of *E. coli* maltose-binding protein (MBP) was obtained as a gift from Dr. Giuliana Zanetti. This construct was transformed into *E. coli* BL21(DE3) cells, and individual colonies were selected for overnight growth (37 °C) in 15 mL of LB containing ampicillin (100 μg/mL). 12 x 1.5 L of LB (2.8 L baffled Fernbach flasks) supplemented with ampicillin (100 μg/mL) and glucose (0.2% (w/v); used to

repress the expression of amylase) were inoculated with the 15 mL overnight seed cultures and incubated at 37 °C (160 rpm). When the OD_{600} reached 0.6-1.0, the 1.5 L cultures were allowed to cool in an ice-water bath (10-20 min) before IPTG (0.1 mM) was added to induce protein expression. The cultures were grown at 18 °C for 22-24 h before the cells were harvested and stored at -80 °C.

All subsequent steps were performed at 4 °C. The cells were thawed and resuspended in 25 mL of lysis buffer (50 mM NaH_2PO_4 (pH = 8.0), 300 mM NaCl, 10% (v/v) glycerol, 1 mM PMSF) per 1.5 L of original overexpression culture (i.e., 3-5 mL per 1 g of cells). The cells were lysed by sonication, and the resulting crude lysate mixture was centrifuged at 38,000 x g for 30 min to remove cellular debris. The resulting clarified lysate was diluted 1:6 with lysis buffer prior to loading onto a pre-equilibrated amylose resin column (60 mL, New England Biolabs) via peristaltic pump. The loaded material was washed with 12 CV of lysis buffer, and the protein was eluted with ~50 mL of elution buffer (50 mM NaH_2PO_4 (pH = 8.0), 300 mM NaCl, 10% (v/v) glycerol, 10 mM maltose). Yellow protein-containing fractions were combined and concentrated with 30 kD MWCO centrifugal filters. Concentrated protein was desalted by loading onto PD-10 columns and eluting with storage buffer (50 mM NaH_2PO_4 (pH = 7.3), 1 mM EDTA, 0.2 mM DTT, 10% (v/v) glycerol). Aliquots of purified protein were flash frozen in liquid N_2 and stored at -80 °C until needed. The concentration of purified ferredoxin reductase was determined by absorption spectroscopy using the reported value for the extinction coefficient of oxidized flavoprotein (ε_{456} = 10,400 $M^{-1}cm^{-1}$).[7] The overall yield was typically 6-7 mg per 1 L of overexpression culture, and the protein's purity index (A_{456}/A_{280}) was ~0.05.

Expression and purification of TylHI

As previously described, two versions of the *tylHI* gene based on different translation start sites were cloned into pET28b vectors for overexpression. The shorter version of the gene (encoding TylHI-2) exhibited improved expression relative to the longer version (encoding TylHI-1) with the start site occurring 16 codons upstream. Since no differences in activity were observed between the two proteins, TylHI-2 was chosen to carry out subsequent characterization experiments. N-terminally His-tagged

TylHI-2 was expressed and purified as described for MycCI. The yield of functional P450 was twice that for MycCI (13-14 mg per 1 L of overexpression culture), and the protein's purity index (A_{420}/A_{280}) was ~1.6.

Expression and purification of TylHI-RhFRED

The longer TylHI-1 fused to RhFRED expressed very poorly, even when it was coexpressed with GroES/GroEL chaperones. However, the shorter TylHI-2-RhFRED construct exhibited greatly improved expression in the presence of these chaperones, so this version of the enzyme was used for all biochemical studies described. N-terminally His-tagged TylHI-2-RhFRED was expressed and purified as described for MycCI-RhFRED, yielding ~3 mg of functional P450 per 1 L of overexpression culture. The protein's purity index (A_{420}/A_{280}) was ~1.0.

Expression and purification of TylHII

The pET28b_TylHII construct containing the codon-optimized *tylHII* gene was used to express and purify N-terminally His-tagged TylHII as described for MycCII with the following modifications. BL21(DE3) cells were cotransformed with pET28b_TylHII and pGro7 (Takara). Overnight seed cultures were grown in TB instead of LB to expedite growth of 1 L overexpression cultures, which were additionally supplemented with chloramphenicol (25 μg/mL) for pGro7 maintenance and L-arabinose (0.5 g/L) to induce expression of the chaperones after the OD_{600} reached 0.6-1.0. The concentration of purified TylHII was determined by the Bradford protein assay using spinach ferredoxin as standard. Based on these results, ε_{410} for TylHII was estimated to be ~2800 $M^{-1}cm^{-1}$. The overall yield was much lower than that for MycCII (typically ~5 mg per 1 L of overexpression culture), and the protein's purity index was also reduced ($A_{410}/A_{280} \approx 0.40$) despite exhibiting about the same level of electrophoretic homogeneity (**Figure A.2**). On the basis of these results, it is likely that TylHII is unstable in the absence of chaperones, and it may readily revert to an "apo" form lacking part or all of its postulated [3Fe-4S] cluster. The inactive protein could conceivably account for a large portion of the total purified material. **Figure A.1** shows the UV-visible spectrum of TylHII in comparison to that of MycCII.

A.4 Protein crystallization and structure determination

Expression and purification of MycCI for crystallization

For crystallization experiments, MycCI (from pET28b_MycCI) was expressed in *E. coli* HMS174(DE3) cells. Following induction with IPTG (0.25 mM), cells were incubated at 18 °C for 20 h. All subsequent steps were carried out at 4 °C. Cells were harvested, resuspended in lysis buffer (50 mM Tris-HCl (pH = 8.0), 100 mM NaCl, 1 mM EDTA, 0.5 mM PMSF, 2.5 μg/mL lysozyme), and disrupted using a Microfluidics M-110P homogenizer. The crude extract was separated from cellular debris via centrifugation, and the clarified lysate was loaded onto a Ni-NTA column. After a series of wash steps, MycCI was eluted by increasing the imidazole concentration from 20 mM to 400 mM. Fractions containing MycCI were pooled, and 3.5 M ammonium sulfate was added to a final concentration of 0.7 M prior to loading the protein solution onto a HiPrepPhenylHP 16/60 hydrophobic interaction column (GE Healthcare). MycCI was eluted by decreasing the concentration of ammonium sulfate from 0.7 M to 0.0 M. Fractions containing MycCI were pooled and loaded onto a Mono Q column (GE Healthcare), and the desired protein was eluted using a 0.1-0.4 M NaCl gradient in 20 mM Tris-HCl (pH = 7.5) and 1 mM EDTA. Fractions containing pure MycCI were pooled, concentrated, and frozen at -80 °C.

Crystallization, data collection, and structure determination

Prior to crystallization, MycCI was diluted to 10 mg/mL by mixing with 10 mM Tris-HCl (pH = 7.5) and 2 mM DTT supplemented with M-VIII (**9**) at a 1:2 enzyme:substrate molar ratio. Crystallization conditions were determined using commercial high-throughput screening kits available in deep-well format (Hampton Research), a nanoliter drop-setting Mosquito robot (TTP LabTech) operating with 96-well plates, and a hanging drop crystallization protocol. Crystals were further optimized in 24-well plates for diffraction data collection. Needle-shaped crystals diffracting in the P1 space group grew from 20% PEG 3350, 0.2 M calcium acetate, 20 mM spermidine, and 0.84 mM TCEP. Prior to data collection, crystals were cryo-protected by plunging them into a drop of reservoir solution supplemented with 20-25% glycerol and flash freezing in liquid N_2.

Diffraction data were collected at 100-110 K at beamline 8.3.1, Advanced Light Source, Lawrence Berkeley National Laboratory, USA. Data indexing, integration, and scaling were conducted using MOSFLM[8] and the programs implemented in the ELVES software suite.[9] The crystal structure was initially determined by molecular replacement using vitamin D hydroxylase CYP105A1 from *Streptomyces griseolus* (PDB 3CV9)[10] as a search model (47% sequence identity to MycCI). Molecular replacement was performed using the automated molecular replacement program package MRBUMP[11,12] implemented in the CCP4 software suite.[13] The MycCI coordinates were built using the BUCCANEER[13,14] and COOT[15] programs. Refinement was performed using REFMAC5 software.[13,16] Data collection and refinement statistics are reported in **Table 2.5** (see Chapter 2).

A.5 Preparation of substrates for enzymatic reactions

Media recipes

All media components were purchased from EMD Millipore, BD (Difco), Sigma-Aldrich, and Thermo Fisher Scientific unless otherwise specified. MOPS was obtained from AK Scientific and glycerol was purchased from BDH (VWR). Components of 23-DMTL/tylactone production medium and *Streptomyces fradiae* strains GS76 and GS14 were obtained as kind gifts from Eli Lilly and Company.

SCM: 1 L = 20 g soytone, 15 g soluble starch, 10.5 g MOPS, 1.5 g yeast extract, 0.1 g $CaCl_2$, pH 7.2 (adjusted with KOH)

10-DML production medium: 1 L = 20 g dextrose, 15 g soybean flour, 5 g $CaCl_2$, 1 g NaCl, 2 mg $CoCl_2 \cdot 6H_2O$, 100 µL Antifoam B, pH 7.2 (adjusted with NaOH)

Narbonolide production medium: 1 L = 10 g dextrose, 10 g glycerol, 10 g polypeptone, 5 g NaCl, 5 g beef extract, 2 g $CaCl_2$, 100 µL Antifoam B, pH 7.3 (adjusted with NaOH)

Tryptic soy broth (TSB): 1 L = 17 g tryptone, 3 g soytone, 2.5 g dextrose, 5 g NaCl, 2.5 g K_2HPO_4, pH 7.3

23-DMTL/tylactone production medium: 1 L = 20 g dextrose, 15 g corn meal, 9 g fish meal, 9 g corn gluten, 1 g NaCl, 0.4 g $(NH_4)_2HPO_4$, 2 g $CaCO_3$, 30 mL crude soybean oil, pH 7.1

*Fermentation, isolation, and purification of 23-DMTL (**12**)*

A variant of *Streptomyces fradiae* designated GS76 was previously generated via chemical mutagenesis, yielding a strain that primarily produces 23-deoxy-desmycinosyl-tylosin (**S1**) due to the presence of mutations in the *tylH* and *tylD* genes encoding a P450/ferredoxin and a ketoreductase involved in 6-deoxyallose biosynthesis, respectively.[17] 50 mL of TSB (250 mL baffled Erlenmeyer flask containing a stainless steel spring) was inoculated with 10 µL of GS76 spore stock, and the seed culture was incubated at 28 °C for 7 days (180 rpm). 3 x 1 L of 23-DMTL/tylactone production medium (2.8 L baffled Fernbach flasks containing a stainless steel spring) were each inoculated with 10 mL of the seed culture, and the resulting production cultures were incubated at 28 °C for 7 days (180 rpm). Following this period of fermentation, the cultures were centrifuged twice at 10,000 x g for 20 min to remove cells and insoluble media components. The pH of the resulting supernatant was adjusted to 11 prior to extraction with XAD16 resin as described below for **2** to yield 2.35 g of crude material. The extract was resuspended in 50% ethyl acetate/hexanes, and hydrophobic impurities (mostly derived from the soybean oil component of the production medium) were removed from the soluble portion via silica gel chromatography (50% ethyl acetate/hexanes). Following removal of these impurities, the remaining material adsorbed to the silica was eluted with 10% methanol/dichloromethane supplemented with 1% triethylamine. This “semipure” material was combined with the ethyl acetate/hexanes-insoluble material to yield ~400 mg of methanol-soluble crude extract. LC-MS analysis revealed that the major component of this extract was the expected fermentation product **S1**. In order to remove mycarose from **S1** to produce 23-DMTL (**12**), the extract was resuspended in 8 mL of 0.2 M HCl and stirred at room temperature for 4 h. The solution was then neutralized by addition of 8 mL of 0.2 M NaOH, and the pH was adjusted to 9 prior to extraction with 3 x 10 mL of chloroform. The combined organic layers were dried over anhydrous Na_2SO_4, and the solvent was removed under reduced pressure to yield 265 mg of crude material. LC-MS analysis indicated that most of **S1** had been converted to **12** (**Scheme A.1**), which was purified by preparative HPLC as described later to afford 39 mg of pure material. During the purification process,

however, some material was sacrificed in order to maximize purity for enzymatic assays.

Fermentation and purification of macrolactones

10-deoxymethynolide (10-DML, **2**) was produced as described previously[18] with minor modifications. Briefly, 6 x 100 mL of SCM (250 mL baffled Erlenmeyer flasks containing a stainless steel spring) were inoculated with 10 µL of *Streptomyces venezuelae* ATCC 15439 (*desI* disruption mutant designated DHS8708) spore stock. Following incubation at 28 °C for 24 h (180 rpm), 20 mL of each seed culture was inoculated into 6 x 1 L of 10-DML production medium (2.8 L baffled Fernbach flasks containing a stainless steel spring). These cultures were incubated at 28 °C for 72 h (180 rpm) prior to centrifugation at 4500 x g for 25 min to remove cells and insoluble media components. The resulting supernatant was extracted by incubating with Amberlite XAD16 resin (30 g of washed wet resin per 1 L of culture supernatant) overnight with shaking. The resin was collected via filtration using a Büchner funnel, rinsed with water, and extracted with 3 x 500 mL of ethyl acetate. The combined organic extracts were washed with brine and dried over anhydrous Na_2SO_4. Solvent was removed under reduced pressure to yield crude **2**, which was purified by flash column chromatography using 35% ethyl acetate/hexanes as the solvent system (R_f = 0.40) to afford 560 mg of **2** as a yellow oil. The identity and purity of the material were confirmed by LC-MS and ^{1}H NMR analysis.

Narbonolide (NBL, **4**) was produced following a similar protocol for the production of **2**. SCM seed cultures were inoculated into 6 x 1 L of narbonolide production medium, and the resulting production cultures were incubated at 28 °C for 26 h (180 rpm). Following extraction as described above, the crude material was purified by flash column chromatography using 35% ethyl acetate/hexanes (R_f = 0.38). Further purification (to remove contaminating **2**) was accomplished via iterative recrystallization from ethyl acetate/hexanes to afford 249 mg of **4** as a white crystalline powder. The identity and purity of the material were confirmed by LC-MS and ^{1}H NMR analysis.

Semipure protomycinolide IV (PML-IV, **8**) was received as a generous gift from Dr. Yojiro Anzai. Prior to use in enzymatic assays, the material was further purified by

preparative HPLC as described later. Tylactone (**10**) was fermented, isolated, and purified following a similar protocol for the production of **12** with minor modifications. A variant of *S. fradiae* designated GS14 was previously generated via chemical mutagenesis, yielding a strain that primarily produces **10** due to the presence of mutations in the *tylA* genes encoding enzymes involved in tylosin sugar biosynthesis.[17] 8 x 40 mL of TSB (250 mL baffled Erlenmeyer flasks containing a stainless steel spring) were each inoculated with 10 µL of GS14 spore stock, and the seed cultures were incubated at 28 °C for 2 days (180 rpm). 8 x 1 L of 23-DMTL/tylactone production medium (2.8 L baffled Fernbach flasks containing a stainless steel spring) were each inoculated with 35 mL of seed culture, and the resulting production cultures were incubated at 28 °C for 7 days (300 rpm). Following this period of fermentation, the cultures were centrifuged at 5,000 x g for 20 min to remove cells and insoluble media components. The supernatant was then filtered through paper towels to further remove cellular debris, stored at 4 °C for 1 day, and extracted directly with 3 x 2 L of ethyl acetate. The combined organic layers were washed with brine (1 L), dried over anhydrous Na_2SO_4, and evaporated under reduced pressure to afford crude **10** as a yellow oil. The residue thus obtained was purified by flash column chromatography using 33% ethyl acetate/hexanes to afford **10** (1.054 g) as a yellow oil that solidified to an off-white, crystalline solid upon standing. Prior to use in enzymatic assays, the material was further purified by preparative HPLC as described later.

Construction of S. venezuelae pikAI-IV/pikC deletion mutant (DHS316)

A knock-out plasmid (pSRP65; **Figure A.12A**) derived from pKC1139[19] containing an apramycin resistance marker was constructed to replace the *pikC* gene with a kanamycin resistance gene. *Streptomyces venezuelae* genomic DNA was used to amplify the left- and right-flanking regions of the *pikC* gene with primer sets SR105/SR106 (5' flanking region) and SR107/SR108 (3' flanking region) (**Table A.1**). The kanamycin resistance gene was PCR amplified from plasmid pYJ276[20] using primer set SR109/SR110 (**Table A.1**). The amplified PCR fragments were cloned into the individual restriction sites of plasmid pLitmus28, generating plasmids pSRP51, pSRP52, and pSRP53 (each verified by sequencing). The *XbaI-HindIII*, *BamHI-XbaI*,

and *EcoRI-EcoRV* fragments from pSRP51, pSRP52, and pSRP53, respectively, were ligated into pKC1139 to produce pSRP65. The resulting plasmid pSRP65 was identified by restriction digestion prior to introduction into *S. venezuelae* Δ*pikAI-IV* (designated DHS2001)[21] by protoplast-based transformation. A single crossover product was first selected in the presence of apramycin and kanamycin. The *pikC* gene was then disrupted by an insertional inactivation via double crossover homologous recombination (**Figure A.12A**) as previously described.[22] The transformants (Δ*pikC*) resulting from double crossover were selected by their apramycin-sensitive and kanamycin-resistant phenotype, and their genotype was verified by Southern blot hybridization (**Figure A.12B**). The resulting *pikAI-IV*/*pikC* double disruption mutant of *S. venezuelae* was designated DHS316.

Biotransformation of macrolactones to macrolides

In order to append desosamine (**1**) to each of the four macrolactones tested in Chapter 2, biotransformations were carried out as described previously[23] with minor modifications. Briefly, 100 mL of SCM (250 mL baffled Erlenmeyer flask containing a stainless steel spring) was inoculated with 10 µL of *S. venezuelae* DHS316 spore stock. The culture was incubated at 28 °C (180 rpm) until the OD_{600} reached ~0.1 (12-15 h), at which point 10 mg of macrolactone as a DMSO solution (50 mg/mL) was added to the culture followed by 0.25 mg of acetyl-narbonolide as a DMSO solution (20 mg/mL). The culture was incubated at 28 °C for 24 h (180 rpm) before isolating desosaminylated macrolactones (i.e., macrolides). To isolate macrolide products, the 100 mL biotransformation culture was added to 200 mL of acetone, and the resulting suspension was incubated at -20 °C for at least 1 h. The mixture was subsequently filtered through a Celite plug to remove cells and other insoluble materials, and the acetone was removed under reduced pressure. The remaining aqueous solution was saturated with NaCl prior to adjusting the pH to 11. The solution was extracted with 3 x 100 mL of ethyl acetate, and the combined organic layers were dried over anhydrous Na_2SO_4 and evaporated under reduced pressure to afford crude macrolides purified directly by preparative HPLC as described later. LC-MS analysis of culture extracts

demonstrated that all macrolactones were efficiently converted into singly desosaminylated macrolides.

Typically, 50-100 mg of each macrolactone was converted to the corresponding macrolide at any given time. It should be noted that a single 1 L culture could be used in lieu of 10 x 100 mL cultures to biotransform up to 100 mg of material with little to no impact on overall conversion. In addition, solid-phase extraction with XAD16 resin could replace direct liquid-liquid extraction for large sample volumes.

Preparative HPLC purification

All compounds were purified using a Beckman Coulter System Gold HPLC equipped with a Phenomenex Luna C18 column with the following specifications: dimensions, 250 x 21.2 mm; particle size, 5 µm; pore size, 100 Å. The flow rate was maintained at 8 mL/min, and the isocratic mobile phase consisted of an acetonitrile/water mixture (**Table A.2**) with triethylamine (0.1%) included as a modifier only for purification of macrolides. All crude material was dissolved in methanol (40-50 mg/mL for crude extracts, 10-30 mg/mL for semipure compounds) and filtered through 0.20 µm PTFE filters (EMD Millipore) prior to manual HPLC injection (typically 1 mL per run). UV absorption was monitored at 288 nm for all compounds except for YC-17 (**3**) and narbomycin (**5**), which were monitored at 240 nm.

A.6 Preparative-scale enzymatic reactions

Preparative-scale enzymatic reactions were performed as previously described with minor modifications.[24,25] Reactions were typically conducted on ~15 mg of each substrate (50-70 mL total reaction volume) and were performed in 250-500 mL Erlenmeyer flasks (capped with a milk filter) at 30 °C overnight (12-24 h) with gentle shaking (100 rpm). Reaction conditions for macrolides **9**, **11**, and **12** were as follows: 2.5-5.0 µM MycCI-RhFRED (semipure), 500 µM substrate, 1 mM $NADP^+$, 5 mM glucose-6-phosphate, and 1 U/mL glucose-6-phosphate dehydrogenase for NADPH regeneration in storage buffer (50 mM NaH_2PO_4 (pH = 7.3), 1 mM EDTA, 0.2 mM DTT, 10% (v/v) glycerol). Reaction conditions for macrolactones **8** and **10** were the same with the exception that MycCI-RhFRED was replaced with a three-component biocatalytic

system consisting of 5 μM MycCI (semipure), 100 μM MycCII, and 5 μM MBP-FdR. Prior to extraction, reaction mixtures were analyzed by LC-MS to determine the percent conversion of starting material to product. Approximate values were as follows: 80% (**9**), 60% (**11**), 40% (**12**), 30% (**8**), and 50% (**10**). To isolate product and remaining starting material, the reaction mixture was added to acetone (2 x total reaction volume) and incubated at 4 °C for 2 h. The mixture was then filtered through Celite, and the acetone was removed under reduced pressure. The remaining aqueous solution was saturated with NaCl, adjusted to pH 11 (only for reactions with macrolides), and extracted with ethyl acetate (3 x 50 mL). The combined organic layers were dried over anhydrous Na_2SO_4 and evaporated under reduced pressure to afford a crude mixture of product and remaining starting material, which were purified by preparative HPLC as described above. Product recovery was typically at least 50%, and isolated yield of pure product averaged around 30% in each case save for **13** (~15%).

A large-scale reaction with **5** was carried out under the same conditions as described above for the macrolactones (**8** and **10**). After overnight incubation, the reaction mixture was extracted and the residue thus obtained was used as a substrate for a second reaction that was identical to the first in all other respects. LC-MS analysis of the final reaction mixture showed that **5** was converted to one major (~2%) and one minor (~0.5%) monohydroxylated product (**Figure A.3**). However, due to the low conversion yields, we were unable to isolate and characterize these compounds further.

A.7 Enzymatic assays

Determination of total turnover number (TTN)

Analytical-scale enzymatic reactions were carried out under the following conditions: 0.5 μM P450, 100 μM ferredoxin (MycCII or TylHII), 10 μM MBP-FdR, 500 μM substrate (2.5% DMSO, final concentration), 1 mM $NADP^+$, 5 mM glucose-6-phosphate, and 1 U/mL glucose-6-phosphate dehydrogenase in storage buffer (50 mM NaH_2PO_4 (pH = 7.3), 1 mM EDTA, 0.2 mM DTT, 10% (v/v) glycerol). Exogenous redox partners (ferredoxin and MBP-FdR) were not included in reactions employing P450-RhFRED fusion proteins. The total volume of each reaction was 100 μL (1.7 mL Eppendorf tube), and reactions were incubated at 30 °C (100 rpm) for 15-16 h prior to

quenching by addition of 100 µL of methanol. Quenched reactions were briefly vortexed and centrifuged at 17,000 x g for 10 min (4 °C), and the supernatant was removed for HPLC or LC-MS analysis. All reactions were performed and analyzed in triplicate.

HPLC analysis was performed on an Agilent 1100 Series HPLC system with UV detection at 285 nm using a Phenomenex Luna C18 column with the following specifications: dimensions, 150 x 4.6 mm; particle size, 5 µm; pore size, 100 Å. For analysis of reactions with macrolides **9**, **11**, and **12**, HPLC conditions were as follows (**Method A**): mobile phase (A = deionized water + 0.1% formic acid, B = acetonitrile + 0.1% formic acid); 15% B for 1 min, 15% to 55% B over 10 min, 95% B for 1 min, 15% B for 2 min; flow rate, 2.0 mL/min; injection volume, 50 µL. For analysis of reactions with macrolactones **8** and **10**, HPLC conditions were the same except for the gradient program, which was as follows (**Method B**): 15% B for 1 min, 15% to 75% B over 5 min, 95% B for 1 min, 15% B for 2 min. Retention times for substrates and products are reported in **Table A.3**.

LC-MS analysis was performed on an Agilent Q-TOF HPLC-MS (Department of Chemistry, University of Michigan) equipped with a high-resolution electrospray mass spectrometry (ESI-MS) source and a Beckmann Coulter reversed-phase HPLC system using a Phenomenex Luna C18 column with the following specifications: dimensions, 150 x 3.0 mm; particle size, 5 µm; pore size, 100 Å. HPLC conditions were as follows: mobile phase (A = deionized water + 0.1% formic acid, B = 95% acetonitrile/deionized water + 0.1% formic acid); 10% to 100% B over 12.5 min, 100% B for 2.5 min, 10% B for 5 min; flow rate, 0.4 mL/min; injection volume, 1 µL. Retention times and observed *m/z* values for substrates and products are reported in **Table A.4**.

In both cases, TTN values were calculated using Equation 1.

$$\mathrm{TTN} = \left(\frac{\mathrm{Area}_{\mathrm{product(s)}}}{\mathrm{Area}_{\mathrm{reactant}}+\mathrm{Area}_{\mathrm{product(s)}}}\right)\left(\frac{[\mathrm{Substrate}]_{\mathrm{total}}}{[\mathrm{P450}]_{\mathrm{total}}}\right) \qquad (1)$$

For all 16-membered ring macrolides and macrolactones, TTN was determined by evaluating the areas of HPLC peaks corresponding to starting materials and products. The extinction coefficients of a given 16-membered ring substrate and the corresponding monohydroxylated product are essentially identical since the α,β,γ,δ-

unsaturated ketone chromophore remains unaltered. Therefore, the amount of product formed in each case could easily be determined without having to generate standard curves to correlate substrate and/or product peak area with concentration. For **5**, TTN was determined by integrating extracted-ion chromatogram (EIC) peaks corresponding to $[M + H]^+$ ions for unreacted substrate and mono- ($[M + H + 16]^+$) and dihydroxylated ($[M + H + 32]^+$) products. The ionization efficiencies of substrate and hydroxylated products were assumed to be identical, as ionization most likely occurs at the *N*,*N*-dimethylamino group of desosamine for these and related compounds.[26] A summary of the results obtained with **5** as substrate is presented in **Table A.5**.

Equilibrium substrate binding assays

Spectroscopic substrate binding assays were performed at room temperature using a SpectraMax M5 UV-visible spectrophotometer (Molecular Devices). Compound parent stocks were prepared by dissolving ~15 mg of each compound in DMSO to 30 mM. Serial dilutions of the parent stocks were made to achieve target concentrations of the stock solutions used for binding assays. Purified P450s were diluted in storage buffer (50 mM NaH_2PO_4 (pH = 7.3), 1 mM EDTA, 0.2 mM DTT, 10% (v/v) glycerol) to concentrations ranging from 0.1 to 5 μM (see **Table A.7**). 0.7 mL of diluted enzyme was transferred to a 1 cm quartz cuvette (Beckman), and substrate was titrated into the solution in varying amounts so as to achieve the desired final concentrations. The same amounts of DMSO alone were added to the protein in the reference cuvette. Generally, DMSO comprised 2-5% of the solution volume at the conclusion of each experiment. Scans were performed from 365 to 439 nm (2 nm steps), and difference spectra were subsequently obtained by subtracting reference spectral data from the experimental spectra. Average absorbance differences ($\Delta A = A_{385} - A_{419}$; for binding of **3** only, $\Delta A = A_{385} - A_{425}$) from experiments performed at least in triplicate were plotted as a function of substrate concentration, and the data were fit to either a rectangular hyperbolic function (Equation 2) for $K_d \geq 5 \times [P450]$ or a quadratic function (Equation 3) for high-affinity ligands ($K_d \leq 5 \times [P450]$) using the KaleidaGraph software package.

$$\Delta A = \frac{\Delta A_{max}[S]}{K_d + [S]} \qquad (2)$$

$$[S] = \text{free substrate} \approx \text{total substrate}$$

$$\Delta A = \frac{\Delta A_{max}\left[([E]+[S]+K_d) - \sqrt{([E]+[S]+K_d)^2 - 4[E][S]}\right]}{2[E]} \qquad (3)$$

$$[S] = \text{total substrate};\ [E] = \text{total enzyme}$$

The percent spin shift of each enzyme at saturating levels of different substrates was estimated by normalizing the ΔA_{max} values acquired from the nonlinear regression analysis previously described to the enzyme concentration. The resulting values were then compared with the largest of these values obtained for MycCI and MycCI-RhFRED to determine percent spin shift as described by Equation 4.

$$\%\ \text{spin shift} = \left[\frac{\Delta A_{max}/[E]}{(\Delta A_{max}/[E])_{max}}\right] \text{ x } 100 \qquad (4)$$

The percentage of each enzyme in the high-spin state at saturating levels of a given substrate was estimated by assuming that both MycCI and MycCI-RhFRED were completely converted to high spin when saturated with **10**. Indeed, $(\Delta A_{max}/[E])_{max}$ was observed with **10** as the substrate for both of these enzymes (**Table A.8**). $\Delta A_{max}/[E]$ for binding of **10** to MycCI was used as $(\Delta A_{max}/[E])_{max}$ to calculate percent spin shifts for MycCI, $MycCI_{S172A}$, and TylHI. Due to the slightly different spectral properties of MycCI-RhFRED and TylHI-RhFRED, $\Delta A_{max}/[E]$ for binding of **10** to MycCI-RhFRED was used as $(\Delta A_{max}/[E])_{max}$ to calculate percent spin shifts for these self-sufficient fusion enzymes. Results are summarized in **Table A.8**.

Steady-state kinetics (product formation)

Reactions performed to assess rates of product formation were carried out under the following conditions: 0.5 μM P450, 100 μM ferredoxin (MycCII or TylHII), 10 μM MBP-FdR, 5-750 μM substrate (2.5% DMSO, final concentration), and 2 mM NADPH in storage buffer (50 mM NaH_2PO_4 (pH = 7.3), 1 mM EDTA, 0.2 mM DTT, 10% (v/v) glycerol). Exogenous redox partners (ferredoxin and MBP-FdR) were not included in

reactions employing P450-RhFRED fusion proteins. For reactions involving TylHI, 1.0 μM P450 was used due to the very slow rates observed. All components save for NADPH (P450-RhFRED reactions) or P450 (P450 + ferredoxin + MBP-FdR reactions) were mixed together in a total volume of 150 μL (1.7 mL Eppendorf tubes) and pre-incubated at 30 °C (200 rpm) for 5 min. Reactions were initiated by addition of 50 μL of either 8 mM NADPH or 2 μM P450 (4 μM P450 for TylHI), and the mixtures were incubated at 30 °C (200 rpm) in a MultiTherm shaker (Benchmark Scientific). Each reaction was quenched at four time points (including t = 0 min) by dispensing 50 μL aliquots into 100 μL of methanol and placing the resulting mixtures on ice. Subsequently, quenched reactions were centrifuged at 17,000 x g for 10 min (4 °C) to separate precipitated protein components, and the supernatant was analyzed by HPLC as described previously for determining TTN with minor modifications as follows. **Method B** was used to analyze all samples save for those derived from reactions between MycCI/MycCII or TylHI/TylHII and **12**, which were analyzed using **Method A** to facilitate separation of product from starting material and other protein-derived contaminants. For reactions containing 5-10 μM substrate, injection volumes were increased to 100 μL in order to improve UV detection of products.

For a given P450, time points varied according to the specific substrate being tested and its concentration in the reaction mixture. Based on the results of preliminary experiments, the time points were chosen to maximize signal-to-noise in the HPLC chromatogram while ensuring that steady-state conditions were maintained (i.e., reactions did not proceed beyond 10% substrate conversion). The concentration of product formed at various time points was estimated using Equation 5, which was feasible given that the extinction coefficients of a particular 16-membered ring substrate and the corresponding monohydroxylated product are effectively equal to one another.

$$[\text{Product}] = \left(\frac{\text{Area}_{\text{product}}}{\text{Area}_{\text{reactant}}+\text{Area}_{\text{product}}}\right)[\text{Substrate}]_{\text{total}} \qquad (5)$$

At each substrate concentration, initial rates of product formation (V_0) were determined by plotting product concentration as a function of time over four data points. Average initial rates derived from experiments performed at least in triplicate were plotted vs

substrate concentration, and the data were fit to the standard Michaelis-Menten equation (Equation 6) or to equations describing single-site (Equation 7) or two-site (Equation 8) substrate inhibition using KaleidaGraph.

$$\frac{V_0}{[E]} = \frac{k_{cat}[S]}{K_m + [S]} \qquad (6)$$

$$\frac{V_0}{[E]} = \frac{k_{cat}}{1 + \frac{K_m}{[S]} + \frac{[S]}{K_i}} \qquad (7)$$

$$\frac{V_0}{[E]} = \frac{k_{cat1}\left(\frac{[S]}{K_{m1}}\right) + k_{cat2}\left(\frac{[S]^2}{K_{m1}K_{m2}}\right)}{1 + \left(\frac{[S]}{K_{m1}}\right) + \left(\frac{[S]^2}{K_{m1}K_{m2}}\right)} \qquad (8)$$

Equation 6 was used to fit data acquired with MycCI-RhFRED acting on **8**–**10** as well as TylHI-RhFRED acting on **12**. Equation 7 provided the best fit for data acquired with MycCI-RhFRED acting on **11** and **12**, yielding very large inhibitory constants (K_i = 6.6 ± 7.4 mM for **11**; K_i = 2.5 ± 1.1 mM for **12**). The results for TylHI-RhFRED are shown in **Figure A.9A**.

Equation 8 was used to fit the data acquired with MycCI and TylHI acting on all substrates tested. This equation provides a good fit to the experimental data when "partial substrate inhibition" is observed. It was originally derived to describe a two-site model in which an enzyme is capable of binding two substrate molecules simultaneously, although it cannot be used to verify whether the binding sites are the same or independent.[27] In the model, the four variable kinetic parameters can be described as follows:

k_{cat1} = catalytic constant when the enzyme is saturated with one substrate molecule
K_{m1} = Michaelis constant describing the binding of the first substrate molecule
k_{cat2} = catalytic constant when the enzyme is saturated with two substrate molecules
K_{m2} = Michaelis constant describing the binding of the second substrate molecule when the first binding site is already fully occupied by the first substrate molecule

Table A.9 presents the values for these parameters that were obtained after fitting Equation 8 to the data acquired with MycCI. The large errors associated with these values render straightforward interpretation of their meaning or importance quite challenging. Nonetheless, it is clear from the values for k_{cat2} that the rates of MycCI-catalyzed hydroxylation at high substrate concentrations converge toward ~1 min^{-1} for all 16-membered ring substrates. If the effect of substrate inhibition were removed in each case, maximum rates would all approach ~3 min^{-1} (k_{cat1}).

Some substrate inhibition was also observed for TylHI/TylHII/MBP-FdR acting on **12**, but the overall rate of product formation was very low compared with that using MycCI/MycCII/MBP-FdR (**Figure A.9B**). However, the rate was improved nearly 12-fold when TylHI was partnered with MycCII (**Table 2.4**). In addition, since the activity of MycCI was greatly diminished when it acted in conjunction with TylHII (**Table A.6**), it is highly probable that the latter ferredoxin was unable to facilitate effective electron transfer from MBP-FdR to the P450 heme domain. The reason for this poor activity is unclear, but it may relate to the instability or suboptimal folding of TylHII when overexpressed in a heterologous host.

Steady-state kinetics (NADPH consumption)

Reactions performed to assess rates of NADPH consumption were carried out under the following conditions: 0.2 μM P450-RhFRED, 1-300 μM substrate (2.5% DMSO, final concentration), and 250 μM NADPH in storage buffer (50 mM NaH_2PO_4 (pH = 7.3), 1 mM EDTA, 0.2 mM DTT, 10% (v/v) glycerol). All components save for NADPH were mixed together in a total volume of 150 μL (96-well plate, Corning Costar) and pre-incubated at 30 °C for 5 min. Reactions were initiated by addition of 50 μL of 1 mM NADPH via multichannel pipette, and the absorbance at 340 nm was monitored over 30 min (15 s read intervals) using a SpectraMax M5 Microplate Reader (Molecular Devices). The temperature of the plate-reading chamber was maintained at 30 °C for the duration of the experiment. The raw absorbance data were converted to NADPH concentration using ε_{340} = 6.22 $mM^{-1}cm^{-1}$ and pathlength = 0.535 cm. Initial rates of NADPH consumption were determined by plotting NADPH concentration as a function of time within the linear range (first 5-10 min). Normalized rates were obtained by

subtracting the observed rate of NADPH consumption in the absence of substrate from that measured in the presence of substrate at various concentrations and dividing the resulting value by the enzyme concentration. Average normalized rates derived from experiments performed in triplicate were plotted vs substrate concentration, and the data were fit to Equation 6 to obtain the reported steady-state kinetic parameters (for MycCI-RhFRED (pure), see **Table 2.3** and **Figure A.10A**; for MycCI-RhFRED (semipure), see **Table A.10** and **Figure A.10B**; for TylHI-RhFRED, see **Figure A.10C**). In contrast to what had been seen for MycCI-RhFRED (pure) with respect to kinetics of product formation (**Figure 2.3A**), no substrate inhibition was observed for substrates **11** and **12** when NADPH consumption rates were monitored (**Figure A.10A**). Therefore, the inhibition must have been occurring after NADPH oxidation but before substrate turnover, likely during the electron transfer steps, indicating a possible interference of these substrates with cooperative interaction between the [2Fe-2S] domain of RhFRED and the P450 heme domain.

NADPH consumption in the presence of P450/ferredoxin/MBP-FdR was independent of substrate concentration, thus precluding determination of relevant kinetic parameters for the tripartite biocatalytic systems. Despite testing a number of different parameters (e.g., enzyme concentration, P450:ferredoxin:MBP-FdR ratios, initiation of reactions with NADPH, P450, or MBP-FdR), we were unable to observe substrate-dependent NADPH depletion. **Table A.11** presents rates of NADPH consumption under some of the conditions tested. The data show that the rate of NADPH consumption in the absence of substrate was about the same as that in the presence of substrate. Moreover, the rate was independent of the presence of P450 itself. The NADPH oxidation rate exhibited a slight dependence on the presence of ferredoxin, however. Rates were ~1.3 μM/min faster when MycCII was present while they were only ~0.6 μM/min faster on average when TylHII was present, indicating a preference for MBP-FdR to reduce MycCII. Nonetheless, the overall rate was observed to change mostly as a function of MBP-FdR concentration (~4 μmol/min per μmol enzyme).

Determination of turnover frequency (TOF) and coupling efficiency

Reactions performed to assess turnover frequency (TOF) were carried out in an identical manner to those described previously for steady-state kinetics where formation of product was monitored. In all cases, substrate was present at 500 μM, and reaction progress was monitored by HPLC after 0, 10, 20, and 30 min. All TOF results are presented in **Table 2.4** (see **Table A.12** for TOF results obtained with MycCI-RhFRED (semipure)). NADPH consumption rates in the presence of 500 μM substrate were determined as described previously. Instead of subtracting rates in the absence of substrate from those measured in the presence of substrate, however, normalized rates were obtained by subtracting the rate of spontaneous NADPH oxidation in the absence of enzyme (experimentally determined to be 0.146 μM/min) from the raw rates and dividing the resulting values by the enzyme concentration. All experiments were performed and analyzed in triplicate. The coupling efficiency for each enzyme/substrate combination was determined by dividing TOF by the rate of NADPH consumption in the presence of 500 μM substrate. NADPH consumption rates and coupling efficiencies are presented in **Tables A.13** and **A.14**, respectively.

A.8 Supplemental discussions

Steady-state kinetics (product formation)

The steady-state kinetics profiles observed for MycCI/MycCII/MBP-FdR are consistent with a two-site model in which the P450 possesses two substrate binding sites that can be occupied simultaneously.[27,28] However, this model cannot be used to determine the relative proximity of these two sites (i.e., orthosteric vs allosteric). Several possible scenarios can be envisioned that would provide an explanation for the atypical kinetics seen for the tripartite biocatalytic system. One such situation that has been widely postulated as an explanation for the cooperativity seen in human drug-metabolizing P450s (e.g., CYP3A4) involves simultaneous binding of more than one substrate in the same pocket.[29] While promiscuous microsomal P450s tend to harbor large substrate binding pockets that have the capacity to bind more than one substrate molecule, the same may not be true for more selective P450s such as those commonly found in bacterial secondary metabolic pathways. Although there are documented

exceptions,[30] the higher substrate specificity of biosynthetic P450s, especially those acting on particularly large pathway intermediates, would likely preclude simultaneous binding of two substrate molecules in the active site. Another more plausible scenario involves binding of the second substrate at a site that is distinct from the first (main and catalytically relevant) substrate binding site. In this case, the observed inhibition could stem from a substrate-induced conformational change in the structure of the P450 such that it is less effective at executing its catalytic cycle.[29] Suboptimal catalysis could conceivably result from disruption of any of the steps in the catalytic cycle, most likely the electron and proton transfer steps that must occur en route to Compound I formation. In turn, it is plausible that binding of substrate at an allosteric site could disrupt these steps by hindering cooperative interactions between the P450 and its ferredoxin partner and/or impeding concomitant electron transfer. There is a great deal of evidence supporting the idea that substrate binding to P450 can modulate its affinity for redox partners.[29] However, this scenario is most well documented in the context of microsomal P450s, wherein substrate binding improves interactions between P450 and its associated reductase/cytochrome b_5.[27,29,31] Substrate-induced conformational transitions could also lead to disruptions in the key proton transfer steps by interfering with the hydration state of the active site and/or the positions of key catalytic residues. Given the data presently available, it is not possible to draw any solid conclusions with respect to the mechanism of partial substrate inhibition seen for the MycCI/MycCII/MBP-FdR catalytic system.

Analysis of "semipure" MycCI-RhFRED

In order to determine if we could further improve the observed activity of MycCI-RhFRED on each of the substrates tested, especially those for which lower TTN values were obtained, we measured the activity of the enzyme following a faster, less rigorous purification procedure. Single-step immobilized-metal affinity chromatography (IMAC) purification using a batch method yielded P450 enzyme that copurified with a number of additional protein impurities, including GroEL/GroES, which were coexpressed with MycCI-RhFRED in order to improve soluble protein expression (**Figure A.2**). When this "semipure" enzyme was tested, TTN values were about double those of the highly

purified enzyme across all substrates (compare results shown in **Tables 2.1** and **A.6**). Interestingly, when some of the impurities discarded during the protein preparation were added to reactions containing the pure enzyme, overall substrate conversion increased, indicating that the effect was not a result of more expeditious purification (data not shown). However, we were unable to recapitulate these results by addition of BSA to the reaction mixtures, suggesting that the effect was also unlikely a consequence of macromolecular crowding. It is possible that the presence of additional proteins, most likely various copurifying chaperones such as GroEL, DnaK, and GrpE, plays a role in stabilizing MycCI-RhFRED and thereby allows it to evade oxidative damage due to uncoupling of NADPH consumption from product formation. We also performed analytical-scale reactions using "semipure" MycCI as well as crude cell lysate, but increases in TTN were typically modest or not observed at all (**Table A.6**). More notable improvements were observed for substrates **12** and **5**, with MycCI crude cell lysate supporting 135 and 13 turnovers of each, respectively. The low expression level of MycCI-RhFRED precluded accurate assessment of its activity when it was prepared as crude cell lysate.

Interestingly, despite the higher TTN values obtained with semipure MycCI-RhFRED, the rates of NADPH consumption were lower for all substrates tested (compare results shown in **Tables 2.3** and **A.10**; see **Figure A.10A/B**). However, the specificity constants were comparable to those for pure MycCI-RhFRED in each case. Additionally, the TOF values for semipure MycCI-RhFRED were all lower than those for pure MycCI-RhFRED (compare results shown in **Tables 2.4** and **A.12**), which accords well with the NADPH consumption data. Even though the rates of both product formation and NADPH consumption were lower for semipure MycCI-RhFRED than for pure MycCI-RhFRED, the activity of the former as assessed by TTN was found to be about twice that of the latter (**Tables 2.1** and **A.6**). Initially, we hypothesized that this apparent inconsistency could relate in some capacity to coupling efficiency. In P450 catalytic systems, coupling of NADPH consumption to substrate oxidation typically positively correlates with structural complementarity between the substrate and the P450 active site.[32] Tighter and more effective substrate binding leads to more favorable displacement of water molecules that are sequestered in the active site and maximizes

productive substrate positioning with respect to the iron-oxo species prior to oxidative attack of the target C–H bond. In turn, these effects minimize uncoupling and the ensuing production of reactive oxygen species (ROS) that are involved in the oxidative degradation of the enzyme, which can lead to lower TTN values. Coupling efficiencies for pure MycCI-RhFRED (**Table A.14**) were estimated by comparing the initial rates of product formation (**Table 2.4**) with those for NADPH consumption at 500 μM substrate (**Table A.13**). A direct correlation was observed between coupling efficiency and the activity of the enzyme on each of its substrates. Nonetheless, the highest coupling efficiency (~12% with **9** as substrate) was still rather low, even when compared with other P450-RhFRED fusion enzymes that have previously been reported (19% for MycG-RhFRED[33] acting on its native substrate mycinamicin IV; 34% for $P450_{cam}$-RhFRED[34] acting on its native substrate camphor). Furthermore, despite the ability of semipure MycCI-RhFRED to support more substrate turnovers, the coupling efficiencies for this enzyme were found to be no higher than those for pure MycCI-RhFRED (**Table A.14**). Therefore, we reasoned that the impurities (e.g., molecular chaperones) present in the semipure preparations were somehow tempering the damaging effects of ROS production on enzyme stability during the in vitro reactions. If this hypothesis is true, then it should be possible to increase the observed activity of MycCI-RhFRED by addition of ROS scavengers like catalase and superoxide dismutase to the reactions.

A.9 Supplemental tables

Table A.1. Primers used to generate constructs described in Chapter 2.

Primer	Sequence (5'–3')	Notes
P1	CCCCGAGCAGTACGCCGAATTTCGCCAGCGGGCCACATTGG	Base modified from original sequence is underlined
P2	GAGTTCCGTACGAGGACCGGGAATTTTTCCAGGAACGCAGCGAACTGGCG	Base modified from original sequence is underlined
P3_forward	GCGCATATGGTGGTCTGGCCCATGG	*NdeI* restriction site is underlined
P3_reverse	GGCGAATTCCCACTCGACCAGCAGC	*EcoRI* restriction site is underlined
P4_forward	CCGCATATGGCCTGGGCACCGGACACGGTGTTTTC	*tylHI* start site 1 (AF147703); *NdeI* restriction site is underlined
P4_reverse	GCGAAGCTTTCACCAGGCGACGGGCAGCTCGTAC	*tylHI* start site 1 (AF147703); *HindIII* restriction site is underlined
P5_forward	GGAATTCCATATGTCCTCGTCCGGGGACGC	*tylHI* start site 2 (AF055922); *NdeI* restriction site is underlined
P5_reverse	CGATCAAGCTTTCACCAGGCGACGGGC	*tylHI* start site 2 (AF055922); *HindIII* restriction site is underlined
P6_reverse	GCGGAATTCCCAGGCGACGGGCAGCTCGTAC	*tylHI* start site 1 (AF147703); *EcoRI* restriction site is underlined
P7_reverse	CGATCGAATTCCCAGGCGACGGGCAG	*tylHI* start site 2 (AF055922); *EcoRI* restriction site is underlined
P8_forward	GGAATTCCATATGCGTGTTCGTATTGATACCG	*NdeI* restriction site is underlined
P8_reverse	CGATCAAGCTTTTATGCATCACGACCTG	*HindIII* restriction site is underlined
P9	GAACGACGACCGCGCCATGCCGGCCCTGATC	Base modified from original sequence is underlined
SR105	CGTGAATTCCGTCGAAGTACAGCCGCA	*EcoRI* restriction site is underlined
SR106	CCGGATATCCGGACCCTCGGCACGCAG	*EcoRV* restriction site is underlined
SR107	CTCTCTAGATGCCCGGACCTCGCCCTG	*XbaI* restriction site is underlined
SR108	CGCAAGCTTTGGTGTGGGAGGCCTGCC	*HindIII* restriction site is underlined
SR109	AAAGGATCCCCCGAACCCCAGAGTCCC	*BamHI* restriction site is underlined
SR110	AAATCTAGAACCTGATACCGCTCGCCGC	*XbaI* restriction site is underlined

Table A.2. Conditions for preparative HPLC purification of macrolactones and macrolides.

Compound	% MeCN[a]	Approx. rt (min)
YC-17 (**3**)	65	33
Narbomycin (**5**)	65	36
PML-IV (**8**)	65	24
M-VIII (**9**)	75	33
Tylactone (**10**)	65	23
DT (**11**)	75	34
23-DMTL (**12**)	55	30
ML-IV (**13**)	35	37
M-VII (**14**)	55	28
23-OH-tylactone (**15**)	35	30
23-OH-DT (**16**)[b]	65	20
MTL (**17**)	35	29

[a]Triethylamine (0.1%) was included as a modifier for the purification of all compounds except **8**, **10**, **13**, and **15**.

[b]**16** copurified with a slightly less polar compound that was later identified as a photoisomer. Effective separation was achieved using 40% MeCN, with **16** eluting at approximately 91 min.

Table A.3. Analytical HPLC retention times of 16-membered ring aglycones and macrolides.

Compound	Method A (min)	Method B (min)
8	12.53	7.14
9	8.22	4.74
10	12.49	7.05
11	8.24	4.76
12	7.10	4.38
13	8.56	5.28
14	5.41	3.81
15	8.09	5.12
16	5.88	3.96
17	4.35	3.46

Table A.4. LC-MS retention times and observed *m/z* values of compounds investigated in Chapter 2.

Compound	Ret. time (min)	*m/z* ($[M + H]^+$)
2[a]	9.65	297.21, 279.20
3	5.91	454.32
4[a]	10.69	353.23, 335.22
5	6.26	510.34
OH-narbomycin (A)	5.02	526.34
OH-narbomycin (B)	4.61	526.34
$(OH)_2$-narbomycin	4.77	542.33
8[a]	11.33	349.24, 331.23
9	6.71	506.35
10[a]	11.16	395.28, 377.27, 359.26
11	6.76	552.39
12	6.1	582.36
13[a]	8.11	365.23, 347.22, 329.21
14	5.21	522.34
15[a]	7.85	411.27, 393.26, 375.25, 357.24
16	5.43	568.38
17	4.65	598.36

[a]Due to the low ionization efficiencies of the macrolactone substrates and products, ions corresponding to dehydrated species ($[M + H - 18n]^+$, n = 1, 2, or 3) were commonly observed.

Table A.5. TTN results with narbomycin (**5**) as substrate. $(OH)_2$:A:B shows the ratio of dihydroxylated **5** to each of the monohydroxylated products (A and B) as assessed by LC-MS.

P450	Ferredoxin	TTN	$(OH)_2$:A:B
MycCI	MycCII	6.8 ± 0.4	1.4 : 0.8 : 1.0
MycCI (semipure)	MycCII	13.1 ± 0.3	1.4 : 0.6 : 1.0
MycCI (lysate)	MycCII	12.9 ± 0.3	1.8 : 1.0 : 1.0
MycCI	TylHII	1.0 ± 0.1	2.1 : 0.6 : 1.0
$MycCI_{S172A}$	MycCII	2.0 ± 0.1	2.7 : 1.0 : 1.0
MycCI-RhFRED		0.6 ± 0.1	2.2 : 3.3 : 1.0
MycCI-RhFRED (semipure)		1.0 ± 0.1	1.2 : 1.3 : 1.0

Table A.6. TTN results for MycCI-RhFRED (semipure), MycCI (semipure), MycCI (lysate), and MycCI paired with TylHII.

Substrate	MycCI-RhFRED (semipure)	MycCI (semipure) / MycCII	MycCI (lysate) / MycCII	MycCI (pure) / TylHII
5	1.0 ± 0.1	13.1 ± 0.3	12.9 ± 0.3	1.0 ± 0.1
8	40.0 ± 1.0	66.0 ± 0.5	54 ± 2	0.7 ± 0.2
9	389 ± 12	86 ± 3	75 ± 1	1.2 ± 0.1
10	104 ± 2	83 ± 5	82 ± 3	1.7 ± 0.2
11	332 ± 20	99 ± 2	107 ± 8	2.2 ± 0.1
12	271 ± 12	110 ± 6	135 ± 14	1.9 ± 0.3

Table A.7. Parameters for equilibrium substrate binding assays. Data from experiments performed at least in triplicate were fit to Equation 2 or Equation 3. Concentrations of enzyme used for a given substrate are also shown.

	MycCI[a]			TylHI[b]		
Substrate	**[Range] (μM)**	**Equation**	**[E] (μM)**	**[Range] (μM)**	**Equation**	**[E] (μM)**
3	2-1024	2	2	--	--	--
5	0.5-128	2	0.5	--	--	--
8	0.5-128	2	0.5	40-1280	2	5
9	0.01-1.28	3	0.1	40-1280	2	5
10	0.5-128	2	0.5	2-1024	2	4
11	0.01-1.28	3	0.1	2-1024	2	2
12	0.01-1.28	3	0.1	0.5-128	3	0.5

[a]Includes MycCI, $MycCI_{S172A}$, and MycCI-RhFRED.
[b]Includes TylHI and TylHI-RhFRED.

Table A.8. $\Delta A_{max}/[E]$ and percent spin shift values (shown in parentheses) obtained from equilibrium substrate binding assays. Results derive from nonlinear regression analysis of data averaged from experiments performed at least in triplicate.

Substrate	MycCI	MycCI-RhFRED	TylHI	TylHI-RhFRED	$MycCI_{S172A}$
3	0.036[a] (29%)[b]	0.040 (30%)	N.B.[c]	N.B.	0.029 (23%)
5	0.098 (79%)	0.105 (79%)	N.B.	N.B.	0.052 (42%)
8	0.100 (80%)	0.102 (77%)	N.B.	0.031 (23%)	0.092 (74%)
9	0.107 (86%)	0.123 (92%)	0.046 (37%)	0.046 (34%)	0.085 (69%)
10	0.124[d] (100%)	0.133[e] (100%)	0.052 (42%)	0.059 (44%)	0.107 (86%)
11	0.097 (78%)	0.117 (88%)	0.091 (73%)	0.098 (74%)	0.076 (61%)
12	0.086 (69%)	0.106 (80%)	0.116 (93%)	0.126 (94%)	0.057 (46%)

[a]$\Delta A_{max}/[E]$
[b]% spin shift
[c]N.B. = no binding detected.
[d]$(\Delta A_{max}/[E])_{max}$ used to calculate % spin shifts for MycCI, $MycCI_{S172A}$, and TylHI.
[e]$(\Delta A_{max}/[E])_{max}$ used to calculate % spin shifts for MycCI-RhFRED and TylHI-RhFRED.

Table A.9. Values obtained for the variable kinetic parameters after fitting Equation 8 to experimental steady-state kinetic data acquired with MycCI acting in conjunction with MycCII and MBP-FdR on each of the substrates listed.

Substrate	k_{cat1} (min^{-1})	K_{m1} (μM)	k_{cat2} (min^{-1})	K_{m2} (μM)
8	3 ± 2	14 ± 16	0.9 ± 0.1	24 ± 41
9	2.6 ± 0.3	0.9 ± 0.9	1.0 ± 0.4	133 ± 120
10[a]	380 ± 26621	1701 ± 119740	0.86 ± 0.04	0.07 ± 4.68
11	2.8 ± 0.4	0.5 ± 1.0	0.8 ± 0.3	92 ± 76
12	3 ± 2	12 ± 14	0.8 ± 0.4	49 ± 94

[a]The particularly large errors associated with the values for these kinetic constants likely arose from the constraint on the allowable error for the curve fit (0.1%), which was imposed in order to obtain a satisfactory fit with a high R value (0.9927). The same constraint was imposed by default for all other fits, but the errors associated with the values thus obtained were much smaller in comparison.

Table A.10. Steady-state kinetic parameters (NADPH consumption) for MycCI-RhFRED (semipure).

Substrate	k_{cat} (min^{-1})	K_m (μM)	k_{cat}/K_m ($\mu M^{-1}min^{-1}$)
8	3.1 ± 0.2	126 ± 15	0.025 ± 0.003
9	4.5 ± 0.1	0.7 ± 0.2	6 ± 1
10	4.11 ± 0.06	20 ± 1	0.20 ± 0.01
11	5.57 ± 0.07	0.65 ± 0.08	9 ± 1
12	5.09 ± 0.06	0.65 ± 0.07	7.9 ± 0.9

Table A.11. Rates of NADPH consumption under various conditions as monitored by UV-visible spectroscopy. When present, the concentrations of P450, ferredoxin, MBP-FdR, and substrate were 0.5 μM, 10 μM, 1 μM, and 250 μM, respectively. Experiments were carried out in a manner analogous to that described for the P450-RhFRED enzymes.

Substrate[a]	P450	Ferredoxin	MBP-FdR present?	Rate[b]
9	MycCI	MycCII	Yes	4.64
9	MycCI	MycCII	No	0.20
9	MycCI		Yes	3.23
9	MycCI		No	0.14
DMSO	MycCI	MycCII	Yes	4.52
DMSO	MycCI	MycCII	No	0.15
DMSO	MycCI		Yes	3.28
DMSO	MycCI		No	0.15
9		MycCII	Yes	4.60
9		MycCII	No	0.13
9			Yes	3.27
9			No	0.15
DMSO		MycCII	Yes	4.31
DMSO		MycCII	No	0.15
DMSO			Yes	3.15
DMSO			No	0.23
12	TylHI	TylHII	Yes	3.89
12	TylHI	TylHII	No	0.14
12	TylHI		Yes	3.12
12	TylHI		No	0.13
DMSO	TylHI	TylHII	Yes	3.58
DMSO	TylHI	TylHII	No	0.18
DMSO	TylHI		Yes	3.21
DMSO	TylHI		No	0.13
12		TylHII	Yes	3.99
12		TylHII	No	0.18
12			Yes	3.18
12			No	0.12
DMSO		TylHII	Yes	3.87
DMSO		TylHII	No	0.21
DMSO			Yes	3.27
DMSO			No	0.13

[a]DMSO was present at a final concentration of 2.5% in all cases.
[b]Units: μM NADPH min^{-1}

Table A.12. Turnover frequencies (TOFs) for reactions involving MycCI-RhFRED (semipure).

Substrate	TOF[a]
8	0.115 ± 0.005
9	0.76 ± 0.01
10	0.240 ± 0.005
11	0.58 ± 0.01
12	0.45 ± 0.02

[a]TOF = mol product/mol P450 per min

Table A.13. NADPH consumption rates in the presence of 500 μM substrate.[a]

Substrate	MycCI-RhFRED	MycCI-RhFRED (semipure)	TylHI-RhFRED
8	6.1 ± 0.1	4.7 ± 0.3	--
9	10.2 ± 0.3	7.6 ± 0.2	--
10	8.0 ± 0.2	6.3 ± 0.2	--
11	11.45 ± 0.08	8.6 ± 0.2	--
12	10 ± 1	7.9 ± 0.7	14.7 ± 0.6

[a]NADPH consumption rate (min^{-1}) = mol NADPH consumed/mol P450 per min

Table A.14. Coupling efficiencies calculated from TOFs and NADPH consumption rates in the presence of 500 μM substrate.[a]

Substrate	MycCI-RhFRED	MycCI-RhFRED (semipure)	TylHI-RhFRED
8	2.6 ± 0.1	2.4 ± 0.2	--
9	11.7 ± 0.6	10.1 ± 0.3	--
10	4.2 ± 0.2	3.8 ± 0.1	--
11	7.1 ± 0.1	6.8 ± 0.2	--
12	5.9 ± 0.6	5.7 ± 0.6	5.2 ± 0.3

[a]Coupling efficiency (%) = (TOF/NADPH consumption rate) x 100

A.10 Supplemental schemes

Scheme A.1. Conversion of **S1** to **12** under mild acidic conditions.

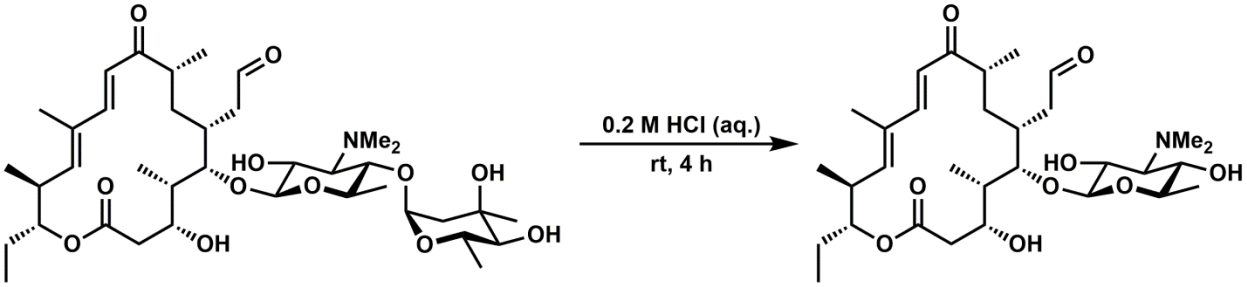

23-deoxy-desmycinosyl-tylosin (S1) **23-DMTL (12)**

A.11 Supplemental figures

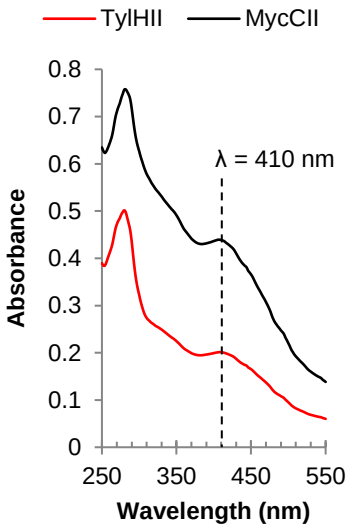

Figure A.1. The UV-visible spectra of TylHII and MycCII.

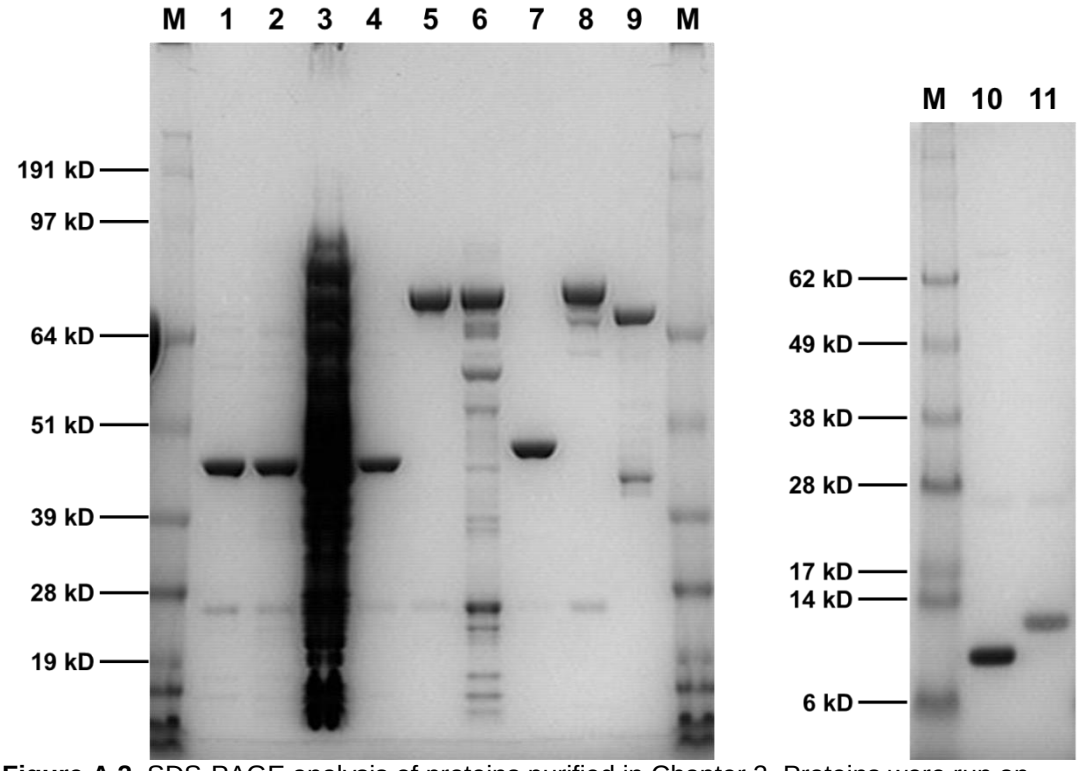

Figure A.2. SDS-PAGE analysis of proteins purified in Chapter 2. Proteins were run on NuPAGE Novex 4-12% Bis-Tris gels (Invitrogen) using MOPS (samples 1-9) or MES (samples 10 and 11) running buffer and subsequently stained with Coomassie Brilliant Blue R-250 dye. Lanes: M (protein MW marker); 1 (MycCI, pure); 2 (MycCI, semipure); 3 (MycCI, lysate); 4 ($MycCI_{S172A}$); 5 (MycCI-RhFRED, pure); 6 (MycCI-RhFRED, semipure); 7 (TylHI); 8 (TylHI-RhFRED); 9 (MBP-FdR); 10 (MycCII); 11 (TylHII).

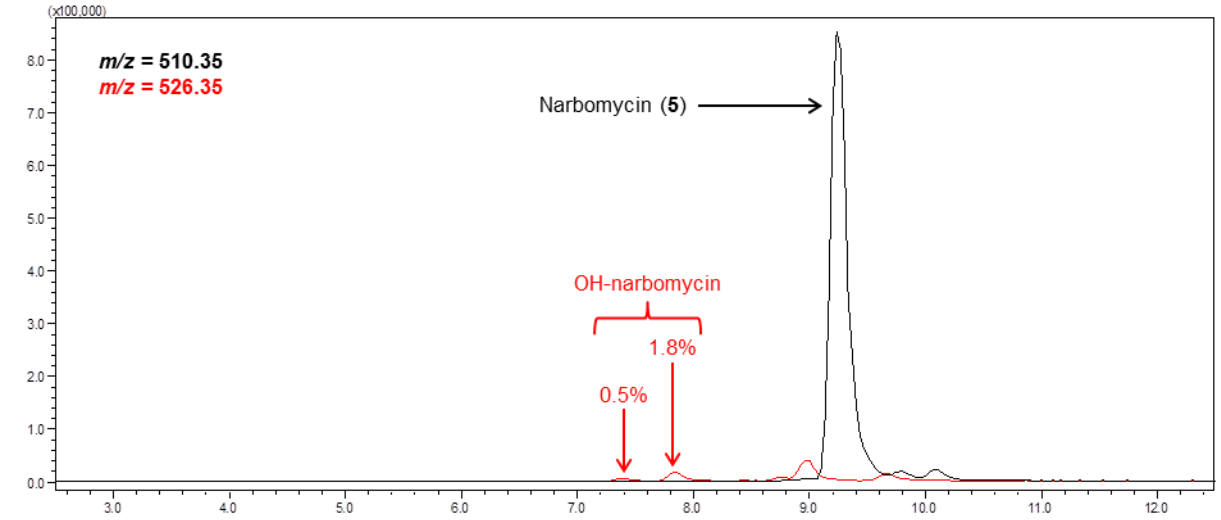

Figure A.3. LC-MS analysis of the large-scale enzymatic reaction between MycCI and narbomycin (**5**) (crude extract). Selected-ion monitoring chromatograms for substrate (black) and products (red) are shown.

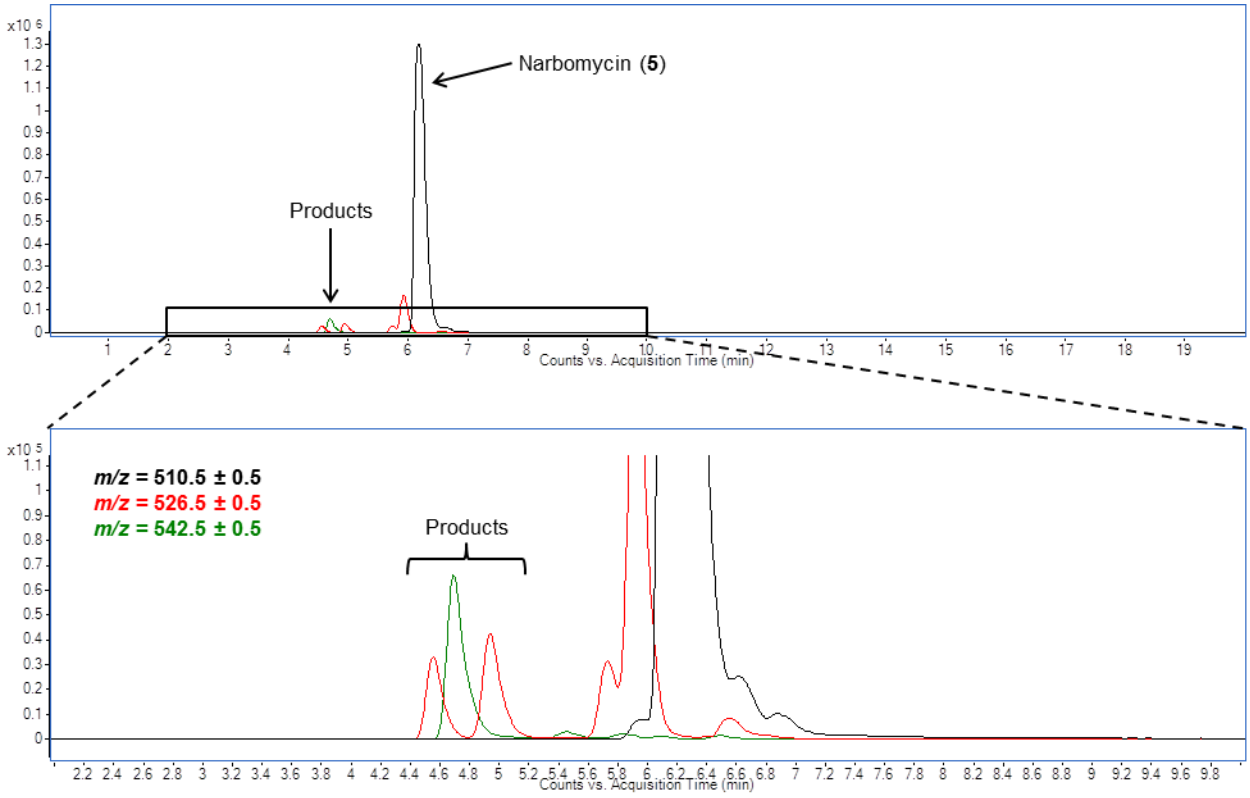

Figure A.4. LC-MS analysis of the analytical-scale enzymatic reaction between MycCI and narbomycin (**5**). Extracted ion chromatograms for substrate (black) and products (red, monohydroxylated; green, dihydroxylated) are shown.

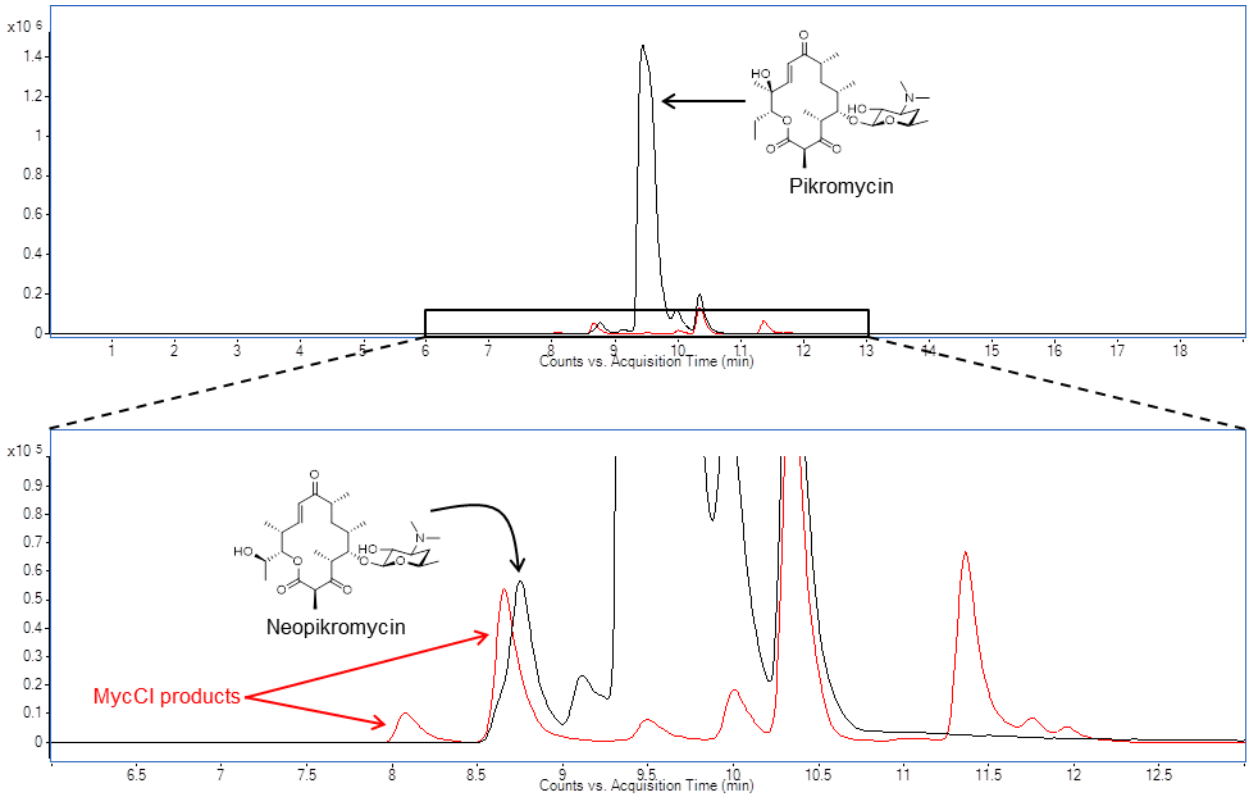

Figure A.5. LC-MS comparison of products from reactions of PikC and MycCI with narbomycin (**5**). Extracted ion chromatograms corresponding to *m/z* = 526.5 ± 0.5 are shown for reactions involving PikC (black trace) and MycCI (red trace).

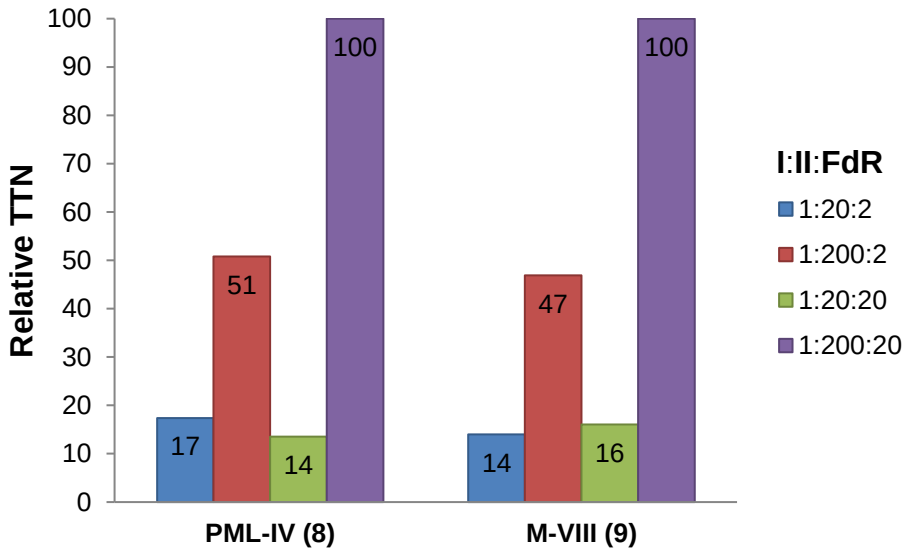

Figure A.6. Activity of MycCI (**I**) as a function of redox partner MycCII (**II**) and MBP-FdR (**FdR**) concentrations. In these assays, [MycCI (semipure)] = 0.5 μM. The results of experiments using different molar ratios of **I**:**II**:**FdR** are depicted for substrates **8** and **9**.

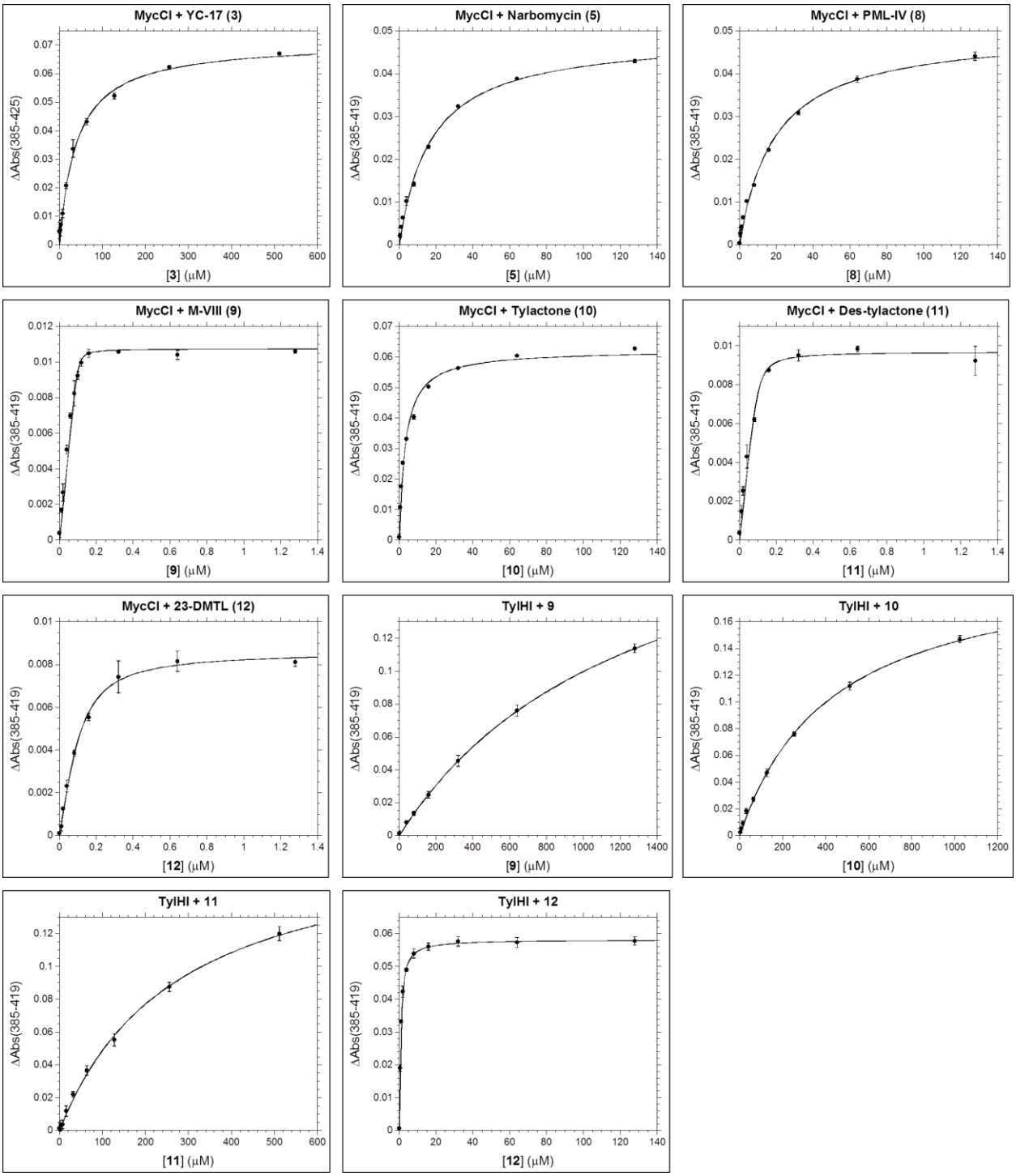

Figure A.7. Plots of substrate-induced heme iron spin shift vs substrate concentration for MycCI and TylHI. Data averaged from experiments performed at least in triplicate (dots/error bars) were fit to either Equation 2 or Equation 3 (solid line).

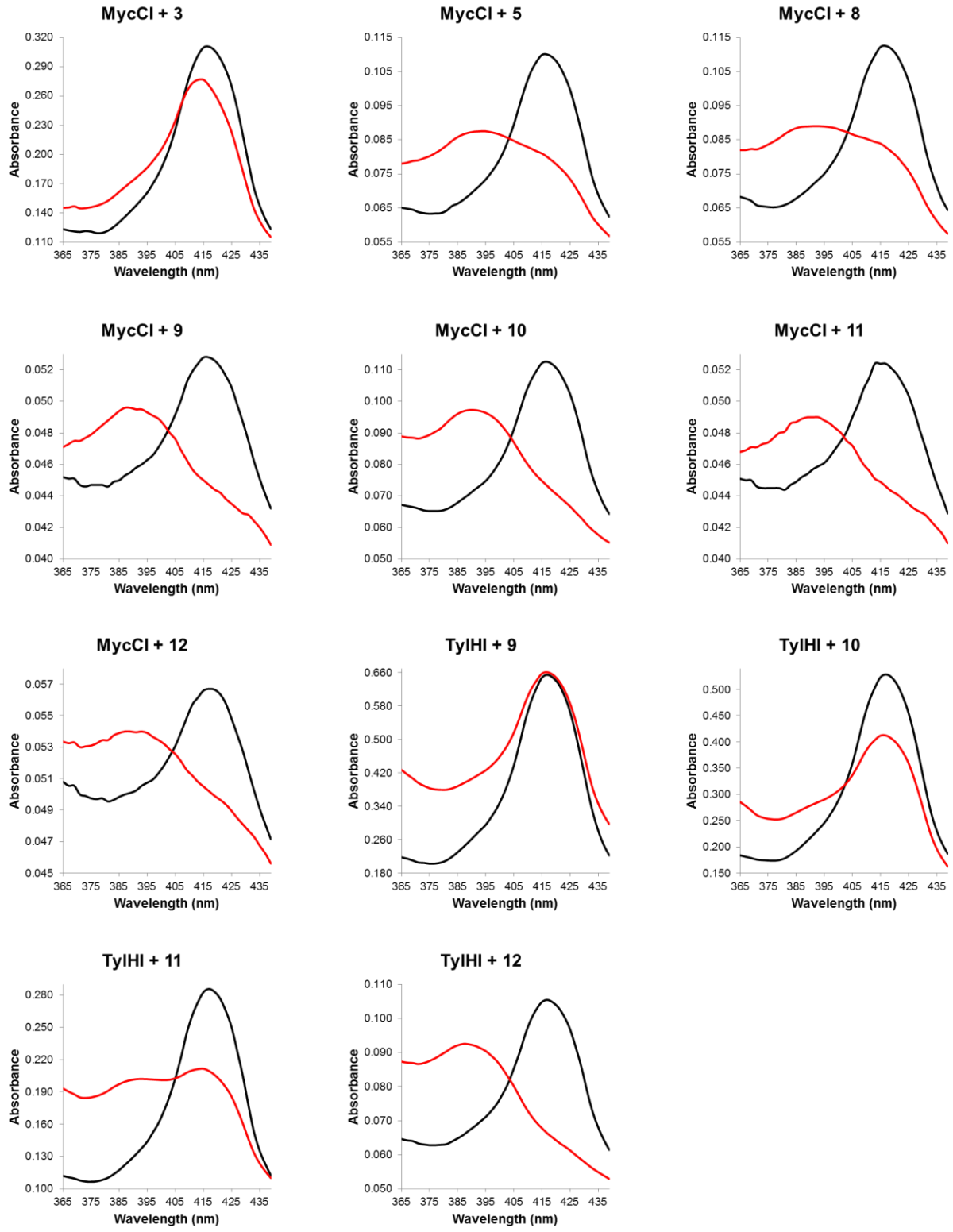

Figure A.8. Absolute UV-visible spectra of MycCI and TylHI in the absence (black traces) or presence (red traces) of different substrates. Enzyme concentrations are as listed in **Table A.7**. Substrate concentrations are as follows: MycCI + **3** (512 μM), **5**/**8**/**10** (128 μM), **9**/**11**/**12** (1.28 μM); TylHI + **9** (1280 μM), **10** (1024 μM), **11** (512 μM), **12** (128 μM).

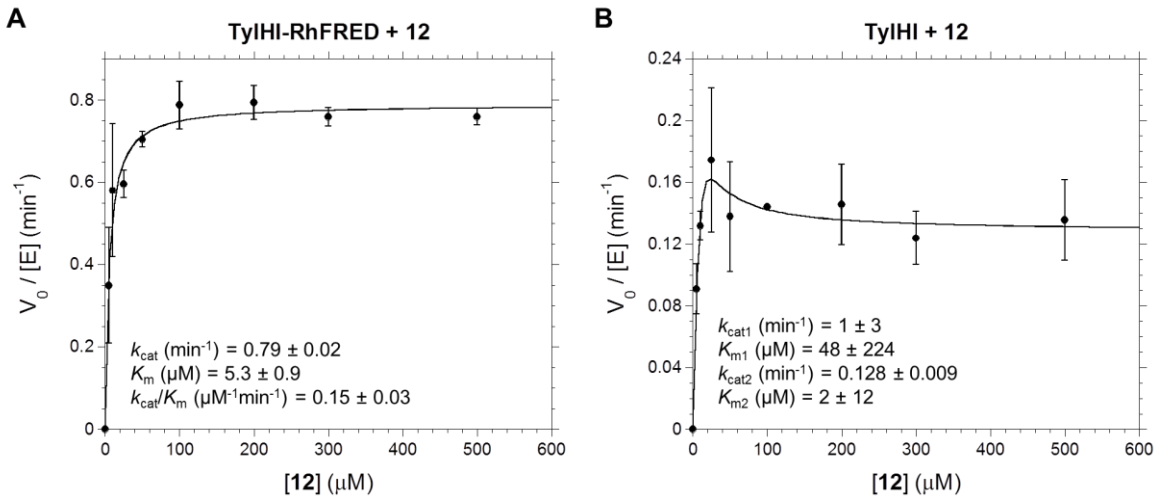

Figure A.9. Steady-state kinetics results (formation of **17** from **12**) for (**A**) TylHI-RhFRED and (**B**) TylHI acting in conjunction with TylHII and MBP-FdR.

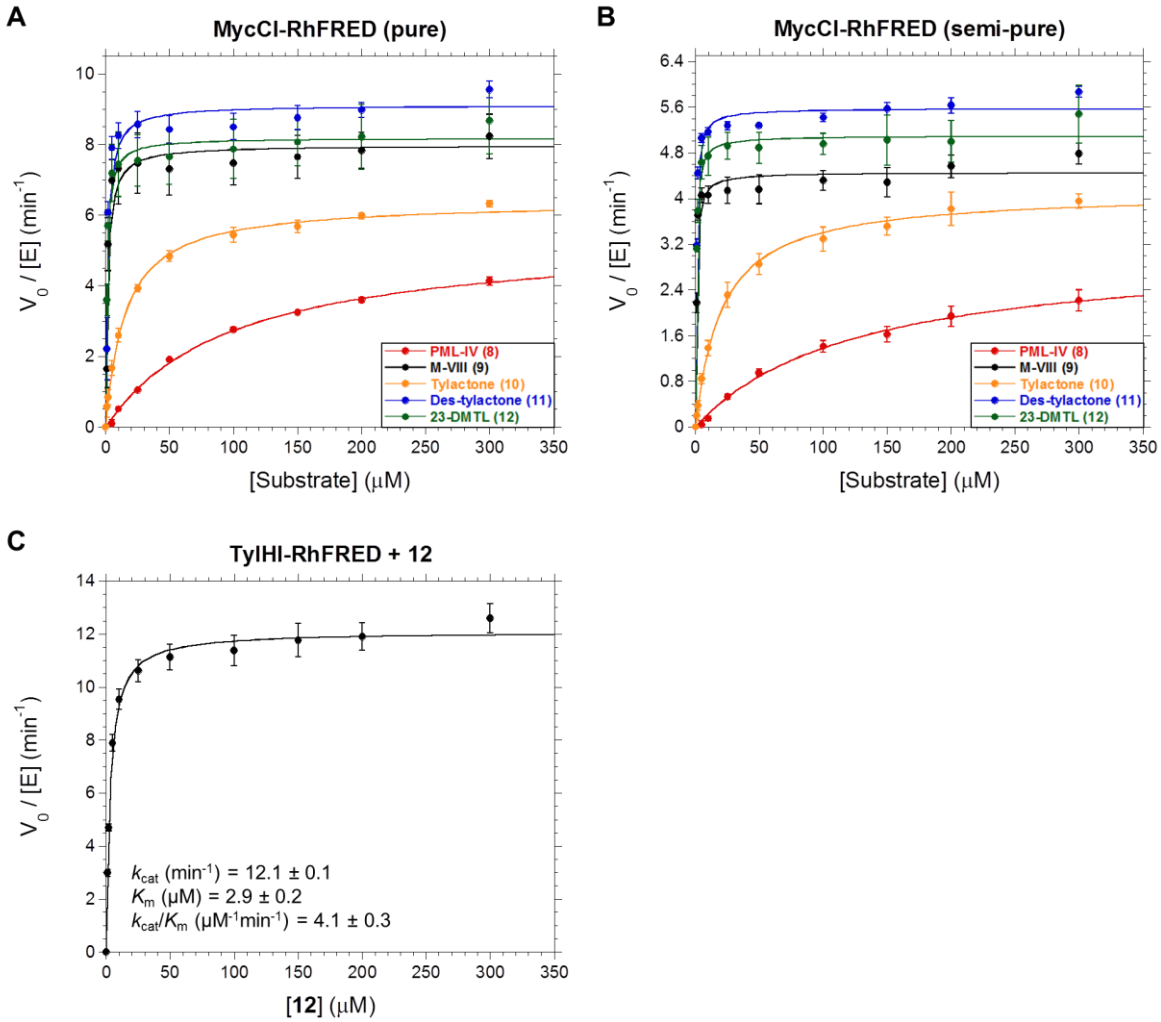

Figure A.10. Steady-state kinetic profiles (NADPH consumption) for (**A**) MycCI-RhFRED (pure), (**B**) MycCI-RhFRED (semipure), and (**C**) TylHI-RhFRED.

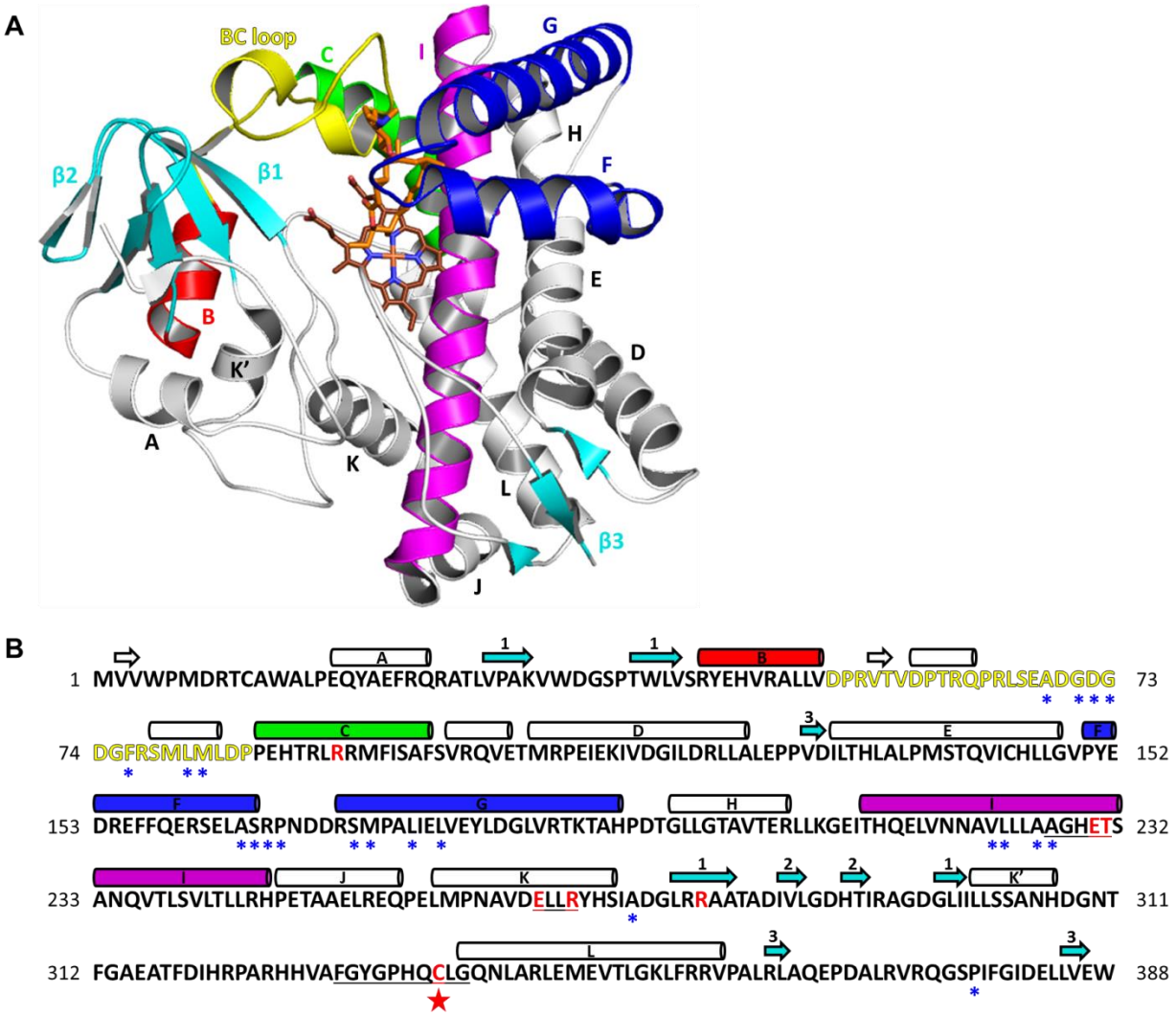

Figure A.11. (**A**) Overall structure of MycCI. The heme cofactor is shown in brown and bound M-VIII (**9**) is shown in orange. Helices are labeled A-L, and β-sheet regions are shown in cyan and labeled accordingly. (**B**) MycCI primary sequence. Helices and β-strands are labeled and colored as in **A**. Key conserved motifs are underlined, and highly conserved residues involved in catalysis and heme binding are highlighted in red. A red star is located below the absolutely conserved cysteine involved in heme ligation. Blue asterisks are shown below residues located within 4 Å of bound **9**.

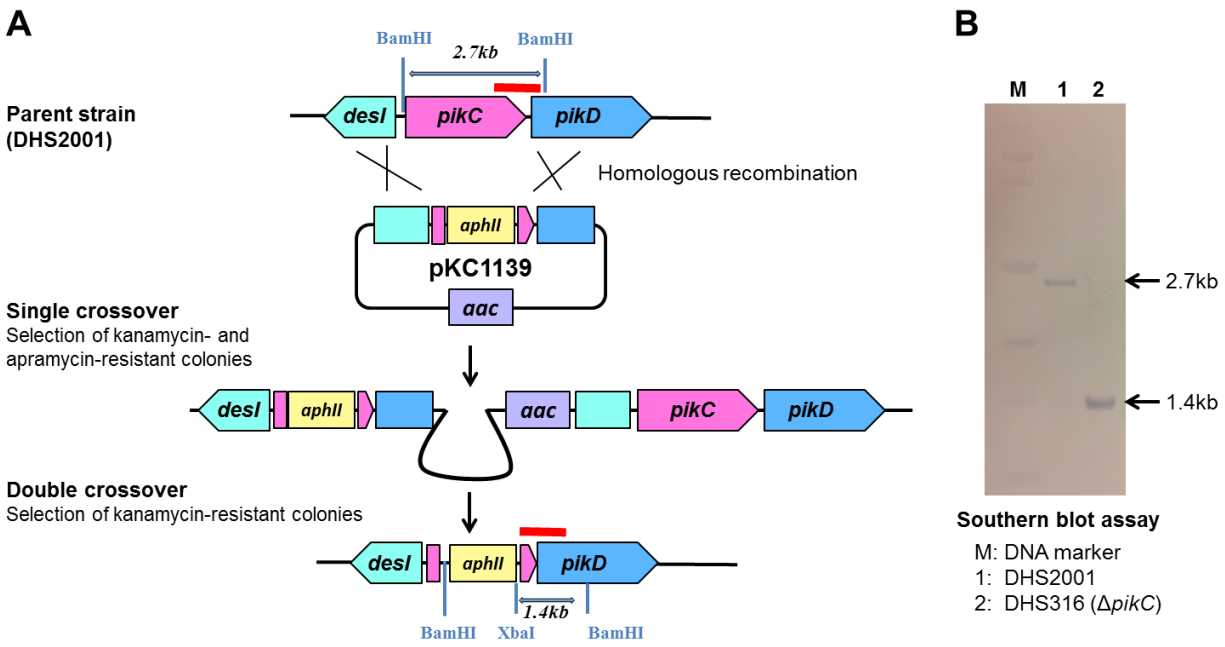

Figure A.12. Replacement of the *pikC* gene with a kanamycin-resistance gene in *Streptomyces venezuelae* by homologous recombination. (**A**) A single crossover between pSRP65 and a homologous region in the genome of *S. venezuelae* DHS2001 resulted in a pSRP65-integrated single crossover strain. A subsequent second crossover event afforded the Δ*pikC* strain designated DHS316. (**B**) Confirmation of the genotype of DHS316 by Southern blot analysis. Abbreviations: *aphII*, kanamycin resistance gene; *aac*, apramycin resistance gene.

A.12 HRMS and NMR data for compounds 8–17

Position	δ_C (ppm)	δ_H (ppm), multi (*J* in Hz)
1	168.3	
2	122.5	5.89, dd (15.5, 0.7)
3	153.3	6.56, dd (15.5, 9.9)
4	41.6	2.55, tq (10.4, 6.8)
5	80.7	3.19, dd (10.5, 1.5)
6	35.4	1.15, m
7	32.7	1.44, ddd (13.9, 12.4, 4.3)
		1.62, ddd (14.0, 12.2, 3.2)
8	46.4	2.49, dqd (13.7, 7.1, 4.9)
9	206.4	
10	124.6	6.45, d (15.0)
11	143.6	7.04, ddd (15.1, 11.1, 0.8)
12	133.2	6.21, dd (15.2, 11.1)
13	146.8	5.74, dd (15.2, 9.4)
14	44.6	2.34, tq (9.6, 6.7)
15	79.0	4.60, td (9.6, 2.6)
16	25.7	1.54, ddq (14.5, 9.3, 7.3)
		1.87, dqd (14.9, 7.5, 2.7)
17	10.1	0.93, t (7.4)
18	19.9	1.09, d (6.6)
19	17.8	0.96, d (6.8)
20	17.9	1.19, d (6.9)
21	15.9	1.10, d (6.6)

*Solvent: CD_3OD

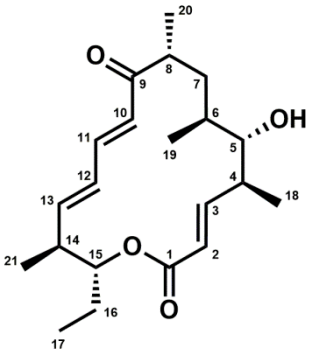

PML-IV (8)

HRMS: *m/z* calculated $[M + H]^+$ 349.2373, found 349.2374

Position	δ_C (ppm)	δ_H (ppm), multi (*J* in Hz)
1	168.3	
2	122.4	5.88, d (15.5)
3	153.3	6.59, dd (15.5, 9.9)
4	42.3	2.79, tq (9.9, 6.7)
5	88.1	3.35, dd (10.4, 1.3)
6	35.5	1.21, m
7	33.7	1.57, m
		1.69, ddd (15.0, 12.2, 3.5)
8	46.3	2.50, m
9	206.6	
10	124.7	6.43, d (15.0)
11	143.6	7.04, dd (15.0, 11.1)
12	133.1	6.21, dd (15.2, 11.1)
13	146.9	5.74, dd (15.1, 9.3)
14	44.6	2.36, m
15	79.1	4.61, td (9.6, 2.7)
16	25.7	1.54, m
		1.87, dqd (14.8, 7.4, 2.6)
17	10.1	0.93, t (7.3)
18	20.0	1.21, d (5.5)
19	17.9	0.98, d (6.8)
20	18.0	1.17, d (6.9)
21	15.9	1.10, d (6.7)
1'	106.1	4.25, d (7.3)
2'	72.2	3.27, dd (10.2, 7.3)
3'	65.9	2.61, ddd (12.2, 10.2, 4.2)
4'	31.9	1.25, m
		1.74, ddd (12.6, 4.3, 2.0)
5'	70.1	3.52, m
6'	21.4	1.20, d (4.8)
7'	40.9	2.33, s

*Solvent: CD_3OD

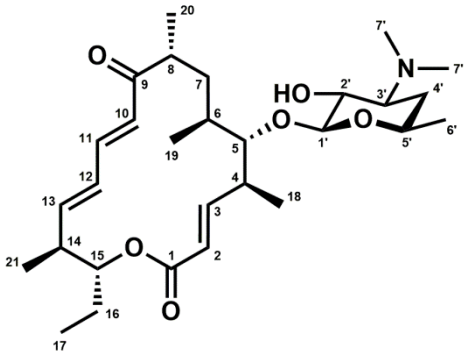

M-VIII (9)

HRMS: *m/z* calculated $[M + H]^+$ 506.3476, found 506.3478

Position	δ_C (ppm)	δ_H (ppm), multi (*J* in Hz)
1	175.3	
2	40.7	2.02, dd (17.2, 1.1)
		2.49, dd (17.2, 10.5)
3	67.7	3.70, d (10.7)
4	41.4	1.51, dtd (16.9, 6.6, 2.5)
5	73.2	3.62, d (10.3)
6	39.7	1.15, m
7	33.9	1.39, ddd (15.0, 11.5, 3.8)
		1.67, ddd (14.2, 12.4, 1.7)
8	46.6	2.63, m
9	206.8	
10	119.7	6.48, d (15.4)
11	149.7	7.25, d (15.4)
12	135.0	
13	147.7	5.67, d (10.4)
14	40.1	2.80, tq (10.2, 6.5)
15	80.0	4.69, td (9.6, 2.6)
16	25.7	1.59, m
		1.88, m
17	10.1	0.94, t (7.3)
18	9.9	0.96, d (6.8)
19	23.8	1.34, m
		1.55, m
20	12.2	0.89, t (7.4)
21	18.0	1.23, d (7.0)
22	13.1	1.85, d (1.2)
23	16.3	1.09, d (6.5)

*Solvent: CD_3OD

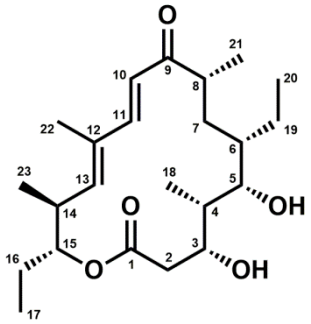

Tylactone (10)

HRMS: *m/z* calculated $[M + H]^+$ 395.2792, found 395.2794

Position	δ_C (ppm)	δ_H (ppm), multi (*J* in Hz)
1	175.1	
2	41.2	2.05, dd (17.4, 1.3)
		2.49, dd (17.4, 9.8)
3	68.4	3.73, d (9.9)
4	42.4	1.69, m
5	80.0	3.76, d (9.6)
6	40.0	1.12, m
7	34.9	1.47, ddd (15.1, 11.6, 4.4)
		1.74, m
8	46.5	2.65, m
9	207.0	
10	119.9	6.46, d (15.5)
11	149.6	7.24, d (15.5)
12	135.0	
13	147.7	5.67, d (10.5)
14	40.0	2.79, tq (10.4, 6.6)
15	80.0	4.69, td (9.5, 2.6)
16	25.7	1.58, ddq (14.6, 9.2, 7.4)
		1.88, m
17	10.1	0.94, t (7.3)
18	9.7	1.05, d (6.9)
19	22.2	1.41, m
		1.63, m
20	12.6	0.85, t (7.2)
21	17.9	1.21, d (4.4)
22	13.1	1.85, d (1.2)
23	16.4	1.08, d (6.5)
1'	105.5	4.22, d (7.3)
2'	72.3	3.24, dd (10.3, 7.3)
3'	65.9	2.62, ddd (12.2, 10.2, 4.2)
4'	32.0	1.24, m
		1.72, m
5'	70.0	3.52, m
6'	21.4	1.20, d (3.7)
7'	40.9	2.33, s

*Solvent: CD_3OD

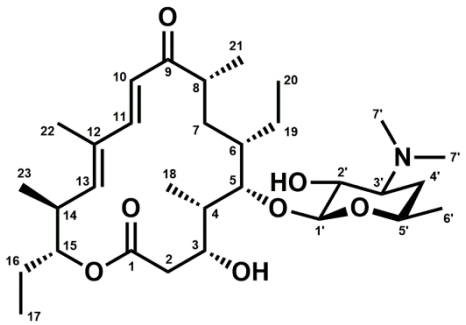

Des-tylactone (11)

HRMS: *m/z* calculated $[M + H]^+$ 552.3895, found 552.3895

Position	δ_C (ppm)	δ_H (ppm), multi (*J* in Hz)
1	174.2	
2	39.6	1.93, dd (16.6, 0.9)
		2.50, m
3	67.4	3.83, d (9.9)
4	40.5	1.65, m
5	81.2	3.72, d (9.0)
6	32.8	2.14, m
7	32.8	1.48, m
		1.65, m
8	44.9	2.59, m
9	203.3	
10	118.5	6.26, d (15.5)
11	148.3	7.28, d (15.6)
12	133.5	
13	146.1	5.65, d (10.4)
14	39.0	2.71, tq (10.2, 6.5)
15	78.9	4.71, td (9.6, 2.6)
16	24.9	1.54, ddq (14.5, 9.2, 7.2)
		1.83, m
17	9.8	0.92, t (7.3)
18	9.2	1.00, d (6.8)
19	43.9	2.40, m
		2.93, ddd (17.9, 9.7, 1.7)
20	203.1	9.69, s
21	17.6	1.21, d (6.9)
22	13.1	1.78, d (1.3)
23	16.4	1.07, d (6.6)
1'	104.1	4.25, d (7.4)
2'	71.2	3.48, dd (10.4, 7.4)
3'	70.2	2.37, t (10.2)
4'	70.9	3.05, t (9.4)
5'	73.5	3.26, m
6'	18.0	1.26, d (6.1)
7'	41.8	2.50, s

*Solvent: $CDCl_3$

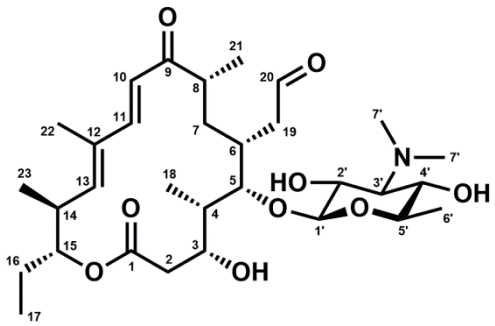

23-DMTL (12)

HRMS: *m/z* calculated $[M + H]^+$ 582.3637, found 582.3641

Position	δ_C (ppm)	δ_H (ppm), multi (*J* in Hz)
1	168.2	
2	122.4	5.91, d (15.5)
3	153.4	6.56, dd (15.5, 10.0)
4	41.7	2.55, tq (10.7, 6.9)
5	80.7	3.20, dd (10.4, 1.5)
6	35.5	1.15, m
7	32.7	1.44, ddd (13.9, 12.5, 4.3)
		1.63, ddd (13.9, 12.2, 3.4)
8	46.4	2.50, dqd (13.7, 7.1, 4.9)
9	206.4	
10	124.6	6.46, d (15.0)
11	143.6	7.08, dd (15.0, 11.1)
12	134.6	6.26, dd (15.3, 11.0)
13	143.3	6.03, dd (15.3, 9.4)
14	52.7	2.41, tt (9.6, 4.7)
15	75.4	4.88, td (9.6, 2.6)
16	26.1	1.58, m
		1.89, dqd (14.8, 7.4, 2.7)
17	10.1	0.94, t (7.4)
18	19.8	1.09, d (6.7)
19	17.8	0.96, d (6.9)
20	18.0	1.19, d (6.9)
21	62.0	3.70, d (4.7)

*Solvent: CD_3OD

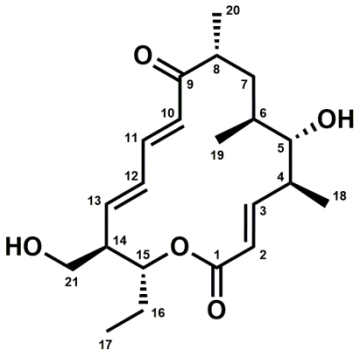

ML-IV (13)

HRMS: *m/z* calculated $[M + H]^+$ 365.2323, found 365.2325

Position	δ_C (ppm)	δ_H (ppm), multi (*J* in Hz)
1	168.2	
2	122.4	5.89, d (15.5)
3	153.4	6.59, dd (15.5, 9.9)
4	42.3	2.80, tq (9.6, 6.7)
5	88.1	3.35, d (10.3)
6	35.5	1.22, m
7	33.7	1.56, m
		1.69, ddd (14.9, 12.0, 3.4)
8	46.3	2.50, m
9	206.7	
10	124.8	6.44, d (15.0)
11	143.6	7.08, dd (15.0, 11.0)
12	134.6	6.27, dd (15.3, 11.0)
13	143.4	6.04, dd (15.3, 9.4)
14	52.6	2.42, tt (9.6, 4.7)
15	75.6	4.88, td (9.6, 2.7)
16	26.1	1.58, m
		1.89, dqd (14.4, 7.3, 2.6)
17	10.1	0.94, t (7.3)
18	20.0	1.22, d (4.6)
19	17.9	0.98, d (6.9)
20	18.0	1.17, d (6.9)
21	62.0	3.70, d (4.8)
1'	106.1	4.26, d (7.3)
2'	72.2	3.27, dd (10.2, 7.3)
3'	65.9	2.63, ddd (12.2, 10.2, 4.2)
4'	31.9	1.25, m
		1.74, ddd (12.5, 3.9, 1.7)
5'	70.1	3.53, m
6'	21.4	1.21, d (4.0)
7'	40.8	2.34, s

*Solvent: CD_3OD

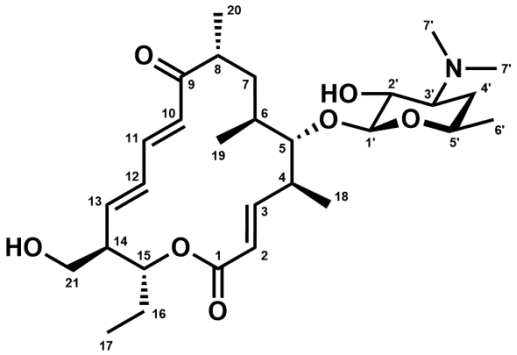

M-VII (14)

HRMS: *m/z* calculated $[M + H]^+$ 522.3425, found 522.3428

Position	δ_C (ppm)	δ_H (ppm), multi (*J* in Hz)
1	175.2	
2	40.7	2.03, dd (17.2, 1.1)
		2.50, dd (17.2, 10.5)
3	67.8	3.71, d (10.2)
4	41.5	1.52, dtd (17.1, 6.6, 2.3)
5	73.2	3.62, d (10.3)
6	39.7	1.16, m
7	33.9	1.39, ddd (15.1, 11.7, 3.7)
		1.68, ddd (14.2, 12.4, 1.7)
8	46.6	2.64, m
9	206.9	
10	119.7	6.49, d (15.4)
11	149.6	7.29, d (15.5)
12	136.7	
13	144.2	5.93, d (10.6)
14	48.4	2.87, tt (10.2, 4.8)
15	76.3	4.95, td (9.7, 2.6)
16	26.2	1.63, m
		1.90, m
17	10.1	0.95, t (7.3)
18	9.9	0.96, d (6.8)
19	23.8	1.35, m
		1.56, m
20	12.2	0.90, t (7.4)
21	18.0	1.23, d (6.9)
22	13.3	1.87, d (1.3)
23	62.6	3.68, d (1.2)
		3.69, d (2.5)

*Solvent: CD_3OD

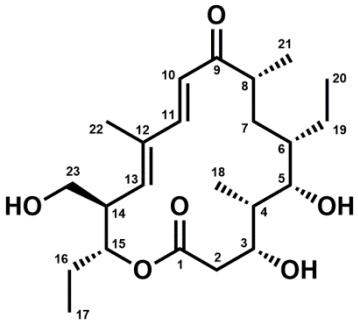

OH-tylactone (15)

HRMS: *m/z* calculated $[M + H]^+$ 411.2741, found 411.2743

Position	δ_C (ppm)	δ_H (ppm), multi (*J* in Hz)
1	174.9	
2	41.2	2.05, dd (17.3, 1.2)
		2.49, dd (17.3, 9.8)
3	68.3	3.74, d (9.9)
4	42.4	1.71, m
5	80.0	3.76, d (9.6)
6	40.8	1.15, m
7	34.9	1.47, ddd (15.1, 11.4, 4.5)
		1.74, m
8	46.4	2.66, m
9	207.0	
10	119.9	6.46, d (15.4)
11	149.6	7.28, d (15.5)
12	136.6	
13	144.1	5.92, d (10.5)
14	48.3	2.86, tt (10.2, 4.8)
15	76.4	4.96, td (9.6, 2.7)
16	26.2	1.63, ddq (14.3, 9.2, 7.0)
		1.90, m
17	10.1	0.95, t (7.3)
18	9.7	1.05, d (6.9)
19	22.2	1.41, m
		1.64, m
20	12.6	0.86, t (7.3)
21	17.9	1.21, d (6.4)
22	13.2	1.87, d (1.2)
23	62.6	3.68, d (1.4)
		3.68, d (2.6)
1'	105.5	4.23, d (7.3)
2'	72.2	3.26, dd (10.3, 7.3)
3'	66.0	2.69, ddd (12.4, 10.0, 4.2)
4'	32.0	1.27, m
		1.76, m
5'	70.0	3.53, m
6'	21.4	1.21, d (6.4)
7'	40.8	2.38, s

*Solvent: CD_3OD

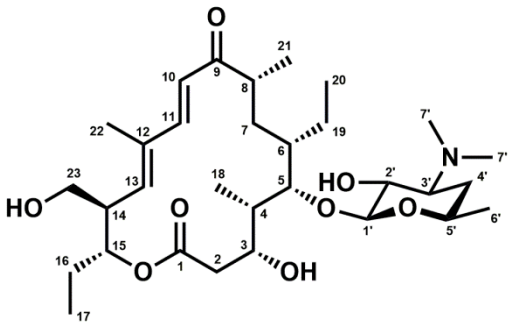

OH-des-tylactone (16)

HRMS: *m/z* calculated $[M + H]^+$ 568.3844, found 568.3846

Position	δ_C (ppm)	δ_H (ppm), multi (*J* in Hz)
1	174.1	
2	39.6	1.95, dd (16.6, 0.9)
		2.52, m
3	67.6	3.84, d (10.1)
4	40.5	1.64, m
5	81.3	3.74, m
6	32.8	2.14, m
7	32.8	1.48, m
		1.64, m
8	44.6	2.62, m
9	203.4	
10	119.2	6.29, d (15.6)
11	147.8	7.31, d (15.4)
12	136.5	
13	141.4	5.84, d (10.6)
14	47.4	2.89, m
15	75.1	4.95, td (9.6, 2.7)
16	25.8	1.61, m
		1.85, m
17	9.9	0.94, t (7.3)
18	9.2	1.01, d (6.8)
19	43.9	2.40, m
		2.94, m
20	203.0	9.69, s
21	17.5	1.22, d (6.8)
22	13.3	1.83, d (1.2)
23	62.8	3.74, m
1'	104.1	4.26, d (7.3)
2'	71.1	3.49, dd (10.4, 7.3)
3'	70.4	2.40, t (10.2)
4'	70.8	3.07, t (9.4)
5'	73.5	3.28, m
6'	18.0	1.27, d (6.1)
7'	41.8	2.52, s

*Solvent: $CDCl_3$

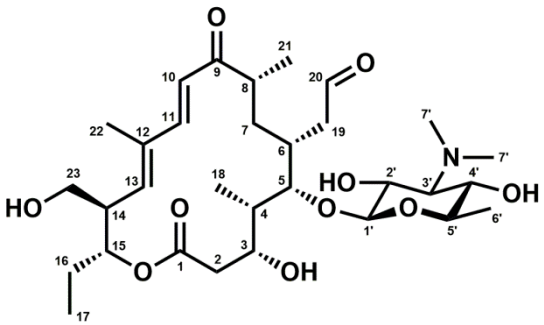

MTL (17)

HRMS: *m/z* calculated $[M + H]^+$ 598.3586, found 598.3590

A.13 References

(1) Inoue, H., Nojima, H., and Okayama, H. (1990) High efficiency transformation of *Escherichia coli* with plasmids. *Gene 96*, 23–28.

(2) Anzai, Y., Li, S., Chaulagain, M. R., Kinoshita, K., Kato, F., Montgomery, J., and Sherman, D. H. (2008) Functional analysis of MycCI and MycG, cytochrome P450 enzymes involved in biosynthesis of mycinamicin macrolide antibiotics. *Chem. Biol. 15*, 950–959.

(3) Li, S., Podust, L. M., and Sherman, D. H. (2007) Engineering and analysis of a self-sufficient biosynthetic cytochrome P450 PikC fused to the RhFRED reductase domain. *J. Am. Chem. Soc. 129*, 12940–12941.

(4) Fouces, R., Mellado, E., Díez, B., and Barredo, J. L. (1999) The tylosin biosynthetic cluster from *Streptomyces fradiae*: genetic organization of the left region. *Microbiology 145*, 855–868.

(5) Bate, N., and Cundliffe, E. (1999) The mycinose-biosynthetic genes of *Streptomyces fradiae*, producer of tylosin. *J. Ind. Microbiol. Biotechnol. 23*, 118–122.

(6) Omura, T., and Sato, R. (1964) The carbon monoxide-binding pigment of liver microsomes: I. Evidence for its hemoprotein nature. *J. Biol. Chem. 239*, 2370–2378.

(7) Hasumi, H., and Nakamura, S. (1978) Studies on the ferredoxin–ferredoxin-NADP reductase complex: kinetic and solvent perturbation studies on the location of sulfhydryl and aromatic amino acid residues. *J. Biochem. 84*, 707–717.

(8) Leslie, A. G. W. (1992) Recent changes to the MOSFLM package for processing film and image plate data. *Joint CCP4 ESF-EAMCB Newslett. Protein Crystallogr. 26*.

(9) Holton, J., and Alber, T. (2004) Automated protein crystal structure determination using ELVES. *Proc. Natl. Acad. Sci. U.S.A. 101*, 1537–1542.

(10) Hayashi, K., Sugimoto, H., Shinkyo, R., Yamada, M., Ikeda, S., Ikushiro, S., Kamakura, M., Shiro, Y., and Sakaki, T. (2008) Structure-based design of a highly active vitamin D hydroxylase from *Streptomyces griseolus* CYP105A1. *Biochemistry 47*, 11964–11972.

(11) Keegan, R. M., and Winn, M. D. (2007) Automated search-model discovery and preparation for structure solution by molecular replacement. *Acta Crystallogr. D Biol. Crystallogr. 63*, 447–457.

(12) Keegan, R. M., and Winn, M. D. (2008) MrBUMP: an automated pipeline for molecular replacement. *Acta Crystallogr. D Biol. Crystallogr. 64*, 119–124.

(13) (1994) Collaborative Computational Project, Number 4. *Acta Crysallogr. D 50*, 760–763.

(14) Cowtan, K. (2006) The Buccaneer software for automated model building. 1. Tracing protein chains. *Acta Crystallogr. D Biol.. Crystallogr. 62*, 1002–1011.

(15) Emsley, P., and Cowtan, K. (2004) Coot: model-building tools for molecular graphics. *Acta Crystallogr. D Biol. Crystallogr. 60*, 2126–2132.

(16) Murshudov, G. N., Vagin, A. A., and Dodson, E. J. (1997) Refinement of macromolecular structures by the maximum-likelihood method. *Acta Crystallogr. D Biol. Crystallogr. 53*, 240–255.

(17) Baltz, R. H., and Seno, E. T. (1981) Properties of *Streptomyces fradiae* mutants blocked in biosynthesis of the macrolide antibiotic tylosin. *Antimicrob. Agents Chemother. 20*, 214–225.

(18) Hansen, D. A., Koch, A. A., and Sherman, D. H. (2015) Substrate controlled divergence in polyketide synthase catalysis. *J. Am. Chem. Soc. 137*, 3735–3738.

(19) Bierman, M., Logan, R., O'Brien, K., Seno, E. T., Rao, R. N., and Schoner, B. E. (1992) Plasmid cloning vectors for the conjugal transfer of DNA from *Escherichia coli* to *Streptomyces* spp. *Gene 116*, 43–49.

(20) Jung, W. S., Jeong, S. J., Park, S. R., Choi, C. Y., Park, B. C., Park, J. W., and Yoon, Y. J. (2008) Enhanced heterologous production of desosaminyl macrolides and their hydroxylated derivatives by overexpression of the *pikD* regulatory gene in *Streptomyces venezuelae*. *Appl. Environ. Microbiol. 74*, 1972–1979.

(21) Jung, W. S., Lee, S. K., Hong, J. S. J., Park, S. R., Jeong, S. J., Han, A. R., Sohng, J. K., Kim, B. G., Choi, C. Y., Sherman, D. H., and Yoon, Y. J. (2006) Heterologous expression of tylosin polyketide synthase and production of a hybrid bioactive macrolide in *Streptomyces venezuelae*. *Appl. Microbiol. Biotechnol. 72*, 763–769.

(22) Yoon, Y. J., Beck, B. J., Kim, B. S., Kang, H.-Y., Reynolds, K. A., and Sherman, D. H. (2002) Generation of multiple bioactive macrolides by hybrid modular polyketide synthases in *Streptomyces venezuelae*. *Chem. Biol. 9*, 203–214.

(23) Hansen, D. A., Rath, C. M., Eisman, E. B., Narayan, A. R. H., Kittendorf, J. D., Mortison, J. D., Yoon,

Y. J., and Sherman, D. H. (2013) Biocatalytic synthesis of pikromycin, methymycin, neomethymycin, novamethymycin, and ketomethymycin. *J. Am. Chem. Soc. 135*, 11232–11238.
(24) Negretti, S., Narayan, A. R. H., Chiou, K. C., Kells, P. M., Stachowski, J. L., Hansen, D. A., Podust, L. M., Montgomery, J., and Sherman, D. H. (2014) Directing group-controlled regioselectivity in an enzymatic C–H bond oxygenation. *J. Am. Chem. Soc. 136*, 4901–4904.
(25) Narayan, A. R. H., Jiménez-Osés, G., Liu, P., Negretti, S., Zhao, W., Gilbert, M. M., Ramabhadran, R. O., Yang, Y.-F., Furan, L. R., Li, Z., Podust, L. M., Montgomery, J., Houk, K. N., and Sherman, D. H. (2015) Enzymatic hydroxylation of an unactivated methylene C–H bond guided by molecular dynamics simulations. *Nat. Chem. 7*, 653–660.
(26) Li, S., Chaulagain, M. R., Knauff, A. R., Podust, L. M., Montgomery, J., and Sherman, D. H. (2009) Selective oxidation of carbolide C–H bonds by an engineered macrolide P450 mono-oxygenase. *Proc. Natl. Acad. Sci. U.S.A. 106*, 18463–18468.
(27) Korzekwa, K. R., Krishnamachary, N., Shou, M., Ogai, A., Parise, R. A., Rettie, A. E., Gonzalez, F. J., and Tracy, T. S. (1998) Evaluation of atypical cytochrome P450 kinetics with two-substrate models: evidence that multiple substrates can simultaneously bind to cytochrome P450 active sites. *Biochemistry 37*, 4137–4147.
(28) Lin, Y., Lu, P., Tang, C., Mei, Q., Sandig, G., Rodrigues, A. D., Rushmore, T. H., and Shou, M. (2001) Substrate inhibition kinetics for cytochrome P450-catalyzed reactions. *Drug Metab. Dispos. 29*, 368–374.
(29) Davydov, D. R., and Halpert, J. R. (2008) Allosteric P450 mechanisms: multiple binding sites, multiple conformers, or both? *Expert Opin. Drug Metab. Toxicol. 4*, 1523–1535.
(30) Cupp-Vickery, J., Anderson, R., and Hatziris, Z. (2000) Crystal structures of ligand complexes of P450eryF exhibiting homotropic cooperativity. *Proc. Natl. Acad. Sci. USA 97*, 3050–3055.
(31) Hutzler, J. M., and Tracy, T. S. (2002) Atypical kinetic profiles in drug metabolism reactions. *Drug Metab. Dispos. 30*, 355–362.
(32) Loida, P. J., and Sligar, S. G. (1993) Molecular recognition in cytochrome P-450: mechanism for the control of uncoupling reactions. *Biochemistry 32*, 11530–11538.
(33) Zhang, W., Liu, Y., Yan, J., Cao, S., Bai, F., Yang, Y., Huang, S., Yao, L., Anzai, Y., Kato, F., Podust, L. M., Sherman, D. H., and Li, S. (2014) New reactions and products resulting from alternative interactions between the P450 enzyme and redox partners. *J. Am. Chem. Soc. 136*, 3640–3646.
(34) Sabbadin, F., Hyde, R., Robin, A., Hilgarth, E.-M., Delenne, M., Flitsch, S., Turner, N., Grogan, G., and Bruce, N. C. (2010) LICRED: a versatile drop-in vector for rapid generation of redox-self-sufficient cytochrome P450s. *ChemBioChem 11*, 987–994.

Appendix B:
Experimental procedures and supplemental information for Chapter 3

B.1 Cloning

Cloning of ChmHI and construction of ChmHI-RhFRED

chmHI was obtained as a synthetic codon-optimized gene from Invitrogen (GeneArt Strings DNA Fragments). The sequence (5'–3') is displayed below:

ATGTTGGACGTAGATCACCTTCTCCCGATTGCATTTCGTGTTCGTAAAAGCATGAAAAGCAGCAAAGTTGTTCAT
AGCCGTCCTGCCGAAGCCGGTGTTGCATGGCCTGTTGCACGTACCTGTCCGTTTACACTGCCGGATCAGTATGC
AGAAAAACGTAAAAATGAACCGATTTGTCGTGCACAGGTTTGGGATGATAGCCGTACCTGGCTGATTACCAAACA
TGAACATGTGCGTGCACTGCTGGCAGATCCGCGTGTTACCGTGGATCCGGCAAAACTGCCTCGTCTGAGCCCG
AGTGATGGTGATGGTGGTGGCTTTCGTAGCCTGCTGACCATGGATCCGCCTGATCATAATGCACTGCGTCGTAT
GCTGATTAGCGAATTTTCAGTTCATCGTGTGCGTGAAATGCGTCCGGGTATTGAACGTACCGTTCATGGTCTGCT
GGATGGTATTCTGGAACGTCGTGGTCCGGTTGATCTGGTTGCAGAACTGGCACTGCCGATGAGCACCCTGGTTA
TTTGTCAGCTGCTGGGTGTTCCGTATGAAGATCGTGAATTTTTTCAAGAACGTAGCGAACAGGCAACCCGTGTTG
GTGGTAGCCAAGAAAGCCTGACAGCCCTGCTGGAACTGCGTGATTATCTGGATCGTCTGGTTACCGCAAAAATT
GAAACACCGGGTGATGATCTGCTGTGTCGTCTGATTGCAAGCCGTCTGCATACAGGCGAAATGCGCCATGCAGA
AATTGTTGATAATGCAGTTCTGCTGTTAGCAGCAGGTCATGAAACCAGCGCAGCAATGGTTGCACTGGGTATTCT
GACCCTGCTGCGTCATCCGGGTGCACTGGCAGAGCTGCGTGGTGATGGCACCCTGATGCCGCAGACCGTTGAT
GAACTGCTGCGCTTTCATAGCATTGCAGATGGTCTGCGTCGTGCAGTTACCGAAGATATTGAATTAGGTGGTATT
ACCCTGCGTGCCGGTGATGGTCTGATTGTTAGCCTGGCAAGCGCAAATCGTGATGAAAGTGCATTTGCAAGTCC
GGATGGTTTTGATCCGCATCATCCGGCAAGTCGTCATGTTGCATTTGGTTATGGTCCTCATCAGTGTCTGGGCCA
GAATCTGGCACGTCTGGAACTGGAAGTTACCCTGGGTGCAGTTGTTGAACGTATTCCGACACTGCGTCTGGCTG
GTGATGCAGATGCCCTGCGTGTTAAACAGGATAGCACCATTTTTGGTCTGCATGAGCTGCCGGTCGAGTGGTGA

The gene was amplified by PCR using primers ChmHI_for and ChmHI_rev1. The amplified fragment was subsequently purified, digested with *NdeI* and *HindIII*, and ligated into pET28b that had previously been digested with the same restriction enzymes to yield pET28b_ChmHI. The plasmid was sequenced to ensure that no mutations were present in the open reading frame.

To construct the ChmHI-RhFRED fusion protein, the *chmHI* gene was further amplified by PCR using primers ChmHI_for and ChmHI_rev2. The amplified DNA fragment was isolated and purified prior to restriction digestion with *NdeI* and *EcoRI*. The cut *chmHI* fragment was ligated into the pET28b_PikC-RhFRED vector[1] that had

previously been digested with the same restriction enzymes to generate pET28b_ChmHI-RhFRED. Sequencing results verified that the entire open reading frame was free of unwanted mutations. The following is the primary amino acid sequence of the entire translated ChmHI-RhFRED protein (yellow = N-terminal His-tag; red = ChmHI; green = RhFRED):

MGSSHHHHHHSSGLVPRGSHMLDVDHLLPIAFRVRKSMKSSKVVHSRPAEAGVAWP
VARTCPFTLPDQYAEKRKNEPICRAQVWDDSRTWLITKHEHVRALLADPRVTVDPAKL
PRLSPSDGDGGGFRSLLTMDPPDHNALRRMLISEFSVHRVREMRPGIERTVHGLLDGI
LERRGPVDLVAELALPMSTLVICQLLGVPYEDREFFQERSEQATRVGGSQESLTALLEL
RDYLDRLVTAKIETPGDDLLCRLIASRLHTGEMRHAEIVDNAVLLLAAGHETSAAMVAL
GILTLLRHPGALAELRGDGTLMPQTVDELLRFHSIADGLRRAVTEDIELGGITLRAGDGL
IVSLASANRDESAFASPDGFDPHHPASRHVAFGYGPHQCLGQNLARLELEVTLGAVVE
RIPTLRLAGDADALRVKQDSTIFGLHELPVEWEFVLHRHQPVTIGEPAARAVSRTVTVE
RLDRIADDVLRLVLRDAGGKTLPTWTPGAHIDLDLGALSRQYSLCGAPDAPSYEIAVHL
DPESRGGSRYIHEQLEVGSPLRMRGPRNHFALDPGAEHYVFVAGGIGITPVLAMADHA
RARGWSYELHYCGRNRSGMAYLERVAGHGDRAALHVSEEGTRIDLAALLAEPAPGV
QIYACGPGRLLAGLEDASRNWPDGALHVEHFTSSLAALDPDVEHAFDLELRDSGLTVR
VEPTQTVLDALRANNIDVPSDCEEGLCGSCEVAVLDGEVDHRDTVLTKAERAANRQM
MTCCSRACGDRLALRL

Cloning of ChmHII

Like *chmHI*, *chmHII* was obtained as a synthetic codon-optimized gene. The sequence (5'–3') is displayed below:

ATGCGGGTGACAGTCGACCAGAGCCGTTGTTTAGGTGCAGGTCAGTGTGAACAGCTGGCACCGGAAGTTTTTC
GTCAGGATGAAGAAGGTCTGAGTCGCGTTCTGGTGCCGGAACCGGATCCTGCAAGCTGGCCTCGTGTTCTGCA
GACCGTTGATCTGTGTCCGGTTCAGGCAGTTCTGATTGATGAAGGTCCGGGTCCAGCGCCGCAGGACACCAAG
TGA

The gene was amplified by PCR using primers ChmHII_for and ChmHII_rev. The amplified fragment was subsequently purified, digested with *NdeI* and *HindIII*, and ligated into pET28H8T (pET28b variant generated in house containing an N-terminal 8xHis-tag followed by a TEV cleavage sequence upstream of the multiple cloning site) that had previously been digested with the same restriction enzymes to yield pET28H8T_ChmHII. The plasmid was sequenced to ensure that no mutations were present in the open reading frame.

Cloning of TylHII

The synthetic *tylHII* gene previously cloned into pET28b (Appendix A)[2] was re-cloned into pET28H8T as described for *chmHII* using primers TylHII_for and TylHII_rev to yield pET28H8T_TylHII. The plasmid was sequenced to ensure that no mutations were present in the open reading frame.

Cloning of MBP-FdR

To allow for purification of MBP-FdR via nickel affinity chromatography, the gene encoding spinach ferredoxin reductase (FdR) was amplified by PCR from the pMAL-c vector (Appendix A)[2] using primers FdR_for and FdR_rev. The amplified DNA fragment was isolated and purified prior to restriction digestion with *NdeI* and *HindIII*. The cut fragment was ligated into pET28H8mbpT (pET28b variant generated in house containing N-terminally 8xHis-tagged maltose-binding protein (MBP) followed by a TEV cleavage sequence upstream of the multiple cloning site) that had previously been digested with the same restriction enzymes to yield pET28H8mbpT_FdR. Sequencing results verified that the entire open reading frame was free of unwanted mutations.

Construction of TylHI$_{\Delta 2\text{-}33}$

The N-terminal truncated variant of TylHI was generated by PCR amplification of the *tylHI* gene using primers TylHI_for and TylHI_rev and previously generated pET28b_TylHI-2 (Appendix A)[2] as template. Following isolation and purification of the amplicon, restriction digestion was carried out with *NdeI* and *HindIII*. The cut *tylHI* fragment was then ligated into pET28b that had previously been digested with the same restriction enzymes to yield pET28b_TylHI$_{\Delta 2\text{-}33}$. The plasmid was sequenced to ensure that no mutations were present in the open reading frame.

Site-directed mutagenesis of TylHI and MycCI

Site-directed mutagenesis was performed via whole-plasmid PCR amplification using KOD Xtreme Hot Start DNA polymerase (EMD Millipore) and associated reagents according to the manufacturer's instructions along with the mutagenic primers listed in **Table B.1**.

Generation of TylHI/MycCI chimeras

The TylHI(MycCI$_{T57\text{-}M81}$) and TylHI(MycCI$_{D72\text{-}F76}$) chimeras were generated by whole-plasmid PCR amplification using the mutagenic primers listed in **Table B.1** and pET28b_TylHI-2 as template.

Table B.1. Cloning and mutagenesis primers for constructs described in Chapter 3.

Primer	Sequence (5'–3')	Notes
FdR_for	CGCATATGACCACCGCTGTCACCGCCGCTGTTTC	*NdeI* site underlined
FdR_rev	GGCCAAGCTTTTAGTAGACTTCAACGTTCCATTGTTCTGCC	*HindIII* site underlined
ChmHI_for	GGAATTCCATATGTTGGACGTAGATCACCTTCTCCCGATTGC	*NdeI* site underlined
ChmHI_rev1	CGATCAAGCTTTCACCACTCGACCGG	*HindIII* site underlined
ChmHI_rev2	CGATCGAATTCCCACTCGACCGGCAGC	*EcoRI* site underlined
ChmHII_for	GGAATTCCATATGCGGGTGACAGTCGACCAGAGC	*NdeI* site underlined
ChmHII_rev	CGATCAAGCTTTCACTTGGTGTCCTGCGGCG	*HindIII* site underlined
TylHII_for	GGAATTCCATATGCGTGTTCGTATTGATACCG	*NdeI* site underlined
TylHII_rev	CGATCAAGCTTTTATGCATCACGACCTG	*HindIII* site underlined
TylHI_for	GGAATTCCATATGGCCTGGCCGGTCGC	*NdeI* site underlined
TylHI_rev	CGATCAAGCTTTCACCAGGCGACGGGC	*HindIII* site underlined
TylHI_R96A	GCGAAGCTCCCGGCGCTCTCACCCTCC	Altered codon is underlined
TylHI_D101A	GCTCTCACCCTCCGCCCGGTGAGGCCGAGG	Altered codon is underlined
TylHI_D101N	GCTCTCACCCTCCAACGGTGAGGCCGAGG	Altered codon is underlined
TylHI_E103A	CCCTCCGACGGTGCGGCCGAGGCGTCC	Altered codon is underlined
TylHI_E105A	GACGGTGAGGCCGCGGCGTCCCGTTCG	Altered codon is underlined
TylHI_E105Q	GACGGTGAGGCCCAGGCGTCCCGTTCG	Altered codon is underlined
TylHI_E105L	GACGGTGAGGCCCTGGCGTCCCGTTCG	Altered codon is underlined
TylHI_R310A	GCCGACGGGCTGGCGCGCTCGGCCACC	Altered codon is underlined
TylHI_D101R	GCTCTCACCCTCCCGTGGTGAGGCCGAGG	Altered codon is underlined
TylHI_R310D	GCCGACGGGCTGGATCGCTCGGCCACC	Altered codon is underlined
MycCI_D70A	CTGTCCGAGGCGGCAGGTGACGGCGAC	Altered codon is underlined
MycCI_D70N	CTGTCCGAGGCGAACGGTGACGGCGAC	Altered codon is underlined
TylHI(MycCI_T57-M81)	GCTGCTGGCCGACCCCCGGGTCACCGTGGACCCGACCCGACA ACCTCGTCTGTCCGAGGCGGATGGTGACGGCGACGGCTTCCGT TCCATGCTGATGCTGGACCCGCCCGACCACGGAGC	
TylHI(MycCI_D72-F76)	GCGGCTCTCACCCTCCGACGGTGATGGCGATGGCTTTCGTTCG CTGCTGACACTGGACC	

B.2 Protein expression and purification

Expression and purification of P450s

All stand-alone P450s (MycCI, TylHI, and ChmHI) and mutants thereof were expressed and purified as previously described (Appendix A)[2] with the exception that each protein was expressed in cultures grown in 1-2 x 1.5 L batches using 2.8 L baffled Fernbach flasks.

Expression and purification of P450-RhFRED constructs

The protocol was similar to that previously described (Appendix A)[2] with a few minor alterations. Each plasmid was cotransformed with pGro7 (Takara) into *E. coli*

BL21(DE3) cells, and individual colonies were selected for overnight growth (37 °C) in 15 mL of TB containing kanamycin (50 μg/mL) and chloramphenicol (25 μg/mL). 2-3 x 1.5 L of TB (2.8 L baffled Fernbach flasks) supplemented with kanamycin (50 μg/mL), chloramphenicol (25 μg/mL), thiamine (1 mM), and glycerol (4% v/v) were inoculated with the 15 mL overnight seed cultures and incubated at 37 °C (160 rpm). When the OD_{600} reached 0.6-1.0, the cultures were cooled in an ice-water bath (15-20 min) before addition of IPTG (0.1 mM), δ-aminolevulinic acid (1 mM), and L-arabinose (0.5 g/L). The cultures were grown at 18 °C for ~20 h before the cells were harvested and stored at -80 °C until used for protein purification.

All subsequent steps were performed at 4 °C. The cells were thawed and resuspended in 30 mL of lysis buffer (50 mM Tris, 50 mM NaCl, 10% (v/v) glycerol, 1 mM PMSF, 0.5 mg/mL lysozyme, 2 mM $MgCl_2$, 2.5 U/mL Benzonase nuclease, pH 7.4) per 1 L of original overexpression culture. The cell suspension was incubated on a nutating shaker for 1 h prior to sonication in 80 mL batches (70% power, 5 s on, 5 s off, 5 min total on time) and centrifugation at 50,000 x g for 30 min to remove cellular debris. To the resulting clarified lysate were added 4 M solutions of NaCl and imidazole such that the final concentrations of each were 300 mM and 10 mM, respectively. The lysate was then incubated with 10 mL of Ni-NTA resin on a nutating shaker for 1 h. The resin slurry was loaded onto an empty column, and the lysate was pushed through with gentle syringe pressure. The resin was washed with 2 x 100 mL of wash buffer (50 mM Tris, 300 mM NaCl, 20 mM imidazole, 10% (v/v) glycerol, pH 7.4) prior to elution of P450-RhFRED with 20 mL of elution buffer (50 mM Tris, 300 mM NaCl, 300 mM imidazole, 10% (v/v) glycerol, pH 7.4). Protein was subsequently concentrated to ~0.5 mL total volume using 30 kD MWCO centrifugal filters and exchanged into anion exchange loading buffer (50 mM Tris, 50 mM NaCl, 10% (v/v) glycerol, pH 7.4) using PD-10 columns. The buffer-exchanged protein was filtered through 4 mm 0.22 μm PVDF filters (EMD Millipore) prior to further purification via anion exchange chromatography. Using an ÄKTA FPLC system (GE Healthcare), 4 mL of protein was loaded onto a 20 mL Mono Q HR 16/10 anion exchange column (GE Healthcare) and washed with 2 CV of loading buffer followed in turn by 3 CV of 5% and 10% anion exchange elution buffer (50 mM Tris, 1 M NaCl, 10% (v/v) glycerol, pH 7.4). P450-

RhFRED was eluted with a linear gradient of 10-25% elution buffer over 10 CV. Fractions containing pure material as assessed by monitoring absorbance (A_{420}/A_{280}) were pooled, concentrated, and desalted on PD-10 columns. Protein was eluted with storage buffer, and aliquots were flash frozen in liquid N_2 and stored at -80 °C until used for analytical-scale reactions.

Expression and purification of ferredoxins MycCII, TylHII, and ChmHII

These proteins were expressed and purified as previously described (Appendix A)[2] with the following details/exceptions. All cultures were grown in 1.5 L batches using 2.8 L baffled Fernbach flasks. TylHII (pET28H8T_TylHII) and ChmHII (pET28H8T_ChmHII) were both coexpressed with GroES/GroEL (pGro7). Concentrations of purified ferredoxins were determined by the Bradford protein assay using spinach ferredoxin (Sigma-Aldrich) as standard. Based on these results, ε_{408} ($M^{-1}cm^{-1}$) was estimated to be 4200 (MycCII) or 3500 (TylHII and ChmHII). See **Figure B.1** below for UV-visible spectra of these ferredoxins.

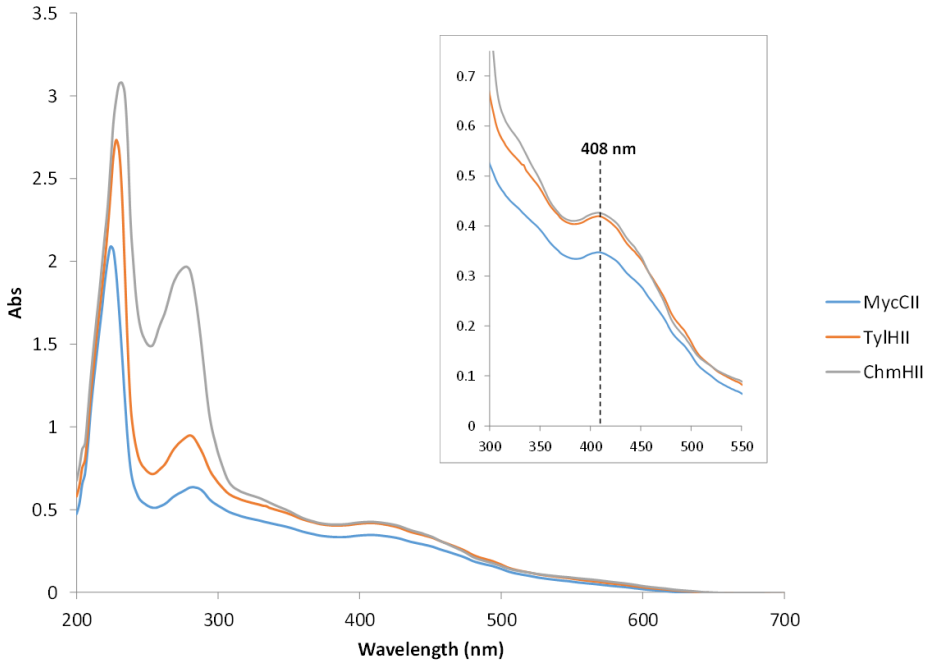

Figure B.1. UV-visible spectra of ferredoxins MycCII, TylHII, and ChmHII.

Expression and purification of MBP-FdR

Plasmid pET28H8mbpT_FdR was transformed into *E. coli* BL21(DE3) cells, and an individual colony was selected for overnight growth (37 °C) in 250 mL of LB containing kanamycin (50 μg/mL). 12 x 1.5 L of LB (2.8 L baffled Fernbach flasks) supplemented with kanamycin (50 μg/mL) and thiamine (1 mM) were each inoculated with 15 mL of overnight seed culture and incubated at 37 °C (160 rpm). When the OD_{600} reached 0.6-1.0, the cultures were cooled in an ice-water bath (15-20 min) before addition of IPTG (0.1 mM). The cultures were grown at 18 °C for 23 h before the cells were harvested and stored at -80 °C until used for protein purification.

All subsequent steps were performed at 4 °C. The cells were thawed and resuspended in 180 mL of lysis buffer (50 mM NaH_2PO_4, 300 mM NaCl, 10 mM imidazole, 10% (v/v) glycerol, 1 mM PMSF, pH 8) prior to lysis in 80 mL batches using a sonic dismembrator (70% power, 5 s on, 5 s off, 5 min total on time). The crude lysate was centrifuged at 50,000 x g for 30 min to remove cellular debris, and the clarified lysate was incubated with 15 mL of Ni-NTA resin on a nutating shaker for 1-2 h. The resin slurry was loaded onto an empty column, and the lysate was pushed through with gentle syringe pressure. The resin was washed with 50-70 mL of lysis buffer prior to elution of yellow MBP-FdR with 40-50 mL of elution buffer (50 mM NaH_2PO_4, 300 mM NaCl, 300 mM imidazole, 10% (v/v) glycerol, pH 8). The protein was subsequently concentrated using 50 kD MWCO centrifugal filters (Millipore) and desalted by loading onto PD-10 columns (GE Healthcare) and eluting with storage buffer (50 mM NaH_2PO_4, 1 mM EDTA, 0.2 mM DTT, 10% (v/v) glycerol, pH 7.3) according to the manufacturer's instructions. The purified enzyme was aliquoted, flash frozen in liquid N_2, and stored at -80 °C until used for analytical-scale reactions. The concentration of purified MBP-FdR was determined by absorption spectroscopy using the reported extinction coefficient of oxidized spinach ferredoxin reductase at 456 nm (10,400 $M^{-1}cm^{-1}$).[3] Thus, the yield of protein was ~13 mg per 1 L of overexpression culture (A_{456}/A_{280} = 0.07).

B.3 Protein crystallization and structure determination

For crystallization experiments (carried out by Nathan Samora and Dr. Larissa Podust), TylHI was purified via Ni-NTA affinity chromatography followed by anion

exchange chromatography using a Mono Q column. Crystals of TylHI supplemented with 23-DMTL (**3**) were grown using a hanging drop vapor diffusion protocol, and those diffracting in the $P2_12_12_1$ space group grew from 14% PEG MME 550, 100 mM HEPES (pH = 7.5), and 6 mM glutathione. Diffraction data were collected at 110 K at beamline 8.3.1, Advanced Light Source, Lawrence Berkeley National Laboratory, USA. The crystal structure was determined by molecular replacement using MycCI (PDB 5FOI) as a search model. Data collection and refinement statistics are reported in **Table 3.2** (see Chapter 3).

B.4 Preparation of substrates for enzymatic reactions

5-*O*-mycaminosyl-tylactone (MT, **2**) was prepared in three steps starting from 23-deoxy-5-*O*-mycaminosyl-tylonolide (23-DMTL, **3**). The latter was isolated from *Streptomyces fradiae* GS76 cultures as previously described (Appendix A).[2] Compound **3** was first reduced to 20-hydroxy-5-*O*-mycaminosyl-tylactone (20-OH-MT, **8**), and the hydroxyl group at C20 was removed via iodination and subsequent reduction (see **Scheme B.1**). All other substrates were prepared as described in recent reports (see Appendices A and C).[2,4]

Scheme B.1. Semisynthesis of MT (**2**).

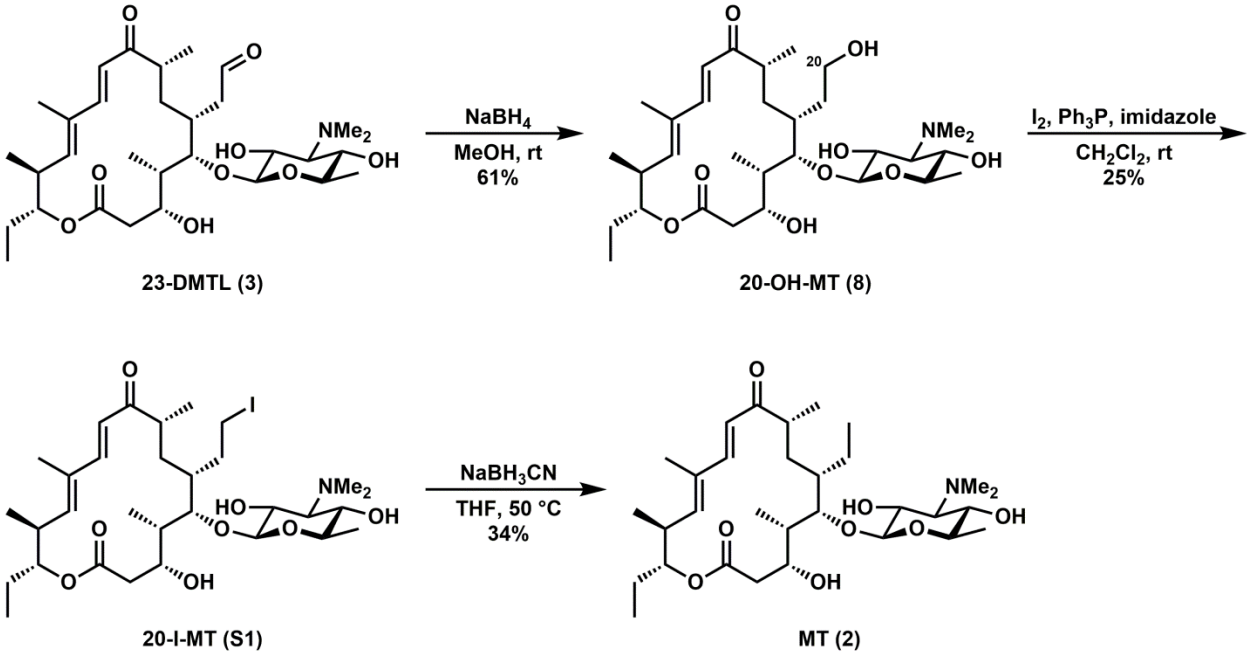

*20-hydroxy-5-O-mycaminosyl-tylactone (20-OH-MT, **8**)*

To a stirring solution of **3** (180 mg, 0.309 mmol) in CH_3OH (3.30 mL) in a 50 mL round-bottom flask was added a solution of $NaBH_4$ (0.330 mmol, 3.30 mL CH_3OH). The reaction mixture was stirred at room temperature open to air in the dark for 45 min prior to addition of more $NaBH_4$ solution (0.165 mmol, 1.65 mL CH_3OH). After an additional 15 min of stirring, the reaction was deemed complete by HPLC analysis. The solvent was evaporated, and the crude material was purified by flash chromatography (10% CH_3OH/CH_2Cl_2 + 1% Et_3N, SiO_2) followed by preparative HPLC (isocratic 45% CH_3CN/H_2O + 0.1% Et_3N, Phenomenex Luna C18 (250 x 21.2 mm, 5 µm, 100 Å), 8 mL/min, monitored at 288 nm) to afford **8** (110 mg, 60.9%) as a white amorphous solid. T_R **8** = 36-40 min.

*20-iodo-5-O-mycaminosyl-tylactone (20-I-MT, **S1**)*

To a flame-dried 50 mL round-bottom flask under N_2 was added CH_2Cl_2 (4.86 mL) followed by triphenylphosphine (58.6 mg, 0.224 mmol). The solution was stirred prior to addition of imidazole (29.6 mg, 0.435 mmol) and I_2 (54.3 mg, 0.214 mmol). A solution of **8** (51.7 mg, 0.0886 mmol) in CH_2Cl_2 (4.00 mL) was added, and the reaction mixture was stirred at room temperature under N_2 in the dark for 24 h. LC-MS analysis indicated full consumption of starting material and the presence of a ~1:1 mixture of mono:diiodinated products. The solvent was evaporated, and the crude material was purified by flash chromatography (10% CH_3OH/CH_2Cl_2 + 1% Et_3N, SiO_2) followed by preparative HPLC (isocratic 70% CH_3CN/H_2O + 0.1% Et_3N, Phenomenex Luna C18 (250 x 21.2 mm, 5 µm, 100 Å), 8 mL/min, monitored at 288 nm) to afford **S1** (15.5 mg, 25.2%) as a white amorphous solid. T_R **S1** = 29-34 min.

*5-O-mycaminosyl-tylactone (MT, **2**)*

To a small glass tube (13 x 100 mm) containing **S1** (40.4 mg, 0.0582 mmol) was added a solution of $NaBH_3CN$ (0.23 mmol, 0.58 mL dry THF). The reaction mixture was stirred at 50 °C under N_2 in the dark for 51 h. The solvent was evaporated, and the crude material was purified by preparative HPLC (isocratic 60% CH_3CN/H_2O + 0.1% Et_3N, Phenomenex Luna C18 (250 x 21.2 mm, 5 µm, 100 Å), 8 mL/min, monitored at

288 nm) to afford **2** (11.1 mg, 33.5%, 39.2% BRSM) as a semitransparent amorphous solid. T_R **2** = 40-44 min. T_R **S1** = 54-59 min.

B.5 Analytical-scale enzymatic reactions

Analytical-scale enzymatic reactions were carried out under the following conditions: 5 μM P450 (or 0.5 μM for determination of total turnover number (TTN)), 100 μM ferredoxin, 10 μM MBP-FdR, 500 μM substrate (2.5% DMSO, final concentration), 1 mM $NADP^+$, 5 mM glucose-6-phosphate, and 1 U/mL glucose-6-phosphate dehydrogenase in storage buffer (50 mM NaH_2PO_4, 1 mM EDTA, 0.2 mM DTT, 10% (v/v) glycerol, pH 7.3). Exogenous redox partners (ferredoxin and MBP-FdR) were not included in reactions employing P450-RhFRED fusion proteins. The total volume of each reaction was 100 μL (1.7 mL Eppendorf tube), and reactions were incubated in the dark at 30 °C (200 rpm) for 15-18 h prior to quenching by addition of methanol (100 μL for HPLC analysis, 900 μL for LC-MS analysis). Quenched reactions were centrifuged at 17,000 x g for 10 min (4 °C), and the supernatant was removed for HPLC or LC-MS analysis. All reactions were performed and analyzed in triplicate. Negative control reactions performed in parallel lacked P450/ferredoxin/MBP-FdR or P450-RhFRED.

HPLC analysis was performed on an Agilent 1100 Series HPLC system with UV detection at 285 nm using a Phenomenex Luna C18 column with the following specifications: dimensions, 150 x 4.6 mm; particle size, 5 μm; pore size, 100 Å. HPLC conditions were as follows: mobile phase (A = deionized water + 0.1% formic acid, B = acetonitrile + 0.1% formic acid); 15% B for 1 min, 15% to 75% B over 12 min, 95% B for 1 min, 15% B for 2 min; flow rate, 2.0 mL/min; injection volume, 50 μL. Percent conversion and TTN values were determined by integrating peaks corresponding to monohydroxylated product and unreacted starting material for each reaction. The results of all reactions save for those involving narbomycin (**S2**) were quantified by HPLC.

LC-MS analysis was performed on an Agilent Q-TOF HPLC-MS (Life Sciences Institute, University of Michigan) equipped with a high-resolution electrospray mass spectrometry (ESI- MS) source and a Beckmann Coulter reversed-phase HPLC system using a Phenomenex Luna C18 column with the following specifications: dimensions,

150 x 3.0 mm; particle size, 5 μm; pore size, 100 Å. HPLC conditions were as follows: mobile phase (A = deionized water + 0.1% formic acid, B = 95% acetonitrile/deionized water + 0.1% formic acid); 10% B (pre-run) for 2.5 min, 10% to 100% B over 12.5 min, 100% B for 2.5 min, 10% B (post-run) for 2.5 min; flow rate, 0.4 mL/min; injection volume, 0.2 μL. Percent conversion and TTN values were determined by integrating extracted-ion chromatogram (EIC) peaks corresponding to $[M + H]^+$ ions for unreacted substrate and potential products (i.e., mono/dihydroxylation and/or demethylation). Only the results of reactions with **S2** as substrate were quantified by LC-MS.

B.6 Equilibrium substrate binding assays

Spectroscopic substrate binding assays were performed essentially as previously described (Appendix A).[2] Purified P450s were diluted in storage buffer to concentrations ranging from 0.5 to 5 μM. Diluted enzyme was transferred to a 1 cm quartz cuvette (Beckman), and substrate was titrated into the solution in varying amounts so as to achieve the desired final concentrations (0.5-1280 μM). The same amounts of DMSO alone were added to the protein in the reference cuvette. DMSO comprised no more than 6.4% of the solution volume at the conclusion of each experiment. Scans were performed from 365 to 439 nm (2 nm steps), and difference spectra were subsequently obtained by subtracting DMSO control spectra from experimental spectra. Average absorbance differences ($\Delta A = A_{385} – A_{419}$) from experiments performed in duplicate were plotted as a function of substrate concentration, and the data were fit to either a rectangular hyperbolic function ($K_d \geq 5$ x [P450]) or a quadratic function for high-affinity ligands ($K_d \leq 5$ x [P450]) using the KaleidaGraph software package.

Percent spin shift of each enzyme at saturating levels of different substrates was estimated by normalizing the ΔA_{max} values acquired from the nonlinear regression analysis previously described to the enzyme concentration. The resulting values were then compared with the largest of these values obtained across all enzyme/substrate combinations to determine percent spin shift as previously described (Appendix A).[2] In the present set of experiments, the percentage of each enzyme in the high-spin state at saturating levels of a given substrate was estimated by assuming that $TylHI_{E103A}$ was completely converted to high spin when saturated with **3** (i.e., $(\Delta A_{max}/[E])_{max}$ was

observed with **3** as the substrate for TylHI$_{E103A}$; a similar value was observed with M-VIII (**10**) as the substrate for MycCI).

B.7 Supplemental tables and figures

Table B.2. Summary of the results of activity assays performed with TylHI and MycCI. Average percent conversion values and standard deviations reflect the results of experiments performed in triplicate.[a]

	Substrate								
Catalytic system	**2**	**3**	**8**	**6**	**7**	**9**	**10**	**11**	**13**
MycCI	96.6 ± 1.4	95.6 ± 0.9	97.8 ± 0.5	98.5 ± 0.4	93.7 ± 1.2	96.3 ± 0.2	97.3 ± 0.5	86.8 ± 1.2	64.2 ± 1.1
TylHI/TylHII	34.2 ± 2.1	57.7 ± 1.8	58.2 ± 0.8	2.8 ± 0.1	10.9 ± 0.5	10.0 ± 0.4	0	0	0
TylHI	39.7 ± 1.0	90.7 ± 2.3	92.3 ± 1.5	0.9 ± 0.1	5.9 ± 0.1	4.7 ± 0.5	0	0	0
TylHI-RhFRED	6.9 ± 0.2	35.1 ± 0.9	36.7 ± 1.9	0.3 ± 0.0	0.9 ± 0.1	1.0 ± 0.1	0	0	0
$TylHI_{\Delta 2\text{-}33}$	36.4 ± 0.4	85.5 ± 1.7	87.0 ± 1.9	0.6 ± 0.1	5.0 ± 0.1	4.0 ± 0.4	--[b]	--	--
$TylHI_{E105Q}$	46.8 ± 1.3	67.9 ± 1.5	61.7 ± 2.0	1.4 ± 0.1	9.5 ± 0.3	6.6 ± 0.2	--	--	--
$TylHI_{E105A}$	53.9 ± 1.6	69.6 ± 2.2	67.5 ± 2.5	2.1 ± 0.2	12.4 ± 0.4	8.7 ± 0.3	--	--	--
$TylHI_{E105L}$	18.6 ± 0.6	36.9 ± 1.6	33.7 ± 0.4	5.0 ± 0.5	18.4 ± 0.9	18.5 ± 0.4	--	--	--
$TylHI_{D101N}$	1.6 ± 0.0	11.1 ± 0.8	5.7 ± 0.2	0.5 ± 0.0	3.0 ± 0.2	2.2 ± 0.2	--	--	--
$TylHI_{D101A}$	1.6 ± 0.1	11.7 ± 0.6	5.5 ± 0.0	0.4 ± 0.0	2.6 ± 0.3	2.0 ± 0.1	--	--	--
$TylHI_{R96A}$	1.9 ± 0.0	13.6 ± 1.0	6.9 ± 0.2	0.3 ± 0.0	2.0 ± 0.1	1.5 ± 0.1	--	--	--
$TylHI_{R310A}$	0.3 ± 0.0	4.9 ± 0.3	2.0 ± 0.1	<0.1	0.9 ± 0.2	0.5 ± 0.1	--	--	--
$TylHI_{D101R/R310D}$	0.1 ± 0.0	0.5 ± 0.1	0.4 ± 0.0	<0.1	0.3 ± 0.0	0.1 ± 0.0	--	--	--
$TylHI_{E103A}$	37.3 ± 1.1	91.7 ± 1.9	90.3 ± 1.9	1.2 ± 0.1	6.6 ± 0.3	5.9 ± 0.1	--	--	--
$TylHI(MycCI_{T57\text{-}M81})$	48.8 ± 1.7	53.8 ± 0.9	66.5 ± 0.9	36.2 ± 0.6	49.5 ± 1.8	62.8 ± 2.9	23.1 ± 0.5	3.2 ± 0.3	0
$TylHI(MycCI_{D72\text{-}F76})$	34.7 ± 0.9	72.9 ± 1.5	62.0 ± 1.6	15.3 ± 0.3	26.5 ± 0.6	39.8 ± 0.6	1.6 ± 0.1	0.2 ± 0.1	0

[a]Reported values are % conversion ± standard deviation from experiments performed in triplicate. Unless otherwise indicated, all catalytic systems employed MycCII as ferredoxin and MBP-FdR as ferredoxin reductase.

[b]Blank space (--) indicates that the corresponding reaction was not performed.

Table B.3. ΔA_{max}/[E] and percent spin shift values (shown in parentheses) obtained from equilibrium substrate binding assays. Results derive from nonlinear regression analysis of data averaged from experiments performed in duplicate.

	Substrate							
Enzyme	**2**	**3**	**8**	**6**	**7**	**9**	**10**	**11**
TylHI (wild-type)	0.086[a] (60%)[b]	0.125 (87%)	0.113 (79%)	0.091 (63%)	0.076 (53%)	0.086 (60%)	0.036 (25%)	0.048 (33%)
$TylHI_{\Delta 2\text{-}33}$	--[c]	0.126[d] (88%)	--	--	--	--	--	--
$TylHI_{E105Q}$	--	0.131 (91%)	--	--	--	--	--	--
$TylHI_{E105A}$	--	0.135 (94%)	--	--	--	--	--	--
$TylHI_{E105L}$	--	0.104 (72%)	--	--	--	--	--	--
$TylHI_{D101N}$	--	0.077 (54%)	--	--	--	--	--	--
$TylHI_{D101A}$	--	0.071 (49%)	--	--	--	--	--	--
$TylHI_{R96A}$	--	0.089 (62%)	--	--	--	--	--	--
$TylHI_{R310A}$	--	0.066 (46%)	--	--	--	--	--	--
$TylHI_{D101R/R310D}$	--	0.045 (31%)	--	--	--	--	--	--
$TylHI_{E103A}$	--	0.144[e] (100%)	--	--	--	--	--	--
TylHI($MycCI_{T57\text{-}M81}$)	0.128 (89%)	0.120 (83%)	--	0.125 (87%)	0.115 (80%)	--	0.126 (88%)	0.065 (45%)
TylHI($MycCI_{D72\text{-}F76}$)	0.137 (95%)	0.138 (96%)	--	0.131 (91%)	0.122 (85%)	--	0.096 (67%)	0.049 (34%)

[a] ΔA_{max}/[E]
[b] % spin shift
[c] Blank space (--) indicates that the corresponding binding experiment was not performed.
[d] K_d = 0.65 ± 0.04 μM
[e] $(\Delta A_{max}/[E])_{max}$ used to approximate % spin shifts for all enzymes.

Table B.4. Summary of the results of activity assays performed with MycCI (wild-type), $MycCI_{D70N}$, and $MycCI_{D70A}$.[a]

Compound	**MycCI (wild-type)**	**$MycCI_{D70N}$**	**$MycCI_{D70A}$**
3	91	88	91
6	76	67	72
10	73	69	77
11	61	64	66
13	52	58	57

[a] Reported values are % conversion from experiments performed once. MycCII and MBP-FdR were employed as ferredoxin and ferredoxin reductase, respectively.

Table B.5. Total turnover numbers (TTNs) for reactions performed in parallel with MycCI, ChmHI, and TylHI.[a]

	Substrate						
Catalytic system	**2**	**3**	**6**	**7**	**10**	**11**	**13**
MycCI/MycCII	154 ± 6	169 ± 7	154 ± 1	170 ± 1	153 ± 2	125 ± 8	93 ± 4
MycCI-RhFRED	92 ± 2	109.0 ± 0.3	157 ± 5	171 ± 5	181 ± 5	53 ± 2	19 ± 2
ChmHI/ChmHII	40 ± 3	55 ± 4	43.6 ± 0.5	55 ± 1	49 ± 5	39 ± 3	10 ± 2
ChmHI/MycCII	125 ± 9	123 ± 6	121 ± 5	139 ± 5	189 ± 2	89 ± 2	33 ± 2
ChmHI-RhFRED	13.1 ± 0.9	16 ± 1	21 ± 1	28 ± 2	29.6 ± 0.9	8.6 ± 0.8	2.4 ± 0.5
TylHI/TylHII	45 ± 2	72 ± 4	3.3 ± 0.3	11.0 ± 0.7	0	0	0
TylHI/MycCII	66 ± 5	171 ± 3	1.2 ± 0.3	10 ± 1	0	0	0
TylHI-RhFRED	13.9 ± 1.0	117 ± 3	0.5 ± 0.2	1.7 ± 0.4	0	0	0

[a]TTN = mol product/mol P450. Reported errors are standard deviations calculated from experiments performed in triplicate. All catalytic systems save for P450-RhFRED included MBP-FdR as ferredoxin reductase.

Table B.6. TTNs for reactions between MycCI/ChmHI and narbomycin (**S2**).[a]

	TTN (reaction type)	
Catalytic system	Hydroxylation	*N*-demethylation
MycCI/MycCII	4.2 ± 0.3	2.3 ± 0.4
MycCI-RhFRED	0.3 ± 0.0	4.3 ± 0.4
ChmHI/ChmHII	0.2 ± 0.0	45 ± 2
ChmHI/MycCII	0.1 ± 0.0	42 ± 3
ChmHI-RhFRED	0	231 ± 8

[a]TTN = mol product/mol P450. Reported errors are standard deviations calculated from experiments performed in triplicate. All catalytic systems save for P450-RhFRED included MBP-FdR as ferredoxin reductase.

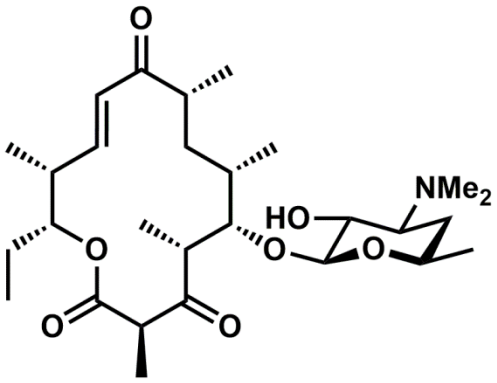

Narbomycin (S2)

Figure B.2. Structure of narbomycin (**S2**).

B.8 NMR data for compounds 2, 8, and S1

Position	δ_C (ppm)	δ_H (ppm), multi (*J* in Hz)
1	175.0	
2	41.2	2.04, dd (17.5, 1.3)
		2.49, dd (17.5, 9.8)
3	68.4	3.72, d (10.5)
4	42.5	1.69, m
5	80.0	3.75, d (9.8)
6	40.8	1.11, m
7	34.8	1.45, ddd (15.0, 11.7, 4.3)
		1.73, m
8	46.5	2.64, m
9	207.0	
10	119.9	6.45, d (15.4)
11	149.6	7.24, d (15.4)
12	135.0	
13	147.7	5.67, d (10.4)
14	40.0	2.79, tq (10.5, 6.5)
15	80.0	4.69, td (9.6, 2.6)
16	25.7	1.58, m
		1.87, m
17	10.1	0.94, t (7.3)
18	9.7	1.04, d (6.9)
19	22.2	1.41, m
		1.60, m
20	12.6	0.85, t (7.2)
21	17.9	1.20, d (6.9)
22	13.1	1.85, d (1.3)
23	16.3	1.08, d (6.5)
1'	105.2	4.26, d (7.5)
2'	71.8	3.34, dd (10.4, 7.5)
3'	71.8	2.40, t (10.1)
4'	72.8	3.13, t (9.5)
5'	74.2	3.23, dq (9.3, 6.1)
6'	18.2	1.24, d (6.1)
7'	42.2	2.51, s

*Solvent: CD_3OD

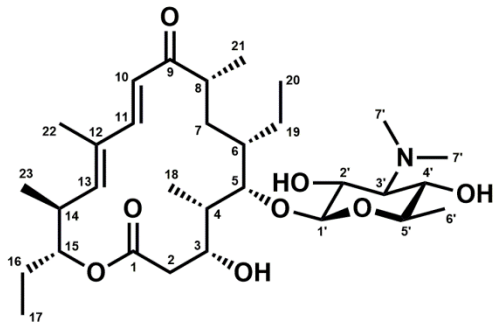

MT (2)

Position	δ_C (ppm)	δ_H (ppm), multi (*J* in Hz)
1	174.8	
2	41.0	2.04, dd (17.2, 1.1)
		2.48, dd (17.5, 10.0)
3	68.2	3.75, d (9.8)
4	42.5	1.71, m
5	80.8	3.66, d (9.7)
6	34.9	1.45, m
7	34.6	1.48, m
		1.79, t (12.5)
8	46.4	2.65, m
9	206.8	
10	119.8	6.46, d (15.4)
11	149.8	7.25, d (15.4)
12	134.9	
13	147.8	5.66, d (10.4)
14	40.0	2.79, tq (10.3, 6.5)
15	79.9	4.68, td (9.6, 2.6)
16	25.7	1.58, m
		1.88, m
17	10.0	0.94, t (7.3)
18	9.7	1.04, d (6.9)
19	32.7	1.58, m
		1.92, m
20	61.4	3.53, m
		3.63, m
21	18.0	1.21, d (6.9)
22	13.1	1.85, d (1.2)
23	16.3	1.08, d (6.5)
1'	105.4	4.27, d (7.5)
2'	71.8	3.34, dd (10.4, 7.5)
3'	71.8	2.39, t (10.1)
4'	72.8	3.13, t (9.4)
5'	74.3	3.23, dq (9.2, 6.2)
6'	18.2	1.24, d (6.1)
7'	42.2	2.51, s

*Solvent: CD_3OD

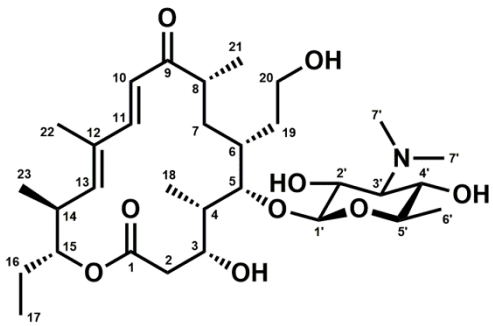

20-OH-MT (8)

Position	δ_C (ppm)	δ_H (ppm), multi (*J* in Hz)
1	175.0	
2	41.1	2.04, dd (17.5, 1.2)
		2.50, dd (17.4, 9.9)
3	68.2	3.75, d (10.0)
4	42.3	1.72, m
5	79.0	3.67, d (10.1)
6	40.5	1.33, m
7	33.8	1.50, ddd (14.8, 12.0, 4.3)
		1.76, m
8	46.5	2.58, m
9	206.5	
10	119.8	6.47, d (15.4)
11	149.9	7.26, d (15.4)
12	135.0	
13	147.8	5.67, d (10.4)
14	40.1	2.79, tq (10.3, 6.5)
15	80.0	4.69, td (9.6, 2.6)
16	25.7	1.58, ddq (14.5, 9.3, 7.3)
		1.88, m
17	10.1	0.94, t (7.4)
18	9.6	1.04, d (6.9)
19	34.9	1.91, m
		2.20, dtd (14.4, 9.9, 4.6)
20	5.3	3.07, td (9.4, 6.8)
		3.35, m
21	17.9	1.21, d (6.9)
22	13.1	1.85, d (1.2)
23	16.3	1.08, d (6.5)
1'	104.9	4.28, d (7.5)
2'	71.7	3.35, m
3'	71.7	2.42, t (10.2)
4'	72.6	3.14, t (9.5)
5'	74.3	3.25, dq (9.0, 6.1)
6'	18.8	1.31, d (6.1)
7'	42.2	2.53, s

*Solvent: CD_3OD

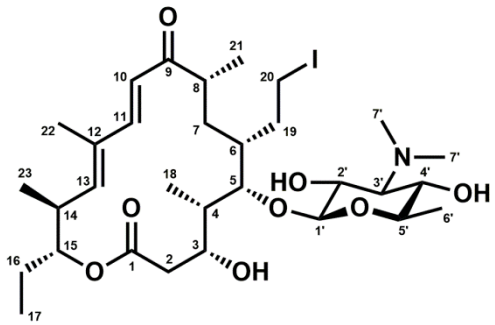

20-I-MT (S1)

B.9 References

(1) Li, S., Podust, L. M., and Sherman, D. H. (2007) Engineering and analysis of a self-sufficient biosynthetic cytochrome P450 PikC fused to the RhFRED reductase domain. *J. Am. Chem. Soc. 129*, 12940–12941.

(2) DeMars, M. D., II, Sheng, F., Park, S. R., Lowell, A. N., Podust, L. M., and Sherman, D. H. (2016) Biochemical and structural characterization of MycCI, a versatile P450 biocatalyst from the mycinamicin biosynthetic pathway. *ACS Chem. Biol. 11*, 2642–2654.

(3) Hasumi, H., and Nakamura, S. (1978) Studies on the ferredoxin–ferredoxin-NADP reductase complex: kinetic and solvent perturbation studies on the location of sulfhydryl and aromatic amino acid residues. *J. Biochem. 84*, 707–717.

(4) Lowell, A. N., DeMars, M. D., II, Slocum, S. T., Yu, F., Anand, K., Chemler, J. A., Korakavi, N., Priessnitz, J. K., Park, S. R., Koch, A. A., Schultz, P. J., and Sherman, D. H. (2017) Chemoenzymatic total synthesis and structural diversification of tylactone-based macrolide antibiotics through late-stage polyketide assembly, tailoring, and C—H functionalization. *J. Am. Chem. Soc. 139*, 7913–7920.

Appendix C:
Experimental procedures and supplemental information for Chapter 4

C.1 Cloning

Cloning of JuvC, JuvD, and TylI and construction of the corresponding RhFRED fusions

The *juvC* gene was amplified from *Micromonospora chalcea* (ssp. *izumensis*) fosmid DNA using primers JuvC_for and JuvC_rev (see **Table C.1**), and the *juvD* gene was similarly amplified using primers JuvD_for and JuvD_rev. The *tylI* gene was amplified from *Streptomyces fradiae* genomic DNA using primers TylI_for and TylI_rev. The amplified DNA fragments were isolated and purified prior to restriction digestion with *NdeI* and *EcoRI*. The cut *juvC*, *juvD*, and *tylI* fragments were ligated into the pET28b_PikC-RhFRED vector[1] that had previously been digested with the same restriction enzymes to generate pET28b_JuvC-RhFRED, pET28b_JuvD-RhFRED, and pET28b_TylI-RhFRED, respectively. Sequencing results verified that the entire open reading frame was free of unwanted mutations in each case.

Table C.1. Primers used to generate P450-RhFRED constructs described in Chapter 4.

Primer	Sequence (5'–3')	Notes
TylI_for	GGAATTCCATATGACGACACAGACGCTCGAAGC	*NdeI* restriction site is underlined
TylI_rev	CGATAGAATTCGTGGCGGGTGACGGTG	*EcoRI* restriction site is underlined
JuvC_for	CCAACCCATATGACGCAGACCCCGAACGCCC	*NdeI* restriction site is underlined
JuvC_rev	CCAACCGAATTCCTTCGGGTGCCGTCCGTCG	*EcoRI* restriction site is underlined
JuvD_for	CCAACCCATATGGAGCACCCAGTAACGGCCGG	*NdeI* restriction site is underlined
JuvD_rev	CCAACCGAATTCCCACGTCACCGGAAGGGACACG	*EcoRI* restriction site is underlined

The following is the primary amino acid sequence of the entire translated JuvC-RhFRED protein (yellow = N-terminal His-tag; red = JuvC; green = RhFRED):

MGSSHHHHHHSSGLVPRGSHMTQTPNAPAGPIDLPKGADAQGLLDWFAYMRKNWP
VSWDETRQAWHVFSYRDYQTVTTNPLIFSSDFTSVFPVPSELALLMGPGTIGGIDPPR

HAPLRKLVSQAFTPRRIAQLELRIGQITADVLDQVRDQDRIDIASDLAYPLPVTVIAELLGI
PTKDHEKFREWVDIILSNEGLEYPNLPDDFTETVGPAIEEWSEFLYAQIAQKRAEPKDD
LISGLCAAEVDGRKLTDEEVVNIVALLLTAGHISSATLLSNLFLVLEEHPQAQAAVRADR
SLVPGVIEETLRYRSPFNCIFRILNEDTDIFGHPMRKGQMVIAWIASANRDTEVFTDPDT
FDIRRESNKHLAFGHGIHHCLGAFLARLEAKVFLNQTLDQFTEFRIDHAGVEFYDADQL
TARRLPVQVVRDGRHPKEFVLHRHQPVTIGEPAARAVSRTVTVERLDRIADDVLRLVL
RDAGGKTLPTWTPGAHIDLDLGALSRQYSLCGAPDAPSYEIAVHLDPESRGGSRYIHE
QLEVGSPLRMRGPRNHFALDPGAEHYVFVAGGIGITPVLAMADHARARGWSYELHYC
GRNRSGMAYLERVAGHGDRAALHVSEEGTRIDLAALLAEPAPGVQIYACGPGRLLAGL
EDASRNWPDGALHVEHFTSSLAALDPDVEHAFDLELRDSGLTVRVEPTQTVLDALRAN
NIDVPSDCEEGLCGSCEVAVLDGEVDHRDTVLTKAERAANRQMMTCCSRACGDRLAL
RL

The following is the primary amino acid sequence of the entire translated JuvD-RhFRED protein (yellow = N-terminal His-tag; red = JuvD; green = RhFRED):

MGSSHHHHHHSSGLVPRGSHMEHPVTAGSCRFYPFSDRTDLNIDPTYGELRSKEPVA
RVRMPYGGDAWLVTRHADAKKALSDPRLSIAAGAGRDVPRASPRLQEPDGLMGLPP
DAHARLRRLVATAFTPKRVRDIAPRVVQLADQLLDDVVETGPPADLVQQLALPLPVMII
CEMMGIGYDEQHLFRAFSDALMSSTRYTADQVDRAVEDFVEYLGGLLAQRRAHRTDD
LLGALVEARDDGDRLTEDELVMLTGGLLVGGHETTASQIASQIFLLLRDRTRYDQLHAR
PELIPTAVEELLRVAPLWASVGPTRIATEDLELNGTTIRAGDAVVFSLASANQDDDVFA
NAADVVLDRDPNPHIAFGHGPHYCIGASLARLEIQAAIGTLARRLPGLRLAVEENELEW
NKGMMVRSLVSLPVTWEFVLHRHQPVTIGEPAARAVSRTVTVERLDRIADDVLRLVLR
DAGGKTLPTWTPGAHIDLDLGALSRQYSLCGAPDAPSYEIAVHLDPESRGGSRYIHEQ
LEVGSPLRMRGPRNHFALDPGAEHYVFVAGGIGITPVLAMADHARARGWSYELHYCG
RNRSGMAYLERVAGHGDRAALHVSEEGTRIDLAALLAEPAPGVQIYACGPGRLLAGLE
DASRNWPDGALHVEHFTSSLAALDPDVEHAFDLELRDSGLTVRVEPTQTVLDALRAN
NIDVPSDCEEGLCGSCEVAVLDGEVDHRDTVLTKAERAANRQMMTCCSRACGDRLAL
RL

The following is the primary amino acid sequence of the entire translated TylI-RhFRED protein (yellow = N-terminal His-tag; red = TylI; green = RhFRED):

MGSSHHHHHHSSGLVPRGSHMTTQTLEAEKPPEPERTANSVHPLAQPAGAGARGLL
EWFARARAEAPVFWDESRQAWQVFRYDDYLTVSTNPQLFSSDFSPVFPVPEELAILM
GPGTFGGIDPPRHGPLRKLVSQAFTPRRIATLEPRIAEITRGLLDGLREKGQIDVVSDLA
YPLPVIVIAELLGIPAEDRDLFREWVDVILNNEGMEYPNLPDDFSETMGPAIKEWGDYL
YRRIALKRETPTDDLMSGLIEAEVEGRRLTDEEIVNIVALLLTAGHISSATLLGNLFLVLD
EHREAQAELRADRDLIPGAIEETLRYRSPFNNIFRLLKEDTDILGHPMKAGQMVVAWIA
SANRDSAHFSDPDTFDVRRQPNKHMSFGHGIHHCLGSFLARLEAKVFLELFFDEFSDY
RVEHDEVEFYEEDELTARRLPVTVTRHEFVLHRHQPVTIGEPAARAVSRTVTVERLDRI
ADDVLRLVLRDAGGKTLPTWTPGAHIDLDLGALSRQYSLCGAPDAPSYEIAVHLDPES
RGGSRYIHEQLEVGSPLRMRGPRNHFALDPGAEHYVFVAGGIGITPVLAMADHARAR
GWSYELHYCGRNRSGMAYLERVAGHGDRAALHVSEEGTRIDLAALLAEPAPGVQIYA
CGPGRLLAGLEDASRNWPDGALHVEHFTSSLAALDPDVEHAFDLELRDSGLTVRVEP

TQTVLDALRANNIDVPSDCEEGLCGSCEVAVLDGEVDHRDTVLTKAERAANRQMMTC
CSRACGDRLALRL

C.2 Protein expression and purification

Expression and purification of TylI-RhFRED for large-scale reactions

Plasmid pET28b_TylI-RhFRED was transformed into *E. coli* BL21(DE3) cells, and an individual colony was selected for overnight growth (37 °C) in 500 mL of LB containing kanamycin (50 μg/mL). 24 x 1.5 L of LB (2.8 L baffled Fernbach flasks) supplemented with kanamycin (50 μg/mL), thiamine (1 mM), and $FeCl_3$ (100 μM) were each inoculated with 15 mL of overnight seed culture and incubated at 37 °C (160 rpm). When the OD_{600} reached 0.6-1.0, the cultures were cooled in an ice-water bath (15-20 min) before addition of IPTG (0.1 mM) and δ-aminolevulinic acid (1 mM). The cultures were grown at 18 °C for 18-20 h before the cells were harvested and stored at -80 °C until used for protein purification.

All subsequent steps were performed at 4 °C. The cells were thawed and resuspended in 360 mL of lysis buffer (50 mM NaH_2PO_4, 300 mM NaCl, 10 mM imidazole, 10% (v/v) glycerol, 1 mM PMSF, pH 8) prior to lysis in 80 mL batches using a sonic dismembrator (70% power, 5 s on, 5 s off, 5 min total on time). The crude lysate was centrifuged at 50,000 x g for 30 min to remove cellular debris, and the clarified lysate was incubated with 40 mL of Ni-NTA resin on a nutating shaker for 1-2 h. The resin slurry was loaded onto an empty column, and the lysate was pushed through with gentle syringe pressure. The resin was washed with 2 x 120 mL of wash buffer (50 mM NaH_2PO_4, 300 mM NaCl, 20 mM imidazole, 10% (v/v) glycerol, pH 8) to remove bulk protein contaminants prior to elution of TylI-RhFRED with 75 mL of elution buffer (50 mM NaH_2PO_4, 300 mM NaCl, 300 mM imidazole, 10% (v/v) glycerol, pH 8). The protein was subsequently concentrated using 50 kD MWCO centrifugal filters (Millipore) and desalted by loading onto PD-10 columns (GE Healthcare) and eluting with storage buffer (50 mM NaH_2PO_4, 1 mM EDTA, 0.2 mM DTT, 10% (v/v) glycerol, pH 7.3) according to the manufacturer's instructions. The purified enzyme was flash frozen in liquid N_2 and stored at -80 °C until used for large-scale reactions. The yield of functional P450 (as assessed by obtaining CO difference spectra according to the established protocol[2]) was ~12 mg per 1 L of overexpression culture.

Expression and purification of TylI-RhFRED and JuvC-RhFRED for analytical-scale reactions

A similar protocol was followed for the parallel expression and purification of TylI-RhFRED and JuvC-RhFRED for use in analytical-scale reactions. Plasmids pET28b_TylI-RhFRED and pET28b_JuvC-RhFRED were transformed into *E. coli* BL21(DE3) cells, and individual colonies were selected for overnight growth (37 °C) in 10 mL of LB containing kanamycin (50 μg/mL). 2 x 1 L of LB (2.8 L baffled Fernbach flasks) supplemented with kanamycin (50 μg/mL), thiamine (1 mM), and $FeCl_3$ (100 μM) were inoculated with the 10 mL of overnight seed cultures and incubated at 37 °C (160 rpm). When the OD_{600} reached 0.6-1.0, the cultures were cooled in an ice-water bath (15-20 min) before addition of IPTG (0.1 mM) and δ-aminolevulinic acid (1 mM). The cultures were grown at 18 °C for 20 h before the cells were harvested and stored at -80 °C until used for protein purification.

All subsequent steps were performed at 4 °C. Each cell pellet was thawed and resuspended in 20 mL of lysis buffer prior to sonication (70% power, 3 s on, 3 s off, 3 min total on time). The crude lysate was centrifuged at 50,000 x g for 30 min to remove cellular debris, and the clarified lysate was incubated with 4 mL of Ni-NTA resin on a nutating shaker for 1-2 h. The resin slurry was loaded onto an empty column, and the lysate was pushed through with gentle syringe pressure. The resin was washed with 3 x 20 mL of wash buffer prior to elution of P450 with 15 mL of elution buffer. The protein was concentrated (MWCO filters), desalted (PD-10 columns), aliquoted, flash frozen in liquid N_2, and stored at -80 °C until used for analytical-scale reactions. The yields of functional TylI-RhFRED and JuvC-RhFRED were ~17 mg and ~16 mg per 1 L of overexpression culture, respectively.

Expression and purification of JuvD-RhFRED and MycCI-RhFRED for analytical- and large-scale reactions

Plasmid pET28b_JuvD-RhFRED or the pET28b_MycCI-RhFRED plasmid previously generated (Appendix A)[3] was cotransformed along with pGro7 (Takara) into *E. coli* BL21(DE3) cells, and an individual colony was selected for overnight growth (37 °C) in 250 mL of TB containing kanamycin (50 μg/mL) and chloramphenicol (25 μg/mL).

12 x 1.5 L of TB (2.8 L baffled Fernbach flasks) supplemented with kanamycin (50 μg/mL), chloramphenicol (25 μg/mL), thiamine (1 mM), and glycerol (4% v/v) were each inoculated with 15 mL of overnight seed culture and incubated at 37 °C (160 rpm). When the OD_{600} reached 0.6-1.0, the cultures were cooled in an ice-water bath (15-20 min) before addition of IPTG (0.1 mM), δ-aminolevulinic acid (1 mM), and L-arabinose (0.5 g/L). The cultures were grown at 18 °C for 18-20 h before the cells were harvested and stored at -80 °C until used for protein purification, which was performed in an analogous manner to the procedure described for TylI-RhFRED with the following modifications. Cells were resuspended in 540 mL of lysis buffer prior to sonication. Clarified cell lysate was incubated on ice with 30 mL of Ni-NTA resin on a Belly Dancer shaker for 1-2 h. The resin was washed via peristaltic pump with 180 mL of wash buffer, and protein was eluted with 45 mL of elution buffer. The yields of functional JuvD-RhFRED and MycCI-RhFRED were ~9 mg and ~14 mg per 1 L of overexpression culture, respectively.

C.3 Analytical-scale enzymatic reactions

Analytical-scale enzymatic reactions were carried out under the following conditions: 5 μM P450-RhFRED, 500 μM substrate (2.5% DMSO, final concentration), 1 mM $NADP^+$, 5 mM glucose-6-phosphate, and 1 U/mL glucose-6-phosphate dehydrogenase in storage buffer (50 mM NaH_2PO_4, 1 mM EDTA, 0.2 mM DTT, 10% (v/v) glycerol, pH 7.3). The total volume of each reaction was 100 μL (1.7 mL Eppendorf tube), and reactions were incubated in the dark at 30 °C (200 rpm) for ~15 h prior to quenching by addition of 900 μL of methanol. Quenched reactions were centrifuged at 17,000 x g for 10 min (4 °C), and the supernatant was removed for LC-MS analysis. All reactions were performed and analyzed in duplicate. Negative control reactions performed in parallel lacked P450-RhFRED. All substrates were acquired as described previously (see Appendices A and B) or via large-scale enzymatic reactions as described below.

LC-MS analysis was performed on an Agilent Q-TOF HPLC-MS (Life Sciences Institute, University of Michigan) equipped with a high-resolution electrospray mass spectrometry (ESI-MS) source and a Beckmann Coulter reversed-phase HPLC system

using a Phenomenex Luna C18 column with the following specifications: dimensions, 150 x 3.0 mm; particle size, 5 µm; pore size, 100 Å. HPLC conditions were as follows: mobile phase (A = deionized water + 0.1% formic acid, B = 95% acetonitrile/deionized water + 0.1% formic acid); 10% B (pre-run) for 2.5 min, 10% to 100% B over 12.5 min, 100% B for 2.5 min, 10% B (post-run) for 2.5 min; flow rate, 0.4 mL/min; injection volume, 0.2 µL. Percent conversion values were determined by integrating extracted-ion chromatogram (EIC) peaks corresponding to $[M + H]^+$ ions for unreacted substrate and potential products. For reactions involving MycCI-RhFRED and JuvD-RhFRED, ions with masses corresponding to hydroxylation/epoxidation and/or demethylation of starting material were extracted. For reactions involving TylI-RhFRED and JuvC-RhFRED, ions with masses corresponding to products of sequential oxidation reactions on a given substrate (i.e., alcohol, aldehyde, carboxylic acid) and/or demethylation were extracted.

C.4 Biotransformation of tylactone (18) to DT (1) and isolation of iso-DT (13)

*Biotransformation of **18** to **1** in Streptomyces venezuelae DHS316*

The following biotransformation reaction was carried out in an analogous manner to the published procedure (Appendix A).[3] To 3 x 1 L of SCM medium (per 1 L in ddH_2O: 20 g soytone, 15 g soluble starch, 10.5 g MOPS, 1.5 g yeast extract, 0.1 g $CaCl_2$, pH 7.2) in 2.8 L baffled Fernbach flasks containing a stainless steel spring was added 100 µL (per 1 L culture) of *S. venezuelae* DHS316 spore stock. The cultures were incubated at 28 °C (180 rpm) until the OD_{600} reached ~0.1 (12-15 h), at which point 100 mg of **18** as a DMSO solution (50 mg/mL) was added to each 1 L culture followed by 2.5 mg of acetyl-narbonolide as a DMSO solution (20 mg/mL). The cultures were incubated at 28 °C for 24 h (180 rpm), after which time HPLC analysis of the culture supernatant indicated complete conversion of **18** to **1** (**Figure C.1**). The cultures were centrifuged at 6000 x g for 10 min, and the resulting supernatant was adjusted to pH 11 and extracted via incubation with Amberlite XAD16 resin (30 g of washed wet resin per 1 L of culture supernatant) overnight with shaking. The resin was collected, rinsed briefly with water, and extracted with ethyl acetate (3 x 400 mL). The combined organic extracts were washed with brine and dried over anhydrous Na_2SO_4. Solvent

was removed under reduced pressure to yield crude **1**, which was purified by flash chromatography (5% CH_3OH/CH_2Cl_2, SiO_2) to give a yellow foam. Further purification under the same conditions yielded pure **1** (0.294 g, 70.0%) as an off-white foam. This material was handled and stored in the dark to prevent photoisomerization to compound **13**. Spectral data were in accord with those previously reported (Appendix A).[3]

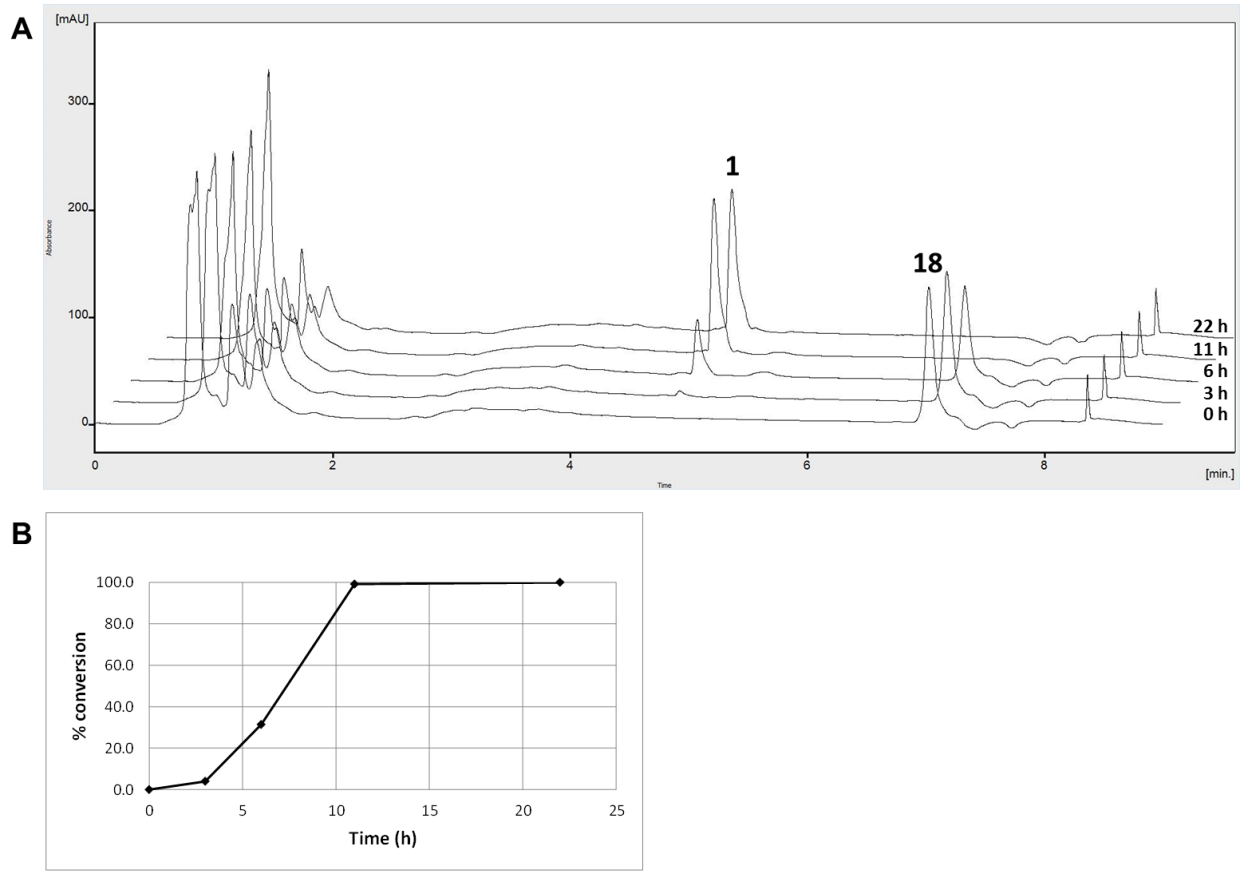

Figure C.1. One-step glycosylation of **18** to **1** via whole-cell biotransformation. (**A**) UV traces of the conversion of **18** to **1** at 0 h, 3 h, 6 h, 11 h, and 22 h post-addition of **18** and acetyl-narbonolide to a 1 L culture of biotransformation strain DHS316. Aliquots (1 mL) of the culture were removed at each time point and centrifuged (17,000 x g, 4 °C, 10 min). Methanol (0.5 mL) was added to the supernatant (0.5 mL), and the resulting mixture was briefly vortexed and centrifuged (17,000 x g, 4 °C, 10 min). The supernatant (50 µL) was analyzed by HPLC using a Phenomenex Luna C18 column (150 x 4.6 mm, 5 µm, 100 Å). HPLC conditions were as follows: mobile phase (A = H_2O + 0.1% formic acid, B = CH_3CN + 0.1% formic acid); 15% B for 1 min, 15% to 75% B over 5 min, 95% B for 1 min, 15% B for 2 min; flow rate, 2.0 mL/min; injection volume, 50 µL; wavelength, 285 nm. T_R **18** = 7.0 min. T_R **1** = 4.8 min. (**B**) Percent conversion of **18** to **1** as a function of time (h).

*Production and isolation of **13***

Following exposure of **1** dissolved in methanol to UV light for ~1 h (HPLC and ^1H NMR analysis indicated ~35% conversion of **1** to **13**), the mixture was purified by

preparative HPLC (isocratic 75% CH_3CN/H_2O + 0.1% Et_3N; flow rate: 8 mL/min; monitored at 288 nm) using a Phenomenex Luna C18 column (250 x 21.2 mm, 5 µm, 100 Å) to afford **13** and recovered **1** as semitransparent amorphous solids (isolated yields not quantified). T_R **1** = 32-37 min. T_R **13** = 40-44 min.

C.5 Large-scale P450 and chemical oxidation reactions

General procedure for P450-catalyzed oxidation reactions

Reactions with catalytically self-sufficient P450-RhFRED fusion enzymes were carried out in an analogous manner to the published procedure (Appendix A)[3] and in the dark to minimize photoisomerization of starting materials and products. To an Erlenmeyer flask containing reaction buffer (50 mM NaH_2PO_4, 1 mM EDTA, 0.2 mM DTT, 10% (v/v) glycerol, pH 7.3) pre-heated to 30 °C were added the following components sequentially: substrate (20 mM stock in DMSO, 0.5 mM final concentration), glucose-6-phosphate (100 mM stock in reaction buffer, 5 mM final concentration), glucose-6-phosphate dehydrogenase (100 U/mL stock in water, 1 U/mL final concentration), P450-RhFRED (varied stock concentrations, 5 µM final concentration), and $NADP^+$ (20 mM stock in reaction buffer, 1 mM final concentration). Reaction mixtures were capped with a milk filter and incubated at 30 °C overnight (typically 14-16 h) with gentle shaking (100 rpm). Prior to extraction, reaction mixtures were analyzed by LC-MS to determine the percent conversion of starting material to product. Subsequently, each reaction mixture was quenched by addition of acetone (2 x total reaction volume) and incubated at 4 °C for 2 h. The mixture was then filtered through Celite, and the acetone was removed under reduced pressure. The remaining aqueous solution was saturated with NaCl, adjusted to pH 11, and extracted with ethyl acetate (3 x total reaction volume). The combined organic layers were dried over anhydrous Na_2SO_4 and evaporated under reduced pressure to afford a crude mixture of product(s) and remaining starting material, which were purified directly by preparative HPLC using isocratic or shallow gradient elution methods (solvent system: CH_3CN/H_2O + 0.1% Et_3N; column: Phenomenex Luna C18 (250 x 21.2 mm, 5 µm, 100 Å); flow rate: 8 mL/min; monitored at 240 or 288 nm as specified).

*Juvenimicin B_1 (**2**)*

The enzymatic reaction with **1** as substrate (165.5 mg, 0.3000 mmol) was performed in a 2.8 L Fernbach flask (600 mL total reaction volume) using purified TylI-RhFRED as biocatalyst. Conversion as assessed by LC-MS was 80%. Following extraction of the reaction mixture, the crude material was purified by flash chromatography (10% CH_3OH/CH_2Cl_2 + 1% Et_3N, SiO_2) followed by preparative HPLC (isocratic 50% CH_3CN/H_2O + 0.1% Et_3N; monitored at 288 nm) to afford **2** (103.1 mg, 60.5%) as a semitransparent amorphous solid. T_R **2** = 36-44 min.

*M-4365 G_2 (**3**)*

The following reaction was carried out in an analogous manner to the published procedure[4,5] with minor modifications. To a stirring solution of **2** (42.6 mg, 0.0750 mmol) in CH_3CN (1.5 mL) in a 25 mL round-bottom flask were added the following solutions sequentially: $[Cu^I(MeCN)_4](OTf)$ (0.075 mmol, 1.5 mL CH_3CN), 2,2'-bipyridine (0.075 mmol, 1.5 mL CH_3CN), TEMPO (0.075 mmol, 1.5 mL CH_3CN), and 1-methylimidazole (0.15 mmol, 1.5 mL CH_3CN). The dark red/brown reaction mixture was stirred at room temperature open to air in the dark for 1.5 h. The mixture was subsequently concentrated to a dark green film and purified by flash chromatography (10% CH_3OH/CH_2Cl_2 + 1% Et_3N, SiO_2) followed by preparative HPLC (isocratic 60% CH_3CN/H_2O + 0.1% Et_3N, Phenomenex Luna C18 (250 x 21.2 mm, 5 µm, 100 Å), 8 mL/min, monitored at 288 nm) to afford **3** (24.2 mg, 57.1%) as a semitransparent amorphous solid. T_R **3** = 35-40 min.

*23-hydroxy-5-O-desosaminyl-tylactone (**7**)*

The enzymatic reaction with **1** as substrate (27.6 mg, 0.0500 mmol) was performed in a 500 mL Erlenmeyer flask (100 mL total reaction volume) using purified MycCI-RhFRED as biocatalyst. Conversion as assessed by LC-MS was 53%. The crude extract was purified by preparative HPLC (55% CH_3CN/H_2O + 0.1% Et_3N for 10 min, linear gradient up to 75% over 40 min, 75% hold for 30 min, column re-equilibration at 55% for 10 min; monitored at 288 nm) to afford **7** (11.0 mg, 38.7%, 54.0% BRSM) as

a semitransparent amorphous solid. T_R **7** = 27-29 min. T_R **1** = 57-60 min. Spectral data were in accord with those previously reported (Appendix A).[3]

*Juvenimicin B_3 (**8**)*

The enzymatic reaction with **2** as substrate (18.5 mg, 0.0326 mmol) was performed in a 250 mL Erlenmeyer flask (65 mL total reaction volume) using purified MycCI-RhFRED as biocatalyst. Conversion as assessed by LC-MS was 56%. The crude extract was purified by preparative HPLC (35% CH_3CN/H_2O + 0.1% Et_3N for 10 min, linear gradient up to 55% over 40 min, 55% hold for 30 min, column re-equilibration at 35% for 10 min; monitored at 288 nm) to afford **8** (10.0 mg, 52.6%, 77.8% BRSM) as a semitransparent amorphous solid. T_R **8** = 29-33 min. T_R **2** = 60-64 min.

*5-O-desosaminyl-tylonolide (**9**)*

The enzymatic reaction with **3** as substrate (18.4 mg, 0.0325 mmol) was performed in a 250 mL Erlenmeyer flask (65 mL total reaction volume) using purified MycCI-RhFRED as biocatalyst. Conversion as assessed by LC-MS was 67%. The crude extract was purified by preparative HPLC (40% CH_3CN/H_2O + 0.1% Et_3N for 10 min, linear gradient up to 60% over 40 min, 60% hold for 30 min, column re-equilibration at 40% for 10 min; monitored at 288 nm) to afford **9** (8.8 mg, 47%, 58% BRSM) as a semitransparent amorphous solid. T_R **9** = 30-34 min. T_R **3** = 64-68 min.

*M-4365 A_1 (**10**)*

The enzymatic reaction with **1** as substrate (27.6 mg, 0.0500 mmol) was performed in a 500 mL Erlenmeyer flask (100 mL total reaction volume) using purified JuvD-RhFRED as biocatalyst. Conversion as assessed by LC-MS was 95%. The crude extract was purified by preparative HPLC (isocratic 65% CH_3CN/H_2O + 0.1% Et_3N; monitored at 240 nm) to afford **10** (15.7 mg, 55.3%) as a semitransparent amorphous solid. T_R **10** = 39-44 min.

*Juvenimicin A_4 (**11**)*

The enzymatic reaction with **2** as substrate (18.5 mg, 0.0326 mmol) was performed in a 250 mL Erlenmeyer flask (65 mL total reaction volume) using purified JuvD-RhFRED as biocatalyst. Conversion as assessed by LC-MS was 99%. The crude extract was purified by preparative HPLC (isocratic 45% CH_3CN/H_2O + 0.1% Et_3N; monitored at 240 nm) to afford **11** (11.9 mg, 62.6%) as a semitransparent amorphous solid. T_R **11** = 38-43 min.

*Juvenimicin A_3 (**12**)*

The enzymatic reaction with **3** as substrate (18.4 mg, 0.0325 mmol) was performed in a 250 mL Erlenmeyer flask (65 mL total reaction volume) using purified JuvD-RhFRED as biocatalyst. Conversion as assessed by LC-MS was 97%. The crude extract was purified by preparative HPLC (isocratic 50% CH_3CN/H_2O + 0.1% Et_3N; monitored at 240 nm) to afford **12** (8.1 mg, 43%) as a semitransparent amorphous solid. T_R **12** = 45-52 min.

*12,13-epoxy-M-VIII (**15**) and 14-hydroxy-M-VIII (**16**)*

The enzymatic reaction with M-VIII (**14**) as substrate (72.1 mg, 0.143 mmol) was performed in a 2 L Erlenmeyer flask (285 mL total reaction volume) using purified JuvD-RhFRED as biocatalyst. Conversion as assessed by LC-MS was 68% (59% **15** + 9% **16**). The crude extract was purified by preparative HPLC (55% CH_3CN/H_2O + 0.1% Et_3N for 10 min, linear gradient up to 75% over 40 min, 75% hold for 30 min, column re-equilibration at 55% for 10 min; monitored at 240 and 288 nm) to afford **15** (32.9 mg, 44.2%, 63.1% BRSM) and **16** (7.1 mg, 9.5%, 13.6% BRSM) as semitransparent amorphous solids. T_R **15** = 48-51 min. T_R **16** = 27-29 min. T_R **14** = 56-59 min.

*Hydroxy-narbomycin (hydroxy-**20**)*

The enzymatic reaction with narbomycin (**20**) as substrate (59.9 mg, 0.118 mmol) was performed in a 2 L Erlenmeyer flask (235 mL total reaction volume) using purified JuvD-RhFRED as biocatalyst. Conversion as assessed by LC-MS was 35%. The crude extract was purified by preparative HPLC (45% CH_3CN/H_2O + 0.1% Et_3N for 10 min,

linear gradient up to 65% over 40 min, 65% hold for 30 min, column re-equilibration at 45% for 10 min; monitored at 240 nm) to afford hydroxy-**20** (12.5 mg, 20.2%, 34.2% BRSM) as a semitransparent amorphous solid. T_R hydroxy-**20** = 28-31 min. T_R **20** = 60-64 min.

C.6 Antimicrobial activity assay

10 mM DMSO stock solutions of each compound were serially diluted two-fold in DMSO to create stock solutions of each ranging in concentration from 0.61 μM to 10 mM. Each of these stock solutions was further diluted 10-fold in water to make working solutions with concentrations ranging from 61 nM to 1000 μM. After overnight growth (37 °C) of the target strains on solid media, cultures were grown (37 °C, 200 rpm) in appropriate liquid media. Overnight seed cultures were diluted to an OD_{600} of 0.05 and subsequently grown to an OD_{600} of ~0.5 (37 °C, 200 rpm) prior to dilution to an OD_{600} of 0.004. These diluted cultures (45 μL per well) were applied to clear 384-well plates (Thermo Scientific) charged with working antibiotic solutions (5 μL per well), incubated at 37 °C for 16 h, and assessed by OD_{600} measurements. Each combination was performed in duplicate. Results are shown in **Table C.3**.

C.7 Supplemental tables and figures

Table C.2. Results of activity assays performed with MycCI-RhFRED, JuvD-RhFRED, TylI-RhFRED, and JuvC-RhFRED showing total *N*-demethylation activity on selected substrates.[a]

Compound	MycCI-RhFRED	JuvD-RhFRED	TylI-RhFRED	JuvC-RhFRED
1	0.1	0.2	0.3	0.1
2	0.2	0.3	0.4	0.3
3	1.0	1.2	1.0	0.9
4	0.2	1.1	0.4	0.3
5	0.3	0.5	0.7	0.7
6	1.2	1.2	0.8	0.5
7	--[b]	1.0	0.9	0.8
8	--	2.0	0.6	0.7
9	--	8.6	1.6	1.9
10	0.3	--	1.3	0.7
11	0.3	--	0.4	0.4
12	1.0	--	1.5	1.8
13	0.5	8.3	1.8	1.9
14	0.1	0.3	--	--
15	0.2	0.8	--	--
16	0.3	0.4	--	--
19	0.4	0.9	--	--
20	0.4	0.7	--	--

[a]Each value (average of duplicate experiments) indicates total percent of *N*-demethylated starting material and product(s) in the reaction mixture.
[b]Blank space (--) indicates that the corresponding reaction was not performed.

Table C.3. Results of antimicrobial assays performed with the 16-membered ring macrolides generated in Chapter 4.[a]

		Compound											
Bacterial strain	Media[b]	**Tylosin**	**Erythromycin**	**13**	**1**	**7**	**10**	**2**	**8**	**11**	**3**	**9**	**12**
Gram positive													
B. subtilis DHS 5333	1	1.6	0.781	>100	>100	>100	>100	>100	>100	>100	3.1	3.1	1.6
B. subtilis 168	1	1.6	0.781	>100	>100	100	100	>100	>100	100	3.1	12.5	0.781
B. anthracis 34f2	1	0.781	3.1	>100	50	50	50	100	>100	50	1.6	3.1	0.781
B. cereus	1	6.3	6.3	>100	>100	100	100	100	>100	100	6.3	25	3.1
S. aureus ATCC 6538P	1	1.6	0.781	>100	50	50	50	50	100	100	1.6	3.1	0.781
S. aureus NorA	1	6.3	1.6	>100	12.5	12.5	25	50	25	25	3.1	3.1	1.6
Methicillin-resistant *S. aureus* ATCC 43300	1	>100	>100	>100	>100	>100	>100	>100	>100	>100	>100	>100	>100
E. faecalis ATCC 29212	2	12.5	25	>100	>100	>100	>100	>100	>100	>100	25	6.3	6.3
Vancomycin-resistant *Enterococcus*	2	6.3	12.5	>100	>100	50	>100	>100	>100	>100	3.1	3.1	3.1
L. monocytogenes ATCC 19115	2	12.5	6.3	>100	>100	100	>100	>100	>100	>100	25	12.5	6.3
K. rhizophilia ATCC 9341	2	0.781	0.781	>100	12.5	6.3	25	12.5	12.5	12.5	0.781	0.391	0.781
S. pneumoniae ATCC 49619	3	1.6	0.781	>100	25	12.5	25	50	25	25	0.781	0.781	0.781
S. pneumoniae ATCC BAA-1409	3	>100	>100	>100	>100	>100	>100	>100	>100	>100	>100	>100	>100
S. pneumoniae D39	3	0.781	0.781	>100	6.3	3.1	12.5	6.3	6.3	6.3	0.195	0.391	0.781
Gram negative													
E. coli TolC	1	1.6	0.781	100	1.6	1.6	3.1	1.6	3.1	3.1	0.391	0.391	0.391
E. coli MC1061	1	25	12.5	50	1.6	0.781	1.6	1.6	1.6	1.6	1.6	1.6	1.6
S. enterica ATCC 14028	1	>100	>100	>100	>100	>100	>100	>100	>100	>100	>100	>100	100
S. flexneri BS103	1	>100	100	>100	>100	>100	>100	>100	>100	>100	50	50	25
K. pneumoniae ATCC 29665	1	>100	>100	>100	>100	>100	>100	>100	>100	>100	100	>100	100
A. baumannii ATCC 17978	1	>100	100	>100	>100	>100	>100	>100	>100	>100	100	>100	100

[a]Reported values are minimum inhibitory concentrations (MICs, μM).

[b]Media composition (solid, seed culture, MIC culture): 1 (LB agar, Mueller-Hinton broth, Mueller-Hinton broth); 2 (TSA, BHI broth, BHI broth); 3 (blood agar, 5% blood broth, 0.5% blood broth).

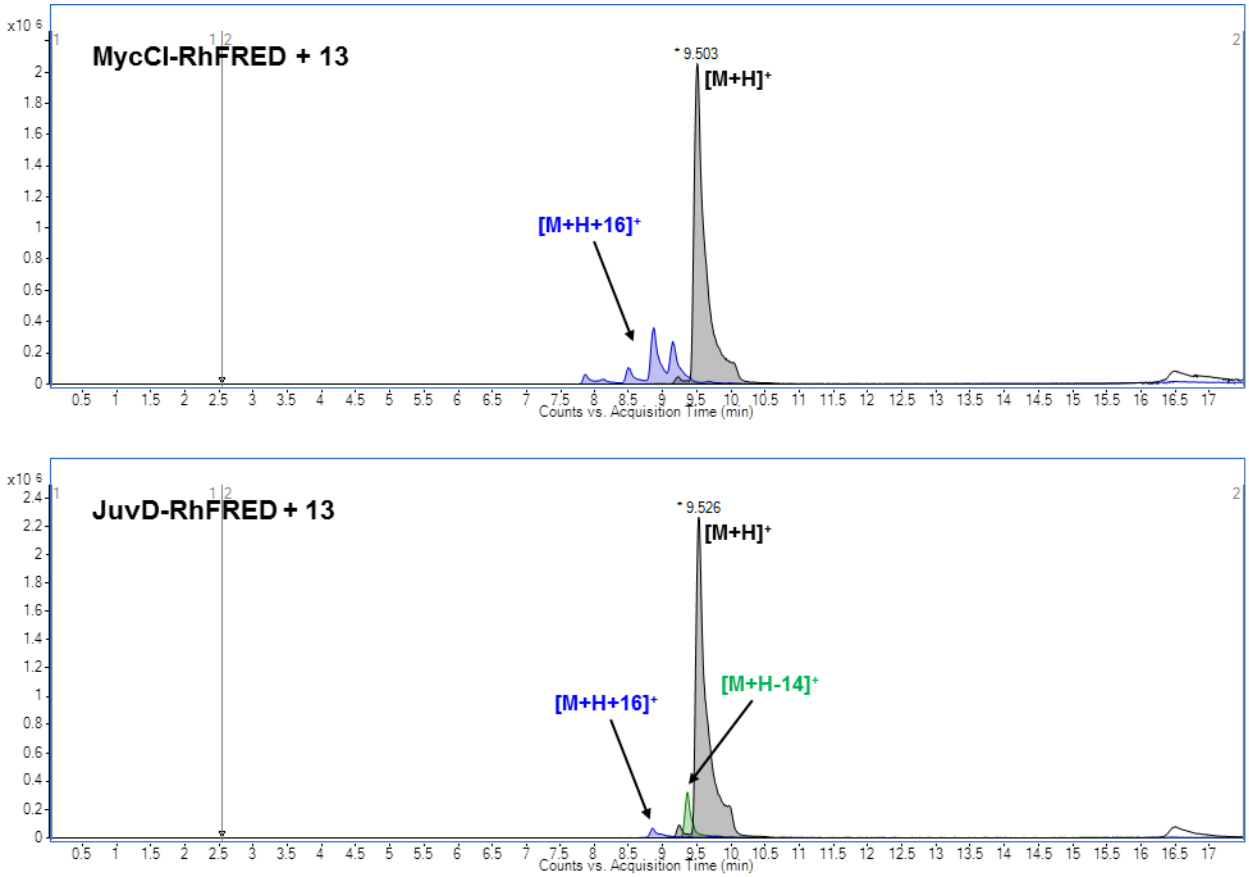

Figure C.2. LC-MS analysis of reactions between MycCl-RhFRED/JuvD-RhFRED and iso-DT (**13**).

C.8 HRMS and NMR data for compounds 2, 3, 8–13, 15, and 16

Position	δ_C (ppm)	δ_H (ppm), multi (*J* in Hz)
1	174.8	
2	41.0	2.04, dd (17.3, 1.2)
		2.47, dd (17.3, 9.9)
3	68.2	3.75, d (9.8)
4	42.5	1.71, m
5	80.5	3.67, d (9.7)
6	35.0	1.45, m
7	34.7	1.49, m
		1.80, t (12.6)
8	46.4	2.66, m
9	206.8	
10	119.8	6.47, d (15.4)
11	149.8	7.25, d (15.5)
12	134.9	
13	147.8	5.67, d (10.5)
14	40.0	2.79, tq (10.2, 6.5)
15	79.9	4.68, td (9.6, 2.6)
16	25.7	1.58, m
		1.87, m
17	10.0	0.94, t (7.3)
18	9.7	1.04, d (6.9)
19	32.8	1.58, m
		1.95, m
20	61.4	3.54, m
		3.63, ddd (11.6, 7.4, 4.7)
21	18.0	1.22, d (6.8)
22	13.1	1.85, d (1.2)
23	16.4	1.08, d (6.5)
1'	105.7	4.23, d (7.3)
2'	72.3	3.25, dd (10.3, 7.3)
3'	65.8	2.61, ddd (12.3, 10.3, 4.3)
4'	32.0	1.24, m
		1.73, m
5'	70.2	3.52, m
6'	21.4	1.20, d (6.0)
7'	40.9	2.32, s

*Solvent: CD_3OD

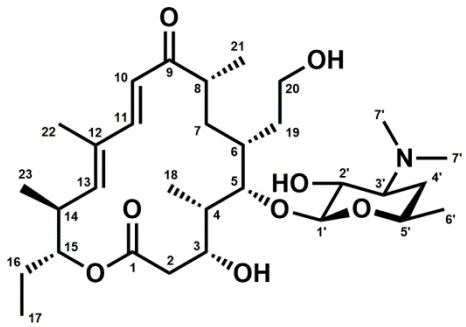

2

HRMS: *m/z* calculated $[M + H]^+$ 568.3844, found 568.3857

Position	δ_C (ppm)	δ_H (ppm), multi (*J* in Hz)
1	174.2	
2	39.6	1.93, d (16.8)
		2.50, dd (16.9, 10.5)
3	67.3	3.84, dd (10.1, 2.1)
4	41.1	1.71, m
5	81.2	3.67, d (10.0)
6	31.4	2.05, t (10.7)
7	32.6	1.57, ddd (15.1, 12.1, 3.8)
		1.74, m
8	45.2	2.54, m
9	203.5	
10	118.3	6.28, d (15.4)
11	148.3	7.29, d (15.4)
12	133.4	
13	146.1	5.65, d (10.4)
14	39.0	2.70, tq (10.2, 6.5)
15	78.7	4.69, td (9.6, 2.6)
16	24.9	1.53, m
		1.82, dqd (14.7, 7.4, 2.6)
17	9.8	0.91, t (7.3)
18	8.9	1.07, d (6.7)
19	43.9	2.44, m
		2.99, ddd (18.1, 10.5, 1.9)
20	203.7	9.70, s
21	17.7	1.19, d (7.3)
22	13.0	1.77, d (1.2)
23	16.3	1.06, d (6.6)
1'	104.3	4.19, d (7.3)
2'	70.5	3.19, dd (10.2, 7.3)
3'	65.8	2.47, m
4'	28.6	1.22, m
		1.64, m
5'	69.7	3.44, m
6'	21.2	1.19, d (5.9)
7'	40.4	2.27, s

*Solvent: $CDCl_3$

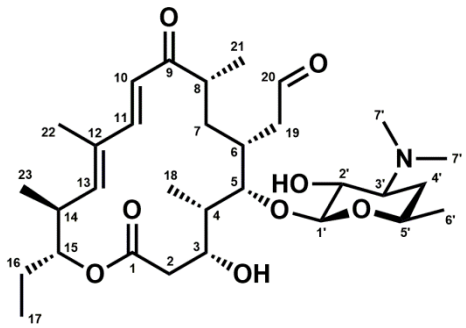

3

HRMS: *m/z* calculated $[M + H]^+$ 566.3687, found 566.3691

Position	δ_C (ppm)	δ_H (ppm), multi (*J* in Hz)
1	174.7	
2	41.0	2.05, d (17.1)
		2.48, dd (17.2, 9.9)
3	68.2	3.76, d (9.8)
4	42.5	1.73, m
5	80.5	3.68, m
6	35.0	1.49, m
7	34.6	1.49, m
		1.80, t (12.5)
8	46.4	2.67, m
9	206.8	
10	119.9	6.48, d (15.4)
11	149.8	7.30, d (15.5)
12	136.6	
13	144.3	5.92, d (10.5)
14	48.3	2.86, tt (10.2, 4.8)
15	76.3	4.95, td (9.9, 2.7)
16	26.2	1.62, m
		1.90, m
17	10.0	0.95, t (7.3)
18	9.7	1.04, d (6.9)
19	32.8	1.58, m
		1.95, m
20	61.4	3.54, m
		3.63, ddd (11.6, 7.3, 4.6)
21	17.9	1.22, d (7.0)
22	13.2	1.87, d (1.2)
23	62.6	3.68, m
1'	105.7	4.23, d (7.3)
2'	72.3	3.25, dd (10.2, 7.3)
3'	65.8	2.62, m
4'	32.0	1.24, m
		1.73, m
5'	70.2	3.52, m
6'	21.4	1.21, d (6.2)
7'	40.9	2.33, s

*Solvent: CD_3OD

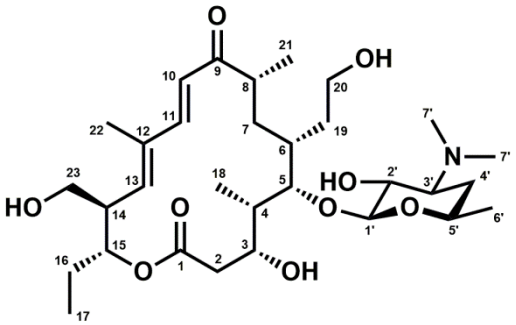

8

HRMS: *m/z* calculated $[M + H]^+$ 584.3793, found 584.3805

Position	δ_C (ppm)	δ_H (ppm), multi (*J* in Hz)
1	174.0	
2	39.7	1.95, d (16.7)
		2.52, dd (16.8, 10.4)
3	67.3	3.86, d (10.4)
4	41.2	1.72, m
5	81.2	3.68, d (10.0)
6	31.4	2.06, t (10.8)
7	32.6	1.58, m
		1.74, m
8	45.1	2.55, m
9	203.6	
10	118.8	6.31, d (15.4)
11	147.9	7.33, d (15.5)
12	136.4	
13	141.6	5.86, d (10.5)
14	47.5	2.88, tdd (10.5, 6.6, 4.1)
15	74.9	4.93, td (9.7, 2.7)
16	25.7	1.61, m
		1.84, m
17	9.8	0.94, t (7.3)
18	8.9	1.08, d (6.8)
19	43.9	2.45, m
		3.01, ddd (18.2, 10.4, 1.8)
20	203.7	9.71, s
21	17.7	1.20, d (4.9)
22	13.2	1.81, d (1.2)
23	62.7	3.74, m
1'	104.3	4.20, d (7.3)
2'	70.5	3.18, dd (10.2, 7.3)
3'	65.8	2.45, m
4'	28.4	1.22, m
		1.63, m
5'	69.8	3.44, m
6'	21.2	1.19, d (4.3)
7'	40.4	2.25, s

*Solvent: $CDCl_3$

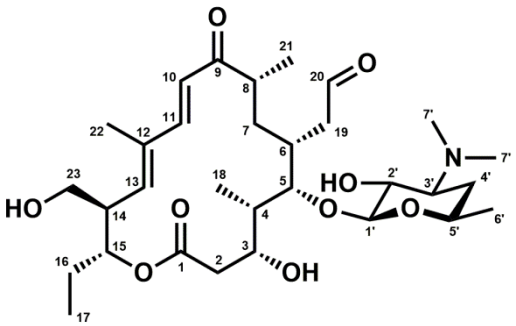

9

HRMS: *m/z* calculated $[M + H]^+$ 582.3637, found 582.3642

Position	δ_C (ppm)	δ_H (ppm), multi (*J* in Hz)
1	174.5	
2	41.3	2.27, dd (17.5, 1.2)
		2.61, dd (17.2, 10.5)
3	67.9	3.80, d (10.3)
4	42.3	1.86, m
5	80.2	3.73, d (9.8)
6	40.4	1.18, m
7	34.1	1.42, ddd (15.1, 11.7, 4.1)
		1.86, m
8	46.8	2.66, m
9	204.1	
10	124.8	6.43, d (15.7)
11	151.9	6.70, d (15.7)
12	61.2	
13	69.6	2.83, d (9.7)
14	39.1	1.74, m
15	77.9	4.86, td (9.7, 2.7)
16	25.6	1.54, m
		1.82, m
17	9.5	0.91, t (7.4)
18	10.1	1.10, d (6.9)
19	22.2	1.41, m
		1.68, m
20	12.5	0.86, t (7.2)
21	17.8	1.17, d (6.9)
22	15.3	1.47, s
23	14.6	1.12, d (6.7)
1'	105.7	4.25, d (7.3)
2'	72.3	3.25, dd (10.2, 7.3)
3'	65.9	2.63, m
4'	31.9	1.24, m
		1.74, m
5'	70.1	3.52, dtt (12.5, 6.3, 3.1)
6'	21.4	1.20, d (6.2)
7'	40.9	2.33, s

*Solvent: CD_3OD

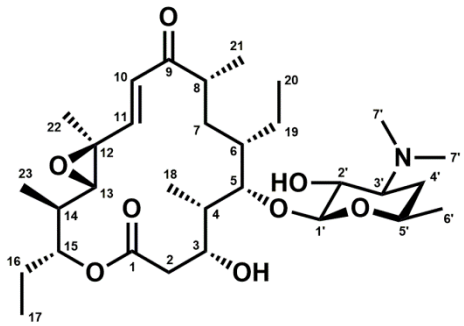

10

HRMS: *m/z* calculated $[M + H]^+$ 568.3844, found 568.3856

Position	δ_C (ppm)	δ_H (ppm), multi (*J* in Hz)
1	174.1	
2	41.1	2.25, d (17.5)
		2.60, dd (17.7, 10.3)
3	67.6	3.82, d (10.3)
4	42.4	1.88, m
5	80.7	3.65, d (9.5)
6	34.4	1.52, m
7	33.8	1.43, ddd (15.3, 11.7, 3.8)
		1.92, m
8	46.7	2.67, m
9	203.9	
10	124.7	6.43, d (15.7)
11	152.1	6.71, d (15.7)
12	61.2	
13	69.7	2.83, d (9.7)
14	39.1	1.74, m
15	77.9	4.84, td (9.6, 2.7)
16	25.6	1.54, m
		1.82, dqd (14.7, 7.5, 2.8)
17	9.5	0.91, t (7.4)
18	10.0	1.09, d (6.8)
19	32.8	1.58, m
		2.00, dddd (14.1, 10.5, 6.1, 4.5)
20	61.3	3.54, m
		3.64, m
21	17.8	1.18, d (6.9)
22	15.3	1.47, s
23	14.6	1.12, d (6.7)
1'	105.7	4.26, d (7.3)
2'	72.3	3.25, dd (10.3, 7.3)
3'	65.8	2.63, m
4'	31.9	1.24, m
		1.73, m
5'	70.2	3.52, m
6'	21.4	1.21, d (6.2)
7'	40.8	2.33, s

*Solvent: CD_3OD

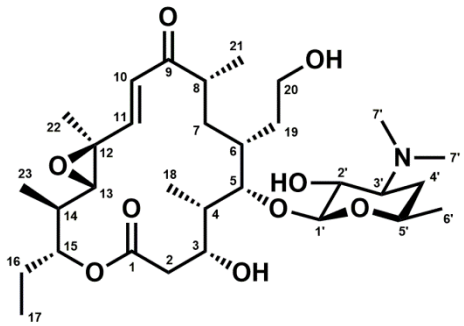

11

HRMS: *m/z* calculated $[M + H]^+$ 584.3793, found 584.3807

Position	δ_C (ppm)	δ_H (ppm), multi (*J* in Hz)
1	173.6	
2	39.8	2.09, d (16.8)
		2.64, dd (17.0, 10.6)
3	66.8	3.91, d (10.6)
4	41.4	1.81, m
5	81.2	3.70, d (10.0)
6	31.3	2.10, m
7	31.9	1.55, ddd (16.4, 12.8, 4.2)
		1.80, m
8	45.2	2.56, m
9	200.5	
10	122.8	6.44, d (15.7)
11	151.0	6.54, d (15.7)
12	59.8	
13	68.1	2.82, d (9.7)
14	38.0	1.70, tq (10.3, 6.8)
15	76.9	4.87, td (9.6, 2.7)
16	24.8	1.50, m
		1.79, m
17	9.2	0.89, t (7.4)
18	9.1	1.14, d (6.7)
19	43.9	2.46, m
		3.07, ddd (18.3, 10.4, 1.6)
20	203.2	9.72, s
21	17.6	1.16, d (6.9)
22	15.2	1.42, s
23	14.7	1.14, d (6.7)
1'	104.5	4.22, d (7.3)
2'	70.5	3.18, dd (10.2, 7.3)
3'	65.8	2.46, m
4'	28.4	1.22, m
		1.64, ddd (12.6, 4.1, 2.0)
5'	69.8	3.44, dqd (12.3, 6.1, 1.8)
6'	21.2	1.19, d (6.2)
7'	40.4	2.26, s

*Solvent: $CDCl_3$

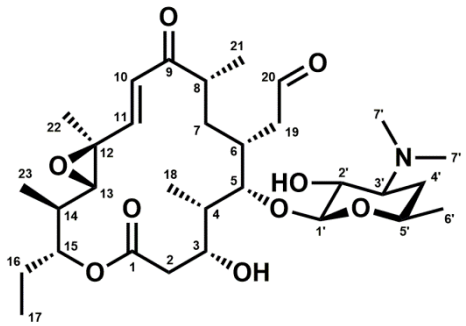

12

HRMS: *m/z* calculated $[M + H]^+$ 582.3637, found 582.3647

Position	δ_C (ppm)	δ_H (ppm), multi (*J* in Hz)
1	173.8	
2	42.1	2.26, d (13.5)
		2.49, dd (14.3, 9.3)
3	69.0	3.76, m
4	42.9	1.57, m
5	79.6	3.74, d (9.4)
6	41.2	1.59, m
7	38.1	1.21, m
		1.61, m
8	44.0	3.07, m
9	208.4	
10	128.6	6.29, d (15.7)
11	140.6	7.67, d (15.7)
12	133.2	
13	144.5	5.62, d (9.9)
14	37.5	2.91, ddq (9.6, 6.8, 6.8)
15	79.1	4.69, td (8.2, 3.1)
16	24.6	1.60, m
		1.76, m
17	9.6	0.92, t (7.4)
18	9.1	1.02, d (7.0)
19	24.6	1.46, m
		1.84, m
20	13.1	0.95, t (7.3)
21	17.3	1.07, d (6.6)
22	20.4	1.89, d (1.3)
23	16.2	1.05, d (6.7)
1'	105.7	4.21, d (7.3)
2'	72.1	3.24, dd (10.2, 7.3)
3'	65.8	2.61, ddd (12.2, 10.1, 4.2)
4'	32.1	1.24, m
		1.73, m
5'	70.0	3.53, m
6'	21.5	1.21, d (6.1)
7'	40.9	2.32, s

*Solvent: CD_3OD

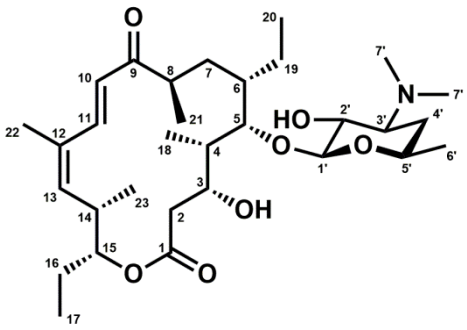

13

HRMS: *m/z* calculated $[M + H]^+$ 552.3895, found 552.3898

Position	δ_C (ppm)	δ_H (ppm), multi (*J* in Hz)
1	167.8	
2	121.8	6.04, d (15.4)
3	153.0	6.62, dd (15.4, 10.6)
4	42.8	2.83, tq (10.4, 6.6)
5	87.7	3.38, dd (9.4, 1.8)
6	35.6	1.12, m
7	32.9	1.55, m
		1.79, m
8	46.2	2.53, m
9	203.7	
10	127.5	6.88, d (15.4)
11	145.2	6.32, dd (15.4, 9.4)
12	59.9	3.38, dd (9.4, 1.8)
13	63.9	2.70, dd (9.1, 1.9)
14	43.2	1.40, ddq (10.9, 9.2, 6.8)
15	76.9	4.90, ddd (11.0, 8.3, 2.9)
16	25.8	1.52, m
		1.82, m
17	9.3	0.88, t (7.4)
18	19.5	1.24, d (6.6)
19	17.7	0.99, d (6.8)
20	17.7	1.18, d (6.9)
21	14.5	1.12, d (6.8)
1'	106.3	4.28, d (7.3)
2'	72.2	3.27, dd (10.2, 7.3)
3'	65.9	2.62, ddd (12.2, 10.1, 4.2)
4'	31.9	1.25, m
		1.74, ddd (12.9, 4.3, 1.9)
5'	70.1	3.53, dqd (12.3, 6.1, 1.8)
6'	21.4	1.21, d (6.2)
7'	40.9	2.33, s

*Solvent: CD_3OD

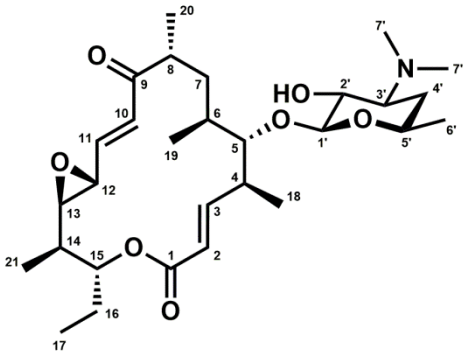

15

12,13-epoxy-M-VIII (15)
600 MHz (CD3OD)

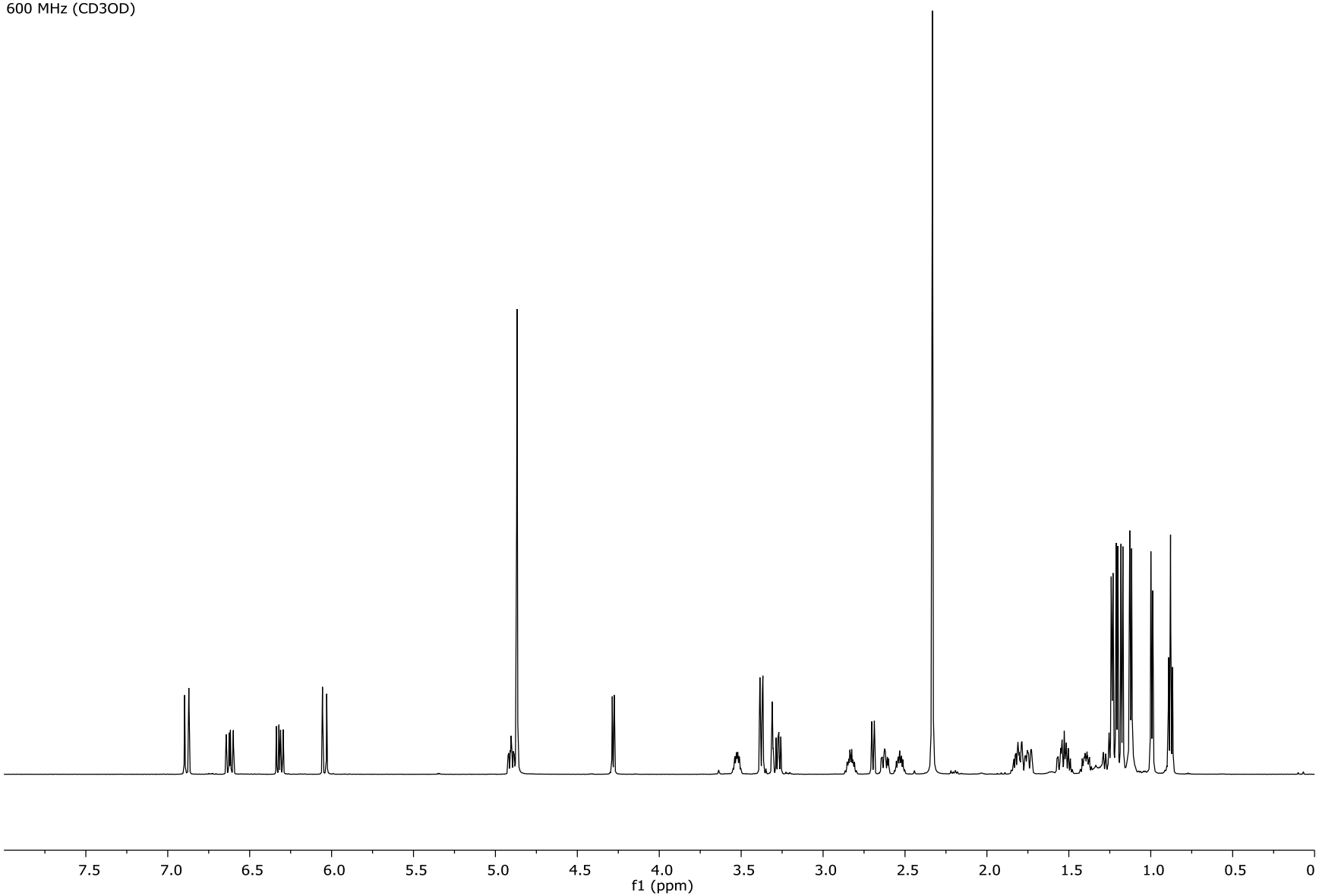

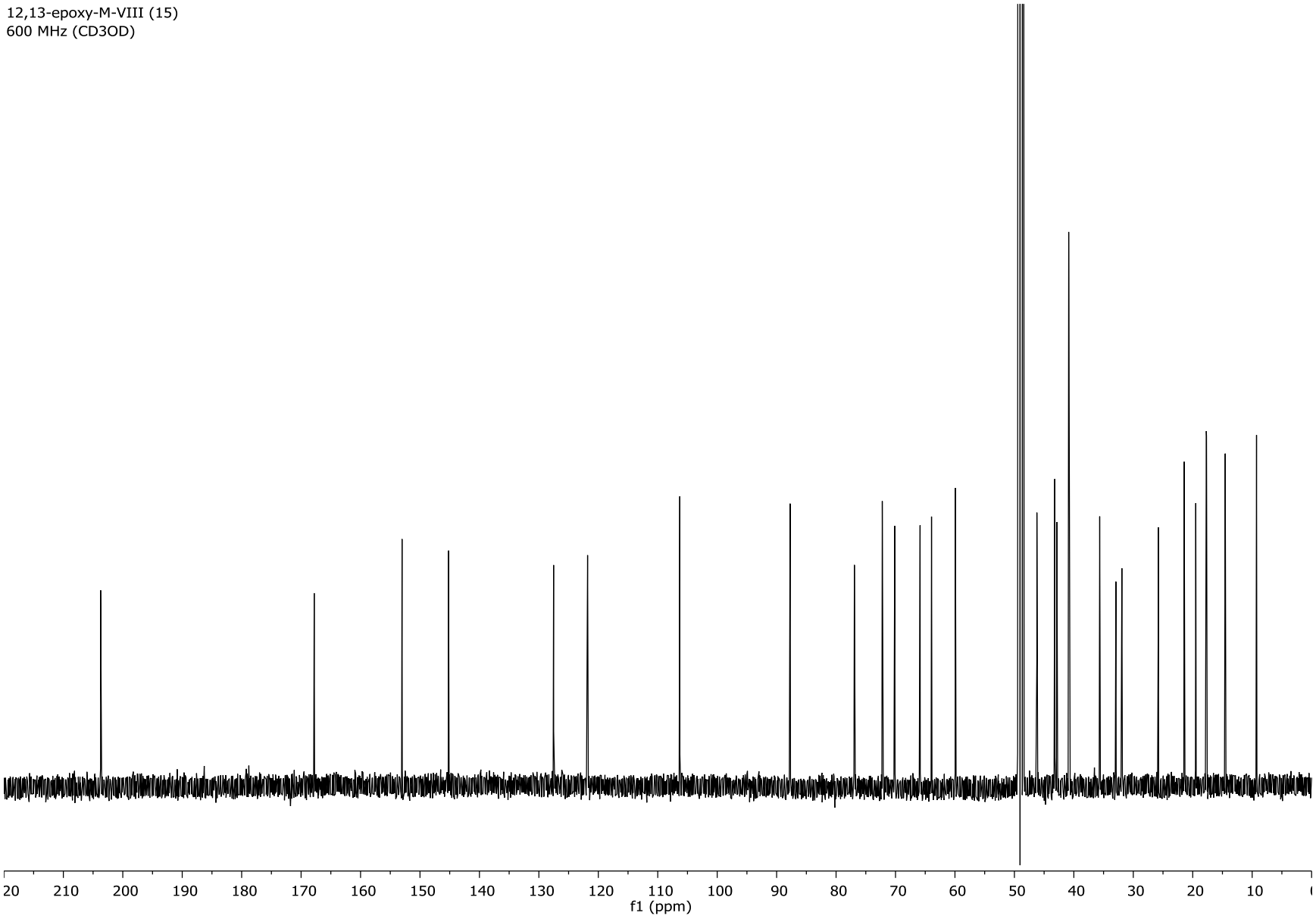
12,13-epoxy-M-VIII (15)
600 MHz (CD3OD)
220
210
200
190
180
170
160
150
140
130
120
110
100
90
80
70
60
50
40
30
20
10
f1 (ppm)

Position	δ_C (ppm)	δ_H (ppm), multi (*J* in Hz)
1	168.5	
2	122.3	5.89, d (15.5)
3	153.5	6.60, dd (15.5, 9.9)
4	42.3	2.78, tq (10.2, 7.0)
5	88.2	3.35, dd (10.2, 1.4)
6	35.5	1.20, m
7	33.8	1.56, ddd (14.5, 12.8, 4.4)
		1.69, ddd (14.5, 12.3, 3.4)
8	46.2	2.51, m
9	206.6	
10	125.3	6.48, d (15.1)
11	143.4	7.10, dd (15.0, 11.1)
12	130.4	6.43, dd (15.3, 11.2)
13	148.5	5.99, d (15.3)
14	76.0	
15	80.5	4.72, dd (10.3, 3.1)
16	21.3	1.78, m
		1.79, m
17	11.0	0.90, t (7.3)
18	20.0	1.21, d (7.2)
19	17.9	0.98, d (6.9)
20	17.9	1.17, d (6.9)
21	24.2	1.32, s
1'	106.1	4.26, d (7.3)
2'	72.1	3.28, dd (10.3, 7.4)
3'	65.9	2.66, m
4'	31.9	1.26, m
		1.75, m
5'	70.1	3.53, m
6'	21.4	1.21, d (5.7)
7'	40.8	2.36, s

*Solvent: CD_3OD

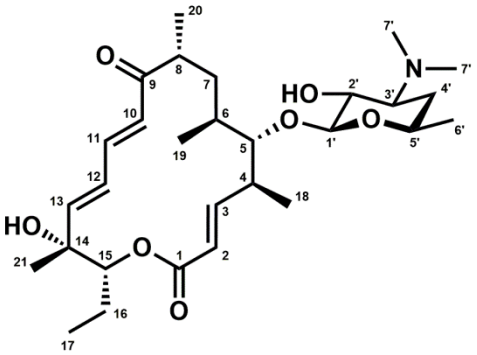

16

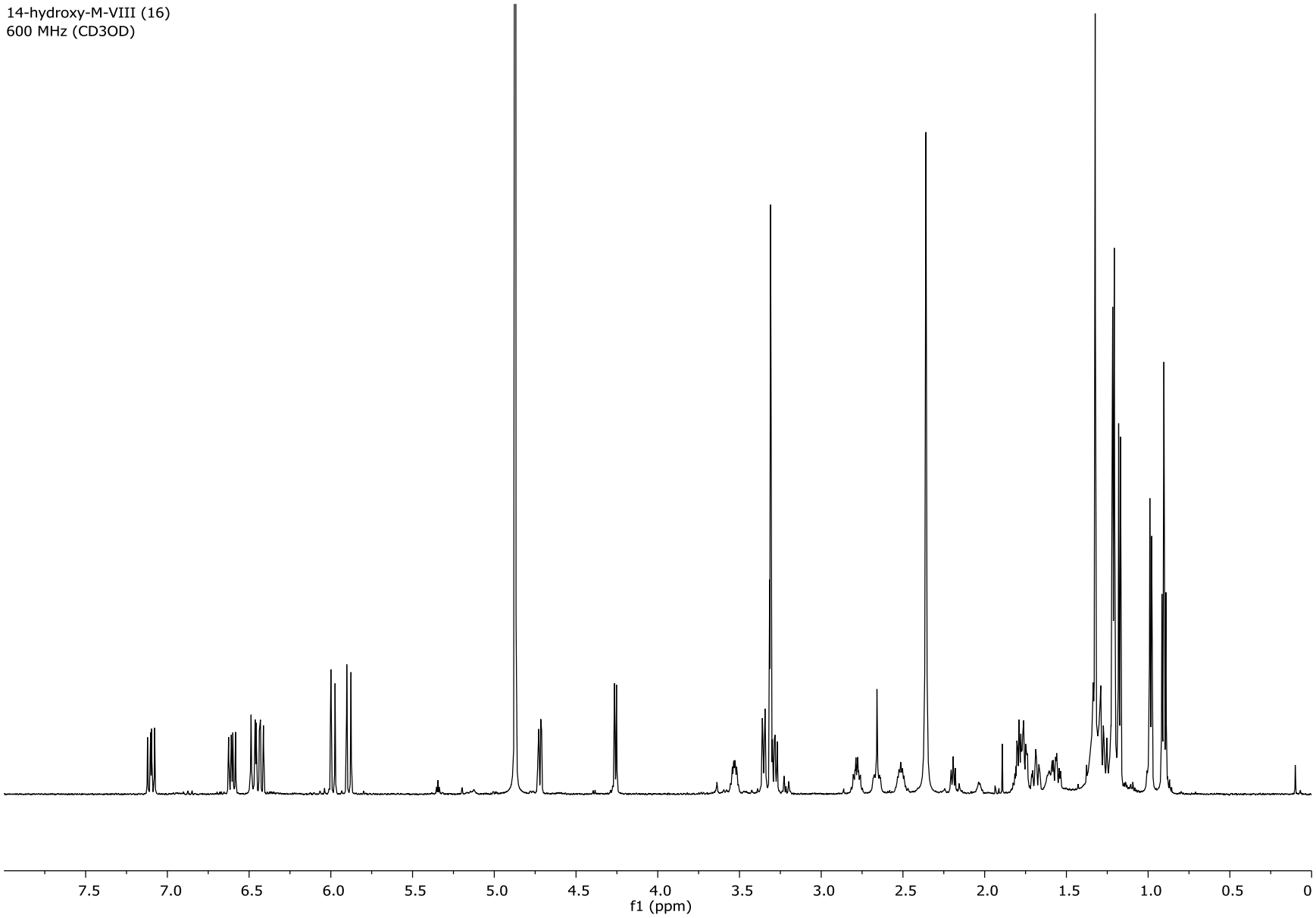
14-hydroxy-M-VIII (16)
600 MHz (CD3OD)
7.5
7.0
6.5
6.0
5.5
5.0
4.5
4.0
3.5
3.0
2.5
2.0
1.5
1.0
0.5
0
f1 (ppm)

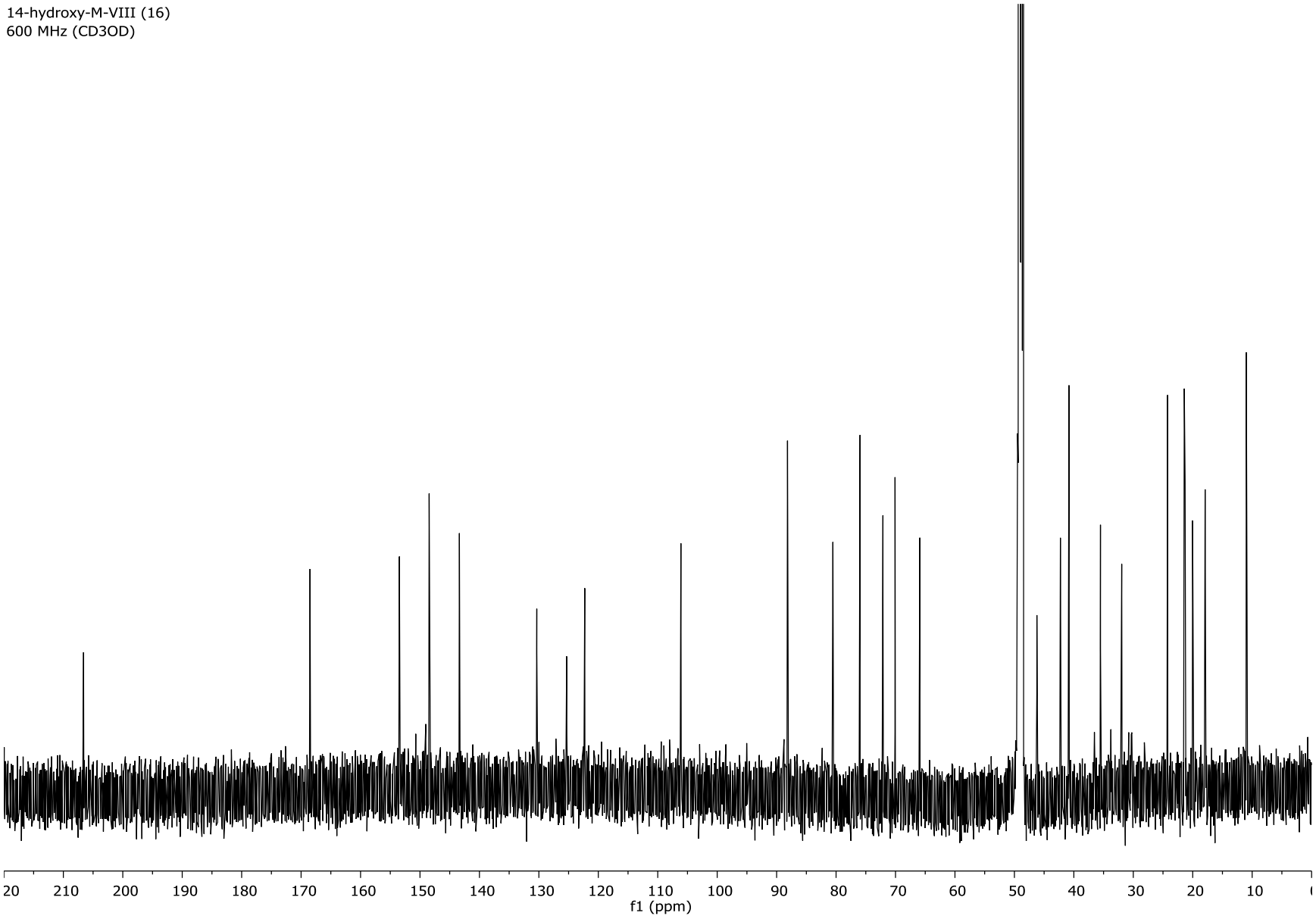
14-hydroxy-M-VIII (16)
600 MHz (CD3OD)
220 210 200 190 180 170 160 150 140 130 120 110 100 90 80 70 60 50 40 30 20 10
f1 (ppm)

C.9 References

(1) Li, S., Podust, L. M., and Sherman, D. H. (2007) Engineering and analysis of a self-sufficient biosynthetic cytochrome P450 PikC fused to the RhFRED reductase domain. *J. Am. Chem. Soc. 129*, 12940–12941.
(2) Omura, T., and Sato, R. (1964) The carbon monoxide-binding pigment of liver microsomes: I. Evidence for its hemoprotein nature. *J. Biol. Chem. 239*, 2370–2378.
(3) DeMars, M. D., II, Sheng, F., Park, S. R., Lowell, A. N., Podust, L. M., and Sherman, D. H. (2016) Biochemical and structural characterization of MycCI, a versatile P450 biocatalyst from the mycinamicin biosynthetic pathway. *ACS Chem. Biol. 11*, 2642–2654.
(4) Hoover, J. M., and Stahl, S. S. (2011) Highly practical copper(I)/TEMPO catalyst system for chemoselective aerobic oxidation of primary alcohols. *J. Am. Chem. Soc. 133*, 16901–16910.
(5) Hoover, J. M., Steves, J. E., and Stahl, S. S. (2012) Copper(I)/TEMPO-catalyzed aerobic oxidation of primary alcohols to aldehydes with ambient air. *Nat. Protoc. 7*, 1161–1166.